

N°: 42158



THESE DE DOCTORAT

Ageing of Flame Retarded Polylactic Acid

Présentée et soutenue publiquement à
L'UNIVERSITE LILLE 1 SCIENCES ET TECHNOLOGIES

Pour obtenir le grade de
DOCTEUR
Spécialité : Molécules et Matière Condensée

Par
Nicolas Lesaffre
Titulaire du Master Ingénierie des Systèmes Polymères de l'Université Lille 1

Thèse dirigée par
Prof. Maude Jimenez et Prof. Gaëlle Fontaine

Soutenue le **10 Novembre 2016** devant la Commission d'Examen composée de :

Prof. Serge Bourbigot, Université Lille 1	Président du Jury
Prof. Carl-Eric Wilén, Abo Akademi University	Rapporteur
DR. Sandrine Thérias, Université Clermont-Ferrand II	Rapporteur
Dr. Xavier Couillens, Solvay	Examineur
Prof. Maude Jimenez, Université Lille 1	Directeur de thèse
Prof. Gaëlle Fontaine, Université Lille 1	Co-directeur de thèse

À Virginie

Acknowledgements

First, I would like to thank Prof. Alexandre Legris, head of the UMET laboratory, and Prof. Serge Bourbigot, head of the team ISP-R2F (Reaction and Resistance to Fire). I would like to thank them for giving me the opportunity to join their labs, work on this project and achieve this PhD in excellent job conditions. I extend my thanks to Mr. Bernard Fontaine, head of the Ecole Nationale Supérieure de Chimie de Lille (ENSCL), where the laboratory is located.

I specially would like to express my gratitude to Prof. Maude Jimenez and Prof. Gaëlle Fontaine who supervised me during my PhD thesis in the R2Fire lab. Working with them was a great pleasure throughout the whole project. They provided me with an unbelievable scientific and moral support that I could ever have desired. Their expertise, their patience and guidance experienced during the whole period of the PhD, combined with continuous and stimulating participation, kept me highly motivated and enthusiastic.

I would like to acknowledge Prof. Serge Bourbigot who agreed to chair the jury but also Prof. Carl-Eric Wilén, DR. Sandrine Thérias and Dr. Xavier Couillens who accepted to take on their time, to bring their expertise as reviewers of this manuscript and to be part of the jury.

I am very grateful to any technique expert such as Bertrand Revel, Bertrand Doumert, Hervé Vezin, Aurélie Malfait, Grégory Stoclet and Séverine Bellayer for their support and expertise on different apparatus or techniques I used outside the lab.

Further, I would like to thank everyone in the lab for just being their selves and for the wonderful atmosphere in the lab. First, thanks to those who left before me but brought me a real pleasure to work in the beginning of this PhD: Bastien, Antoine, Marianne, Marion, Nico Renaud (my dear homonymous), Gwen, Carmen and in particular my friend Andrea *alias* Francis. Thanks to all the lab's permanent members: Maude, Gaëlle, Sophie, Serge, Fabienne, Mathilde, Michel, Charaf', Catherine and Severine. Of course, I am very thankful to Bridget (the small red hair crazy woman with a big heart) who really acted as a mother for all of PhD students in the lab. Thanks to Agnès, Anil, Audrey, Ben (PlaymoBen), Chi, HIRAK, JoJo, Laurie, Maryem, Nitayooooo, Pauline (Mother Christmas), Redgy, Sawsen, Sarah, and Tatenda for all great moments we shared together. A very special thanks to Mathieu (our little Corky), el Midgetator, Pierlouse, Berthy "Enrico" la menace and Benji "Ballon d'or" Balavoine for being who they are. More than colleagues they became a real friend. I will never forget all the unbelievable moments we shared together. A page had been turned but as the poet said, "Show must go on"...

Finally, I would like to thank my friends for having supported me during these last three years. Of course I am also so grateful to my family, my mother, my father and my sister for their invaluable support. Last but not least, thank you to Virginie to whom I dedicate this manuscript, for her patience, her love and her invaluable daily support in the best and worst moments.

Table of contents

ACKNOWLEDGEMENTS	V
TABLE OF CONTENTS.....	VII
ABBREVIATIONS	XI
GENERAL INTRODUCTION	17
CHAPTER I: STATE OF THE ART	23
1. Poly(lactic acid).....	24
1.1. PLA synthesis	24
1.2. Properties of PLA	25
1.2.1. Structure	26
1.2.2. Optical properties	28
1.2.3. Thermal properties	30
1.2.4. Crystallization properties	32
1.2.5. Mechanical properties	35
1.3. Conclusion	36
2. Flame retardancy of PLA	36
2.1. Basics on flame retardancy of polymers.....	36
2.1.1. Physical action	38
2.1.2. Chemical action.....	38
2.2. Flame retardancy of PLA by conventional flame retardants	38
2.3. Flame retardancy of PLA by nanoparticles	40
2.4. Intumescent PLA.....	41
2.5. Conventional flame retardants and nanoparticles: synergy in PLA.....	42
2.6. Conclusion	43
3. Ageing of polymers	43
3.1. Chemical ageing of polymers.....	44
3.1.1. Chemical degradation mechanisms	44
3.1.2. Photo-chemical degradation.....	46
3.1.2.1. Photo-initiation step	46
3.1.2.2. Propagation step	48
3.1.2.3. Termination step	50
3.1.3. Thermal degradation	50
3.1.4. Hydrolytic degradation	52
3.1.5. Bio-chemical degradation	54
3.2. Ageing of Poly(lactic) acid.....	55
3.2.1. Photo-degradation of PLA.....	55
3.2.2. Hydrolysis and bio-chemical degradation of PLA.....	57
3.2.3. Thermal degradation of PLA	59

Table of contents

3.2.4.	Synergy between temperature, relative humidity and/or UV light exposure	60
3.3.	Ageing of flame retarded polymers	60
3.3.1.	Thermal degradation of FR polymers	61
3.3.2.	Hydrolytic degradation of FR polymers	62
3.3.3.	Photo-chemical degradation of FR polymers.....	62
3.4.	Conclusion	65
4.	Conclusion	65
CHAPTER II: MATERIALS AND METHODS		67
1.	Materials preparation and processing	68
1.1.	Materials.....	68
1.1.1.	Poly(lactic acid) (PLA).....	68
1.1.2.	Flame retardants and nanoparticles	68
1.2.	Material preparation and processing	69
1.2.1.	Extrusion	69
1.2.2.	Molding.....	71
1.2.3.	Powders	71
2.	Accelerated ageing methods	71
2.1.	Ageing in presence of temperature and relative humidity	71
2.2.	Ageing in presence of UV-rays.....	72
3.	Physico-chemical characterization.....	73
3.1.	Microscopies.....	73
3.1.1.	Digital microscopy.....	73
3.1.2.	Electron probe micro analysis (EPMA).....	73
3.1.3.	Scanning electron microscopy (SEM).....	74
3.1.4.	Transmission electron microscopy (TEM).....	74
3.2.	Thermal analysis	74
3.2.1.	Thermo-gravimetric analysis (TGA).....	74
3.2.2.	Differential scanning calorimetry (DSC).....	75
3.3.	Color changes measurements	76
3.4.	Gel permeation chromatography (GPC)	77
3.5.	Melt flow index (MFI)	78
3.6.	X-ray diffraction (XRD)	78
3.7.	X-ray photoelectron spectroscopy (XPS)	79
3.8.	Fourier transform infrared spectroscopy (FTIR)	79
3.9.	Chemical derivatisation	80
3.10.	Solid state nuclear magnetic resonance (NMR)	80
3.11.	Electron paramagnetic resonance spectroscopy (EPR)	81
4.	Fire testing methods	83
4.1.1.	Mass loss calorimeter (MLC).....	83
4.1.2.	Limiting oxygen index (LOI).....	83
5.	Conclusion	84

CHAPTER III: IMPACT OF AGEING ON PLA	85
1. Visual measurement of ageing	86
1.1. Visual evaluation	86
1.2. Surface morphology of PLA after ageing	87
1.3. Color changes	88
2. Physico-chemical properties after ageing	89
2.1. Impact of ageing on molecular mass	90
2.2. Thermal behavior	93
2.2.1. Thermogravimetric analysis	93
2.2.2. Glass transition and melting temperature	94
2.3. Effect of ageing on crystallization behavior	98
2.4. Conclusion	103
3. Elucidation of the mechanisms of degradation	104
3.1. Degradation under T/RH exposure	104
3.2. Degradation under T/UV and T/UV/RH exposure.	106
3.2.1. Identification of radical species	106
3.2.2. Secondary products formed during degradation	111
4. Conclusion	116
CHAPTER IV: INFLUENCE OF FLAME RETARDANTS ADDITIVES ON THE AGEING OF PLA	119
1. Impact of ageing on the morphology of FR-PLAs	120
1.1. Visual observations	120
1.2. Surface morphology of FR-PLAs after ageing	122
1.3. Conclusion	125
2. Physico-chemical properties of FR-PLAs during ageing	125
2.1. Molecular mass	125
2.1.1. Impact of fillers on molecular mass of FR-PLAs	125
2.1.2. Impact of ageing on the molecular mass of FR-PLAs	127
2.2. Thermal properties	130
2.2.1. Effect of fillers on glass transition and melting temperature	130
2.2.2. Behavior of glass transition and melting temperatures during ageing	130
2.3. Crystallization behavior	135
2.3.1. Crystallization compartment of unaged FR-PLAs	135
2.3.2. Influence of ageing exposure on crystallization behavior of FR-PLAs	137
2.4. Conclusion	140
3. Mechanisms of degradation of PLA in presence of fillers	141
3.1. Surface chemical analysis of aged FR materials	142
3.2. Role FR additives during hydrolysis	144
3.2.1. Hydrolysis of flame retardant additives	144
3.2.2. Evaluation of the migration of flame retardant additives	148
3.3. Impact of FR additives during UV irradiation of PLA	152

4. Conclusion	155
CHAPTER V: IMPACT OF AGEING ON THE FLAME RETARDANT PROPERTIES OF FR-PLAS...159	
1. Flame retardant performances of FR-PLAS.....	160
1.1. Thermal stability of FR-PLAS	160
1.2. Reaction to fire	161
1.2.1. Behavior under mass loss cone calorimeter (MLC).....	161
1.2.2. Limiting oxygen index (LOI) test results	164
1.3. Mechanism of action of FR-PLAS	164
1.4. Conclusion	166
2. Thermal stability and flame retardant properties after ageing	167
2.1. Effect of ageing on thermal stability of FR-PLAS.....	167
2.2. Limiting Oxygen Index (LOI) test results after ageing.....	170
2.3. Viscosity of FR-PLAS	172
2.4. Mass loss cone performances after ageing	176
2.5. Mass loss cone behavior of FR-PLAS loaded at 20 wt.-%.....	178
2.6. Molecular mass of FR-PLAS loaded at 20 wt.-%.....	182
3. Conclusion	185
GENERAL CONCLUSION	187
OUTLOOK	191
LIST OF FIGURES, TABLES AND EQUATIONS	195
REFERENCES	205
APPENDIX.....	219

Abbreviations

ABS	Acrylonitrile butadiene styrene
ATH	Aluminium trihydroxide
ATR	Attenuated total reflectance
APP	Ammonium polyphosphate
BDP	Bisphenol A bis(diphenyl phosphate)
BSE	Back scattered electron
C	Carbon
C20A	Cloisite 20A
C30B	Cloisite 30B
CIE	Commission internationale de l'éclairage
CCD	Charge-coupled device
CDCl₃	Deuterated chloroform
CNa⁺	Cloisite Na ⁺
Cp	Heat capacity
DecaBDE	Decabromodiphenylether
DSC	Differential scanning calorimetry
DTG	Differential Thermogravimetric analysis
E_a	Activation energy
E&E	Electrical and electronic
EG	Expanded graphite
EPMA	Electron probe micro-analysis
EPR	Electron paramagnetic resonance
ESEEM	Electron spin-echo envelope modulation
EVA	Ethyl vinyl acetate
FR	Flame retarded

Abbreviations

FR-PLA	PLAMEL ₅ APP ₂₅
FR-PLA-C30B	PLAMEL ₅ APP ₂₅ C30B
FTIR	Fourier transform infrared spectroscopy
FTT	Fire testing technology
GPC	Gel permeation chromatography
HIPS	High impact polystyrene
HRR	Heat release rate
K	Kelvin
LDPE	Low density polyethylene
LIG	Lignin
LOI	Limiting oxygen index
M_c	Critical molecular mass
M_e	Entanglement molecular mass
M_n	Number average molecular mass
M_w	Weight-average molecular weight
MAH	Maleic anhydride
MAS	Magic angle spinning
MC	Melamine cyanurate
MDH	Magnesium dihydroxide
MEL	Melamine
MFI	Melt flow index
MLC	Mass loss calorimeter
MMT	Montmorillonite
MP	Melamine polyphosphate
MWNT	Multi-walled carbon nanotubes
N	Nitrogen

Abbreviations

NFPA	National Fire Protection Association
NH₃	Ammonia
NMR	Nuclear magnetic resonance
n_t	number of chain scission
O	Oxygen
P	Phosphorus
PA	Polyamide
PA6	Polyamide 6
PC	Polycarbonate
PC2	Multicouche Ni/C
PCL	Polycaprolactone
PE	Polyethylene
PEA	Poly(esteramide)
PEEK	Poly(ether ether ketone)
PER	Pentaerythritol
PET	Poly(ethylene terephthalate)
PHAs	Polyhydroxyalkanoates
pHRR	Peak of heat release rate
PI	Polydispersity index
PLA	Poly(lactide) / Poly(lactic acid)
PMMA	Poly(methyl methacrylate)
PP	Polypropylene
PS	Polystyrene
PVC	Poly(vinyl chloride)
Py-GC/MS	Pyrolysis – gas chromatography - mass spectroscopy
r	Rotational deformation

Abbreviations

RDP	Resorcinol bis(deiphenyl phosphate)
RI	Refractive index
ROP	Ring opening polymerization
Si	Silicon
SEM	Scanning electron microscopy
ST	Starch
T_c	Crystallization temperature
T_g	Glass transition temperature
T_m	Melting temperature
TAP	Thallium acid phthalate
TBP-DP	2,4,6-tribromophenyl-2',3'-dibromopropylether
TEM	Transmission electron microscopy
TGA	Thermo-gravimetric analysis
THR	Total heat release
TiO₂	Titanium dioxide
THF	Tetrahydrofuran
TMS	Tetramethylsilane
TPP	Triphenyl phosphate
TTI	Time to ignition
UV	Ultraviolet
WAXD	wide-angle X-ray diffraction
XRD	X-ray diffraction
XPS	X-ray photoelectron spectroscopy
ZFS	Zero field splitting
2D HYSCORE	2D Hyperfine sublevel correlation spectroscopy
ΔH_c	Enthalpy of crystallization

Abbreviations

ΔH_m	Enthalpy of melting
X	Crystallinity
δ	Chemical shift
δ_{asym}	Asymmetric deformation (scissoring)
δ_{sym}	Symmetric deformation (scissoring)
ν	Elongation vibration

General Introduction

Plastics are present in the human life since Antiquity, when the ancient Mesoamericans first processed natural rubber into balls or figurines, but it is most of all at the end of XIXth century that they have been developed. During this period, synthetic plastics were developed to be used in a broad range of applications. However, the improvements in chemical technology after the First World War permitted the expansion of new forms of plastics and mass production which began around the 1940s. The production of plastics has grown up and has never decreased since that time (**Figure 1**), except during the oil shocks in 1973 and 1979, and during the crisis in 2008. The European production of synthetic plastics has reached about 58 million tons in 2011 compared to less than half a million tons in the 50's. The production market of synthetic plastics is dominated by China, Europe and North American Free Trade Agreement (NAFTA) with ca. 64 % of the worldwide plastic production (**Figure 1**) [1, 2].

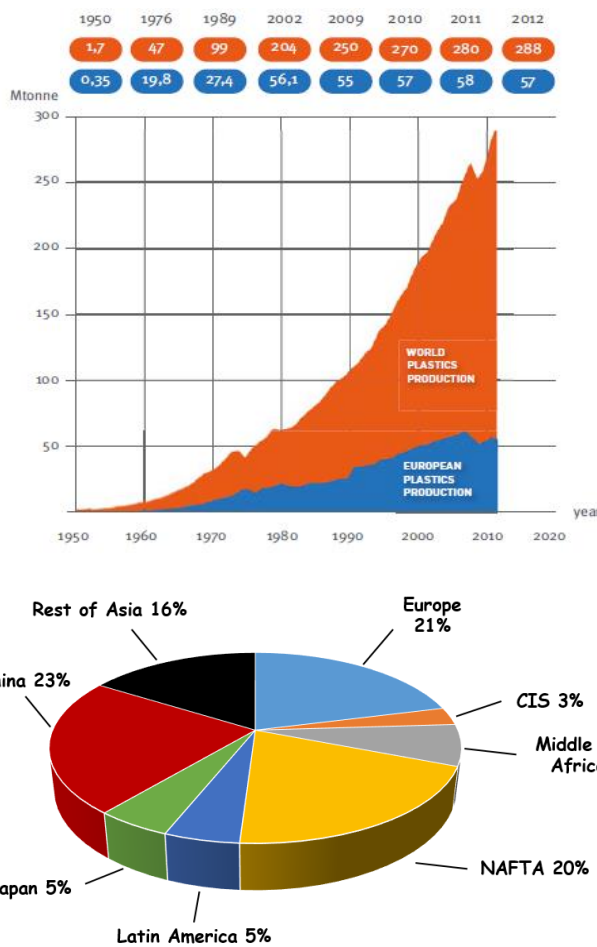


Figure 1: World plastic production from 1950 to 2012 [1, 2].

For more than 50 years, plastics have thus gradually replaced traditional materials such as wood or metal in many applications. They present a great variety of properties and a processing versatility, which make them part of our everyday life. Most of these plastic materials are produced from non-renewable and natural gas-resources. Thus, as the use of synthetic polymers has grown during the past decades, the environmental pollution has extended in dangerous proportions last few years mainly due to (i) the production of these

plastics and (ii) their disposal in landfills after use [1]. Therefore, a move from fossil-based polymers to new polymers exhibiting further properties, especially bio-based polymers, would be appropriate. The worldwide capacity of bio-based plastics production, according to company announcements, will increase from 1.58 Mt in 2013 to 7.85 Mt in 2019 [3, 4]. It is projected that the most important representatives by 2020 will be starch based plastics (1.3 Mt), polylactic acid (PLA) (0.8 Mt) and bio-based polyethylene (PE) (0.6 Mt) [3]. Of the above mentioned bio-based plastics, PLA has drawn attention these last years as an interesting material in several applications areas, particularly in packaging, electrical and electronic (E&E) and automotive [3, 5]. PLA is very easy to process and its production requires 20 to 50% less fossil fuel resources than the production of petroleum based polymers [3].

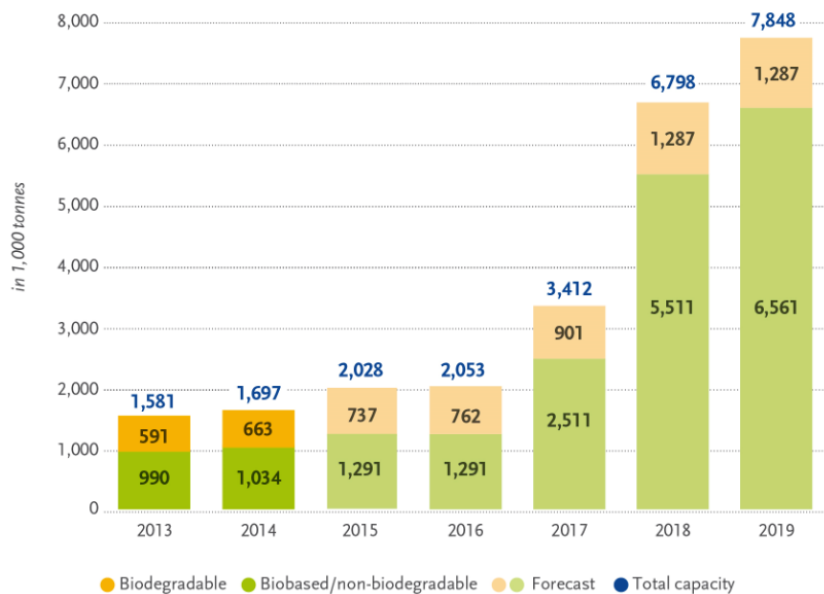


Figure 2: Global production capacities of bioplastics in 2014 (by material type) [4].

In spite of their properties and their numerous applications, plastics exhibit one major drawback: most of them are highly flammable. In case of fire, these materials will tend to release fuel and toxic smokes. The US National Fire Protection Association (NFPA) report that 1.300.000 fires occurred in the United States in 2014 [6], corresponding to a fire every 25 second, and more tragically caused civilian fire deaths and casualties. Plastics are heavy contributors to the development and propagation of a fire. Hence, to be used in certain sectors (e.g. E&E), plastics have to be flame retarded and their flame retardant (FR) properties as well as their properties of use must be kept for the product lifetime. Looking at bio-based plastics, the interest for flame retarded PLA kept growing these past few years (Figure 3); more than 145 papers are dedicated to flame retardancy of PLA in 2015.

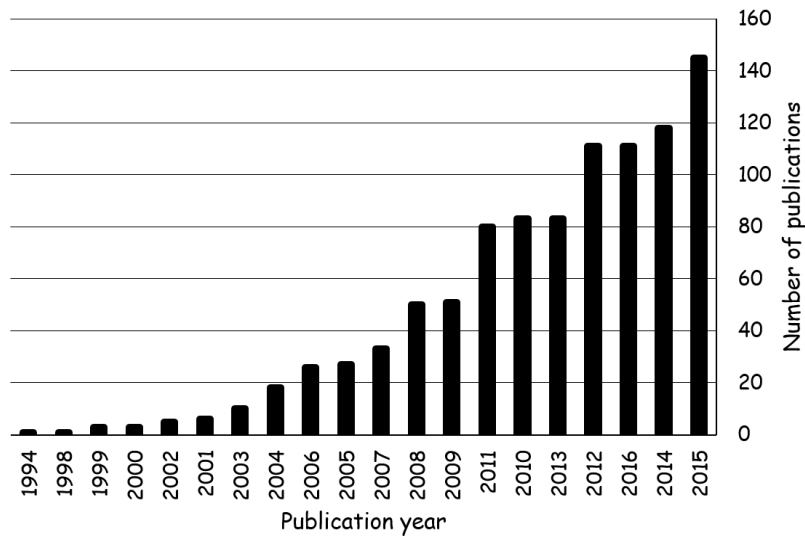


Figure 3: Evolution of number of publications versus time with keyword “flame retardancy” and “PLA” (Scifinder Sept 2016).

Plastics materials can be fire retarded by different methods [7, 8]: (i) by physical methods, i.e. the incorporation of flame retardants (FRs) into polymers via melt blending, (ii) by chemical methods, i.e. the incorporation of FRs into the chemical structure of polymers, e.g. via copolymerization or grafting and (iii) by the coating of a FR layer on the surface of the material. Various kinds of FRs are used in polymers, such as mineral fillers and boron-, phosphorus-, halogen- and nitrogen-based FRs. Concerning PLA, flame retardancy can be obtained by incorporating conventional flame retardants such as metal hydroxides (e.g. Aluminium trihydroxide (ATH), Magnesium hydroxide (MDH) ...), phosphorus-containing compounds (e.g. Ammonium polyphosphate (APP), Melamine polyphosphate (MP) ...) halogenated (e.g. Decabromodiphenylether (DecaBDE), Triphenylphosphate (TPP) ...) and nitrogenated compounds (e.g. Melamine (Mel), Melamine cyanurate (MC) ...) which can be combined with nanoparticles (e.g. organoclays, carbon nanotubes ...) [8-24].

Fire standard tests for polymer-based materials are however usually carried out on newly manufactured samples. However, exposure to various natural ageing conditions (e.g. sun, rain, temperature ...) can impair flame retardant properties throughout the lifetime of the material. Therefore, it is necessary to evaluate the influence of different kinds of ageing conditions on the FR properties of these FR polymers. Numerous studies can be found in the literature concerning the effect of temperature and relative humidity or light (UV-rays) on the degradation of neat PLA [25-35]. The degradation of a PLA matrix containing fillers (sepiolite, fluorohectorite, calcium sulphate, nanoclays ...) has for example been investigated [32, 34-39]. It is demonstrated that PLA is extremely sensitive to hydrolysis and photo-degradation phenomenon, which are accelerated when temperature increases [29]. These kinds of ageing exposure involve the scission of the polymer chains, leading to the complete degradation of the material. Most of the time hydrolysis and photo-degradation lead to a decrease (i) of the molecular mass of the material, (ii) of its glass transition temperature and (iii) of the

mechanical properties of the polymer [29, 33-35, 38]. The incorporation of fillers such as nanoclays or calcium sulphate could accelerate the degradation of the PLA matrix due to the affinity of fillers with water and UV radiations [35, 37]. Few papers however deal with the ageing of flame retarded materials [40-48]. In all the works reported in the literature, the effect of accelerated ageing on the FR properties is mainly evidenced, but the authors do not establish clear relations between these properties and the changes in thermo-physical properties of the polymers during ageing process. This relationship is however needed to elucidate the ageing mechanism and thus design long-term durable flame retardant formulations.

A recent study of our group reported the effectiveness of the combination of Melamine, Ammonium polyphosphate (APP) and organomodified montmorillonite (Cloisite 30B) on the FR properties of PLA [12]. In this way, two formulations were developed, i.e. FR-PLA (containing Melamine and APP) and FR-PLA-C30B (containing Melamine, APP and Cloisite 30B). Thus, based on this study, this work deals with the impact of accelerated ageing on flame retarded PLA and the role of flame retardant additives during ageing of this polymer. Three different kinds of ageing will be investigated: (i) temperature and UV exposure (T/UV), (ii) temperature and relative humidity exposure (T/RH) and (iii) a combination between temperature, relative humidity and UV radiations (T/UV/RH).

This work is divided into five chapters. The first chapter gives a general background about PLA. The synthesis, structure and the different properties of this polymer are reported. Then, a literature review investigates the flame retardancy of polymers and of PLA in particular. The last section of this chapter gives an overview of the chemical ageing of polymers and some examples are given concerning the impact of ageing on PLA and flame retarded materials in general.

The second chapter reports the materials and experimental methods used in this study. The polymer (PLA) and flame retardant additives as well as the material preparation process are described. Then, accelerated ageing tests and characterization methods are presented followed by experimental techniques permitting to evaluate fire retardant properties of the materials.

The third chapter reports the impact of ageing tests on neat PLA as a reference material. The objective of this chapter is to identify the effects of T/UV, T/RH and T/UV/RH exposure on the physico-chemical properties of neat PLA in order to evidence the mechanisms of degradation involved. First the visual modifications as well as the impact on the molecular mass, glass and melting temperatures, crystallinity and thermal stability are investigated for each kind of exposure. Furthermore, hydrolytic and photo-oxidative mechanisms of degradation occurring during ageing are proposed.

Chapter four studies the impact of the incorporation of FR fillers on the properties of PLA. Then, the impact of ageing on the physico chemical properties of flame retarded PLAs, i.e. FR-

PLA and FR-PLA-C30B is evaluated. Finally, the role of fillers on the mechanisms of degradation of PLA is investigated.

The last chapter deals with the impact of ageing on the flame retardant properties of PLA. The fire properties and the mechanism of action of FR-PLAs are firstly reminded. Thereafter, fire retardant properties after ageing are investigated. Finally, the relationship between the change in both physico-chemical and flame retardant properties is examined. The role of ageing on the behavior of flame retardant properties is thus detailed.

At the end of this work a general conclusion is given and outlook for future studies on this subject are proposed.

Chapter I: State of the Art

This first chapter starts by an overview of a biodegradable polymer, i.e. PLA. In particular its production process and properties, are fully commented. As this study mainly deals with ageing of flame retarded materials, the different ways to obtain flame retardant PLA are described. At the end of the chapter, the different types of chemical ageing affecting polymeric materials and especially PLA are discussed with focus on the mechanisms of degradation occurring during ageing. Moreover, some examples of aged flame retarded systems are presented.

1. Poly(lactic acid)

The aim of this study is to evidence and understand the impacts of ageing on flame retarded polymers, and thus determine the FR durability of such materials. In this way we've decided to focus this study on polylactic acid (PLA) which has recently received some great deal of attention [3, 5] and especially in the field of flame retardancy [8, 10, 12-15, 20-23, 49-51]. Before investigating in details the ageing of flame retarded PLAs, the strategy is to first understand the effect of ageing on raw PLA. Hence, determining the mechanisms of degradation occurring during ageing as well as the ageing effect on the physico-chemical properties of the raw PLA. Then the effect of the incorporation of flame retardant fillers on the (i) FR behavior, (ii) the physico-chemical properties and (iii) degradation of PLA during ageing will be investigated.

PLA is nowadays the first commodity biodegradable polymer produced from annually renewable resources. It is a potential good candidate to replace traditional petroleum derived polymeric materials [3]. PLA is relatively cheap and has some remarkable properties that make it suitable for various applications such as packaging, textile or transportation like automobile [3, 5, 52]. PLA can be modified, plasticized, filled, chemically modified, reactive blended and processed like many other conventional polymers. Nevertheless, PLA must be studied carefully due to its unique properties: structural, thermal, crystallization and rheological properties of PLA must be taken into account during its converting process [52]. Hence, an overview of this biodegradable polymer (i.e. the synthesis pathways, its structure and properties) is reported in this part, in order to have a wide background knowledge of the material, before investigating its ageing behavior.

1.1. PLA synthesis

Using an appropriate catalyst and heat, two major routes exist to produce PLA (**Figure 4**): (i) direct condensation polymerization of lactic acid or (ii) conversion of lactic acid to the cyclic lactic dimer and ring opening polymerization (ROP) through the lactide intermediate [5, 52].

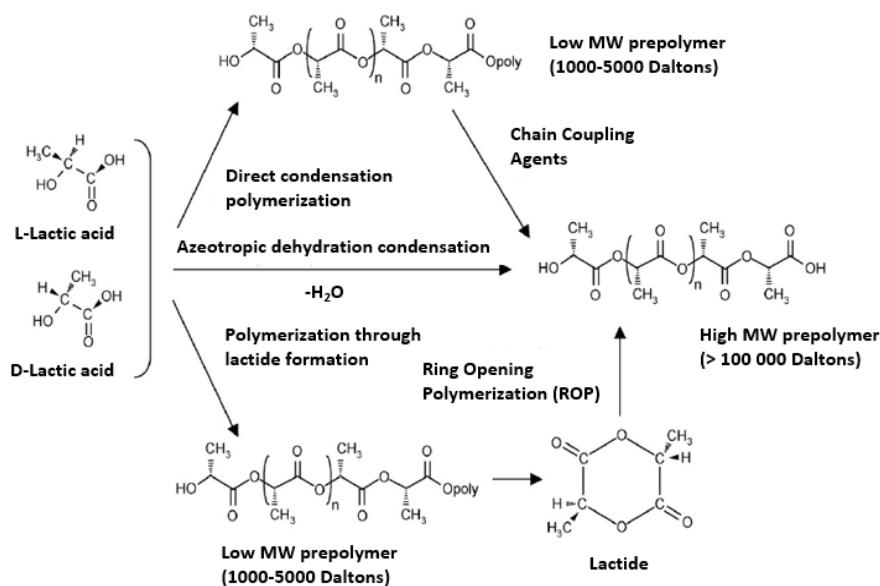


Figure 4: Synthesis of PLA from L- and D-lactic acids, adapted from Lim et al. [52].

ROP is the most common way to produce high molecular weight PLA. In fact, water must be eliminated during polymerization of lactic acid to obtain high molecular weight polymer. As water remains during the direct condensation polymerization, the molecular mass of PLA is decreased [5]. Thus, it is necessary to add a step during the process including chain coupling agents in order to extend the chain length of the polymer and then obtain high molecular weight PLA [53].

The ROP of lactide monomer avoids using coupling agents. Indeed, poly(lactic acid) oligomers, also called pre-polymers (with low molecular weight) are formed by polycondensation in a first step. Then, in a second step, the depolymerization of poly(lactic acid) oligomers produces a cyclic dimer called lactide monomer. Lactide monomer is then finally polymerized by ROP to form high molecular weight polylactide (**Figure 4**).

Among numerous processes allowing obtaining polylactide, ROP is the most commonly used in the industry. However, this kind of process requires the use of a catalyst in order to initiate the polymerization [53]. Numerous catalysts can be used for ROP but previous researches have demonstrated the efficiency of tin octanoate $S_n(\text{Oct})_2$ as catalyst [51]. In fact, tin octanoate is preferred as catalyst for the bulk polymerization of lactide due to its solubility in molten lactide, high catalytic activity, and low rate of racemization of polymer [51, 54-56].

1.2. Properties of PLA

The ability to control both PLA production and structural architecture permits to predict and evaluate its different physico-chemical properties (e.g. crystallinity, mechanical, thermal or optical properties). As these latter play a key role on the lifetime of the material, the next section is dedicated to the different properties of PLA.

1.2.1. Structure

The polymer architecture and its molecular mass are responsible of the different properties of the high molecular weight PLA. According to Auras et al. [5] the ability to control the stereochemical architecture permits precise control over the speed of crystallization and finally the degree of crystallinity, the mechanical properties and the processing temperatures of the material. It is thus of primary importance to study the structure of PLA.

PLA is a linear aliphatic polyester (**Figure 5**) that is composed of repeating units of lactic acid (72 g/mol) containing an asymmetric carbon atom. This stereo center can be either in (S)L or (R)D configuration. L-lactic acid and D-lactic acid, the two isomers of lactic acid are shown in **Figure 6**.

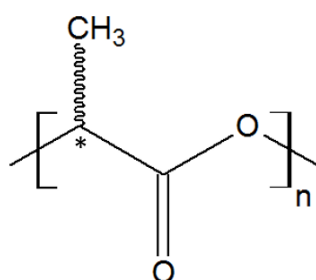


Figure 5: Poly(lactic acid) structure.

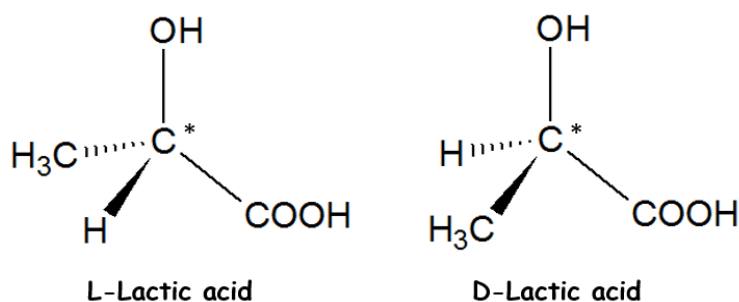


Figure 6: The stereoisomers of lactic acid.

Most of the biological organisms producing lactic acid provide mainly L-lactic acid and no major source of D-lactic acid is available [5]. Theoretically, these two isomers of lactic acid are able to produce four distinct materials; poly(D-lactic acid) (PDLA), poly(L-lactic acid) (PLLA), poly(D,L-lactic acid) (PDLLA) and meso-PLA, obtained by the polymerization of meso-lactide (L,D-Lactide).

Depending on the optical configuration of the lactic acid three main stereoisomers of lactide result from the depolymerization of poly(lactic acid) pre-polymers: L,L-lactide, D,D-lactide and L,D-lactide (**Figure 7**).

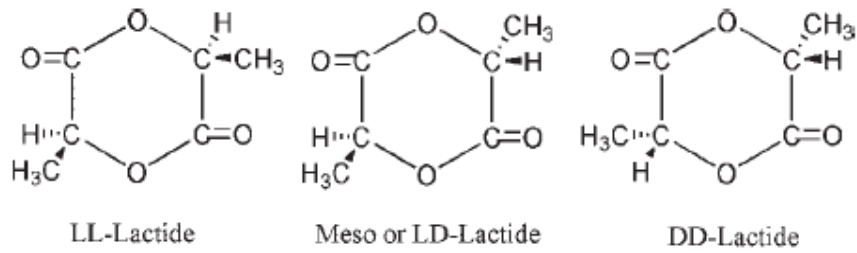


Figure 7: Chemical structures of L,L-, L,D- and D,D-lactides [5].

PLA can also be found in stereocomplex form. Stereocomplexation of polymers corresponds to the formation of complex between two kinds of stereoisomers. This is for example the case of poly(methyl methacrylate) (PMMA) [57], poly(γ -benzyl glutamate) [58], and PLA [59, 60]. In the case of PLA, stereocomplexation happens between PLLA and PDLA. Hydrogen bonds are formed between hydrogen and carbonyl group, contributing to the formation of crystalline structure (**Figure 8**) different from the α -, β - and γ -forms commonly observed [60]. These stereocomplex can be formed in solution or by melt blending.

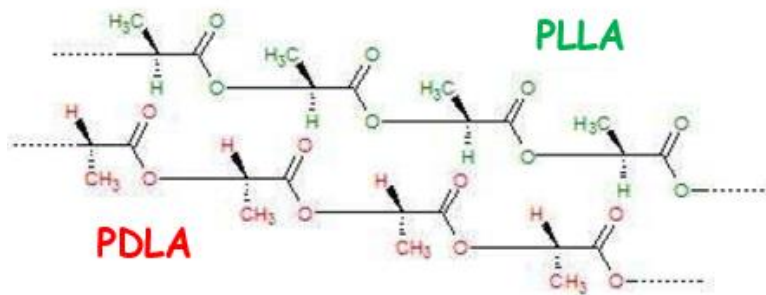


Figure 8: Stereocomplex of PLLA and PDLA [61].

Multi-step polymerization is another way to achieve stereocomplex, in order to obtain PDLLA diblock or multiblock poly-(L,L)-(D,D)-lactide. Depending on the process used, it is possible to obtain different PDLLA chains (**Figure 9**) [60].

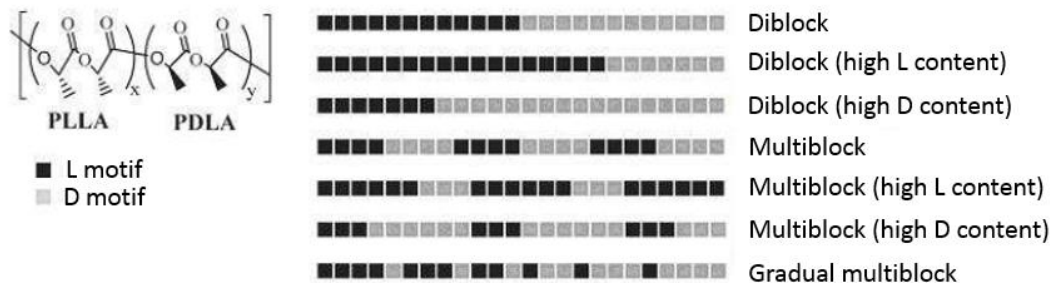


Figure 9: PDLLA multiblocks as function of D and L content, adapted from Kakuta et al. [60].

1.2.2. Optical properties

Figure 10 presents the transmission percentage versus wavelength for different polymers, including PLA in the wavelength range of 180 – 600 nm [5]. As reported by Auras, Harte and Selke [5], PLA does not transmit ultra-violet (UV) rays in the range of 190 – 220 nm whereas at 225 nm the amount of UV light transmitted by PLA increases significantly. Indeed, 85 % of the UV light is transmitted at 250 nm compared to 95 % at 300 nm. Thus, while UV-C is not transmitted, nearly all the UV-B and UV-A light passes through the PLA films. Therefore, the application of transparent PLA films to, for example, dairy products may require additives to block UV light transmission.

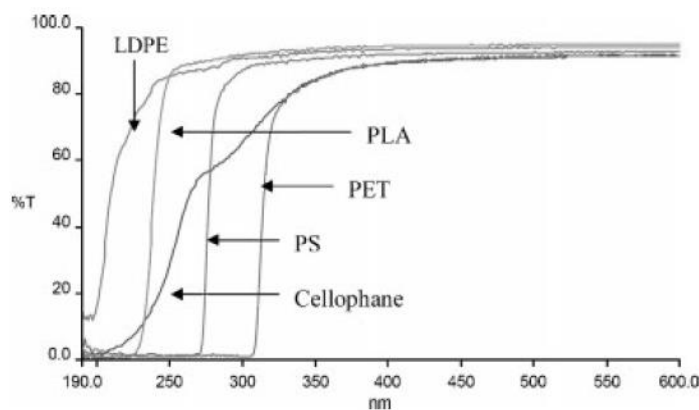


Figure 10: Transmission percentage versus wavelength for PLA, PS, LDPE, PET and cellophane films, adapted from Auras et al. [5].

Effective UV stabilizers are able to absorb UV light and thus to prevent damage to light sensitive packaged foods, resulting in retention of taste and appearance, extension of shelf life and improvement of product quality. PLA transmits less UV-C light than LDPE (**Figure 10**), but PET, PS and Cellophane transmit less UV-B and UV-A than PLA and LDPE. Moreover, PET does not transmit UV-C and UV-B wavelengths, which are the most damaging for food.

PLA also shows some characteristic bands by Fourier Transform Infrared (FTIR) spectroscopy (**Figure 11**). For this polymer, maximum absorbance occurs at 240 nm and is attributed to ester group present in the backbone (**Figure 5**). The main PLA absorption bands in the infrared range are summarized in **Table 1** [29, 32, 34, 35, 62, 63].

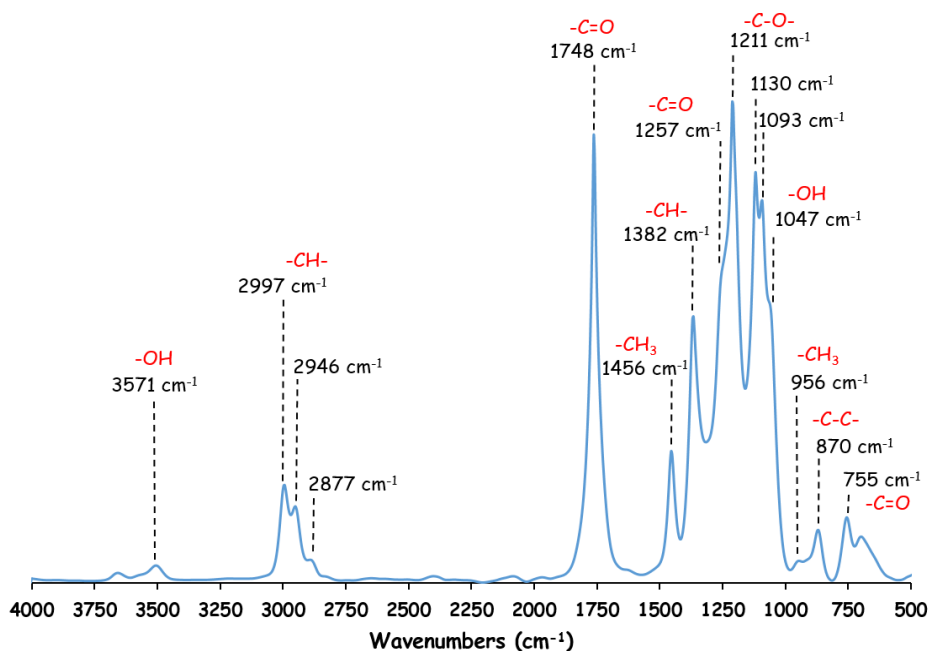


Figure 11: FTIR (ATR) spectrum of PLA in the range 500 to 4000 cm^{-1} .

Table 1: Infrared spectroscopy data for PLA.

Assignment	Peak position (cm^{-1})
-OH stretch (free)	3571
-CH- stretch	2997 (asym), 2946 (sym), 2877
-C=O carbonyl stretch	1748
-CH ₃ bend	1456
-CH- deformation including symmetric and asymmetric bend	1382, 1365
-CH- bend	1315 (not shown), 1300 (not shown)
-C=O bend	1257
-C-O- stretch	1211, 1130, 1093
-OH bend	1047
-CH ₃ rocking modes	956, 921 (not shown), 912 (not shown)
-C-C- stretch	926 (not shown), 870
-C=O deformation	755

These different bands correspond to characteristics bonds of PLA such as –OH groups located at the extremity of the polymer chain (3571 cm^{-1} and 1047 cm^{-1} corresponding to stretching and bending regions). The bands at 2997 , 2946 and 2877 cm^{-1} are assigned to the CH stretching region, $\nu_{\text{as}} \text{CH}_3$, $\nu_{\text{s}} \text{CH}_3$ and νCH modes. The C=O stretching region appears as a large band at 1748 cm^{-1} . The region between 1500 cm^{-1} and 1360 cm^{-1} is characterized by the 1456 cm^{-1} CH₃ band. The CH deformation and asymmetric bands appear at 1382 cm^{-1} and 1365 cm^{-1} , respectively. The bands at 1315 cm^{-1} and 1300 cm^{-1} are due to CH bending modes. Furthermore, in the region of 1300 cm^{-1} to 1000 cm^{-1} , it is possible to observe the C-O

stretching modes of the ester groups at 1211 cm^{-1} and the ν C-O asymmetric mode at 1093 cm^{-1} . Between 1000 cm^{-1} and 800 cm^{-1} , peaks can be observed at 956 cm^{-1} , 921 cm^{-1} and 912 cm^{-1} which can be attributed to the characteristic vibrations of the CH_3 rocking modes (peaks of PLA that had the α - and β -form crystals were observed at 921 and 912 cm^{-1} , respectively). Bands related to the crystalline and amorphous phase of PLA can be observed. The peaks at 956 cm^{-1} and 871 cm^{-1} can be assigned to the amorphous phase and the ones at 921 cm^{-1} and 756 cm^{-1} to the crystalline phase [64, 65].

1.2.3. Thermal properties

In the solid state, PLA can be either amorphous or semi-crystalline, depending on the overall optical composition, primary structure, thermal history, and molecular weight. Semi-crystalline PLA exhibits a glass transition temperature (T_g) and a melting temperature (T_m). Most of the physical characteristics (density, heat capacity, mechanical and rheological properties) of PLA are to a great extent dependent on its glass transition temperature.

The T_g (50 - 60°C) and T_m (130°C - 230°C) of PLA are important in order to define the commercial applications. Above T_g (around 58°C) PLA is rubbery, while below T_g , it is still able to creep until it is cooled to its β -transition temperature at around -45°C , below which it behaves as a brittle polymer [52, 64, 66]. As displayed in **Figure 12** the T_g of PLA is very dependent on both the molecular weight and stereoisomer content of the polymer. According to Dorgan et al. [67], T_g increases with molecular weight until a maximum value at infinite molecular weight. These maximum values reach 60°C , 56°C and 54°C for PLAs with 100, 80 and 50 % L-stereoisomer respectively. It may be noted that, for similar content of L-lactic acid and D-lactic acid, the PLA containing L-lactide has higher T_g values [67].

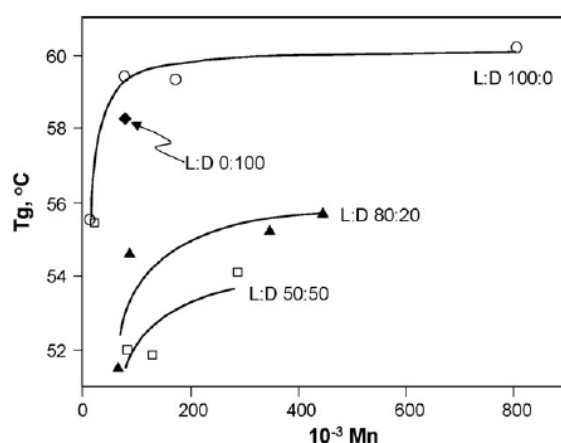


Figure 12: Glass transition temperatures for PLAs of different L-contents as a function of molecular weight, adapted from Dorgan et al. [67].

The relationship between T_g and molecular weight of a polymer can be represented by the Flory-Fox **Equation 1**:

$$T_g = T_g^\infty - \frac{K}{M_n}$$

Equation 1

Where T_g^∞ is the T_g at the infinite molecular weight, K is a constant representing the excess free volume of the end groups of polymer chains, and M_n is the number average molecular weight. The values of T_g^∞ and K are around 57 and 58°C and 55000 and 73000 as reported in the literature for PLLA and PDLA, respectively [68]. The thermal history of the polymer also plays an important role concerning the T_g value of PLA. Quenching the polymer from the melt at a quick cooling rate (>500°C/min, such as during injection molding) will lead to a highly amorphous PLA. The PLA obtained has a tendency to rapidly undergo ageing in matter of days under ambient conditions [69, 70] and this phenomenon contributes in an important manner to the embrittlement of PLA.

As well as T_g , the melting temperature (T_m) of PLA also depends on its stereoisomer content. Hence, the T_m for stereo-chemically pure PLA (either L or D) is around 180°C with an enthalpy between 40-50 J/g. The presence of meso-lactide in the PLA structure can depress the T_m by as much as 50°C, depending on the amount incorporated to the polymer. **Figure 13** shows the variation of the T_m as a function of % meso-lactide introduced in the PLA based on data from Witzke and Hartmann [52, 71, 72].

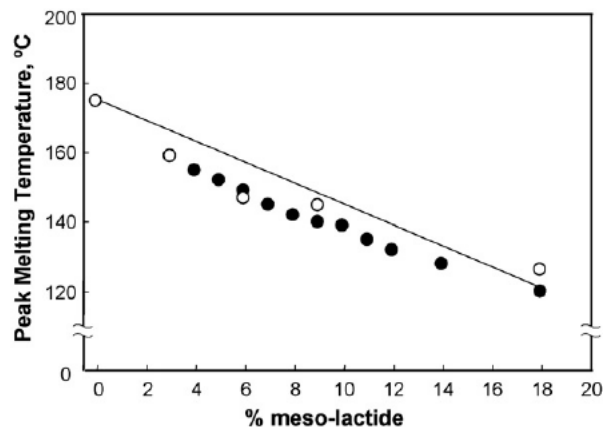


Figure 13: Peak melting temperature of PLA as a function of % meso-lactide [52]. (○) represents values reported by Witzke [71]; (●) represents values reported by Hartmann [72].

The relationship between T_m and meso-lactide content can be approximated reasonably well by the following **Equation 2** [71]:

$$T_m (\text{°C}) \approx 175^\circ\text{C} - 300W_m$$

Equation 2

Where W_m is the fraction of meso-lactide below 18 % level, and 175°C is the melting temperature of PLA made of 100% L-lactide. Typical T_m values for PLA are in the range of

130 - 160°C. The T_m decrease induced by meso-lactide has several important implications as it helps (i) expanding the process window, (ii) reducing thermal and hydrolytic degradation, and (iii) decreasing lactide formation [52].

1.2.4. Crystallization properties

PLA produced from more than 93 % L-lactic acid can be semi crystalline whereas PLA from 50 to 93 % of L-lactic acid is strictly amorphous. It is well known that commercial PLAs are copolymers of PLLA and PDLLA, which are produced from L-lactide and D,L-lactide (maxi 10% of D), respectively [52, 64, 65]. The L-isomer constitutes the main fraction of PLA derived from renewable sources since the majority of lactic acid from biological sources exists in this form. Depending on the compositions of the optically active L- and D-L enantiomers as well as on the preparation conditions, PLA can crystallize principally in three forms (α , β and γ).

The α -form crystal is the most stable and exhibits a well-defined diffraction pattern [73]. It has a melting temperature (T_m) of 185°C compared to 175°C for the β -form [5, 52]. As described in **Table 2**, the α -form has an orthorhombic space group, with a unit cell containing two antiparallel chains. The lattice parameters are $a = 10.66 \text{ \AA}$, $b = 6.16 \text{ \AA}$ and c (chain axis) = 28.88 \AA , with a crystal density of 1.26 g.cm^{-3} [74].

The chain conformation of the β -form is a left-handed 3-fold helix [74]. It has an orthorhombic or a trigonal unit cell containing a 3_1 (3 \AA rise/1 monomeric unit) polymeric helix. The unit cell dimensions are as follows: $a = 10.31 \text{ \AA}$, $b = 18.21 \text{ \AA}$ and $c = 9.0 \text{ \AA}$ for the orthorhombic and $a = 10.52 \text{ \AA}$, $b = 10.52 \text{ \AA}$ and $c = 8.8 \text{ \AA}$ for the trigonal (**Table 2**) [73].

Finally, the γ -form, found by epitaxial crystallization, contains two antiparallel ($s(3/2)$) helices in the pseudo orthorhombic unit cell ($a = 9.95 \text{ \AA}$, $b = 6.25 \text{ \AA}$ and $c = 8.8 \text{ \AA}$) and it assumes the known three-fold helix of PLA (**Table 2**) [75].

Table 2: Unit cell parameters for PLLA and stereocomplex crystals [5].

Crystalline Phase	Space Group	Helix	Helical conformation	a (nm)	b (nm)	c (nm)	α (°)	β (°)	γ (°)
α	P-orthorhombic	2	10_3	1.07	0.645	2.88	90	90	90
α	P-orthorhombic	2	10_3	1.06	0.61	2.88	90	90	90
α	Orthorhombic	2	10_3	1.05	0.61	-	90	90	90
β	Orthorhombic	6	3_1	1.031	1.821	0.90	90	90	90
β	Trigonal	3	3_1	1.052	1.052	0.88	90	90	120
γ	Orthorhombic	2	3_1	0.995	0.625	0.88	90	90	90
Stereo complex	Triclinic	2	3_1	0.916	0.916	0.87	109.2	109.2	109.8

Generally, the faculty of PLLA or PDLA to crystallize is highly linked to the thermal process implementation [76], the nature and quantity of fillers that they contain as well as the ratio between L-lactide/D-lactide [61].

Many researchers investigated the crystallization behavior of PLA [64, 65, 72, 77]. Accordingly, Differential Scanning Calorimetry (DSC) is commonly used to determine the crystallinity of PLA. By measuring the heat of fusion ΔH_m and heat of cold crystallization ΔH_{cc} , the crystallinity can be determined based on the following **Equation 3**:

$$\text{Crystallinity (\%)} = \frac{100 * (\Delta H_m - \Delta H_{cc})}{\Delta H_m(100\%)}$$

Equation 3

$\Delta H_m(100\%)$ is the melting enthalpy for 100% crystalline PLLA or PDLA homopolymers and is 93.1 J/g [52]. Quenching the optically pure PLA from the melt at quick cooling rate leads to a decrease in crystallinity (%) and results in a quite amorphous polymer. The quenched PLA (**Figure 14**) resulted in an exothermic crystallization peak and a glass transition temperature upon subsequent reheat, while slow cooling produces a polymer with higher crystallinity with much lower enthalpy of crystallization [77].

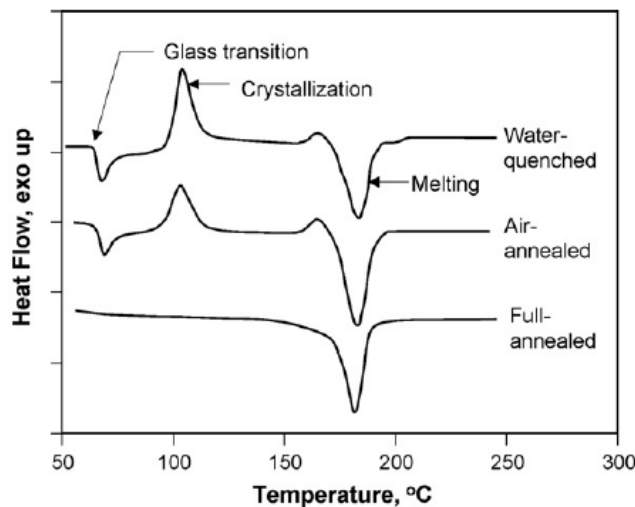


Figure 14: DSC thermograms of water quenched, air-annealed (cooled from 220°C to ambient temperature in 5 min), and full-annealed (cooled from 220°C to ambient temperature in 105 min) PLLA samples. DSC scans were performed at a heating rate of 10°C/min, adapted from Sarasua et al. [77].

The tendency for PLA to crystallize upon reheat also depends on the heating rate. In fact, **Figure 15** illustrates a set of the heat capacities of amorphous poly(L-lactide) after cooling from the melt at 10 K/min, followed by heating with heating rates from 0.3 to 30 K/min. These results indicate that the quenched poly(L-lactide) crystallizes to different degrees on heating rates slower than 30 K/min, and undergoes additional reorganization, melting, and

recrystallization between the glass transition and final melting. The stereoisomer content plays as well an important role in the tendency for PLA to crystallize upon reheat (**Figure 16**). As shown in **Figure 16**, PLA polymers containing more than 8% D-isomer remain amorphous even after 15 h of isothermal treatment at 145°C. In contrast, at 1.5% D-isomer level, although the quenched PLA has a minimal crystallinity, the isothermal treatment at 145°C resulted in a large endothermic melting peak around 450 K.

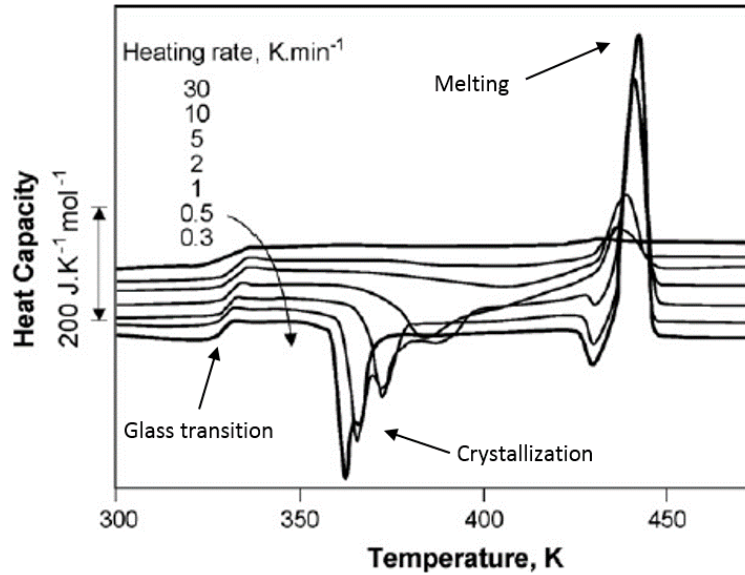


Figure 15: DSC scans for 1.5% D-lactide PLA samples cooled from the melt at 10K/min and then reheated at different heating rates from 30 to 0.3 K/min, adapted from Pyda et al. [78].

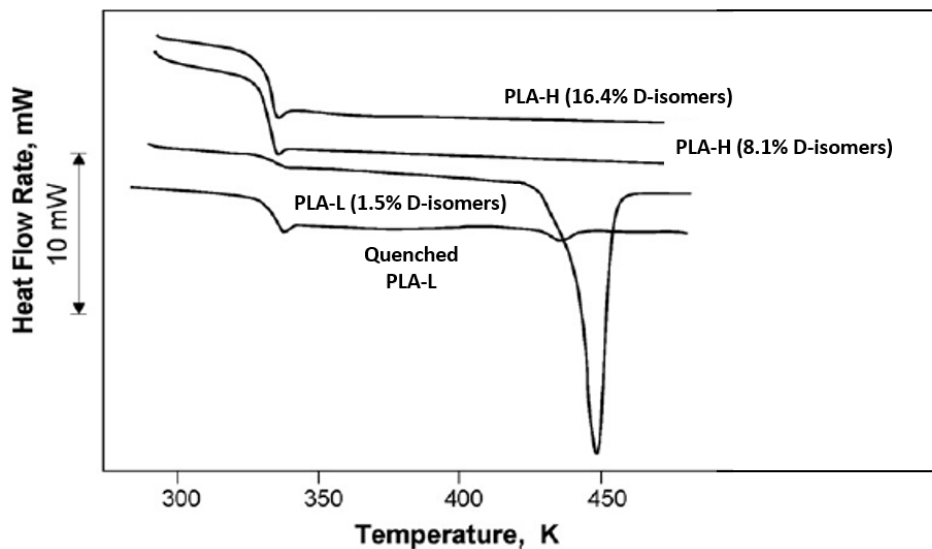


Figure 16: DSC scans at 20 K/min for PLA with 1.5% (PLA-L), 8.1% (PLA-M) and 16.4% (PLA-H) D-isomers. All samples were cooled quickly from the melt and isothermally crystallized at 145°C for 15h. The quenched PLA-L sample was cooled similarly from the melt but did not undergo the 15 h isothermal crystallization, adapted from Pyda et al. [78].

In general, the half time crystallization of PLA increases about 40% for every 1% meso-lactide (L,D-Lactide) in the polymerization mixture, which is mainly driven by the reduction of the melting point for the copolymer [79]. It also has been demonstrated by Vasanthakumari et al [80, 81] that the kinetics of crystallization depends on the molecular mass of the polymer. In fact, authors reported that the rate of crystal formation increases with a decrease of the molecular weight.

Overall, the formation of crystals may or may not be favorable depending on the end-use requirements of PLA articles. As an example, high crystallinity will not be optimal for injection molded preforms that are intended for further blow molding, since rapid crystallization of the polymer would hamper the stretching of the preform and optical clarity of the resulting bottle. On the contrary, an increased crystallinity will be desirable for injection molded articles for which good thermal stability is important. Crystallization of PLA articles can be initiated by annealing at temperatures higher than T_g and below T_m to improve their thermal stability.

1.2.5. Mechanical properties

The mechanical properties of PLA have been widely studied over the years [5, 64, 72, 82]. Despite its numerous advantages such as high strength and high modulus, the inherent brittleness is problematic in many commercial applications. Compared to Polystyrene (PS), PLA not only has comparable tensile strength and modulus but also exhibits very similar inherent brittleness as shown in **Table 3**. In fact, T_g of PLA is between 55 and 65°C, tensile strength at break and modulus are 53 MPa and 3.4 GPa, respectively, whereas elongation at break is 6%.

Table 3: PLA mechanical properties compared to those of most common polymers used in commodity applications [83].

	PLA	PET	PS	HIPS	PP
T_g (°C)	55-65	75	105	-	10
Tensile strength at break (MPa)	51	54	48	23	31
Tensile modulus (GPa)	3.2	2.8	3.0	2.1	0.9
Elongation at break (%)	6	130	7	45	120

These last years PLA toughening has become the focus of numerous investigations. Many strategies have been more or less successfully developed to improve the toughness of PLA, including plasticization, copolymerization, addition of fillers and blending with a variety of flexible polymers or rubbers [36, 77, 84-86].

1.3. Conclusion

In this part, it was reported that PLA is undoubtedly one of the most promising candidates in the market of biodegradable polymers, for further developments. In fact, depending on its structure and chemical composition, PLA can reach good physical, thermal and mechanical properties. This makes it a good candidate to be used in several applications areas such as packaging, electrical and electronic (E&E) and automotive.

However, to be used in some of these sectors (e.g. E&E), PLA has to be flame retarded, which implies the incorporation of fire retardant fillers during PLA processing. Of course, these flame retardant properties must be kept for the product lifetime. The next part is thus dedicated to the different types of additives used to enhance flame retardant properties of PLA.

2. Flame retardancy of PLA

Nowadays, PLA is primarily used in packaging and textile sectors, but its expected market should be susceptible to extend to transportation and E&E sectors in order to substitute thermoplastics like PP, PA or PET. For instance, Fujitsu is making injection molded computer keys and computer housing made from polycarbonate (PC)/PLA blends [16]. Another recent development which should enable wider applications of PLA in electronics products is NEC's process for imparting flame resistance to PLA without the use of halogen or phosphorous compounds [8]. The product is reported to have heat resistance, moldability and strength comparable to fiber-reinforced polycarbonate used in desktop type electronic products. According to these PLA applications, fire hazard is an issue and flame retardancy of PLA is required. That is why the interest for developing flame retardant PLA kept growing these past few years; more than 110 papers are dedicated to FR-PLA in 2014. Literature revealed that the flame retardancy of PLA can be obtained by different ways such as: (i) the use of conventional FR additives, (ii) nanoparticles, (iii) combination of both, and (iv) intumescent additives [8]. In this section, some basics on flame retardancy as well as the different approaches used to flame retard PLA will be developed.

2.1. Basics on flame retardancy of polymers

As polymeric materials are made up mainly of carbon and hydrogen, most of them are highly combustible [87]. This is why it is primordial to flame retard them to decrease risks in limiting fire spread. The combustion of polymers is a very complex process which has already been widely studied in the literature [88, 89].

The combustion reaction of polymers involves three components: one or more combustible materials (polymers), a combustion agent which can be an oxidizing agent (generally oxygen in air) and heat. The whole process usually starts with an increase in the temperature of the polymeric material due to an external heat source, coming from either an inner (e.g.

exothermicity of the combustion reaction) or outer heat source. Polymer bond scissions are then induced and the resulting volatile fractions of polymer fragments diffuse into air and create a combustible gaseous mixture. Then ignition occurs. The combustion of a polymer is the result of a combination of the effects of heat, represented by two mechanisms [87] (**Figure 17**):

- Non oxidizing thermal degradation (pyrolysis): initiated by chain scission under the effect of temperature increase
- Oxidizing thermal degradation: reaction with oxygen to produce a variety of low molecular weight products.

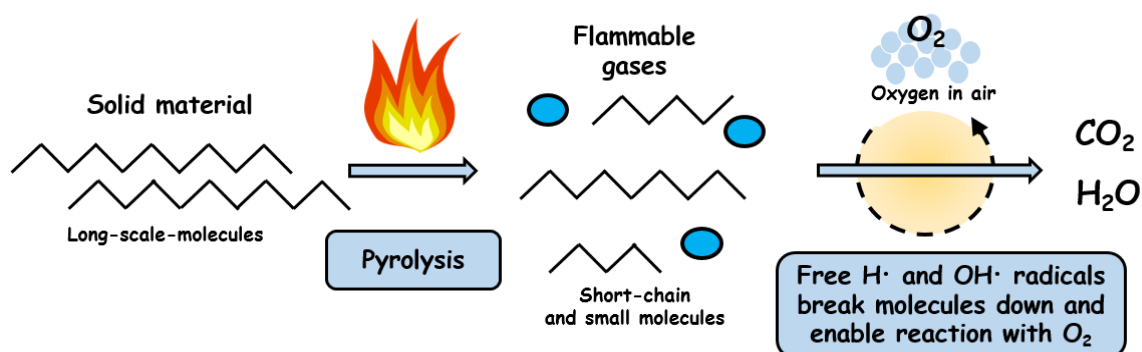


Figure 17: Combustion of a polymer [90].

The concept of “flame retardancy” was introduced in order to inhibit or stop the combustion process of polymeric materials, by modifying the “actors” of fire development. Flame retardants are efficient at improving the fire safety of plastics; they can increase resistance to ignition, reduce the rate of burning, flame spread, smoke emission and minimize dripping during combustion [91]. On the contrary, flame retardants can negatively affect material properties, producing unwanted side effects and add unnecessary cost. Hence, this highlights the difficulty of developing an efficient flame retarded system.

To flame retard a polymer, various methods can be used like the chemical modification of the polymer itself. As an example, it is possible to copolymerize the flame retardant directly with the monomers to yield an intrinsic FR polymer [92, 93]. The use of inherently flame retardant polymers such as poly(tetrafluoroethylene) or polyimides is another possibility to inhibit the combustion of a material [94, 95]. Surface coating is also used to protect polymeric materials against the influence of an external heat source [96-99]. This kind of flame retardant method has some benefits, as the material bulk is not modified during treatments, but adhesion issues can reduce the FR properties of the coating. The last and most widely used method to protect polymers consists in incorporating flame retardants into the polymer during its processing (e.g. extrusion). This is the cheapest method to fire retard polymers. The following part will thus only deal with bulk fire retarded PLAs. The fire retardants added in the PLA matrix can have physical and/or chemical mode of action and can act in the gas or condensed phase. These modes of action are detailed hereafter.

2.1.1. Physical action

The physical action of fire retardant additives takes place through the formation of a protective layer, by cooling and/or dilution. In the first case, a protective layer of low thermal conductivity is formed when the material is submitted to an external heat source, which protects the material through reduction of the heat and mass transfers between the external heat source and the material [50, 100]. In the second case, materials can be protected by cooling through the endothermically decomposition of fire retardant fillers, leading to a decrease in temperature by absorbing the external heat [101]. Concerning the dilution, the protection takes places through the addition of compounds releasing inert gases (e.g. carbon dioxide, water) upon decomposition. These kinds of additives dilute the fuel in the solid and in the gaseous phases and thus lower the concentration of combustible gases in the surrounding atmosphere.

2.1.2. Chemical action

Chemical mode of action is the other possibility by which polymers can be protected. This mode takes place in the condensed and/or gas phase. Two kinds of reactions can occur in the condensed phase: (i) the formation of a carbon layer (charring) on the polymer surface, allowing to limit the volatilization of the fuel but also the oxygen diffusion and insulating the polymer underneath from the external heat [102]; or (ii) the acceleration of the polymer decomposition leading to a pronounced flow of the polymer. Hence, a withdrawal from the sphere of influence of the flame that breaks away. Charring is the most common condensed phase mechanism [103, 104].

In the gaseous phase, the reaction takes place via interruption of the radical mechanism of the combustion process by flame retardants or by their decomposition products. Therefore, the exothermic processes that occur in the flame are stopped and the system cools down. Hence, the supply of flammable gases is reduced or even completely suppressed. In particular, halogens can act as flame inhibitors [105].

It is possible that flame retardants such as magnesium hydroxide (MDH) show exclusively a physical mode of action. However, flame retardants acting exclusively through a chemical mode of action are rare. In fact, one or several physical mechanisms generally take part in chemical mechanisms, which are commonly endothermic dissociation or dilution of fuel.

2.2. Flame retardancy of PLA by conventional flame retardants

FRs additives are mainly constituted by metal hydroxides (aluminium trihydroxide (ATH), magnesium hydroxide (MDH) ...), phosphorus-containing compounds, halogenated compounds and nitrogenated compounds which act in gas and/or condensed phase to provide low flammability of the material [8, 102]. These conventional FRs have been widely evaluated in PLA over the last few years [8, 9, 12-18].

Some researchers studied the use of aluminium trihydroxide (ATH) in PLA to make it flame retardant [13, 14, 16]. Even if the mechanism is not completely elucidated by the authors, the fire behavior of the material is similar to typical thermoplastics flame retarded with ATH. For instance, Kimura et al.[16] demonstrated that the use of ATH allows increasing the UL 94-V (3.2 mm) value of PLA from non-classified to V-2. Flame retardancy of the material is in his case due to physical effects requiring relatively large amount of ATH (between 50 and 65 wt.- %). Bourbigot et al. [101] reported that the activity of ATH consists in:

- a) The dilution of the polymer in the condensed phase
- b) Decreasing the amount of available fuel
- c) Increasing the amount of thermal energy needed to raise the temperature of decomposition to the pyrolysis level, due to the high heat capacity of the fillers
- d) Emission of water vapor - enthalpy of decomposition
- e) Dilution of gaseous phase by water vapor – decrease of amount of fuel and oxygen in the flame
- f) Possible endothermic interactions between the water and decomposition products in the flame
- g) Decrease of feedback energy to the pyrolysing polymer
- h) Insulative effect of the oxides (Al_2O_3) remaining in the char
- i) Charring of the materials

Others researchers such as Yanagisawa et al. [14] have recently studied the flame retardancy of PLA (at UL 94-V (3.2 mm)) using high load ATH (50%) in combination with phenolic resins. Applications was housings of electronic products where the required level of flame retardancy is high. The action mechanism of the flame retarded system is reported to occur via the formation of a homogenous char layer, resulting from the phenolic resins degradation at the surface of the material upon heating. This latter is not fully described in this paper but an assumption concerning the mechanism of action is that phenolic resin should provide high char yield, which could be reinforced by the formation of aluminum oxide from ATH. Hence the ceramic char becomes then protective enough to yield good FR properties to PLA.

Textile is a major application for PLA and it is also required to achieve good level of flame retardancy. In this way, Kubokawa et al [15, 17, 18] have investigated the flame retardancy of PLA fabrics using bromine and triphenylphosphate (TPP), as flame retardants. It was found that limiting oxygen index (LOI) increases from 24 vol.-% to 28 vol.-% with TPP and to 26 vol.-% with the bromine-containing FR. According to the authors, TPP FR treatment promotes charring, suggesting a mechanism of action in the condensed phase. In the case of brominated treatment, action in gaseous phase should occur.

Other phosphorus based FRs are also efficient to achieve low flammability of PLA. For instance, PLA material filled with 30 wt.-% of phosphinate-based FR (OP1311 of Clariant, Germany) is V-0 classified at UL 94-V (3.2 mm) with a LOI value superior to 30 vol.-% and a

decrease of the peak of heat release rate (PHRR) of around 15% observed by cone calorimetry. As well as OP1311, Melamine polyphosphate (MP) presents good fire performances in PLA matrix [10]. In fact, V-0 rating (3.2 mm) is achieved at UL 94-V for 20 wt.-% of MP and the peak of heat release rate (PHRR) determined by cone calorimetry (35 kW/m²) is decreased by 33%.

As described in this section, many conventional flame retardants can be used to achieve flame retardancy of PLA. However, literature report that the interest for nanoparticles to flame retard PLA kept growing these past few years. The next section is thus dedicated to the flame retardancy of PLA using nanoparticles.

2.3. Flame retardancy of PLA by nanoparticles

One interest in the use of nanoparticles is the development of efficient polymer/nanoparticles systems at very low loading of nanoparticles (less than 10 wt.-%). The nanocomposites exhibit remarkably improved properties (e.g. mechanical ...) as compared with those of virgin polymer [106]. It was reported that PLA nanocomposites exhibit a high storage modulus both in solid and melt states, an increased flexural properties, a decrease in gas permeability, an increased heat distortion temperature, an increase in the rate of biodegradability of PLA, and also a decrease of reaction to fire of some polymers [107].

Indeed, it was demonstrated that adding a small amount of clay into the polymer matrix allows reducing pHRR for numerous polymer nanocomposites [108, 109], especially PLA. The use of nanoparticles is then an interesting way to flame retard plastics while reducing both cost and quantities of FR fillers used.

Bourbigot et al. [20] reported that 3 wt.-% of montmorillonite (MMT) platelets dispersed into PLA matrix reduced significantly the pHRR by about 40%. In the case of pure PLA, vigorous bubbling is observed when the polymer is burning and no residue is left at the end of the experiment. But when the clay nanocomposite burns, char formation is observed. This char serves as a barrier limiting both mass and energy transport. In addition to clay, multi-walled carbon nanotubes (MWNT) are also known to significantly improve the fire behavior of polymers when they are nanodispersed in the polymer matrix [10, 21, 110]. PLA/MWNT exhibits limited enhancement in cone calorimetry [20] but the flame spread is much lower compared to virgin PLA when testing samples in vertical position at UL-94 [61]. Virgin PLA flows, drips, and burns quickly while PLA/MWNT does not flow and does not drip. It is suspected that MWNT incorporated in PLA increases the apparent viscosity of the material and so, it avoids dripping as it was previously evidenced by Kashiwagi et al. [21]. PLA/MWNT burns very slowly, keeping in an upright position but the ignition does not stop. This test then shows the interest to incorporate MWNT in PLA.

Graphite that has a two dimensional structure as clays, is another nanoparticle that has already shown great potential when incorporated in polymers. Dispersed in the nanosize range in polymeric matrix, graphite can improve overall properties of the system as clay does

[111, 112] but can also provide its own characteristic properties of thermal and electrical conductivity. Murariu et al. [22] incorporated expanded graphite (EG) at different loadings into PLA. Whereas PLA easily burns and drips without charring when exposed to a flame in horizontal position, PLA/EG nanocomposites at 6 wt.-% loading burn with no dripping and present a decrease by 30% of pHRR in cone calorimetry experiment. It is shown that the nanocomposite swells during burning in order to form a porous foamed carbonaceous char that acts as a barrier to limit the combustion. The high amount of char formed during burning is ascribed to additional expansion of graphite nanolayers. This expansion is provoked by both the heat and gases/products of combustion. Hence, authors reported that the PLA/EG system presents an “intumescent-like” behavior.

2.4. Intumescent PLA

“Intumescence” comes from Latin “intumescere” meaning “to swell up”, which describes rightly the behavior of an intumescent material. Indeed, when heating an intumescent system beyond a critical temperature, the material begins to swell and then to expand resulting in the formation of a foamed cellular charred layer on the surface. This latter protects the underlying material from the action of the heat flux or the flame [50, 113]. The concept of intumescence was applied to flame retard polyesters such as PLA and it was proven to be efficient for this kind of polymers.

An intumescent system is composed of different ingredients which are usually (i) an acid or a material yielding acidic species upon heating, (ii) a char former and (iii) a component that decomposes at the right temperature and at the right time to enable the blowing of the system. Concerning the acidic source, acids, ammonium salts, and phosphates can be used. Char formers are mainly hydroxyl-containing compounds, such as polyols and starch and blowing agents can be Melamine (MEL) compounds which can release gases upon heating, in the temperature range corresponding to the development of the intumescence process.

A typical example of intumescent system is the combination of ammonium polyphosphate (APP) with pentaerythritol (PER) in which APP plays the role of both acid source (yielding phosphoric acid) and blowing agent (releasing NH_3) and PER is the char former [114]. Researchers such as Reti et al. investigated the substitution of PER by lignin (LIG) or starch (ST) in the APP/char former system [9]. At 40 wt.-% loading of APP/char former (PER, LIG or ST), high LOI values are observed (up to 58 vol.-% with PER) and in all cases an intumescent protective layer was formed at the surface of the material. The interesting features of the bio-based systems are V-0 classification at the UL-94 test (3.2 mm) while PLA-APP/PER is only V-2 rated. Under an external heat flux of 35 kW/m^2 exposure on cone calorimetry experiment, those systems exhibit a reduction of pHRR by 65% for APP/PER and by 40% for APP/LIG and APP/ST. An intumescent layer protecting the underlying material is formed under the heat flux, limiting heat and mass transfers.

In order to reinforce mechanical properties of the polymers, fibers can also be incorporated in the intumescent material. Shumao et al. [23] combined natural fibers (ramie fibers) with APP to make an intumescent system for PLA. At 40 wt.-% loading, LOI reaches 35 vol.-% and the FR system exhibits V-0 rating at UL-94 (3.2 mm). Authors report that APP releases phosphoric acid, polyphosphoric acid and non-flammable gases when exposed to flame. Hypothesis of mechanism is that the resulting acid contributes to intramolecular or intermolecular ramie dehydration, then dehydrogenizing, charring and rupture of chemical bonds.

2.5. Conventional flame retardants and nanoparticles: synergy in PLA

Polymer nanocomposites exhibit low flammability in terms of cone calorimetry but they fail to pass other tests, in particular when samples are in vertical position (e.g. LOI, UL-94) [8]. The mechanism of protection involves the formation of a char layer covering the entire sample surface, acting as insulative barrier and reducing volatiles escaping to the flame. The formation of such a layer which does not crack during burning is critical to obtain low heat release rate from nanocomposites [102]. Hence, nanoparticles have been combined with flame retardants fillers in order to see if a synergistic effect is obtained.

As shown in the section above, intumescence is one of the efficient methods existing to limit the flammability of PLA. In our group, Fontaine and Bourbigot [12] investigated the combination of APP with Melamine (MEL) (30 wt.-% in a 5 to 1 ratio respectively) as efficient intumescent combination in PLA (namely FR-PLA). They demonstrated that the incorporation of an additional nanofiller such as organomodified montmorillonite (e.g. cloisite 30B (C30B)) presents positive effects on reaction to fire of the materials meaning that APP, MEL and C30B have a positive synergistic effect in term of fire retardancy in PLA. The intumescent PLA containing C30B does not burn and the small peak of heat release is only due to a very short ignition of the material which goes off very quickly. At 30 wt.-% loading of APP/MEL/C30B in PLA (namely FR-PLA-C30B), the material achieves very good fire performances. Indeed, high LOI values up to 52 vol.-% and V-0 rating (3.2 mm) were measured. Moreover, FR-PLA-C30B exhibits a large decrease of about 90% of the pHRR measured by cone calorimetry (35 kW/m²). These great performances were partially explained by the increase in thermal stability of the FR-PLA-C30B formulation compared to FR-PLA. Cloisite 30B can react with APP to form alumino- and silicophosphates stabilizing the intumescent structure at high temperature [115, 116]. The intumescent PLA was also evaluated with a total loading of 10 wt.-%. This loading is still sufficient to get relatively high LOI (33 vol.-%) and a synergistic effect is also observed with C30B (35 vol.-%). It is outstanding that V-0 at UL-94 is achieved for the formulation with and without Cloisite 30B. This study exhibiting very good results in terms of flame retardancy shows that combination of nanoparticles and intumescent agents offers promising way to design flame retarded PLA.

2.6. Conclusion

This part has reviewed the state of the art of the flame retardancy of PLA. The basics of flame retardancy were firstly reminded, and a focus of the methods providing flame retardancy to PLA was detailed. Very high performances in terms of fire behavior can be reached in certain cases (e.g. intumescence).

PLA was mainly used for non-durable applications but it is turning to durable ones. Hence, because of the growing market for PLA for durable applications, flame retardancy is required and of course these flame retardant properties must be kept for the product lifetime. However, due to its structural and chemical composition as well as its bio-degradable character, PLA is very sensitive to ageing and chemical degradation such as hydrolysis or photo-degradation. Whereas many papers are related to the ageing of raw PLA under various constraints, ageing of filled PLA has not been widely studied yet.

The next part is therefore focused on the ageing of polymeric materials, especially chemical ageing and associated mechanisms of degradation. A particular attention is paid to the ageing of PLA and its consequences on the properties of this material. Moreover, some examples of flame-retarded polymers are given in order to understand the effects of ageing on the fire behavior and thereafter correlate them to our FR systems.

3. Ageing of polymers

During their lifetime, polymeric materials are submitted to different constraints depending on their environment of use. In outdoor applications, polymers undergo principally the action of light, oxygen, water, pollution, heating, etc. An important number of papers deals with ageing issues related to polymeric materials. This is explained by the necessity of understanding the failure observed, in order to prevent (or ensure) the lifetime of the materials. This is also explained by the multiplicity of systems, ageing tests (natural and accelerated) as well as analytical techniques.

In materials science the term ageing is used when engineering properties, physical or chemical characteristics of a material change over a period of time. It may be useful to distinguish physical and chemical ageing. In the first case, there is no alteration of the chemical structure of the macromolecules, only the spatial configuration or composition of the material is affected. In the second case, the chemical structure of the macromolecules is modified. All ageing mechanisms at molecular level lead to changes in morphology and macroscopic properties. Sometimes a number of age-related phenomena operate simultaneously and/or interactively [117, 118]. Usually, effects of ageing are not desired in advanced materials (except maybe for biodegradation) and therefore understanding and fighting ageing phenomena play an essential part in polymer science.

This part gives an insight in the common mechanisms involved in chemical ageing of polymeric materials, including change of properties due to external stimuli such as temperature, humidity and ultra-violet (UV) radiations. Then, as the objective of these researches is to study the ageing behavior of fire retarded PLA, a special focus will be done on the ageing of PLA and flame retarded polymers. The first section is dedicated to the generalities of chemical ageing of polymers.

3.1. Chemical ageing of polymers

Chemical ageing is certainly the most important cause of ageing, involving irreversible changes in the molecular structure of the polymer chains. In the case of chemical ageing, two different situations can be distinguished, whether it occurs in presence or absence of oxygen. For instance, chemical ageing without oxygen involves reactions such as hydrolysis, depolymerization or elimination, radiochemical and photochemical processes. In presence of oxygen, one can mention thermo-oxidative or photo-oxidative ageing. In that case, the role of oxygen is really crucial. In fact, it contributes to the chemical reactions leading to the ageing of the material. Consequently, chemical ageing generally leads to chain scission phenomena, depolymerization/elimination or cross linking. **Figure 18** presents the most usual parameters involving chemical ageing as well as their consequences. These one then lead to the deterioration of the characteristics of polymers (e.g. mechanical, physical ...), to a color change and to the appearance and growth of cracks at the surface that sometimes result in destruction of the polymer [118-121]. Others parameters such as immersion in liquids, acids, oils, etc can induce chemical ageing [30, 122, 123]. These additional factors are not investigated in this PhD thesis and thus are not detailed further in this chapter.

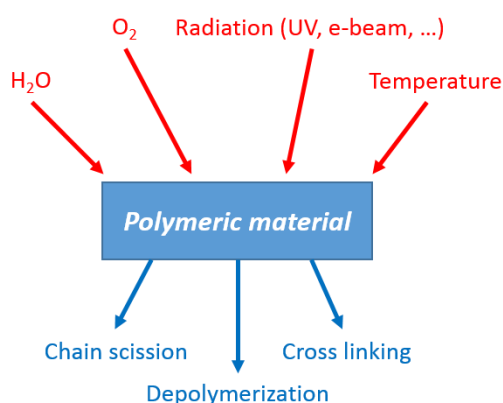


Figure 18: Main chemical ageing factors and consequences on polymeric materials.

3.1.1. Chemical degradation mechanisms

There are many different types of possible chemical reactions causing degradation of polymers, however the most common ones are photo-chemical, thermal, hydrolytic and bio-chemical reaction. These different types of chemical degradation mechanisms are reported and detailed hereafter.

Generally, four common mechanisms of polymer degradation are identified (**Figure 19**). These reactions can be divided into two groups: (i) those involving atoms in the main polymer chain (chain scission and crosslinking) and (ii) those involving principally side chains or groups (side chain elimination and side chain cyclization). The degradation of polymers can be explained by one of these general mechanisms or by a combination of some of them [124].

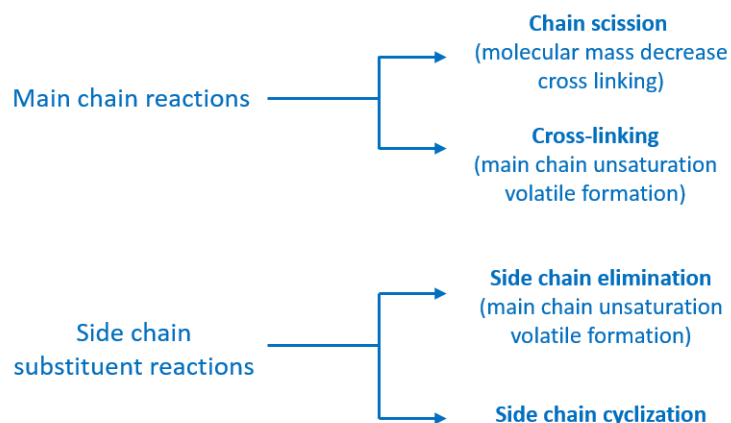


Figure 19: General degradation mechanisms, adapted from Beyler, et al. [124].

The most common reaction mechanism involving the break of bonds in the main polymer chain is usually called “chain scission”. It may occur at the end or at random locations in the polymer chain. End chain scission results in the production of monomer, and the process is commonly called “unzipping”. Random-chain scission generally results in the generation of both monomers and oligomers as well as in some other chemical species.

Another general chemical degradation mechanism is “Cross-linking” that involves the main polymer chain. It generally occurs after some stripping of substituents and involves bonding between two adjacent polymer chains [124].

Elimination and cyclization are the two main reaction types involving side chains or groups. In the case of elimination reactions, the bonds connecting side groups of the polymer chain to the chain itself are broken, the side groups often reacting with other eliminated side groups. The products resulting from elimination are usually small and thus volatile. In cyclization mechanism, two adjacent side groups are bound together, resulting in a cyclic structure.

These degradation mechanisms lead to “a deterioration of any property of the polymer” [125]. In fact, the degradation of polymers by chain scission generally leads to a decrease of the molecular weight of the material as the polymer chains are broken down to smaller units [121]. Thus leading to a decrease of some properties such as glass transition and melting temperatures of the material [27, 29, 34, 35, 52, 123, 126]. Moreover, the crystallinity of the polymer can be affected by degradation during ageing. For instance, in semi-crystalline polymers such as PLA, the amorphous phases are more susceptible to be degraded than crystalline ones. The degradation of amorphous phases leads to an increase in crystallinity of the material. In fact, chain scission occurring in amorphous phases of PLA produces molecule

segments which can integrate crystalline phase if they have sufficient mobility and will thus increase the crystallinity of the material. This phenomenon is called “chemi-crystallization” [5, 38, 127]. Mechanical properties of polymers such as tensile strength or Young’s modulus are also usually affected by the ageing of the material [29, 52, 123, 128]. Some other effects of ageing are reported in literature such as yellowing [129] or formation of cracks at the surface of the material [32, 121] but generally the effects of ageing are dependent on the nature on the material but also of the external stimuli applied to the polymer.

3.1.2. Photo-chemical degradation

Photo-degradation is a phenomenon inducing degradation of a photodegradable molecule by the absorption of photons, particularly those from wavelengths found in sunlight, such as infrared radiation, visible light and ultraviolet (UV). Photons are considered as one of the primary sources of damages exerted upon polymeric substrates at ambient conditions.

It is reported that photo-degradation is able to change the physical, chemical and optical properties of polymers. Thereby the loss of mechanical properties, the changes in molecular weight and visual effects like “yellowing” are the most damaging effects which can be observed [28, 34, 35, 129-132].

A common photo-degradation reaction is photo-oxidation, which is the process of decomposition of the material by the combined action of light and oxygen, which can be accelerated at elevated temperature [29, 129]. Most of synthetic polymers may be degraded by UV and visible light. The near-UV radiations (between 290 and 400 nm) in the sunlight determine the lifetime of polymeric materials in outdoor applications [133-135]. Photo-oxidation process can also be photo-induced by chromophoric impurities (catalyst, peroxides ...).

UV radiations have sufficient energy to cleave C-C bonds [125]. The most damaging UV wavelength for a specific plastic depends on the bonds present and the maximum degradation therefore occurs at different wavelengths for different types of plastics, e.g. around 300 nm for PE and around 370 nm for PP.

Focusing on the mechanism of action, photo-oxidative degradation of polymers includes various processes such as chain scission, cross-linking and secondary oxidative reactions which take place via a radical process [129, 136]. Many researches detail the mechanism of photo-oxidation of polymers by involving the production of radicals and subsequent reactions with oxygen [125, 129, 137, 138]. This mechanism proceeds through a chain reaction into steps gathering initiation, propagation and termination. These steps are detailed below.

3.1.2.1. Photo-initiation step

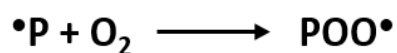
The absorption of UV light that has sufficient energy to break the chemical bonds in the main polymer chain is responsible for the initiation of the photo-oxidation mechanism. In fact,

the polymer (PH) absorbs light and produces low molecular weight radicals (R•) and/or polymeric macro radicals (P•) as follows (**Equation 4**).

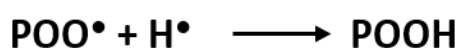


Equation 4

The photo-initiation step may be initiated by various physical factors such as UV radiation, heat, ionization and chemical factors (e.g. direct reaction with O₂ or atomic oxygen ...). In photo-oxidation process, hydroperoxides (POOH) are the most significant and most widespread initiators. Whatever the initial mechanism of radical formation, hydroperoxides are created just after reaction with oxygen and are key intermediates in the oxidation of polymers (**Equation 5** and **Equation 6**) [129].

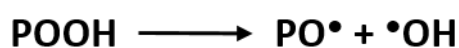


Equation 5



Equation 6

As shown in **Equation 7**, hydroperoxides usually decompose to form radicals (PO• and •OH) that can abstract hydrogen atoms from the polymer and thus initiate photo-oxidation. In this way, hydroperoxides are extremely photolabile [136].



Equation 7

The formation of hydroperoxide and its photolysis illustrate the formation of other effective functional groups such as carbonyls during β-scission of the alkoxy radical [129]. Besides the initiation step by photolysis of hydroperoxide groups, ketone photolysis is the second major contributor to the photo-degradation of polymers. It proceeds through two major reactions known as Norrish I and Norrish II (**Figure 20**) [125, 129, 138-140].

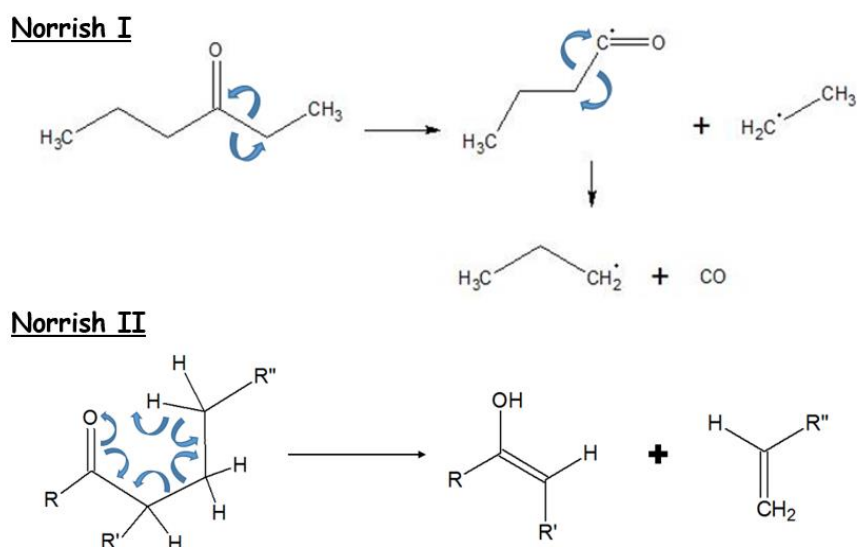


Figure 20: Norrish I and II mechanisms.

As described in **Figure 20**, ketones present onto the polymers backbones are able to absorb photons of appropriate energy when they are exposed to light. Thus, C-C bonds break and scission of the polymer backbone occurs [129, 138].

3.1.2.2. Propagation step

According to Rabek et al. [141] as well as Yousif et al. [129], propagation can be divided into six different steps:

1. Subsequent reaction of low molecular radicals (R^\bullet) or polymer alkyl radical (P^\bullet) in a chain process similar to the abstraction of hydrogen from the polymer molecule (**Equation 8**).



Equation 8

2. Reaction of the polymer macro radicals with oxygen which forms polymer peroxy radicals POO^\bullet (**Equation 5**).
3. Abstraction of a hydrogen from the same or from another polymer molecule ('PH) by polymer alkyl-peroxy radical (POO^\bullet) with the formation of a hydroperoxide group (**Equation 9**).



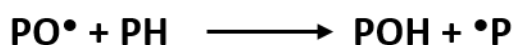
Equation 9

4. Photo-decomposition of hydroperoxide groups with the formation of polymer alkyloxy (PO^\bullet), polymer peroxy (POO^\bullet), and hydroxyl ($^\bullet\text{OH}$) radicals (**Equation 7** and **Equation 10**).



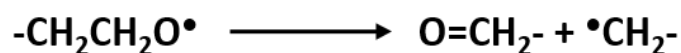
Equation 10

5. Abstraction of hydrogen from the same or another polymer molecule by polymer alkyloxy radical (PO^\bullet) with formation of hydroxyl function groups ($-\text{OH}$) in polymer (**Equation 11**).



Equation 11

6. Scission process of polymer alkoxy radicals ($\text{CH}_2\text{CHO}^\bullet$) with the formation of aldehyde end groups and end polymer alkyl radicals (**Equation 12**).



Equation 12

Generally, the overall processes of photo-oxidative degradation can be simplified by photo-oxidation cycle as described in **Figure 21**.

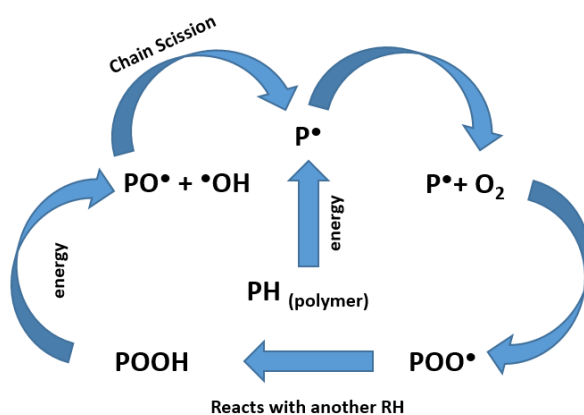


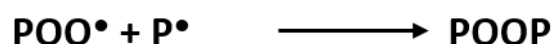
Figure 21: simplified photo-oxidation cycle of polymers, adapted from Yousif et al [129].

3.1.2.3. Termination step

The termination of photo-degradation is achieved by “mopping up” the free radicals to create inert products [125]. In fact, the radicals can be terminated by numerous different combination reactions between two polymer radicals, as detailed in **Equation 13**, **Equation 14** and **Equation 15**:



Equation 13



Equation 14



Equation 15

The polymer radicals may combine to give crosslinked or branched product [125]. If the oxygen pressure is relatively high, the termination follows **Equation 13** and **Equation 14**. In comparison, if the oxygen pressure is low, other termination reactions take place to some extent. When sufficient oxygen content cannot be maintained during the degradation, **Equation 14** becomes significant. Finally, as shown in **Equation 15**, polymer radicals can recombine together [129].

As developed in this part, photo-oxidative degradation takes place via a radical process. As well as photo-chemical degradation, thermal degradation proceeds through a radical process [129, 136]. In fact, under normal conditions, photo-chemical and thermal degradations are similar and classified as oxidative degradation [125]. The next part will be focused on the thermal degradation of polymers as well as the description of mechanisms of degradation.

3.1.3. Thermal degradation

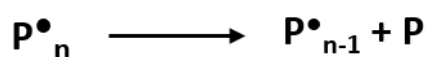
Generally, temperature is one of the parameters that plays a major role in chemical ageing. Thermal degradation of polymers can be defined as “molecular deterioration as a result of overheating”. At high temperatures the components of the long backbone chain of the polymer can start to break up (molecular scission) and react with another molecule to change the polymer properties [142].

Under normal conditions, photochemical and thermal degradations are similar and are classified as oxidative degradations. The main difference between both is the sequence of initiation steps leading to auto-oxidation cycle. Another difference is that thermal reactions

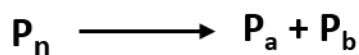
occur throughout the bulk of the polymer sample, whereas photochemical reactions generally occur at the surface [143].

Another important fact concerning the thermo-oxidation is the chain scission phenomenon. In fact, crosslinking and chain scission have both consequences on the polymer properties [118, 144]. The degradation via crosslinking includes hardening, skinning, gel formation, a decrease in tack, and an increase in viscosity. Degradation via chain scission results in softening, a decrease in viscosity, an increase in tack, and a loss of cohesive strength. In addition, discoloration also might occur upon oxidation. Even though discoloration normally does not lead to significant changes in engineering properties, it might be not wanted for application.

From a mechanistic point of view, as for photo-oxidative degradation the thermal degradation in presence of oxygen is divided into three steps, i.e. initiation, propagation and termination [125, 145]. The initiation step of degradation follows either chain end degradation (also known as unzipping route) as shown in **Equation 16**, or random degradation route as shown in **Equation 17**.

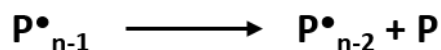


Equation 16

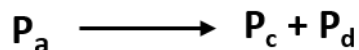


Equation 17

The chain-end degradation (depolymerization reaction) presented in **Equation 16** starts from the end of the polymer chain and consecutively releases monomer units from the chain-ends. Similar to photo-oxidative degradation, it occurs via free radical mechanism. This kind of reaction is the opposite of the propagation step in addition polymerization. During depolymerization, the molecular weight of the polymer decreases and large quantity of monomers is released simultaneously [125, 137]. The random degradation route presented in **Equation 17** occurs at any random point along the polymer chain. As for random degradation to happen, the polymer chain does not require necessarily to carry active sites (sensitive to radical reaction) such as for chain-end degradation [125]. During propagation step, the monomer is formed as depicted in **Equation 18** and **Equation 19**.



Equation 18



Equation 19

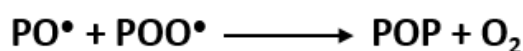
Finally, termination takes place through radical coupling [125, 146] as previously reported for photo-oxidative degradation (Equation 13, Equation 14 and Equation 15, p.50) but also following Equation 20, Equation 21 and Equation 22.



Equation 20



Equation 21



Equation 22

During termination, crosslinking can form some larger molecules induced by reaction of radicals P^{\bullet} with other radicals P^{\bullet} , alkoxy radicals PO^{\bullet} or peroxy radicals POO^{\bullet} . Alkoxy radicals PO^{\bullet} and peroxy radicals POO^{\bullet} can also react together to form POOP or POP molecules.

As photo and thermal degradation, hydrolytic degradation (hydrolysis) of polymers is one of the most common and important ageing mechanism.

3.1.4. Hydrolytic degradation

Hydrolytic degradation occurs in polymers that have water sensitive active groups, especially those that are very hygroscopic. Polymers that are concerned by hydrolytic destruction usually have heteroatoms in the main or side chain of the polymer. In that case we can also talk about hydrolysis of polymers, which involves the scission of chemical functional groups by reaction with water as an example is shown in Figure 22. In fact, hydrolysis of ether compounds leads to the formation of alcohols functional groups. The degree of degradation will depend on both exposure time and temperature.

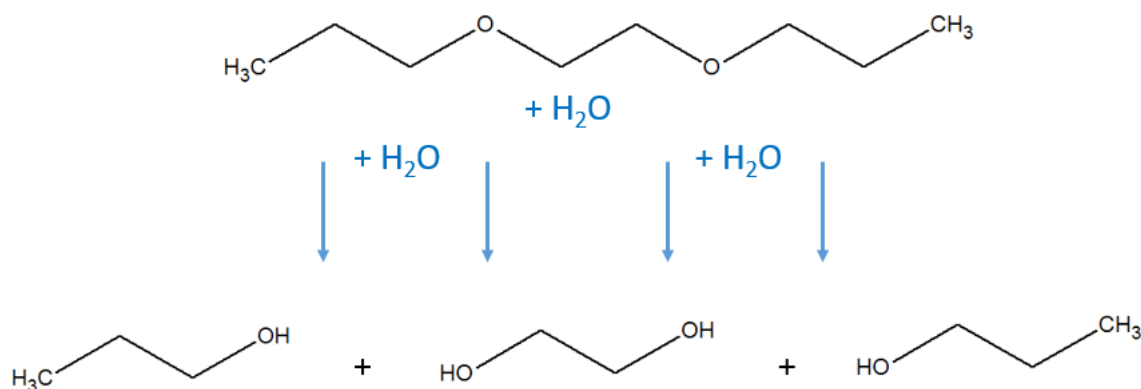


Figure 22: Example of hydrolysis of polyether.

Hydrolytic degradation can be harmful but also helpful in some cases. For example, hydrolytic chain scission of the ester linkage of polyester is the fastest and the most “harmful” degradation process, as it causes a considerable reduction in the molecular weight and in the mechanical properties of the polymer. However, in the case of drug delivery system, the polymer degradation is useful [147].

Two basic types of hydrolytic degradation are discussed: surface erosion and bulk erosion. During surface erosion mechanism, the mass loss of the polymer occurs at the water/polymer interface (**Figure 23 (a)**) and in that case, the rate of hydrolysis is higher than the water rate diffusion [147, 148]. As an example, most of the enzymatically resorbable polymers show surface erosion. Surface-eroding polymers have a better ability to achieve zero-order release kinetics and are therefore ideal candidates for developing drug delivery devices [149].

During bulk erosion, water diffuses rapidly into a polymer structure, leading to hydrolysis. Then, the subsequent mass loss occurs throughout the bulk of the material (**Figure 23 (b)**). In this case, the water diffusion rate into the polymer is higher than the hydrolysis rate. Hence, the water that penetrates the substrate leads to hydrolysis from the inside to the surface [147, 148]. The sudden and rapid loss of strength and structural integrity as the resorption continues over time is a characteristic behavior of bulk eroding polymers.

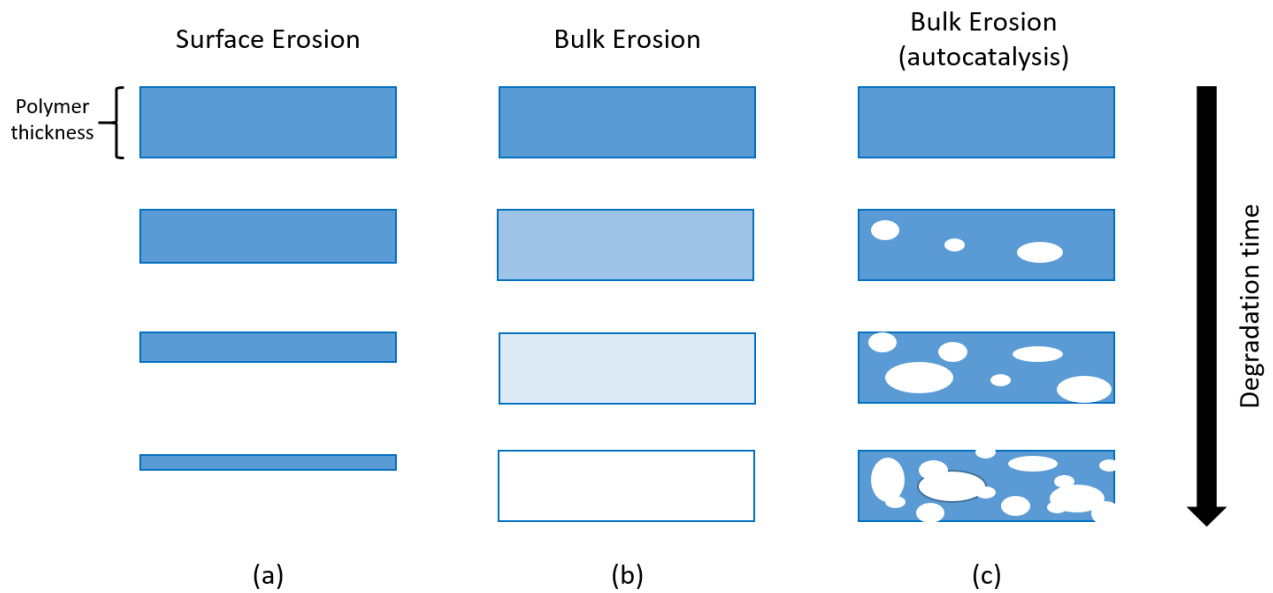


Figure 23: Illustration of the hydrolytic mechanisms: (a) surface erosion, (b) bulk erosion without autocatalysis, and (c) bulk erosion with autocatalysis, adapted from Viera et al. [150].

Autocatalytic degradation is another factor that complicates the degradation behavior of polymers [151]. The phenomenon of autocatalysis occurs when the reaction product is itself the catalyst for the same reaction. In the case of bulk eroding polymers, the oligomeric hydrolysis products (usually carboxylic and other acids) are retained within the material, causing a localized decrease in pH which accelerates the rate of degradation [152]. As a result of this autocatalytic hydrolysis, hollow structures are formed within the polymeric material, which induce a rapid deterioration of the mechanical properties of the material as well as a sudden loss of its structural integrity, as shown in **Figure 23 (c)**. For instance, in the case of polyesters such as PLA, when the thickness of the substrate is larger than 2 mm, the entrapment and accumulation of acidic oligomers and monomers result in autocatalytic degradation [153].

3.1.5. Bio-chemical degradation

The bio-chemical degradation, which is also known as “biodegradation”, is a biochemical transformation of compounds by micro-organisms. Mineralization of organic compounds yields carbon dioxide and water under aerobic conditions, and methane and carbon dioxide under anaerobic conditions [154, 155]. Hydrolysis, photo-oxidation and physical disintegration may enhance biodegradation of polymers by increasing their surface area for microbial colonization or by reducing their molecular weight [154-156].

Biodegradability is also defined as the propensity of a material to get breakdown into its constituent molecules by natural processes (often microbial digestion). The metabolites released by degradation are also expected to be non-toxic to the environment and

redistributed through the carbon, nitrogen and sulfur cycles. Biodegradation is chemical in nature (catalytic nature e.g. enzymes) but the source of attacking chemicals is from micro-organisms. Researchers such as Singh et al. [125] or Lucas et al. [154] have reported that biodegradation of polymers occurs via four different mechanisms: (i) solubilization, (ii) charge formation followed by dissolution, (iii) hydrolysis and (iv) enzyme-catalyzed degradation. Petrochemical-based plastic materials are not easily degraded in the environment because of their hydrophobic character, additionally the three-dimensional structure interferes with the formation of a microbial bio-film, leading to a reduced biodegradation extent [125].

After having identified and developed the different kinds of chemical ageing, this chapter will now focus on the ageing of Poly(lactic) acid. Indeed, this researches are dedicated to PLA and more precisely to the ageing of flame retarded (FR) PLA. In this context, it is crucial to examine the ageing of the raw PLA material in order to understand the phenomena occurring during ageing of filled PLA.

3.2. Ageing of Poly(lactic) acid

Aliphatic polyesters such as PLA currently deserve a particular interest as environmentally degradable polymeric materials. However, due to its chemical composition, PLA is very sensitive to ageing, leading to degradation of the polymer, such as hydrolysis [153], photo-degradation [29], etc. Hence, the development of PLA based materials must find a compromise between sustainability and performances. Therefore, this part will deal with the ageing behavior of PLA under different kinds of chemical degradation.

3.2.1. Photo-degradation of PLA

Many studies have been led over the years, investigating the influence of photo-degradation on PLA properties. It is reported for example that UV irradiation light decreases the physical integrity and enhances the degradation of the material. Thus leading to a decrease of both M_n and mechanical properties (e.g. stress at break, percentage elongation at break and strain energy). Focusing on thermal properties, a decrease of both T_g and T_m is observed for PLA exposed to UV treatment [29, 33, 157]. As already mentioned, PLA chains are photodegradable in both crystalline and amorphous regions but their photo-degradability is higher in the amorphous regions [27] thus leading to an increase of the crystallinity of PLA when irradiated by UV light.

At the state of the art, two main photo-degradation mechanisms of PLA have been reported, depending on the UV irradiation wavelength. In fact, for irradiation under 300 nm, the photo-degradation of Poly(lactic) acid proceeds via the Norrish II mechanism at ester and ethylidene groups adjacent to ester oxygen, as shown in **Figure 24** [27, 32, 33, 158, 159].

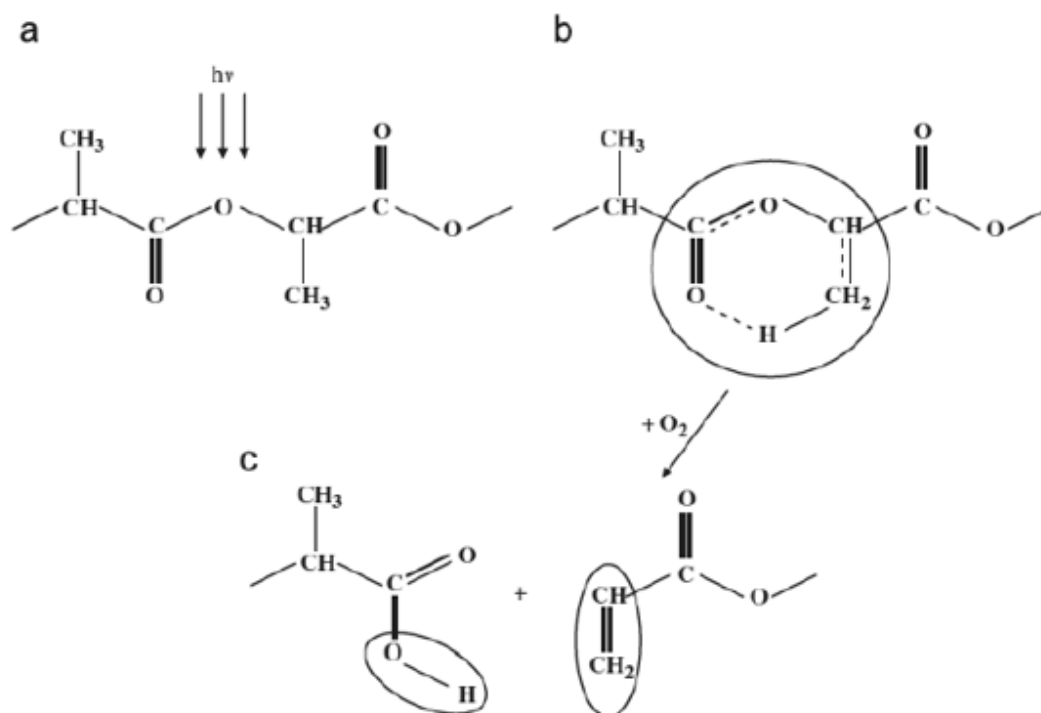


Figure 24: Norrish II mechanism for PLA photo-degradation: (a) PLA chain under UV irradiation, (b) photophysical excitation and (c) oxidation/scission reactions in PLA chains, adapted from Belbachir et al. [33].

This kind of mechanism causes the chain cleavage of the material, the decrease of the molecular weight and the formation of carbon-carbon double bonds [159]. The photo-degradation of PLA films under UV irradiation proceeds via a bulk erosion rather than a surface erosion [159]. During photo-degradation, no formation of specific low-molecular-weight peaks are observed, which strongly suggests that the chains in crystalline regions are photodegradable even at early stage of degradation, in marked contrast with the case of hydrolytic degradation [159].

Bocchini et al. [34] reported that Norrish II mechanism occurs when UV irradiation is under 300 nm, in a region where the carbonyl groups of aliphatic polyester can absorb energy and consequently lead to photo-reaction. Conversely, Bocchini as well as many other researchers [28, 29, 34, 35] evidenced a second mechanism of photo-degradation of PLA proceeding when UV irradiation is in the range 300 to 400 nm [34]. In that, photo-degradation usually starts by radicals formed from impurities during UV-irradiation or thermal decomposition (**Figure 25**).

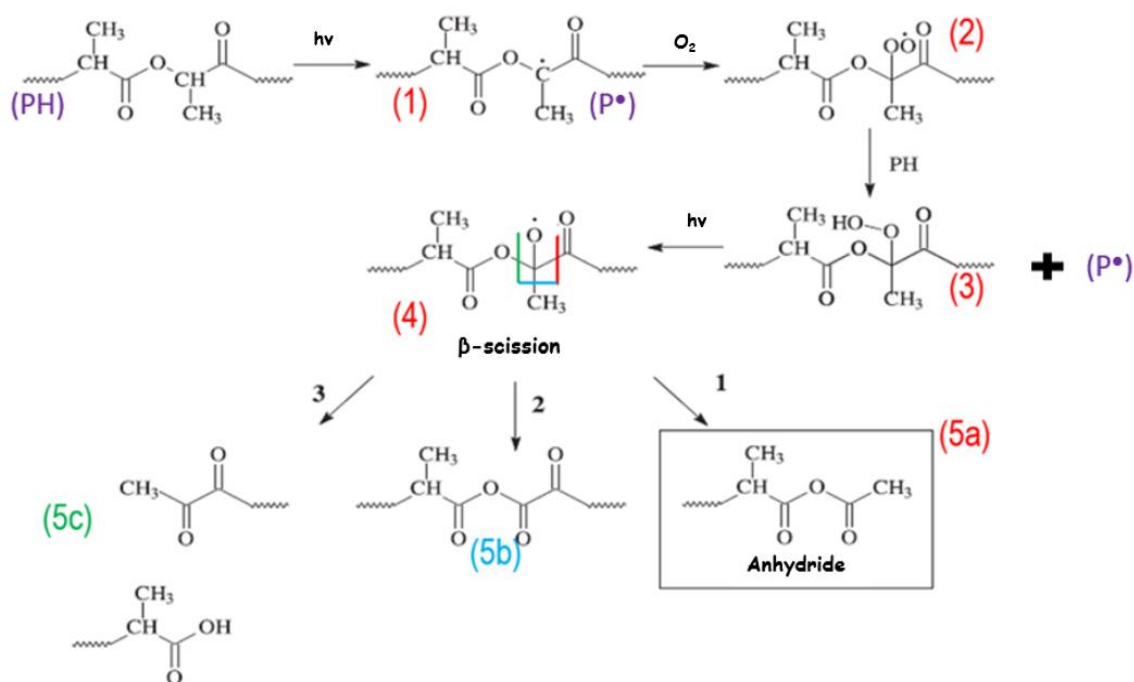


Figure 25: Photo-degradation (radical oxidation) process of irradiated PLA: hydroperoxides chain propagation and formation of anhydrides by photolysis of hydroperoxides, adapted from Gardette et al. [35].

In this mechanism, the most probable reaction is the abstraction of tertiary hydrogen from PLA chain, leading to the formation of a radical P^\bullet (Figure 25 (1)). This radical can react with oxygen to form a peroxide radical (Figure 25 (2)), which may easily abstract another hydrogen from a tertiary carbon with formation of a hydroperoxide and the initial radical P^\bullet (Figure 25 (3)). Then, the hydroperoxide undergoes photolysis (Figure 25 (4)) with the formation of the $\bullet OH$ and PO^\bullet radicals that can further evolve by β -scission (Figure 25 (5)). Furthermore, taking into account the stability of the different fragments the most probable β -scission appears to be the reaction leading to the formation of anhydride groups (5a) [34, 35].

As well as photo-degradation, hydrolysis is another kind of degradation known to be very harmful for the durability PLA based materials.

3.2.2. Hydrolysis and bio-chemical degradation of PLA

PLA like other polyesters is naturally hydrophilic due to its polar oxygen linkages. Its affinity for water makes it very sensitive to hydrolysis (Figure 26) via an autocatalytic mechanism of degradation [5, 31, 125, 153, 160]. In presence of water, ester is hydrolyzed into carboxylic acid and alcohol according to Figure 26.

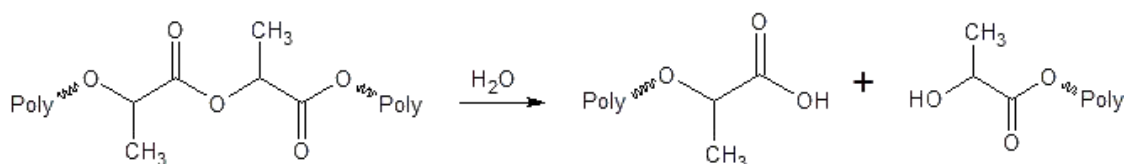


Figure 26: Hydrolysis of PLA.

Hydrolysis of PLA is the first step of the biodegradation of the material which is composed of two steps (Figure 27) [5].

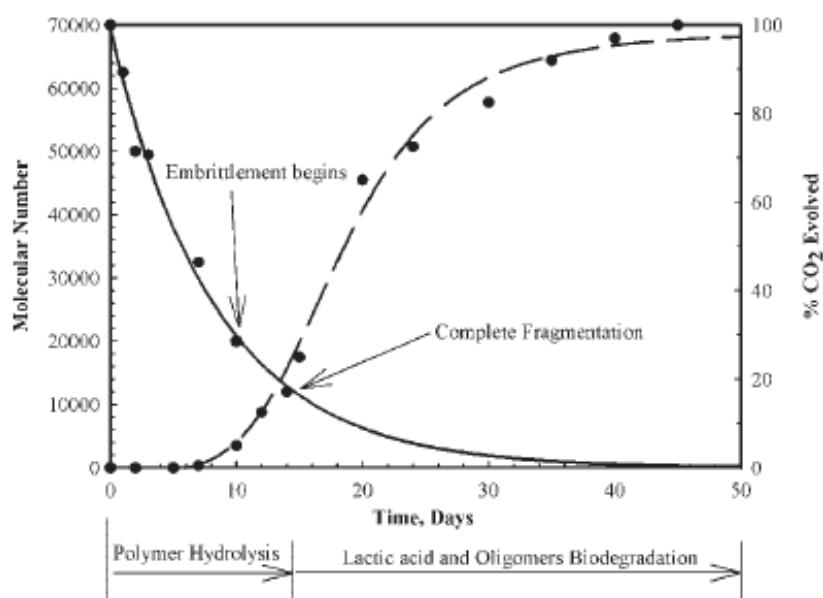


Figure 27: Biodegradation of PLA in 60°C, adapted from Auras et al. [5].

As reported in Figure 27, PLA degradability is driven in a first place by hydrolysis and cleavage of ester linkages in the polymer backbone. The hydrolysis of PLA is auto-catalyzed by the carboxylic acid end groups. The process follows first order kinetics [5]. The duration of the degradation is determined by the initial molecular weight of the polymer as well as by its chemical structure [125]. As hydrolysis degradation mainly takes place in the amorphous regions, degradation results in an increase in the crystallinity of PLA. A decrease of mechanical and thermal properties (T_g and T_m) as well as of molecular weight is also observed during hydrolysis of PLA [29-31, 38, 52, 121, 123, 128, 161, 162]. It can be accelerated by acids or bases and it is also affected by both temperature [29] and moisture levels [66].

In the second step (Figure 27), the low molecular weight PLA resulting from the hydrolysis is then able to diffuse out of the bulk polymer and be used by micro-organisms, yielding carbon dioxide, water and humus [5, 125, 162].

Many researches have been led on the combination of temperature and other factors like humidity, UV irradiation, oxidation and generally, the combination of these parameters enhance the degradation rate of PLA [26, 29, 127, 157, 163, 164].

3.2.4. Synergy between temperature, relative humidity and/or UV light exposure

According to literature, temperature is a key parameters in chemical ageing of polymers as it is able to catalyze reactions such as photo-degradation and/or hydrolytic degradation of PLA [26, 29, 37, 38, 121, 123, 128, 167]. In fact, it is known that the combination between temperature (50 to 60°C) and humidity cause PLA to degrade rapidly [29, 121, 123, 128]. In this case, the increases of temperature favors the diffusion of water and thus increases the hydrolysis of PLA as well as the loss of its physico-chemical properties (M_n , T_g , T_m ...). Moreover, researchers such as Copinet et al. [29] demonstrated the synergistic effect obtained when combining temperature, UV-light and relative humidity. They emitted the hypothesis that in conditions of humidity and temperature, UV treatment catalyzed the hydrolysis of ester linkage. When temperature and relative humidity increase, effect of UV treatment on the degradation of PLA matrix increases too, as it causes a faster autocatalysis process during hydrolysis.

The ageing of PLA under temperature, humidity and/or UV irradiation generally leads to some complex phenomena, as several ageing mechanisms can occur simultaneously. Whereas ageing of raw PLA have been widely studied in this section, it is now useful to discuss concerning the ageing of flame retarded polymers as our study is focused on the ageing of flame retarded PLA.

3.3. Ageing of flame retarded polymers

Nowadays, the fire standard tests for polymer-based materials are currently carried out on newly manufactured samples. However, various ageing conditions can impair flame retardancy throughout the lifetime of a material [40]. Therefore, it seems necessary to evaluate the influence of different kinds of ageing on the flammability of flame retarded polymers.

It was previously reported that many ageing conditions promote structural modifications of a polymer, like crosslinking and more generally chain scissions. For example, this latter leads to a decrease of the molecular weight and then of the material viscosity. However, viscosity is an important parameter controlling flammability. Indeed, in some fire tests, materials are rated according to their ability to drip. Dripping is obviously more severe for low-viscosity materials. Viscosity influences many other phenomena involved in flame retardancy: accumulation and migration of fillers at the surface [168], formation of a protective layer [169], intumescence [170], bubbling [171], etc. Moreover, low-molecular-weight molecules are volatile and can decrease thermal stability and promote early ignition. Nevertheless, this

significant effect of ageing is rarely taken into account in studies dealing with the influence of ageing on flame retardancy.

Thus, in this part, the influence of major chemical ageing scenarios (thermal, hydrolytic and photo-chemical degradation) on the flame retardancy of polymeric materials is discussed.

3.3.1. Thermal degradation of FR polymers

The migration of low molecular-weight FR fillers to the surface is the first effect induced by thermal ageing of FR polymers. Researchers such as Inata et al. [41] investigated the influence of thermal ageing (at 110, 130 and 145°C) on the migration of 16 halogenated compounds incorporated into polypropylene (PP). They reported that the weight loss of filled PP during ageing is attributed to the migration of FRs. However, the migration is not only dependent on the temperature and the molecular weight of the FR but also on its structure. Migration is higher for aliphatic brominated additives, followed by molecules containing only one aromatic ring. Molecules containing double aromatic rings, phosphate or isocyanuric groups hardly migrate. In these experiments, thermal ageing was carried out at high temperatures. Nevertheless, the authors have calculated the activation energy of migration to estimate the migration rate at lower temperatures (corresponding to service life). In some cases, migration can be significant. For 2,4,6-tribromophenyl-2',3'-dibromopropymether (TBP-DP), which exhibits the highest migration rate, the half-value period (corresponding to the loss of 50% of additive) at 30°C is only 5000h, i.e. 200 days. LOI was also measured after ageing for some FRs. It is reported that during ageing, the FR content decreases due to exudation and thus LOI decreases too. These observations seem to indicate that the relation between LOI and FR content is roughly linear.

Nanoparticles incorporated into FR polymers may also be concerned by the migration under the effect of temperature. In fact, Colonna et al. [42] studied the effect of thermal ageing on the combustion behavior of an ethylene–vinyl acetate (EVA) containing organically modified clay nanocomposite. Thermal ageing was carried out close to, but below the melting point of the polymer matrix (90°C). It was evidenced that during ageing, the nanoparticles dispersion changed from intercalated to an exfoliated structure. Consequently, the fire behavior of the EVA system was modified. It was observed that nanoclays move rapidly to the surface, promoting the formation of a physical barrier preventing the development of flames and thus delaying ignition on MLC experiment. However, the pHRR was increased significantly from 430 to 657 kW/m² but no explanation is given in the paper to explain this phenomenon.

Thermal ageing was also reported by Zuo et al. [120] who studied the effect of thermo-oxidative ageing on flammability of long glass fiber-reinforced PA6 composite containing tris(tribromophenyl) cyanurate and antimony trioxide. The samples were aged for 10, 30 and 50 days under thermal-oxidative conditions at 160°C. UL-94 (3.2 mm) rating remains V-0 even after 50 days of ageing. A positive effect of ageing is observed for LOI test (from 25.6 to 37.4 vol.-% after 50 days of ageing) and the pHRR observed in cone calorimetry decreases

from 108 to 72 kW/m². From the author's point of view, the improvement of the flame retardancy is explained by the enrichment of the surface in FRs due to migration. Thus, it allows FRs to act sooner, leading to the reduction of the pHRR. Moreover, the charring effect is promoted after ageing (from 31.5 to 35 % after 50 days of ageing) but the mode of action in the gas phase is not modified even if the effective heat of combustion appears to slightly decrease for 50 days of ageing.

3.3.2. Hydrolytic degradation of FR polymers

As previously reported, the presence of water can lead to dramatic changes in molecular weight and viscosity, which are important factors controlling the flame retardancy. Recent work investigating the influence of ageing in presence of water/moisture evidenced water can modify chemically FR materials but also affect their flame retardancy.

Oztekin et al. [43] recently highlighted the influence of water on the flame retardancy of poly(ether ether ketone) (PEEK). When a small amount of moisture is present in PEEK, water is released just after the polymer melts (343°C). This release leads to vigorous bubbling and results in shorter time to ignition (from 207 to 110 s at an irradiance of 50 kW/m² in cone calorimeter) but lower pHRR (from 355 to 280 kW/m²).

Levchik et al. [44] studied the impact of hydrolytic degradation induced by artificial ageing on the fire performance of flame retarded polycarbonate (PC)/acrylonitrile butadiene styrene (ABS) blends. Three aryl phosphates, triphenyl phosphate (TPP), resorcinol bis(deiphenyl phosphate) (RDP) and bisphenol A bis(diphenyl phosphate) (BDP) were tested as flame retardants. They demonstrated that these three additives show comparable FR efficiency at the same phosphorus level. However, under artificial ageing at 70°C and in the presence of water (85% RH), hydrolysis of aryl phosphates leads to the release of acidic species, which attack the polycarbonate. It results in a decrease of the fire retardant properties of the PC/ABS blend compared to those before artificial ageing. This demonstrates that the integrity of FR structure also plays a crucial role in the lifetime of the flame retardancy.

3.3.3. Photo-chemical degradation of FR polymers

It was reported that thermal ageing may promote migration of FRs. But while service temperature is generally much lower than processing temperature (which sets the minimal temperature of stability of FRs), it is doubtful that thermal ageing can degrade a FR structure. On the contrary UV radiation can induce such modifications. For instance, it was pointed out that viscosity is an important parameter controlling flammability. Therefore, flame retardancy can significantly decrease after photo-ageing due to the detrimental effect of FRs on the photo-stability of polymers [40].

It is known that FRs, and particularly halogenated ones, can promote fast ageing of polymers. Papers have been devoted by Sinturel et al [45, 46] concerning the study of the photo-oxidation of fire retarded PP. Authors reported that oxidation rate of PP increases in the presence of 5 wt.-% decabromodiphenylether (decaDBE) and the induction period is dramatically decreased. These effects are observed from 5% of FR and do not increase very much for higher contents. It is evidenced that when exposed to UV radiation, decaDBE degrades through the homolytic cleavage of the carbon-bromine bond [46]. Hence, the formation of a reactive bromine radical leads to hydrogen abstraction on the backbone and promotes the degradation of the system.

Other types of FR do not show the same trends. Researchers such as Chantegraille et al. [172] investigated a flame retarded PP with an intumescent system based on APP and a synergist containing nitrogen. UV-light irradiation was carried out under polychromatic light with wavelengths higher than 300 nm in a SEPAP 12.24 unit, in the presence of oxygen at 60°C. The authors reported that the FR can be photo-oxidized but not degraded by photolysis in the absence of oxygen. Moreover, even if the oxidation of FR starts much earlier than the oxidation of PP, both oxidations occur independently and no influence of the FR on the photo-oxidation of PP matrix was detected. Lonkar et al. [173] also studied the effect of 5 and 10 wt.-% of layered double hydroxide and organomodified montmorillonite on PP photo-oxidation. Whereas good dispersion of nanoparticles was achieved, it is shown that photo-oxidation of PP is significantly enhanced by the presence of organomodified montmorillonite. The influence of layered double hydroxide depends on divalent cations. In fact, Mg^{2+} has a degrading effect while Zn^{2+} does not accelerate the oxidation of the polymer. This study demonstrates that metallic compounds can exhibit a catalytic effect on the degradation of flame retarded polymers. These metallic impurities increase the decomposition rate of hydroperoxide, thus, accelerating the overall radical process [34]. However, a high ratio of metallic compounds should be needed to observe this catalytic effect.

Vahabi et al. [40] explained that flammability of a FR polymer may be mainly driven by the properties of a thin surface layer and in all these cases, photo-chemical ageing may have an influence on flame retardancy. It was demonstrated by Diagne et al. [47, 48] that PP grafted maleic anhydride (MAH) exhibits better fire performances measured in a cone calorimeter after UV irradiation. Ageing scenarios may promote the crosslinking of PP-MAH in a thin surface layer (oxidation profile shows that UV radiation modifies only a 150 μm thick layer). However, when nanoclays are incorporated into PP-g-MAH, flame retardancy is poorer after ageing. Indeed, nanoclays can reduce the formation of radicals by attenuating the UV penetration and by preventing radical mobility and thus, inhibiting crosslinking. Nevertheless, it must be pointed out that the cone calorimeter results are unclear due to the large standard deviation in the data. Others researchers such as Tidjani and Wilkie [174] also have investigated the flammability and ageing of PP-g-MAH containing nanoclays. They showed that nanoclays enhance the photo-oxidation of the material. The absorbance related to ketones and carboxylic acids observed at 1715 cm^{-1} by Fourier Transform Infrared

Spectroscopy (FTIR) increases faster than the one of PP-g-MAH without nanoclays. Moreover, no significant changes were observed in cone calorimeter data after ageing. It is possible that the enhanced photo-degradation of the material observed in presence of nanoclays results from the degradation of the polymer matrix during the incorporation of nanoparticles, instead of a catalytic effect of nanoparticles. Indeed, if the incorporation of nanoparticles decrease the molecular mass of the material even before ageing, it will lead to a faster degradation of the material.

Generally, UV ageing is combined with other sources of ageing like heat and water. Hence, it is sometimes difficult to identify the main source of ageing. Chen et al. [175] observed a strong decrease of LOI and UL-94 rating of PLA/ramie composites flame retarded by APP after several days of weathering combining UV, heat and relative humidity. Ageing was carried out under UV irradiation (UV-B313 fluorescent UV lamp) at 0.6 W/m^2 , ageing cycle in two phases: 8 h at 60°C and 4h at 50°C for 7, 14 and 21 days (exposure to humidity is not specified). Even if the reasons of the lower fire performances after ageing are not explained, it appears at least that water as well as UV irradiation play a major role in degradation. Indeed, migration of APP to the surface is assigned to its hydrolysis. APP is initially water-insoluble and becomes soluble when its molecular weight decreases. The migration of APP leads to a heterogeneous distribution of APP into the material. Moreover, authors reported that the coating of fibers by APP is decreased, thus promoting the candelwick effect. Nevertheless, the synergistic effect of UV radiation with water seems to be well proven [29]. Almeras et al [176] investigated effect of ageing on the flame retardancy of a PP/polyamide 6 (PA6)/APP/ethyl vinyl acetate (EVA₂₄) blend. Ageing was carried out under a xenon lamp exposure (1.1 W/m^2), rain and temperature cycling for 200 h (18 min of wetting and 102 min of drying at 65°C , 50% relative humidity). Fire performances were measured using cone calorimeter (50 kW/m^2), LOI and UL-94 tests (3.2 mm). Whereas the unaged samples exhibited a LOI of 33 and were V0 rated in UL-94 test, LOI decreased to 23 after ageing and aged samples were not classified at UL-94. Concerning cone calorimetry, pHRR increases from 200 kW/m^2 for the initial sample to 300 kW/m^2 after ageing. The formation of a smaller intumescent protective structure is reported. The decrease in terms of fire performances after ageing is attributed to the degradation of APP by hydrolysis and to its migration (or to the migration of its degradation products, e.g. ortho, pyro and polyphosphates of shorter chains). In fact, water diffusion into the material and migration are both facilitated by the surface degradation. However, these different modifications need the combination of UV and water.

The studies reported above show that UV irradiation can induce a decrease in flame retardancy of polymers but other studies suggest that is not always the case. Larché et al. [177] who studied the photo-oxidation of crosslinked EVA filled with aluminium trihydroxide (ATH) and kaolin show that UV irradiation leads to a strong enrichment of the surface in fillers. The hypothesis of fillers migration is excluded by the authors who explained this phenomenon by the formation and release of low-molecular-weight products due to the EVA oxidation. The composition profile shows that the enrichment occurs in the first $350 \mu\text{m}$. In the first $100 \mu\text{m}$,

the polymer content is less than half of its value in the bulk after 500 h of ageing (60°C, irradiance in the range of 300-400 nm, 100 W/m²). Flammability was not measured but authors were convinced that the enrichment of the surface would promote a barrier effect and improve the flame retardancy. Some works have already shown that EVA filled with mineral fillers exhibited better flame retardancy if these fillers migrate quickly to the surface during cone calorimeter test [178].

3.4. Conclusion

In this part, it was reported that polymers and particularly PLA performances in terms of durability are limited because of multiple chemical ageing mechanisms such as photo-degradation, hydrolysis or thermal degradation. Chemical ageing is responsible for the degradation of the material into low-molecular weight products (carboxylic acids, alcohols ...) and thus the decrease of the thermal and mechanical properties. Many papers are related to the ageing of raw PLA under various constraints, but few of them describe ageing of filled PLA.

Concerning flame retarded polymers, published papers investigate mainly fire behavior evolution but correlations between physico-chemical properties and fire performances after ageing are rarely made. Nevertheless, the relationship between physico-chemical properties and fire performances is a key parameter to investigate in order to develop durable flame retardant systems. Actually, only few studies have been devoted to the ageing of FR polymers generally filled with decaBDE or APP, which is clearly very few among all the FR fillers. According to the wide range of ageing conditions, polymers and FRs, several phenomena can be highlighted, impacting or not the flame retardancy of FR polymers.

4. Conclusion

Poly(lactic) acid is the first commodity biodegradable polyester produced from annually renewable resources. Due to its low cost production and its interesting mechanical and thermal properties, PLA is one of the best candidates among bioplastics. However, to be used in transportation fields for example, PLA has to be flame retarded, and these flame retardant properties must be kept for the product lifetime. Besides, due to its chemical composition and its biodegradable character, PLA is sensitive to ageing and its environment of use. That is why the development of PLA based materials must be based on a compromise between sustainability and performances.

In this chapter, it was highlighted that many possibilities exist to fire retard PLA. The use of conventional flame retardants, nanoparticles, and combination of both in PLA was detailed. FR PLA (loaded at 30 wt.-%) usually exhibits good fire properties with (i) LOI increase up to 58 vol.-% [114], (ii) V-0 classification achieved at UL-94 (3.2 mm) [10, 12, 114] and (iii) PHRR decrease by 90% as observed by cone calorimetry [12].

It was also showed that polymeric materials and especially polyesters such as PLA are extremely sensitive to ageing. Hence, an overview was given about the ageing and general mechanisms of degradation of PLA under hydrolysis, thermal or photo-degradation. It appears that during ageing, PLA turn into to low-molecular-weight products, leading to the decrease in both thermal and mechanical properties but tending to increase the crystallinity of the material [27, 29, 34, 35, 38, 125, 165, 166]. A focus was also done concerning the effects of ageing on the fire behavior of flame retarded polymers, which is a complex subject depending on the ageing conditions as well as on the nature of both polymer and FRs. Different phenomena were evidenced during ageing of FR polymers such as migration [41, 42, 120] or degradation and hydrolysis of fillers and nanoparticles [44, 175, 179]. Moreover, depending on the authors, FR can protect or accelerate UV degradation of the FR material [45-48, 172, 173, 176].

As the development of PLA based materials must be a compromise between fire performances and sustainability, the goal of this study is to characterize and understand the ageing of flame retarded PLAs containing 30 wt.-% of FR additives (i.e. APP, MEL and C30B). Up to now, only a few scenarios have extensively studied the flame retardancy of polymers. Concerning PLA, whereas this polymer has been widely studied in terms of flame retardancy, literature reveals that investigations about ageing of flame retarded PLA are still needed.

The strategy of this work is to study the effect of accelerated ageing in a raw PLA in presence of temperature (T), relative humidity (RH), UV light and oxygen. Hence, the effects on the properties of the raw material as well as on the mechanisms of degradation will be determined. Then, the impact of the addition of FR fillers on the PLA properties, ageing and degradation will be investigated. As previously evidenced by our team, Melamine, APP and organoclays (C30B) have demonstrated their efficiency as FR in PLA intumescent system. The impact of ageing on the fire behavior of both PLA and FR-PLAs will be finally assessed and elucidated.

Chapter II: Materials and Methods

This chapter aims at describing the presentation of the materials, techniques and experimental protocols used in this work. In a first part, the materials, namely PLA, fire retardants and nanoparticles are presented. The different formulations process is also described. Apparatus used to investigate the behavior of materials under accelerated ageing are then presented. Finally, the techniques related to ageing characterization and fire tests are detailed.

1. Materials preparation and processing

1.1. Materials

1.1.1. Poly(lactic acid) (PLA)

The polymer used during this study is an Ingeo PLA 4032D, a polyester supplied by NatureWorks LLC (Ravago distribution center, Arendonk, Belgium). Before used, PLA was dried overnight at 70°C. Properties of this PLA are reported in **Table 4**.

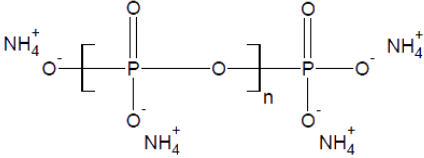
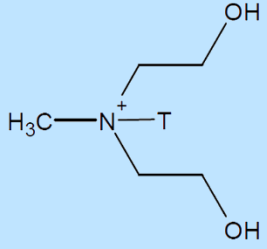
Table 4: Properties of Ingeo PLA 4032D.

Properties	PLA 4032D	Units
Residual monomer content	0.2	%
D-isomer content	1.5	%
Density	1.24	g/cm ³
Glass transition temperature (T _g)	61.5	°C
Melt Flow Index (MFI) (190°C, 2.16 kg)	9	g/10 min
Melt density (at 230°C)	1.08	g/cm ³
M _n	± 68 000	g/mol
Tensile Strength, psi	7.7 (53)	MPa
Tensile Yield Strength, psi	8.7 (60)	MPa
Tensile Modulus, kpsi	500 (3.5)	GPa
Tensile elongation	6	%
Melting Point	155 - 170	°C

1.1.2. Flame retardants and nanoparticles

As previously mentioned, this study is based on the ageing of flame retarded PLA. Hence, the flame retarded systems chosen are based on a previous work done in R₂FIRE team by G.Fontaine and S.Bourbigot [12]. A combination of Melamine, ammonium polyphosphate with and without organomodified montmorillonite Cloisite 30B is incorporated into the PLA matrix. **Table 5** summarizes all additives that have been used in this study, their supplier and their chemical nature.

Table 5: Summary of additives used.

Name	FR type	Supplier	Chemical structure
Melamine 99% (Mel)	Nitrogen FR	Sigma Aldrich	
Exolit® AP422 (APP)	Ammonium polyphosphate FR	Clariant	
Cloisite 30B (C30B) surfactant	Sheet-like nanoparticle (MMT modified with methyl tallow bis-2-hydroxyethyl ammonium chloride)	Southern Clay Product Inc.	 Where T is Tallow (65% C18; 30% C16; 5% C14) Anion: Chloride

Melamine (99%) was obtained from Sigma Aldrich (St Louis, MO). Ammonium polyphosphate (APP, Exolit AP 422, soluble fraction in water < 1 wt.-%) in powder was supplied by Clariant (Charlotte, NC). Nanoparticles, Cloisite 30B, a montmorillonite modified by bis-(2-hydroxyethyl)methyl tallowalkyl ammonium cations, was supplied by Southern Clay products (San Antonio, TX). The FRs and nanoparticles were dried for 24h at 70°C before use.

1.2. Material preparation and processing

1.2.1. Extrusion

Three different formulations, i.e. PLA, FR-PLA and FR-PLA-C30B (**Table 6**) were prepared by using a co-rotative twin screw extruder from Thermo Fischer Scientific (**Figure 29**) (HAAKE Rheomix OS PTW 16 twin screw extruder) with a barrel length of 400 mm and a screw diameter of 16 mm (L/D = 25). Both FR-PLA and FR-PLA-C30B were prepared by incorporating 30 wt.-% of FR fillers. Moreover, for the comprehension of the effects of ageing on flame retardancy of PLA, two additional formulations were prepared with 20 wt.-% of FR fillers, i.e. FR-PLA-20% and FR-PLA-C30B-20% (**Table 7**).



Figure 29: Thermo Scientific extruder.

Table 6: Composition and name of the formulations PLA, FR-PLA, FR-PLA-C30B at 30 wt.-% loading.

PLA (wt.-%)	FR loading (wt.-%)	Formulation name	Mel (wt.-%)	APP (wt.-%)	C30B (wt.-%)
100	0	PLA	0	0	0
70	30	FR-PLA	5	25	0
70	30	FR-PLA-C30B	4.83	24.17	1

Table 7: Composition and name of the formulations FR-PLA, FR-PLA-C30B at 20 wt.-% loading.

PLA (wt.-%)	FR loading (wt.-%)	Formulation name	Mel (wt.-%)	APP (wt.-%)	C30B (wt.-%)
90	20	FR-PLA-20%	3.18	16.14	0
90	20	FR-PLA-C30B-20%	3.18	16.14	0.66

The extruder is composed of a heater barrel divided in ten zones, in which the polymer melts. The polymer, fire retardant additives and nanoparticles were added using a volumetric side feeder. Before each experiment, a calibration of the volumetric feeders was performed in order to obtain a good control of the composition of the final blends. Temperature profile of the ten heating elements was set as reported in **Table 8** and the rotational speed of the screw was fixed at 100 rpm.

Table 8: Temperature profile of the extruder from hopper to die.

Zone	1*	2	3	4	5**	6	7	8	9	10
Temperature (°C)	205	200	195	190	185	180	175	165	165	165

*PLA was fed in zone 1, **FR and nanoparticles mixed together were fed in zone 5

At the end of the extruder, PLA and FR-formulations forms a strip which is cut into pellets.

1.2.2. Molding

Mass loss cone calorimeter (MLC) plates of 100x100x3 mm³ were obtained by pressing the material, previously extruded and pelletized, with a hydraulic hot press in specific molds. Two plates heated at 185°C in between a mold containing 35 g of formulation were used. A force of 20 kN was applied for 2 minutes and then a force of 40 kN was applied for 8 minutes. Prior being removed from the mold, each sample was cooled down with water cooling system until it reaches 50°C. LOI samples size was 100x10x3 mm³ were obtained by cutting them into MLC plate using a bandsaw. Dimension of samples were selected according to the ISO-4589-2 and ISO-13927 standards [180, 181]. Barrels and plates were then stored at room temperature in sealed bags before tests.

1.2.3. Powders

A high speed rotor mill (Retch – Ultra centrifugal Mill ZM 200) was used to obtain fine powder (< 500 µm) from the extruded pellets. The material remains in the grinding chamber for a very short period and liquid nitrogen is used to cool down the sample, which means that the characteristic features of the sample (i.e. thermal properties) to be determined are not altered. Then the formulations were stored at room temperature in sealed bags before analyses.

2. Accelerated ageing methods

As previously mentioned, one objective of this work is to screen the impact of ageing on virgin PLA and both FR-PLA and FR-PLA-C30B, by submitting them to accelerated ageing tests under constraints of their environment of use. Temperature (T), relative humidity (RH) and ultra-violet light (UV) are the main parameters investigated during experiments. PLA as well as both FR-PLAs were submitted for four months to three different kinds of ageing experiments respectively; (i) temperature and relative humidity, (ii) temperature and UV, and (iii) temperature, UV and relative humidity. Accelerated ageing tests are described and detailed below.

2.1. Ageing in presence of temperature and relative humidity

In order to evaluate the impact of temperature and relative humidity on our materials, PLA and both FR-PLAs were subjected to constant heating 50°C and relative humidity (75%) for four months. Swelling, oxidation and hydrolysis of the materials should be accelerated by combining temperature and relative humidity. This temperature/relative humidity treatment will be further addressed to as T/RH treatment. For this purpose, a humidity chamber test HCP 108 (**Figure 30**) supplied by Memmert was used to simulate ageing conditions.



Figure 30: Humidity chamber test HCP 108.

The experiments were carried out on barrels, plates and extruded pellets which were regularly (i.e. each week) taken out of the oven to be characterized. All samples removed from the oven were dried overnight at 50°C before testing, in order to eliminate the excess of humidity and to perform all characterizations in the same and controlled conditions. Effects of each period of ageing on the behavior of PLA and FR-PLAs specimens were investigated by comparing the changes of properties of aged materials to those of unaged material.

2.2. Ageing in presence of UV-rays

The accelerated weathering under UV-rays of PLA and both FR-PLAs was carried out by two distinct experiments. The first ageing test was realized by exposing the samples to both temperature and UV-rays (T/UV), and the second one consisted in exposing the samples to temperature, UV-rays and relative humidity (T/UV/RH). For this purpose, two accelerated weathering chambers from Q-LAB (**Figure 31**) were used: (i) QUV/se for T/UV and (ii) QUV/spray for T/UV/RH.



Figure 31: Q-LAB, QUV/spray weathering chamber.

The weathering conditions chosen are derived from a ISO 4892-3 standard [182]. Both Q-UV devices are equipped with 4 UV lamps (UVA 351) with 0.76 w/m² irradiance. Wavelengths under 300 nm are filtered using these kinds of lamps. The Q-UV/spray tester is also equipped

with humidification unit, distilled water vessel, pump and piping system for circulation of the water to the humidification unit.

Cycles of 4 hours UV irradiation at 50°C, followed by 4 hours dark at 50°C for T/UV or 4 hours dark and water condensation at 50°C for T/UV/RH were applied as listed in **Table 9**. The specimens (extruded pellets, plates and barrels) attached to the test panels were exposed to these consecutive cycles without interruption for four months. As for T/RH ageing, effects of accelerated weathering were investigated each week. Samples aged under T/UV/RH were dried overnight at 50°C after ageing before testing, in order to eliminate the excess of humidity and to perform all characterizations in the same conditions

Table 9: Conditions in accelerated weathering chambers for T/UV and T/UV/RH ageing.

Experiment	Cycle period	Cycle time (minutes)	Temperature (°C)	Relative humidity
T/UV	UV	240	50	No
	Dark	240	50	No
T/UV/RH	UV	240	50	No
	Dark and condensation	240	50	Yes

3. Physico-chemical characterization

3.1. Microscopies

3.1.1. Digital microscopy

Digital microscopes are a variation of a traditional optical microscope that uses optics and a charge-coupled device (CCD) camera to output a digital image to a monitor. In our case, the microscope enables to get a clear view of the surface of PLA and FR-PLAs plates thanks to the high depth of field. The expansion of the char after mass loss cone experiment was also evaluated using the digital microscopy. Images of plates and chars were taken with a VHX-1000 microscope (Keyence) at 50x magnification and stitched together in order to get a clear “3D” image of the whole plate.

3.1.2. Electron probe micro analysis (EPMA)

Electron probe microanalysis (EPMA) is an analytical technique that is used to establish the composition of small areas on specimens. This is one of several particle-beam techniques. Technically, a beam of accelerated electrons is focused on the surface of a specimen using a series of electromagnetic lenses, and these energetic electrons produce characteristic X-rays within a small volume (typically 1 to 9 μ^3) of the specimen. The characteristic X-rays are detected at particular wavelengths, and their intensities are measured to determine

concentrations. Excepting H, He and Li, all elements can be detected, they emit at a specific set of X-rays. EPMA has a high spatial resolution (10 kV-1 μ A-150 nm) and sensitivity (around 3.0 microamperes), and this analytical technique allows obtaining highly magnified secondary and backscattered electron images of a sample.

In this work, FR-PLA and FR-PLA-C30B were analyzed by EPMA to assess a possible migration of fillers during ageing. In this regard, the samples were first carbon coated with a Bal-Tec SCD005 sputter coater. A camera SX100 electron probe micro analyzer was used to perform elemental analysis on the surface of the samples (electron interaction $1\mu^3$). Back scattered electron (BSE) images were carried out at 6 kV and 15 kV, 40 nA and phosphorus, nitrogen and silica X-ray mappings were carried out at 6 kV 15 kV, 40 nA. On BSE pictures, the darkest parts correspond to the “lightest” elements. For mappings, the crystals used to detect the $K\alpha$ of phosphorus, nitrogen and silica were respectively, a PER (pentaerythritol) crystal, a PC2 (multicouche Ni/C) crystal and a TAP (thallium acid phthalate) crystal.

3.1.3. Scanning electron microscopy (SEM)

Scanning electron microscopy (SEM) is a technique that uses the interactions occurring between electrons and matter. An electron beam is applied on the sample, leading to the emission of secondary electrons and backscattered electrons (among other species), which are then used to obtain topographic and chemical information respectively. The surface of PLA and both FR-PLAs was observed before and after ageing using a Scanning Electron Microscope FEG field emission gun JEOL JSM-7800F LV. SEM (Secondary electrons) experiments were performed on carbon coated samples at 6 kV. Images were taken at x75 x400, x700, x1300 and x2500 magnifications.

3.1.4. Transmission electron microscopy (TEM)

Transmission electron microscopy (TEM) is a technique used to qualitatively evaluate the dispersion of additives in a polymeric matrix. This technique was used to analyze the dispersion of organomodified montmorillonite, i.e. Cloisite 30B in the PLA matrix. All the samples were ultra-microtomed with a Leica Ultracut UCT ultramicrotome with a Diatome diamond knife at room temperature to give section with a nominal section of 100 nm. The section were transfered to Cu/Rh grid of 400 mesh. Bright-field TEM images of the samples were obtained at 200 kV under low-dose conditions with a FEI Technai G2 electron microscope.

3.2. Thermal analysis

3.2.1. Thermo-gravimetric analysis (TGA)

Thermo-gravimetric analysis (TGA) is a technique allowing to monitor the weight loss of a sample versus temperature while the sample is heated following a defined temperature ramp. The measurements can be carried out in oxidative (air) atmosphere.

TGA measurements were carried out using a SETARAM (TG92-16). Balance and purge flow rates were set at 15 and 100 mL/min respectively. Experiments were performed under air. Samples of about 10 mg were positioned in open vitreous silica pans with gold foil and submitted to an isotherm at 50°C for 10 minutes, then followed by a heating ramp of 10°C/min up to 800°C. The precision on the temperature measurements is $\pm 1.5^\circ\text{C}$ in the temperature range of 50-800°C. Each TG analysis was repeated at least twice to ensure the repeatability of the measurements. Theoretical TGA curves of FR-PLA and FR-PLA-C30B were calculated by linear combination according to **Equation 23**.

$$\text{wt.-% (theo)} = (h \times \text{wt. \%PLA}) + (i \times \text{wt. \%Mel}) + (j \times \text{wt. \%APP}) + (k \times \text{wt. \%C30B})$$

Equation 23

Where h , i , j and k are the mass fraction of PLA, Melamine, APP and Cloisite, 30B, respectively ($h + i + j + k = 1$) and wt.-% is the residual weight in percentage.

3.2.2. Differential scanning calorimetry (DSC)

DSC is widely used for the characterization of polymers. All experiments in this work have been performed on a TA Instrument Discovery DSC and monitored with Trios software. This technique is used to study the behavior of polymers when exposed to a temperature gradient (rise and / or decrease of the temperature at a controlled rate) under nitrogen atmosphere. This type of analyses allows the measurement of glass transition temperature (T_g , characterized by a change in the slope of the thermogram), the heat capacity (C_p) and, for semi-crystalline polymers, the melting temperature (T_m), the melting enthalpy (ΔH_m), the crystallization temperature (T_c) and the crystallization enthalpy (ΔH_c). Experimentally, two pans are heated during the analysis: one pan containing 5.0 ± 0.5 mg of the sample previously grounded, and a second empty pan used as a reference. Each sample has been exposed to 2 cycles of heating/cooling (**Figure 32**). Experiments were carried out at 10°C/min from room temperature to 180°C, then an isotherm of 3 minutes was performed, after what a decrease of temperature of 1°C/min until -20°C was followed by an isotherm of 3 minutes. At the end of the experiment, the device returns to ambient temperature.

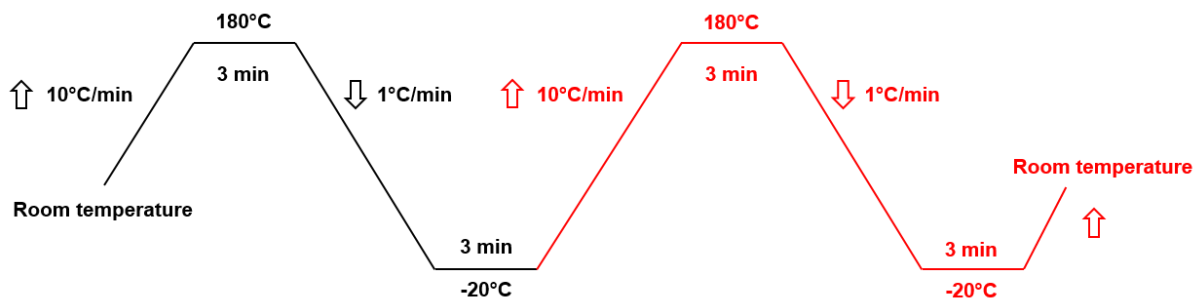


Figure 32: Temperature/time ramp used for the DSC analysis.

The thermal history of the sample is suppressed during the first cycle. Concerning the characterization of the different samples, only the second cycle was taken into account. All information such as melting temperature (T_m), melting enthalpy (ΔH_m), crystallization temperature (T_c), crystallization enthalpy (ΔH_c) and cold crystallization enthalpy (ΔH_{cc}) were obtained from these thermograms. The degree of crystallinity (χ) was calculated from the melting enthalpy by the following **Equation 24**.

$$\chi = \frac{100 * (\Delta H_m - \Delta H_{cc})}{\Delta H_m(100\%)(1 - x)}$$

Equation 24

In this equation, χ allows measuring the proportion of material in the crystalline state. ΔH_m (100%) corresponds to the melting enthalpy of a 100% crystalline PLA (93.1 J/g) and x is the additive content (FRs, nanoparticles). The temperature precision is estimated to $5.10^{-3}^{\circ}\text{C}$. The enthalpy precision is $\pm 0.04\%$.

3.3. Color changes measurements

The color changes and reflectance of unaged and aged samples were recorded using a Datacolor CHECK 3 portable spectrophotometer from Datacolor Industry. The CIE (French “Commission internationale de l'éclairage”) L^*a^*b color system was employed for the color measurement. This system is commonly used in textile characterization [183]. In the CIE L^*a^*b system the three coordinates presented in **Figure 33** represent (i) the lightness of color ($L^* = 0$ corresponds to black and $L^* = 100$ corresponds to diffuse white; specular white may be higher), (ii) the color position between red/magenta and green (negative values of a^* indicate green and positive values indicate magenta), and (iii) the color position between yellow and blue (negative values of b^* indicate blue and positive values indicate yellow).

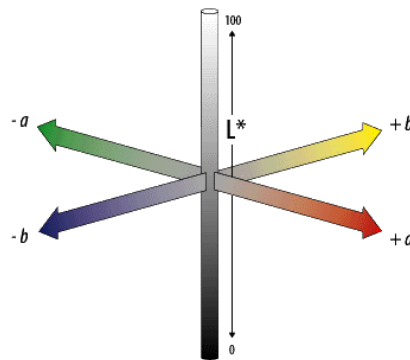


Figure 33: color space of CIE Lab system.

The difference between unaged and aged samples (ΔE) was calculated according to the **Equation 25** where ΔL^* represents the lightness difference; Δa^* and Δb^* , the differences in a and b values.

$$\Delta E = \sqrt{(\Delta L^*)^2 + (\Delta a^*)^2 + (\Delta b^*)^2}$$

Equation 25

The a^* and b^* coordinates are close to zero for neutral colors (white and gray) and increase in magnitude for more saturated or intense colors. The advantage of CIE Lab system is that color differences can be expressed in units that can be related to visual perception [184]. Three reflectance measurements were made on each sample; the samples were rotated 90° before each measurement.

3.4. Gel permeation chromatography (GPC)

In order to determine the number average molecular mass (M_n) of materials, all samples were characterized by gel permeation chromatography (GPC). GPC is a type of high performance liquid chromatography used to determine the molecular weight distribution of polymers which can be performed in a wide range of solvents, from non-polar organics to aqueous ones. Experimentally, columns packed with very small, round and porous particles are used, allowing separation of molecules contained in the solvent that is passed through them. Molecules are separated on the basis of their size, hence “size exclusion”. The first GPC columns were packed with materials referred to as gels, hence “gel permeation”. The particles in the columns are made from polymers that have been cross-linked to make them insoluble, or from inorganic materials, such as spherical silica.

Experimentally, GPC is performed in tetrahydrofuran (THF) at 40°C, with a flow rate of 1 mL/min and a polymer concentration of 2 mg/mL after filtration through a 0.2 μm pore-size membrane, to eliminate FR additives and nanoparticles. Measurements were performed on a Waters system (Separation Module Waters e2695) equipped with three columns (Styragel HR1, Styragel HR3 and Styragel HR4) placed in series and coupled with a differential refractive index (RI) Wyatt detector (WYATT Optilab T-Rex). It was established, however, that in order to get the correct M_n value of PLA, the experimental value obtained from the GPC traces using polystyrene standards have to be multiplied by 0.58 [185]. In fact, when using polystyrene standards for GPC analysis of Polylactic acid, the PLA molecular weights obtained by GPC are typically larger than the actual molecular weights. Multiplication of the GPC data by a factor of 0.58 has been suggested to get a more accurate number average molecular mass. The polydispersity index (PI) was calculated as M_w/M_n . Moreover, in order to analyze an autocatalysis process that can occur during degradation of PLA based materials, the number of chain scission n_t , was calculated according to **Equation 26** [186].

$$n_t = \frac{1}{M_{nt}} - \frac{1}{M_{n0}}$$

Equation 26

Where M_{nt} and M_{n0} are the number average molecular masses at time t and at the initial time, respectively. Considering the precision of the equipment and all the multiple stages of purification and dissolution of compounds, the error of measurement is estimated at 10%.

3.5. Melt flow index (MFI)

In order to characterize the viscosity of the formulations as a function of ageing, the melt flow index (MFI) has been determined. In fact, when the MFI of a blend increases, its viscosity decreases. The device used is a Melt Indexer MP1200 provided by Tinius Olsen (**Figure 34**) and all the experiments were done in accordance to ISO 1133 Procedure B [187], i.e. under a weight constraint of 2.16 kg and at 165°C. Using this procedure, the time taken by the piston to run through 5 mm in the barrel is measured with the help of a sensor and with the weight of the different collected rods, it allows obtaining directly the Melt Flow Index (MFI, g/10min), the density (d , g/cm³) and the dynamic viscosity (η , Pa/sec) from the device. The error of measurement is estimated to 15%.

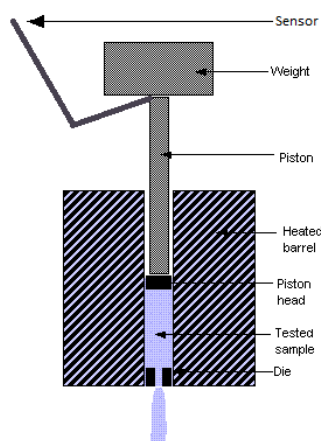


Figure 34: Melt flow Index tester.

3.6. X-ray diffraction (XRD)

X-ray diffraction is a rapid analytical technique widely used as to determine and characterize one or several crystalline phases of a material, providing information about the structure of the material at the molecular scale. Besides, the recent technical and computing developments allow obtaining precise information on the structure of the amorphous phase of a polymer.

In this work, XRD was used in order to identify crystalline phases of our PLA based materials. To this end, the experimental device was equipped with a Genix micro-source (Xenocs, France)

which produces a parallel beam wavelength of 1.54 Å (K_{α} Cu line). A charge coupled device (CCD) Very High resolution camera (Photonic Sciences) was used as a detector. Distance between sample and detector was 8 cm, binning 4x4, and the samples were exposed for 15 minutes.

3.7. X-ray photoelectron spectroscopy (XPS)

X-ray photoelectron spectroscopy (XPS) measurements were carried out on an AXIS Ultra^{DL}D Kratos analytical apparatus using a monochromatic Al KR X-ray source ($h\nu = 1486.6$ eV) in the following conditions: the emission voltage was set to 15 kV, the current 10 mA, the pressure in the analyzing chambers was maintained at 10^{-9} Torr or lower during the analysis, and the size of the analyzed area was $300 \mu\text{m} \times 700 \mu\text{m}$ with a depth of 10 nm. High-resolution C1s spectra were recorded at pass energies of 160 eV with a step of 1 eV. Data treatment and peak-fitting procedures were performed using Casa XPS software. Obtained spectra were rescaled by shift of C1s C–C at 285 eV. Thus, it is possible to determine the atomic percentage of carbon, oxygen nitrogen, phosphorus and silica at the surface of the plates. XPS is an analytical technique permitting to quantify the amount of targeted elements and to identify their chemical or electronic state to get detailed information about the bonding of elements at the sample surface. Samples are irradiated by an X-ray beam ($E = h\nu$) generated by an high power aluminum monochromator. The energy of the X-rays is adsorbed by an atom leading to emission of a core photoelectron. The emitted photoelectron exhibits a kinetic energy (E_{kinetic}) depending on the incident X-ray and the binding energy (E_{binding}) of the atomic orbital (**Equation 27**).

$$h\nu = E_{\text{kinetic}} + E_{\text{binding}}$$

Equation 27

3.8. Fourier transform infrared spectroscopy (FTIR)

Room temperature infrared spectra of the initial and degraded thin films of PLA were recorded between 500 and 4000 cm^{-1} using a Fourier Transformed Infrared spectrometer (ThermoScientific) Nicolet IS 50 in ATR and transmission. Final spectra in ATR resulted from 32 scans using a resolution of 2 cm^{-1} . Final spectra in transmission resulted from 16 scans using a resolution of 2 cm^{-1} and 32 cm^{-1} . Both ATR and transmission spectra were processed by OMNIC software. Electromagnetic waves belonging to the infrared domain are sent towards the molecules composing the sample, inducing transitions between the vibration levels. Links between atoms are targeted and information about these links are obtained. Thus, FTIR allows to evidence chemical modifications on the structure of PLA based materials after ageing and then permit to determine mechanisms of degradation. To avoid the differences due to the thickness of the films, spectra were normalized according to the band at 2997 cm^{-1} vC-H characteristic vibration stretching band of PLA [34].

3.9. Chemical derivatisation

The T/UV and T/UV/RH aged samples were submitted to chemical treatment in order to identify the photoproducts formed and to establish the mechanism of degradation. The irradiated films were exposed to a reactive gas such as ammonia (NH_3) at room temperature. NH_3 saturated atmosphere was obtained under glass bell in presence of concentrated NH_3 solution. The ammonia used in the experiment was provided from Sigma Aldrich. In parallel to these treatments, we verified that the polymeric samples non-irradiated did not react with the gas. As illustrated in **Figure 35**, the reaction of NH_3 with anhydride leads to the formation of ammonium carboxylates and amide groups.

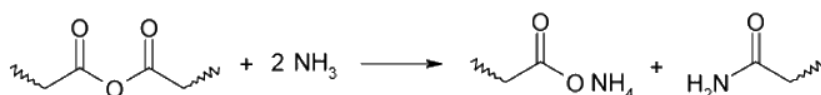


Figure 35: Reaction of anhydride with ammonia.

The ammonium carboxylates and primary amide groups are characterized by an infrared absorption band above 1600 cm^{-1} and 1675 cm^{-1} respectively.

3.10. Solid state nuclear magnetic resonance (NMR)

The solid-state nuclear magnetic resonance (NMR) is an effective tool to analyze the changes in the chemical environment of an atom inside a material. In the solid state (on the contrary to liquid state), the chemical shift anisotropy (anisotropy of magnetic moment, CSA), has a strong effect on the spectra, by broadening peaks. Through a tensorial analysis of the magnetic moments in a molecule, it is possible to demonstrate that a “Magic Angle” exists, with respect to the applied magnetic field at which the spinning of the sample leads to a minimization of absorption line broadening due to CSA. This method of analysis is so called “Magic Angle Spinning” (MAS).

In the case of carbon, the resonance of atoms is only possible in their isotopic form (^{13}C). However their low abundance leads to poor signal. This poor signal can be overcome by an excitation of protons in the sample which makes them resonate at the same frequency than that of target atom (Hartman-Hahn condition). This process is called cross-polarization (CP), and the time of polarization is also called contact time. CP leads to a high enhancement of the excitation of studied nuclei. However an interference exists between the large number of protons and the decay of isolated nuclei, due to weak spin interactions. In this case, the dampening of the signal can be removed with a strong radiofrequency signal which holds the protons in a high resonance state so that they do not absorb resonance from the nuclei. This is called ^1H decoupling.

^{31}P NMR measurements were performed on a Bruker Avance II 400 spectrometer with a 4 mm probe. The Larmor frequency was 40.5 MHz (9.4 T). Measurements were performed with ^1H

dipolar decoupling at MAS of 10 kHz. 120 s delays was used between two pulses. Phosphoric acid (H_3PO_4) in aqueous solution (85%) was used as reference.

3.11. Electron paramagnetic resonance spectroscopy (EPR)

Electron paramagnetic resonance (EPR) spectroscopy is a very powerful and sensitive method for the characterization of the electronic structures of materials. In EPR spectroscopy, microwave radiation is used to probe species with unpaired electrons, such as radicals, radical cations, and triplets in the presence of an externally applied static magnetic field. This technique is used to study: (i) free radicals, i.e. atoms, molecules or ions containing one unpaired electron either in the solid, liquid or gaseous phases, (ii) transition ions including actinide ions (these routinely may have up to five or seven unpaired electrons), (iii) various “point” defects in solids / localized imperfections, (iv) systems with more than one unpaired electron such as triplets state systems, biradicals and multiradicals and (v) systems with conducting electrons such as semiconductors and metals.

Theoretically, when a molecule or compound with an unpaired electron is placed in a strong magnetic field, the spin of the unpaired electron can align in two different ways creating two spin states, $m_s = \pm \frac{1}{2}$. The alignment can either be along the direction (parallel) to the magnetic field which corresponds to the lower energy state $m_s = -\frac{1}{2}$ or opposite (antiparallel) to the direction of the applied magnetic field $m_s = +\frac{1}{2}$. The two alignments have different energies and this difference in energy lifts the degeneracy of the electron spin states. The energy difference is given by **Equation 28**.

$$\Delta E = E_+ - E_- = h\nu = g\mu_B B$$

Equation 28

Where h is the Planck's constant (6.626×10^{-34} J/s), ν is the frequency of radiation, μ_B is the Bohr magneton (9.274×10^{-24} J/T), B represents the strength of the magnetic field in Tesla and g is the g -factor. During the experiment the values of h , ν and μ_B does not change and g value decrease as B increases. The g -factor is a unit measurement of the intrinsic magnetic moment of the electron, and its value for a free electron is 2.0023. The concept of g can be roughly equated to that of chemical shift in NMR. EPR spectrum is the absorption of microwave frequency radiation plotted against the magnetic field intensity.

In an EPR experiment the field of the spectrometer magnet is swept linearly to excite some of the electrons in the lower energy level to the upper energy level while the sample is exposed to fixed microwave irradiation. The free of the unpaired electrons have a small magnetic field and orient themselves parallel to the larger field produced by the spectrometer's magnet. At a particular magnetic field strength the microwave irradiation will cause some of the free electrons to “flip” and orient against the spectrometer's magnetic field. This separation between the lower and the higher energy level is exactly matched by our microwave frequency. The condition where the magnetic field and the microwave frequency

are “just right” to produce an EPR resonance (or absorption) is known as the resonance condition is detected by the spectrometer. EPR spectroscopy can be carried out either by (i) varying the magnetic field and holding the frequency constant or (ii) varying the frequency and holding the magnetic field constant (as in the case of NMR spectroscopy). It exist two typical methods to record an EPR spectra: (i) the continuous wave method where the sample is irradiated continuously with microwave radiation of fixed frequency while the magnetic field is slowly swept and the microwave absorption is measured for each field position. The second one (ii) is the pulse EPR method where a short pulse of high microwave radiation are sent to the sample and the response in the absence of radiation is recorded.

Experimentally, all chosen samples were measured at room temperature on a Bruker E500 A/A/X TMHS spectrometer using X-band continuous wave mode. Converse time and time constant were set to be 40.96 ms and 20.48 ms respectively. Microwave power and modulation amplitude were respectively set to 2 mW and 1 G. The first order baseline correction was applied to all recorded EPR. The weight of samples and measuring Q values were normalized for the spectra to analyze the intensity of all paramagnetic species. Formation of radical species under irradiation was performed in situ using Shimadzu irradiation system with a filter operating in the range of 300-400 nm. For each samples a kinetic was measured by recording spectrum each minute.

EPR image collection: The signals were acquired with a field-of-view of 4mm and gradient strength of 175 Gcm^{-1} . The sample was placed closest to the center of the resonator to minimize the inhomogeneity of the B1 field of the resonator. The two-dimensional (2D) images were acquired with a size of 512x512 pixels resulting in a pixel size of $5 \mu\text{m}$.

EPR image processing: The image processing involves deconvoluting the whole signal acquired under a magnetic field gradient from the reference signal collected without gradient. After deconvolution process signals were backprojected using Fourier Transform, giving the spatial distribution of paramagnetic species

Pulsed-EPR measurements were carried out at X-band ($\sim 9.7 \text{ GHz}$) with a Bruker ELEXSYS E580 equipped with an Oxford Helium flow cryostat for low temperature measurements, typically 4 K. Echo field sweep were achieved with $\pi/2$ and π pulse length values of 10 ns and 22 ns respectively. The hyperfine sublevel correlation spectroscopy (2D-HYSCORE) measurements were also carried at 4.2 K with the four pulse sequence $\pi/2-\tau-\pi/2-t_1-\pi-t_2-\pi/2-\tau$ echo, and a time delay τ is 136 ns. This echo time were chosen by previously performing a 2D 3 pulses electron spin echo envelope modulation (ESEEM) versus t in order to minimize the “blind spot” effect. The principle of the 2D HYSCORE is given in **Appendix 5, p.228**.

4. Fire testing methods

4.1.1. Mass loss calorimeter (MLC)

The mass loss calorimeter (MLC) allows simulating the fire conditions at a small bench scale according to ISO 13927 [181]. A schematic representation of the mass loss calorimeter is given in **Figure 36**. The core of the instrument is a radiant electrical heater in the shape of a truncated cone, irradiating a flat horizontal sample ($100 \times 100 \times 3 \text{ mm}^3$) placed beneath it, at a chosen heat flux (e.g. $35 \text{ kW}\cdot\text{m}^{-2}$ to simulate a mild fire in this study). The distance between the sample holder and the heat source can be chosen as well (e.g. 25 mm in this study). Ignition is provided by an intermittent spark igniter located 13 mm above the sample.

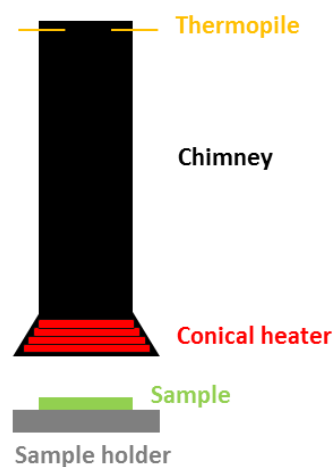


Figure 36: Schematic representation of mass loss calorimeter.

The mass loss calorimeter measures the temperature of the evolved gases using a thermopile located at the top of the chimney. The calibration of the heat release rate (HRR) is performed with methane. A methane flow of 0 to $6.7 \text{ mL}\cdot\text{min}^{-1}$ is burnt above the sample holder to obtain a calibration curve of the heat release as a function of temperature.

The values obtained by mass loss calorimeter testing are: the heat release rate (HRR), the peak of heat release rate (pHRR), the total heat release (THR), the time to ignition (TTI) and the mass loss of the sample during combustion (ML). In this work, the MLC measurements were performed on a Fire Testing Technology mass loss calorimeter device at $35 \text{ kW}/\text{m}^2$ and 25 mm, according to the ISO 13927, on specimens of $100 \times 100 \times 3 \text{ mm}^3$. All measurements were performed three times. The presented curves are the worst case of repeatable results. The acceptable error of measurement is estimated at 10 % for all values.

4.1.2. Limiting oxygen index (LOI)

The limiting oxygen index (LOI) is a small heat source ignition test. With the LOI test (ISO 4589-2 [180]), the relative flammability of materials, their ignitability and inflammation can be evaluated. The experimental set-up of the LOI device is shown in **Figure 37**. LOI

measurements are performed on a Fire Testing Technology (FTT) device with barrels of $100 \times 10 \times 3 \text{ mm}^3$ at room temperature. The specimen is clamped vertically into a glass cylinder in a controlled oxygen-nitrogen mixture atmosphere. The measured LOI value corresponds to the minimal oxygen concentration required to sustain the combustion of a material. It is calculated according to **Equation 29** and expressed as the percentage of oxygen in an oxygen-nitrogen mixture.

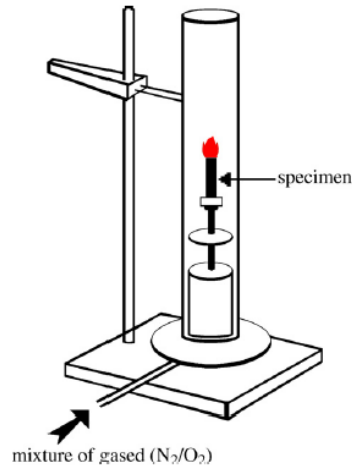


Figure 37: Experimental set-up of the LOI test.

Materials having a LOI value below 21 vol.-%O₂ are called combustible, those with a LOI value above 21 vol.-%O₂ are flame retarded. Thus, the higher the LOI value, the better the fire retardancy of the material.

$$\text{LOI} = 100 \times \frac{[\text{O}_2]}{[\text{O}_2] + [\text{N}_2]}$$

Equation 29

5. Conclusion

In the first part of chapter II, the polymer, the additives as well as the preparation methods of the materials used in this study were presented. Afterwards, materials and protocols used to simulate accelerated ageing of materials were described. Experimental techniques investigated to characterize the impact of ageing on PLA and FR-PLAs, as well as methods to assess fire retardancy before and after ageing were finally discussed.

The following Chapter III will further detail the impact of accelerated ageing on raw PLA. Properties of this material before and after ageing, as well as its mechanisms of degradation will be investigated. Comprehension of the degradation of raw PLA is a key parameter to investigate, before investigating ageing of FR-PLAs in Chapter IV, so as to understand thereafter the role of fire retardant additives on the degradation of PLA.

Chapter III: Impact of ageing on PLA

This chapter deals with the impact of ageing on neat PLA. As reported in chapter I, PLA is extremely sensitive to its environment, leading to a degradation of the material. In this way, before investigating ageing of FR-PLAs, it is necessary to understand the effect of ageing (temperature, UV and relative humidity) on neat PLA. The first section of this chapter presents the visual and surface changes occurring on PLA over time as a function of ageing conditions. Then, the impact of ageing on physico-chemical properties of the material is investigated. Finally, mechanisms of degradation implied during ageing are proposed.

1. Visual measurement of ageing

Even if the effects of ageing on PLA are widely reported in literature as stated in chapter I (p.23), the objective of this chapter is to compare the already published results with the PLA used in this study. Aim is to (i) evidence change in physico-chemical properties and (ii) elucidate the mechanisms of degradation while bringing a complementary insight through the use of unconventional experimental techniques such as electron paramagnetic resonance spectroscopy (EPR). Hence, the first part of this chapter will be dedicated to the effects of temperature, UV and relative humidity (i.e. T/UV, T/RH and T/UV/RH) on the physico-chemical properties of PLA: the surface topography of the materials will be examined using digital microscopy and SEM and the color changes and reflectance of aged samples will be compared to the unaged ones using $L^*a^*b^*$ device.

1.1. Visual evaluation

The impact of the three kinds of ageing experiments on raw PLA was first evaluated visually. The numerical pictures of PLA before ageing and after 60 days ageing under T/UV, T/RH and T/UV/RH exposure (Figure 38) show that ageing promotes the “bleaching” of the plates. This effect is even more pronounced for PLA aged for 60 days under T/UV/RH (Figure 38 (d)), followed by T/RH (Figure 38 (c)) and T/UV (Figure 38 (b)) conditions.

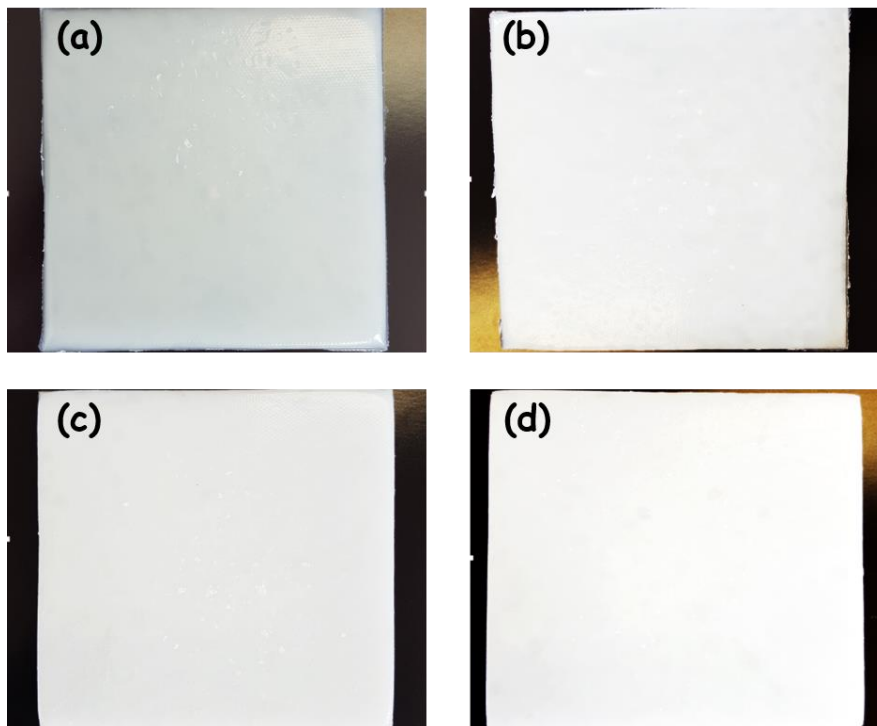


Figure 38: Pictures of PLA at 0 d (a), 60 d T/UV (b), 60 d T/RH (c) and 60 d T/UV/RH (d) exposure.

In order to investigate in more detail these surface modifications, digital microscopy, scanning electron microscopy (SEM) and L*a*b* were performed on PLA plates before and after ageing.

1.2. Surface morphology of PLA after ageing

Whereas PLA surface is completely smooth before ageing, holes and cracks, slightly visible to the naked eyes, appear during ageing. Digital microscopy was thus first used to compare neat PLA before ageing (**Figure 39 (a)**) and aged PLA. Under T/UV/RH exposure cracks are formed in the entire surface of the PLA after 60 days (**Figure 39 (d)**), whereas under T/UV and T/RH they are dispatched in low amount at the surface (**Figure 39 (b)** and **Figure 39 (c)**, respectively).

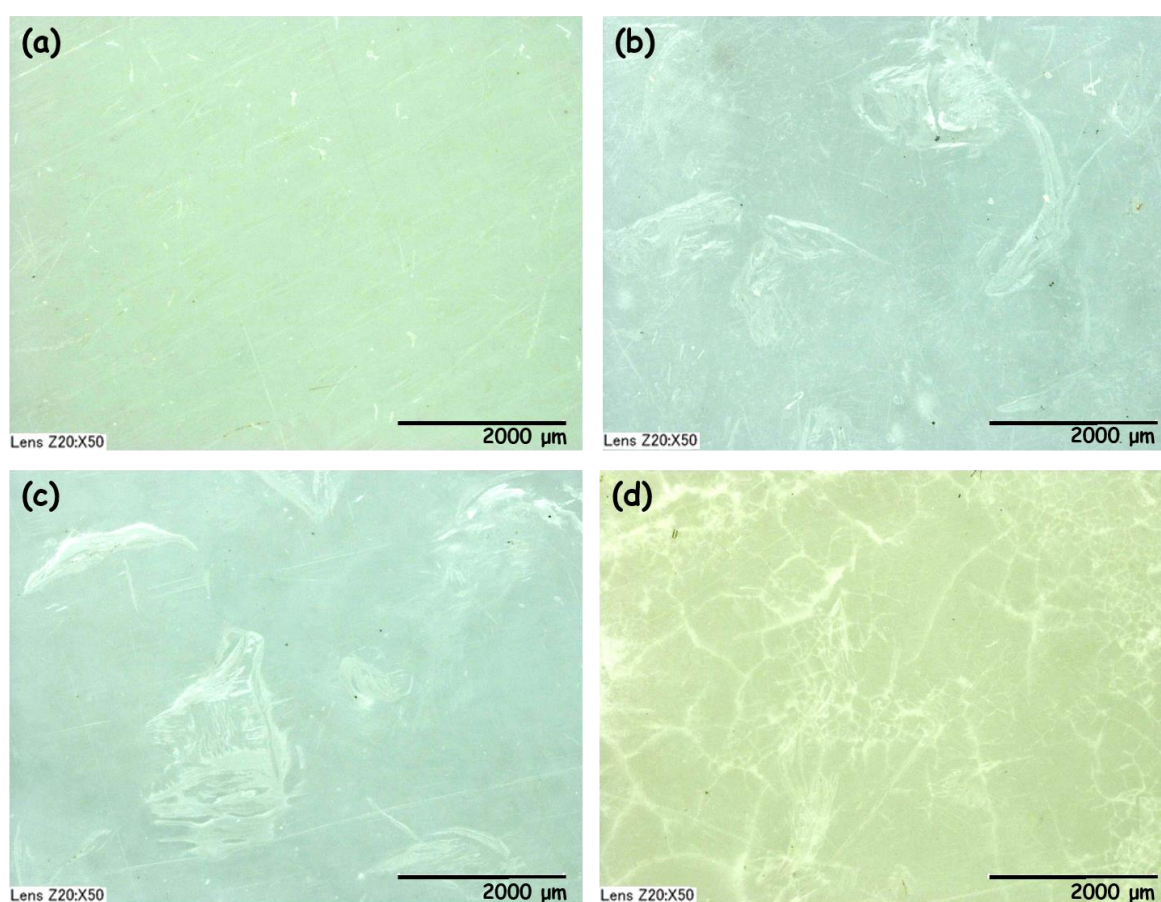


Figure 39: Digital microscopy pictures of unaged PLA (a), 60 d T/UV (b), 60 d T/RH (c) and 60 d T/UV/RH (d).

Pictures of unaged and aged PLA obtained by SEM (**Figure 40**) support these observations. In fact, holes and cracks are observed by SEM (circled in red in the pictures) and the phenomenon is more pronounced for PLA aged for 60 days under T/UV/RH (**Figure 40 (d)**) where cracks are observed on the entire surface of the plate. As previously reported, PLAs aged for 60 days under T/UV (**Figure 40 (b)**) and T/RH (**Figure 40 (c)**) are less damaged.

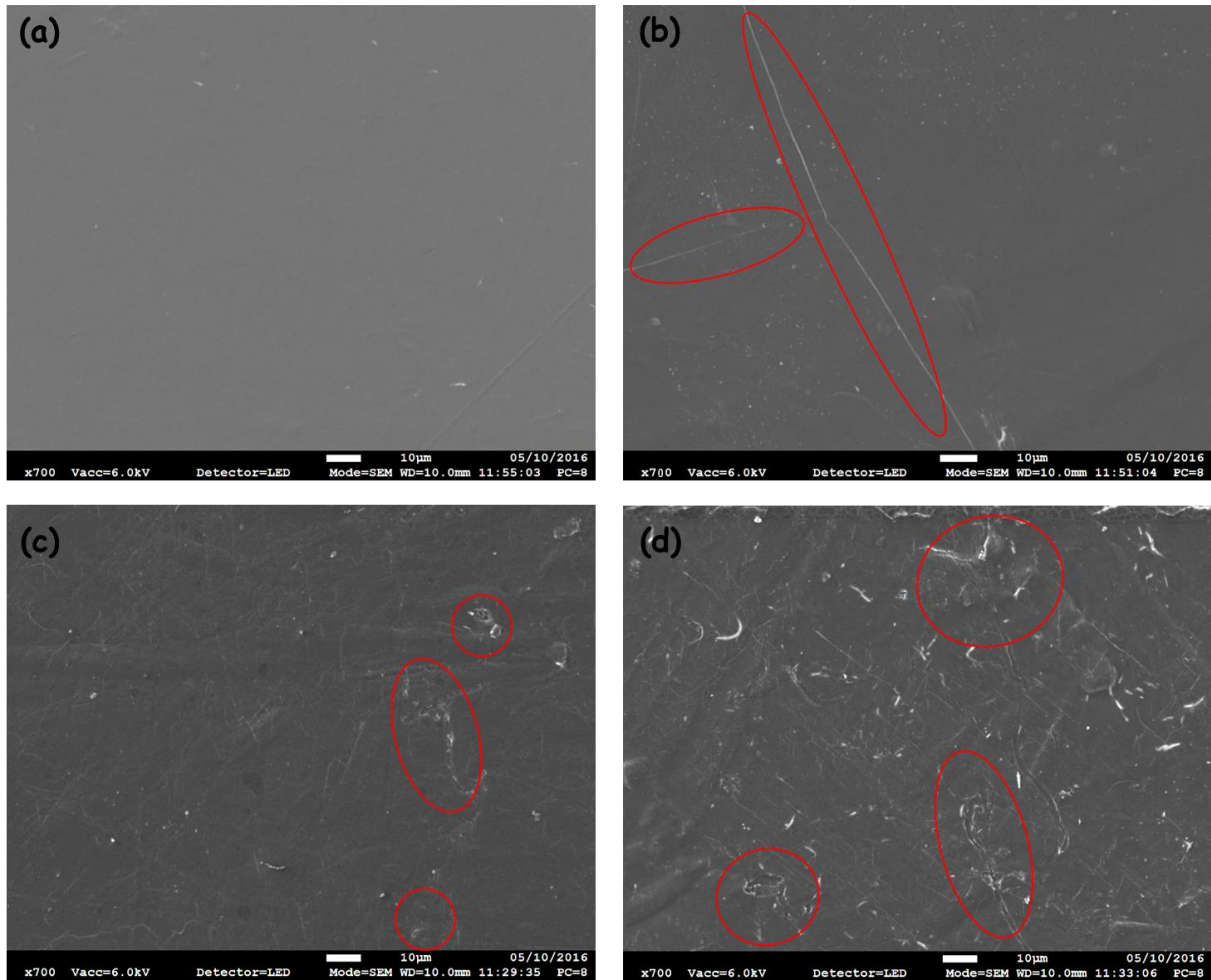


Figure 40: SEM pictures obtained for unaged PLA (a), 60 d aged under T/UV (b), T/RH (c) and T/UV/RH (d) conditions.

1.3. Color changes

The “bleaching” of PLA evidenced when submitted to environmental constraints is not in accordance with data reported in literature. Indeed, as described in chapter I (p.44), ageing of PLA usually leads to a “yellowing” of the material [28, 34, 35, 129].

Hence, in order to quantify the color changes during ageing, $L^*a^*b^*$ measurements were performed on PLA plates before and after 60 days ageing under T/UV, T/RH and T/UV/RH conditions. Results reported in **Table 10** typically show an evolution of the color of the plates during ageing. In fact, ΔE , which represents the difference between two colors, is 7.5 after 60 days exposure to T/UV and reaches 12.7 and 17.5 after 60 days exposure to T/RH and T/UV/RH respectively. L^* , which represents the lightness of color, increases from 52.0 before ageing to 58.8, 64.4 and 69.4 for PLA aged for 60 days under T/UV, T/RH and T/UV/RH respectively. The increase in both ΔE and L^* values indicates that plates become whiter after ageing, which corroborates the “bleaching” phenomenon. For a^* which represents the color between red/magenta and green, values vary from -2.1 for PLA before ageing to -1.9, -1.6 and -1.3 for

PLA aged for 60 days under T/UV, T/RH and T/UV/RH respectively. Concerning b^* , which represents the color between yellow and blue, values increase from -1.0 to -4.0, -3.4 and -2.8 after 60 days ageing under T/UV, T/RH and T/UV/RH conditions, respectively. Due to the relatively low values of a^* and b^* , no conclusion can be drawn. Indeed, generally, a^* and b^* coordinates are close to zero for neutral colors (i.e. white and grey).

*Table 10: $L^*a^*b^*$ values of unaged and 60 days aged PLA under T/UV, T/RH and T/UV/RH conditions.*

$L^*a^*b^*$ values	PLA	PLA T/UV 60 d	PLA T/RH 60 d	PLA T/UV/RH 60 d
L^*	52.0	58.8 (+6.8)	64.4 (+12.4)	69.4 (+17.4)
a^*	-2.1	-1.9 (+0.2)	-1.6 (+0.5)	-1.3 (+0.8)
b^*	-1.0	-4.0 (-3.0)	-3.4 (-2.4)	-2.8 (-1.8)
ΔE	-	7.5	12.7	17.5

Hence, $L^*a^*b^*$ permits to quantify the change in PLA color when exposed to T/UV, T/RH and T/UV/RH conditions and then corroborates the “bleaching” of materials. However, one can notice that this “bleaching” phenomenon do not support literature which mainly report a “yellowing” of PLA during ageing [28, 34, 35, 129]. This case provides an excellent example of the complexity of the problem of quantifying for color changes. It is possible that the difference observed against literature is due to the experimental parameters used during ageing exposure (kind of device, light ...). As an example, exposure to one light source may cause principally bleaching and another, yellowing. Generally, exposure to the Xenotest apparatus source results in increased yellowing. A fluorescence blue light, with radiation peaked at 420 nm results chiefly in bleaching. Sunlight, which contains both ultraviolet and visible radiation, also results in bleaching [188].

Results obtained by digital microscopy, SEM and $L^*a^*b^*$ measurements demonstrate that whatever ageing conditions, visual impacts of ageing on PLA are similar (i.e. bleaching and cracking), but dependent on the external stimuli applied to the polymer. Indeed, the effects of ageing on the visual appearance of PLA are more pronounced when exposed to T/UV/RH than when exposed to T/RH and T/UV conditions. As it was demonstrated that ageing impacts the appearance of PLA, it is now necessary to understand what can be the effects of T/UV, T/RH and T/UV/RH exposure on the physico-chemical properties of PLA. In fact, these latter are responsible for the integrity of the material during its lifetime.

2. Physico-chemical properties after ageing

This part details the impact of ageing on the physico-chemical properties of PLA, especially through the number average molecular mass (M_n), the thermal properties such as T_g and T_m as well as the crystallinity. These properties are investigated until 125 days of ageing under T/UV, T/RH and T/UV/RH conditions.

2.1. Impact of ageing on molecular mass

PLA, like many other polyesters, is known to be extremely sensitive to ageing conditions, leading to hydrolysis [5, 31, 125, 153] or photo-oxidation [27, 29, 33, 34]. These reactions involve the scission of ester bonds, leading to the decrease of the number average molecular mass (M_n) of the material. Thus, M_n was studied as a function of ageing exposure using gel permeation chromatography (GPC). The evolution of M_n and polydispersity index (PI) as a function of time for different ageing conditions is plotted in **Figure 41** and data are reported in **Table 11**.

Table 11: M_n and polydispersity index (PI) data as a function of ageing of PLA exposed to T/UV, T/RH and T/UV/RH conditions.

Exposure time (days)	T/UV M_n (g/mol)	T/UV PI	T/RH M_n (g/mol)	T/RH PI	T/UV/RH M_n (g/mol)	T/UV/RH PI
0	68000	1.8	68000	1.8	68000	1.8
5	64600 (-5%)	1.7 (-0.1)	64250 (-6%)	1.7 (-0.1)	61600 (-11%)	1.8
15	61200 (-10%)	1.6 (-0.2)	59500 (-13%)	1.6 (-0.2)	51400 (-24%)	1.7 (-0.1)
30	57600 (-15%)	1.6 (-0.2)	52100 (-23%)	1.7 (-0.1)	39300 (-42%)	1.8
45	52100 (-23%)	1.7 (-0.1)	42000 (-38%)	1.7 (-0.1)	30950 (-54%)	1.8
60	47000 (-31%)	1.7 (-0.1)	34200 (-50%)	1.7 (-0.1)	21500 (-68%)	1.9 (+0.1)
75	44000 (-35%)	1.8	30300 (-56%)	1.8	15900 (-77%)	1.9 (+0.1)
90	38600 (-43%)	1.7 (-0.1)	25300 (-63%)	1.8	9100 (-87%)	1.8
105	33400 (-51%)	1.8	22600 (-67%)	1.7 (-0.1)	5100 (-92%)	1.9 (+0.1)
125	30000 (-66%)	1.7 (-0.1)	21500 (-71%)	1.8	3200 (-95%)	1.9 (+0.1)

It appears that M_n decreases as a function of time for all samples (**Figure 41 (a)** and **Table 11**). In fact, M_n decreases from 68000 g/mol before ageing to 30000 g/mol (-66%), 21500 g/mol (-71%) and 3200 g/mol (-95%) after 125 days ageing in T/UV, T/RH and T/UV/RH conditions, respectively. This drop of M_n suggests that chain scission mechanism is largely predominant during ageing under T, UV and/or RH. One can notice that the degradation of PLA does not exhibit an induction period, i.e. that the hydrolysis and/or photo-oxidation start as soon as the sample is exposed to ageing constraints. Moreover, these results indicate that the decrease of M_n is even more pronounced when UV is combined with T and RH compared to T/RH and T/UV.

The polydispersity index of PLA (**Figure 41 (b)**) is independent of ageing conditions, as it remains stable between 1.6 and 1.9. This result indicates that chain scissions occur randomly along the polymer macromolecules under hydrolysis and/or photo-oxidative conditions [124, 127, 189] and suppose the fact that degradation is homogeneous through the plates.

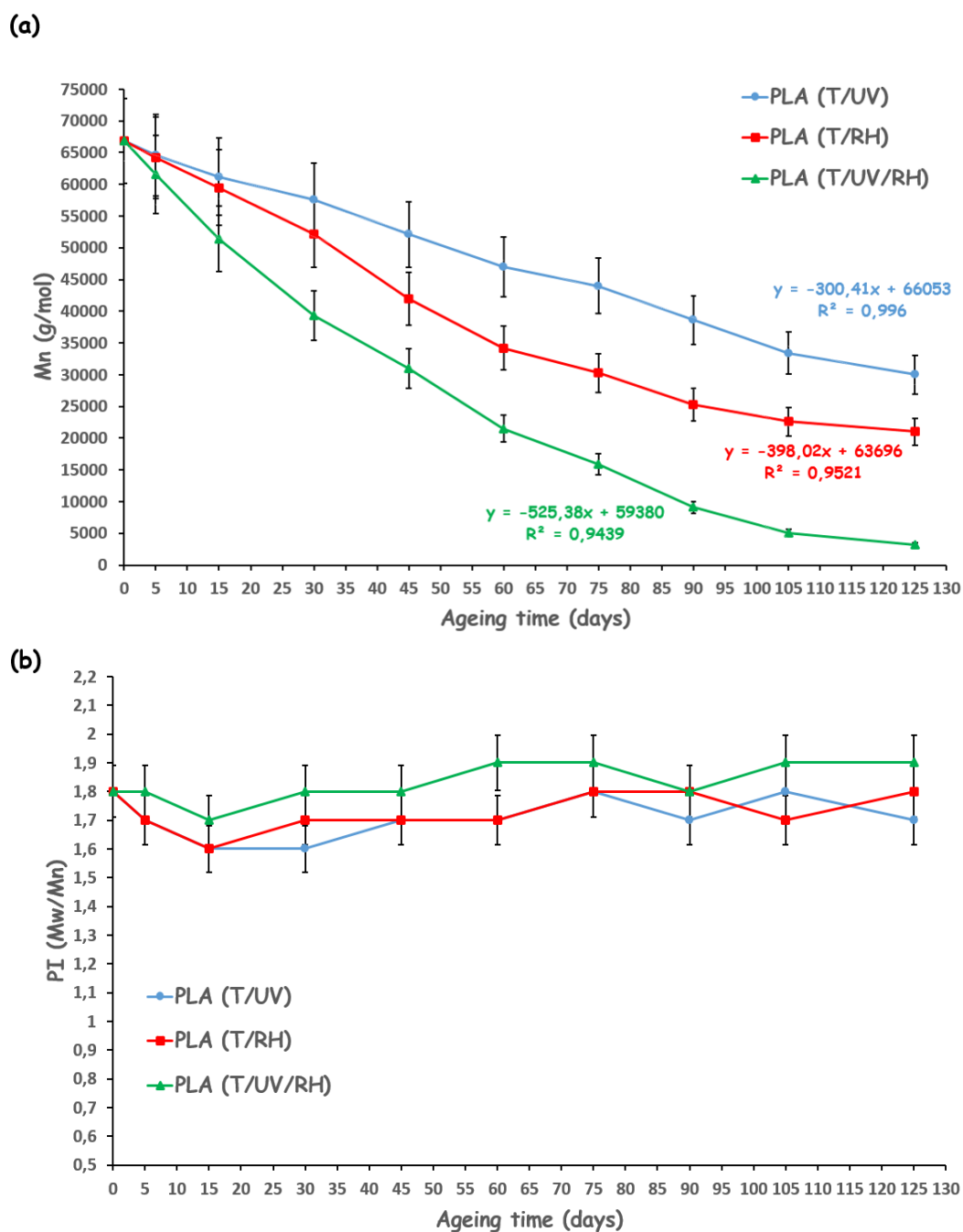


Figure 41: M_n (a) and polydispersity index PI (b) versus ageing time of PLA samples aged under T/UV (●), T/RH (■) and T/UV/RH (▲) conditions.

According to previous observations concerning PI, the drop of M_n observed in **Figure 41 (a)** is attributed to a chain scission process: indeed if depolymerisation process had occurred at the same time, it would have caused a remarkable PI increase, which is clearly not the case in this study.

The number of PLA chain scission (n_t) as a function of time and ageing conditions (**Figure 42**) determined according to **Equation 26 (p.78)**, increases as a function of ageing time. This

phenomenon depends on the ageing conditions: it is even more pronounced for PLA aged under T/UV/RH conditions compared to T/RH and T/UV.

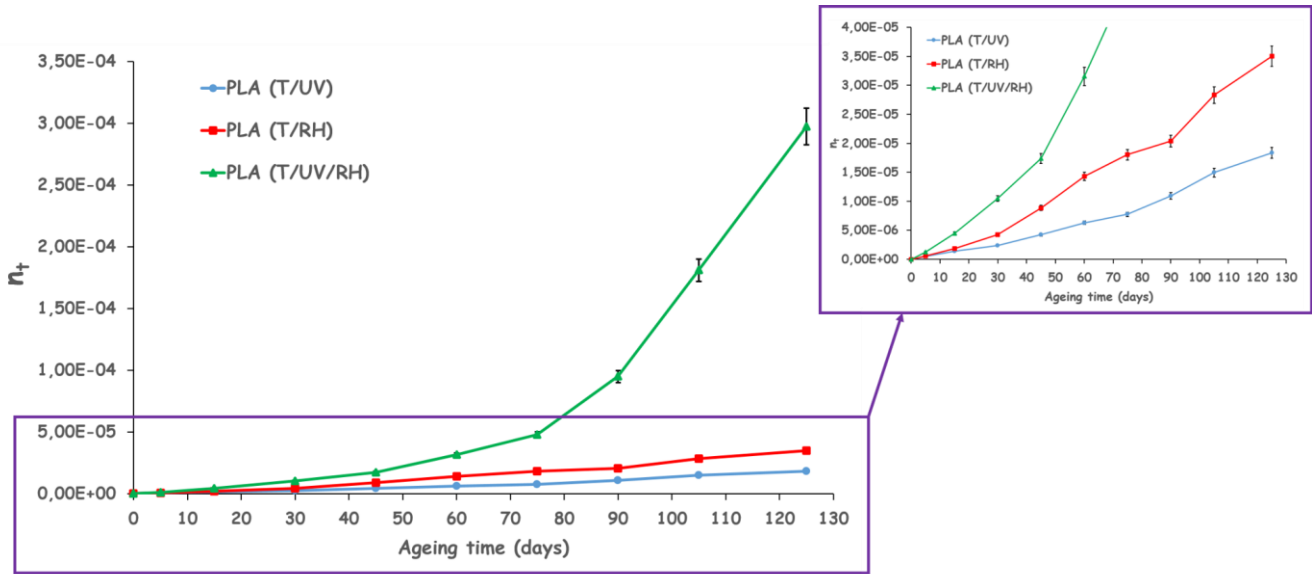


Figure 42: Average number of random chain scissions per unit mass (n_t) for PLA as function of ageing time for different ageing conditions; T/UV (●), T/RH (■) and T/UV/RH (▲).

Many studies led on PLA reveal that chain scission occurring during degradation leads to the formation of carboxylic acid, which is reported to be responsible for an autocatalysis process [5, 31, 125, 150, 153]. Indeed, autocatalysis occurs when the reaction product of degradation is itself the catalyst for the same reaction [151]. In the case of PLA, carboxylic acids formed during degradation are retained within the material, causing a localized decrease in pH which accelerates the rate of degradation and induces a sudden loss of the structural integrity of the material [152, 153]. Taking this into consideration, the behavior of n_t (Figure 42) indicates an increase in the number of chains broken during ageing, thus increasing the formation of secondary products such as carboxylic acid in the medium. These ones are thus able to promote the auto accelerated character of the degradation, which is in agreement with literature [123, 128, 153]. In addition, the combination between UV, T and RH accelerates the degradation of PLA. Indeed, under T/UV/RH n_t is around 3.2×10^{-5} after 60 days against 1.7×10^{-5} and 6.3×10^{-6} under T/RH and T/UV, respectively.

Investigations led by GPC reveal that the molecular mass of PLA decreases when the material is submitted to T/UV, T/RH and T/UV/RH exposure. Moreover, it is evidenced that this behavior depends on the ageing conditions. Indeed, the decrease of M_n is even more important for PLA aged under combination of T, UV and RH compared to T/RH and T/UV. It is well known that the decrease of molecular mass of PLA due to chain scission is followed by a decrease of the thermal properties of the material [29, 33, 38, 121, 123, 157]. Hence, the evolution of thermal properties versus ageing is studied in the following section, using thermogravimetric analysis (TGA) and differential scanning calorimetry (DSC).

2.2. Thermal behavior

2.2.1. Thermogravimetric analysis

The thermal stability of PLA as a function of ageing was evaluated using TGA. Data collected from the TGA of PLA aged under T/UV, T/RH and T/UV/RH exposure are reported in **Table 12**: the onset temperature ($T_{10\%}$) corresponding to 10 wt.-% degradation of the material, the temperature corresponding to its maximum rate of degradation (DTG), and the residual weight obtained at 800°C are considered in this table.

Table 12: TGA data (10°C/min under air) obtained after ageing of PLA exposed to T/UV, T/RH and T/UV/RH conditions.

Exposure / time	$T_{10\%}$ (°C)	Max DTG (°C)	Residual weight (%)
0 d	332	358	0
T/UV 125 d	322 (-10)	355 (-3)	0
T/RH 125 d	300 (-32)	347 (-11)	0
T/UV/RH 125 d	279 (-53)	337 (-21)	0

Unaged PLA decomposes in one step from 280°C (**Figure 43**) and shows a maximum temperature of degradation at 358°C with no residue left at 800°C. Aged PLAs also decompose in one step and lead no residue as well. However, it appears that the onset temperature of degradation ($T_{10\%}$) decreases upon ageing. Indeed, $T_{10\%}$ decreases from 332°C before ageing to 322°C, 300°C and 279°C after 125 days ageing under T/UV, T/RH and T/UV/RH exposure, respectively. The DTG also decreases after ageing, from 358°C to 355°C, 347°C and 337°C after 125 days under T/UV, T/RH and T/UV/RH, respectively.

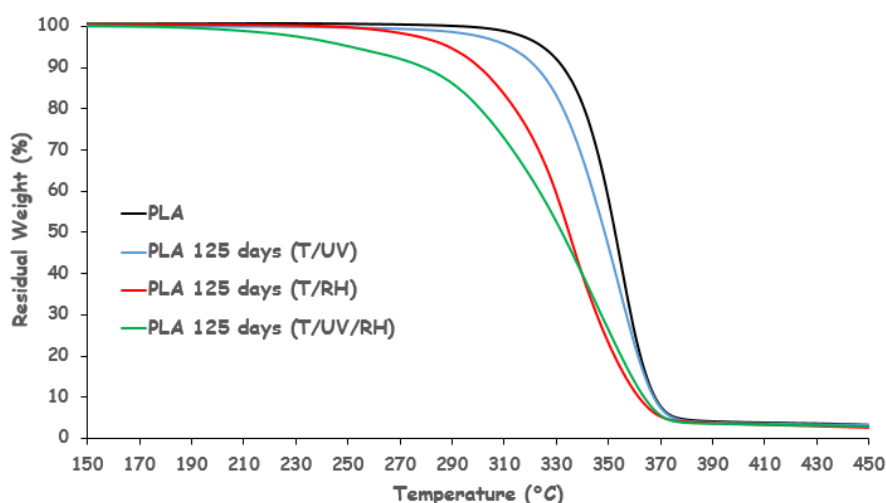


Figure 43: TGA curves as a function of time for unaged PLA (-), T/UV (-), T/RH (-) and T/UV/RH (-) 125 days aged (10°C/min under air).

This decrease in onset temperature of degradation could be linked to the decrease in molecular mass occurring during hydrolysis and photo-oxidation [174]. Indeed, the thermal stability of PLA depends on the strength of its bonds. If the molecular mass decreases, it creates new species with thermally weak bonds (e.g. hydroperoxides, carboxylic acids and peroxides). These ones can quicker initiate the thermal degradation and then decrease the thermal stability of PLA [174, 190-192]. Overall, TGA investigations demonstrate that ageing decreases the thermal stability of PLA until 125 days. This phenomenon depends on the ageing conditions. Indeed, the decrease of thermal stability is reported to be more significant under T/UV/RH exposure compared to T/RH and T/UV. Under T/UV exposure, thermal stability is only slightly affected.

2.2.2. Glass transition and melting temperature

The thermal properties of PLA before and after ageing were also evaluated by DSC. The DSC data of PLA aged until 125 days under T/UV, T/RH and T/UV/RH conditions were compared to those obtained for non-aged PLA. The glass transition temperatures (T_g) and melting temperatures (T_m) are listed in **Table 13**.

It appears that both T_g and T_m are affected by ageing (**Figure 44**, **Figure 45** as well as **Table 13**). In fact, T_g decreases from 61.5°C to 58.8°C (-2.7°C), 57.4°C (-4.1°C) and 30.2°C (-31.3°C) after 125 days under T/UV, T/RH and T/UV/RH conditions, respectively. T_m decreases from 160.2°C to 158.4°C (-1.8°C), 156.2°C (-4°C) and 122.3 (-37.9°C), after 125 days under T/UV, T/RH and T/UV/RH conditions, respectively.

Table 13: DSC data of PLA reported as a function of ageing exposure to T/UV, T/RH and T/UV/RH conditions.

Ageing exposure (days)	T/UV T_g (°C)	T/UV T_m (°C)	T/RH T_g (°C)	T/RH T_m (°C)	T/UV/RH T_g (°C)	T/UV/RH T_m (°C)
0	61.5	160.2	61.5	160.2	61.5	160.2
15	61.1	160.2	61.1	160.1	61.0	159.9
30	61.0	159.9	60.9	159.7	60.8	159.7
45	61.0	159.4	60.8	158.5	59.9	158.2
60	60.9	158.9	59.9	158	58.9	157.1
75	60.7	158.7	59.5	157.9	55.5	154.4
90	60.4	158.9	59.4	157.4	45.5	150.6
105	59.8	158.9	58.1	156.6	40.7	129.9
125	58.8	158.4	57.4	156.2	30.2	122.3

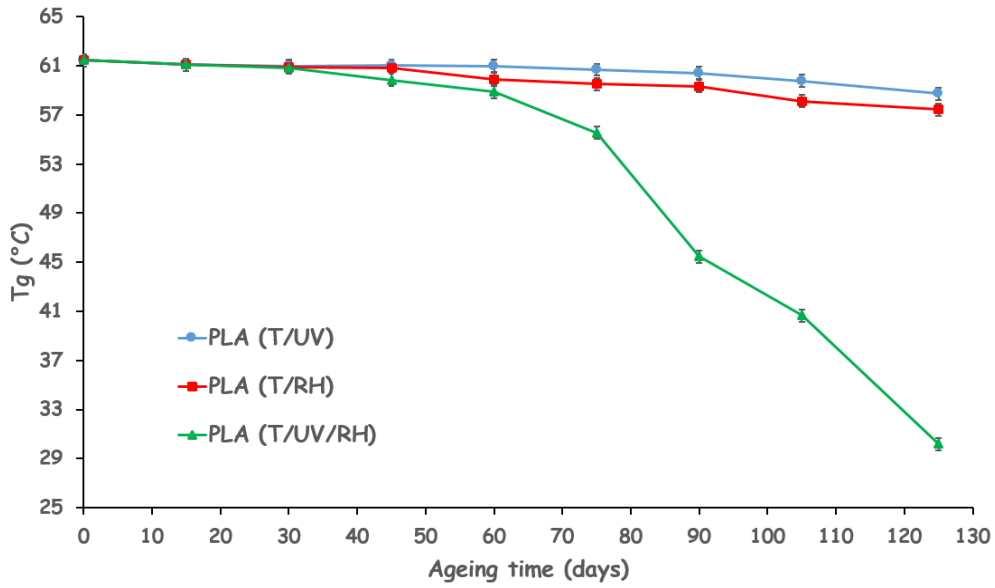


Figure 44: Evolution of glass transition temperature (T_g) of PLA as a function of exposure to T/UV (●), T/RH (■) and T/UV/RH (Δ) conditions.

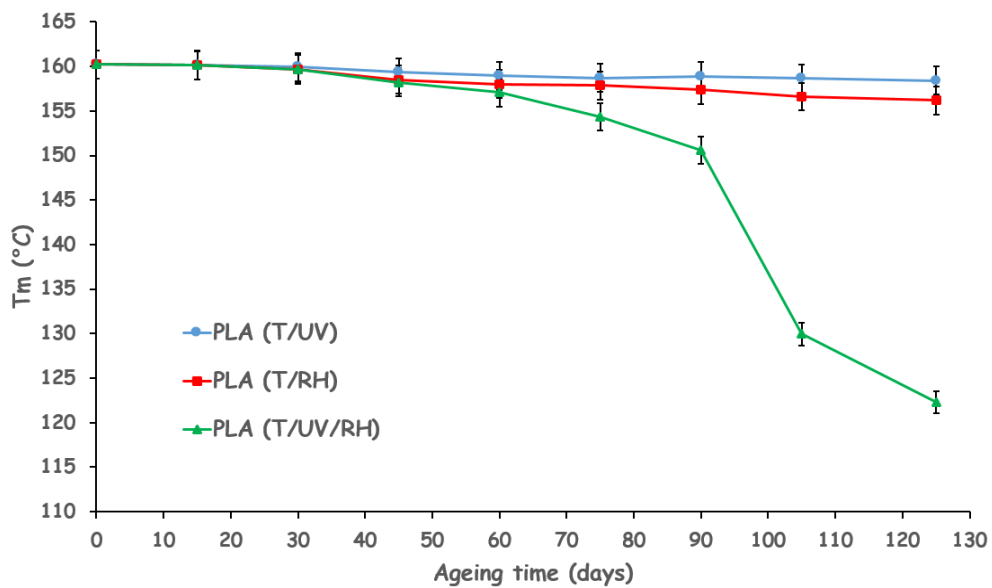


Figure 45: Evolution of melting temperature (T_m) of PLA as a function of exposure to T/UV (●), T/RH (■) and T/UV/RH (Δ) conditions.

As evidenced it appears that both T_g and T_m of PLA are only slightly affected when the material is exposed to T/UV or T/RH for 125 days. However, in the case of exposure to T/UV/RH, the decrease of both T_g and T_m is quite obvious. After 125 days under T/UV and T/RH exposure, PLA matrix is certainly not sufficiently degraded as under T/UV/RH to observe the same decrease of its thermal properties (i.e. T_g and T_m). Hence, to confirm this assumption, investigations were led on the impact of the molecular mass on the behavior of thermal properties during ageing.

It is well known that M_n has a direct influence on the T_g of a polymer [29, 32]. In fact, in the case of linear polymers, T_g and M_n are linked according to the Fox and Flory relationship (**Equation 30**), where k (K.kg.mol^{-1}) is the Fox-Flory constant and $T_{g,\infty}$ the glass transition temperature of PLA having an infinite molar mass.

$$T_g = T_{g,\infty} - k/M_n$$

Equation 30

Thus, if the degradation of PLA under T/UV, T/RH and T/UV/RH exposure fits this equation, when the molecular mass of the material decreases, the T_g should decrease too. Hence, T_g of PLA was plotted against M_n for the three ageing conditions (**Figure 46**). It appears that the decrease of T_g as a function of M_n is quite stable during exposure to T/UV and T/RH conditions. However, in the case of T/UV/RH exposure, the drop of T_g is obvious from $M_n \pm 20000$ g/mol.

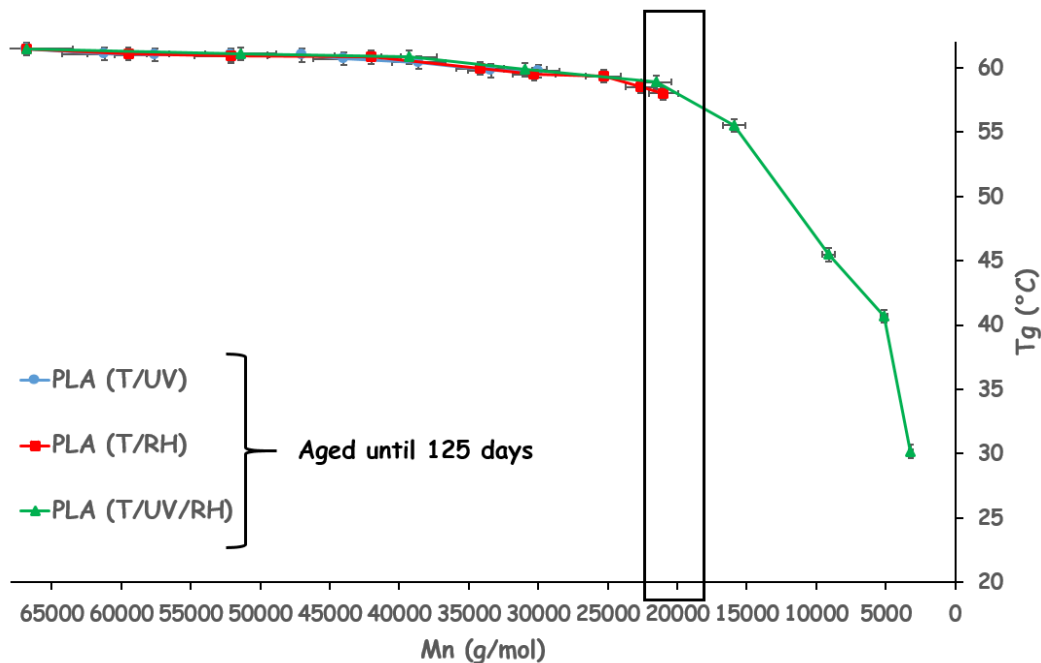


Figure 46: T_g as a function of M_n for PLA aged under T/UV (\bullet), T/RH (\blacksquare) and T/UV/RH (\blacktriangle) exposure.

This suggests that the drop of T_g occurs from a critical M_n of approximately 20000 g/mol. The term of critical molecular mass (M_c) is considered as a characteristic parameter for any polymer as an indicator of entanglement [193-195]. Indeed, the concept of entanglement in polymer system is commonly accepted to interpret viscoelastic properties of high molecular weight polymers. An important parameter for entangled macromolecules is the average molecular mass spacing between entanglement junctions, i.e. the entanglement molecular mass M_e or the critical molecular mass M_c , where some polymer properties of viscoelastic nature are changed. Both M_c and M_e are interrelated according to **Equation 31**:

$$M_c = 2.M_e$$

Equation 31

The value of M_c is considered as a characteristic parameter for any polymer, as a kind of “passport number”. Entanglement behavior of polymers is correlated with parameters of their molecular geometry. The M_c parameter denotes the transition from which the material becomes fragile, starting to lose its structural integrity [193-195]. This critical molecular mass reported at 20000 g/mol for PLA is in accordance with the literature [66, 196-199]. Indeed, many researchers reported a M_e of ± 9000 g/mol which evidences a M_c of ± 18000 g/mol according to **Equation 31**.

Hence, results reported in **Figure 46** evidenced that after 125 days of ageing under T/UV/RH the critical M_n of PLA is reached, leading to the rapid degradation of PLA. Due to this low M_n , the mobility of the polymer chain is really high, explaining why the T_g of the material decreases. After 125 days exposure to T/UV/RH, both M_n and T_g of PLA reach very low values, i.e. 3200 g/mol and 30.2°C, respectively. Taking into account this critical molecular mass around 20000 g/mol, PLA is not sufficiently degraded under T/UV (30000 g/mol) and T/RH (21500 g/mol) even after 125 days, to start the complete loss of its properties. It appears that T_m follows the same evolution as T_g during ageing. The high mobility of the polymer chain under T/UV/RH exposure affects the backbone flexibility and intermolecular interactions, leading to the decrease of T_m . [38]. As for T_g , PLA is not sufficiently degraded under T/UV and T/RH exposure, even after 125 days, to start the decrease of T_m .

As expected, it was demonstrated that the degradation of the polymer, due to random chain scission, leads to a decrease of the molecular mass of the material. The polymer chains are broken into smaller units, thus leading to a decrease of some properties such as glass transition and melting temperature of the material. Generally this decrease of thermal properties also leads to changes in crystallinity (e.g. increase/decrease of crystallinity, formation of new crystal-forms ...) [5, 26, 38, 127, 157]. Hence, the next section is dedicated to the crystallization behavior of PLA after ageing.

2.3. Effect of ageing on crystallization behavior

As mentioned in the state of the art, PLA can be either amorphous or semi-crystalline, depending on its stereochemistry and thermal history [5, 52]. In the case of a semi-crystalline material, PLA can crystallize into three forms, i.e., α , β and γ . The evolution of the crystallinity (χ) of PLA as a function of ageing for the three ageing conditions was measured by DSC according to **Equation 3 (p.33)**. Data are reported in **Table 14** and **Figure 47**. First observation is that the PLA used in this study is almost amorphous with a relatively low crystallinity of about 6.5%.

Table 14: Crystallinity of PLA as a function of ageing duration under T/UV, T/RH and T/UV/RH exposure.

Ageing time (days)	χ (%) – T/UV	χ (%) – T/RH	χ (%) – T/UV/RH
0	6.5	6.5	6.5
15	7.4 (+0.9)	8.1 (+1.6)	13 (+6.5)
30	9 (+2.5)	10.6 (+4.1)	16.5 (+10)
45	10.5 (+4)	15.1 (+8.6)	28.7 (+22.2)
60	12.3 (+5.8)	19.8 (+13.3)	37.8 (+31.3)
75	16.1 (+9.6)	21.3 (+14.8)	41.3 (+34.8)
90	14.8 (+8.3)	22.3 (+15.8)	43.5 (+37)
105	17.4 (+10.9)	24.5 (+18)	46.7 (+40.2)
125	19.8 (+14.3)	30.1 (+23.6)	52.9 (+46.4)

It is evidence that crystallinity increases when PLA is exposed to T/UV, T/RH and T/UV/RH. Indeed, crystallinity is enhanced by 14.3% and 23.6% after 125 days exposure to T/UV and T/RH, respectively. However, the most significant increase is observed for PLA aged under T/UV/RH conditions, where 52.9% of crystallinity is achieved after 125 days. The higher crystallinity of PLA after ageing is related to a high state of degradation of the material [5, 26, 27, 29, 38, 157]. Hence, the high crystallinity value reported after 125 days exposure to T/UV/RH, indicates that this kind of exposure is more detrimental for the lifetime of PLA compared to T/RH and T/UV conditions. This relationship between crystallinity and degradation is further developed in this section.

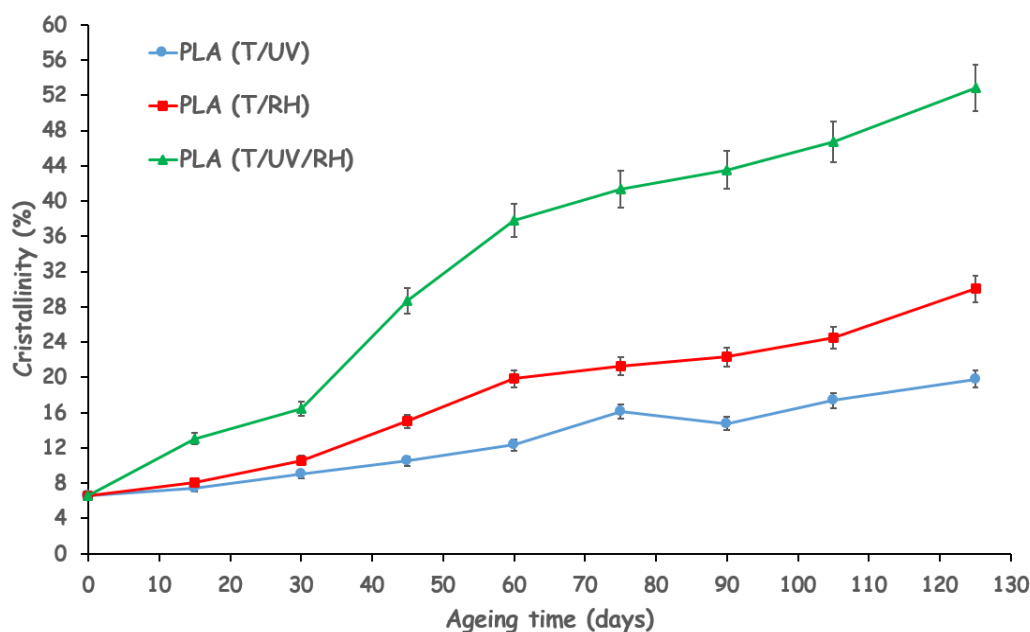


Figure 47: Evolution of crystallinity of PLA as a function of ageing time, for T/UV (●), T/RH (■) and T/UV/RH (△) exposure.

To support these results and determine the kind of crystalline form of PLA, FTIR analyses were performed on thin films (± 0.1 mm) of PLA aged under T/UV, T/RH and T/UV/RH conditions, similarly to the plates. FTIR is one of the simplest ways to evidence the evolution of the crystallinity of a polymer. Indeed, the bands at 870 cm^{-1} and 950 cm^{-1} are assigned to the amorphous phase of PLA, whereas the ones at 755 cm^{-1} and 694 cm^{-1} are linked to the crystalline phase [161, 200]. Moreover, some studies report that during crystallization of PLA, the intensity of the band located at 950 cm^{-1} decreases and a new one appears at 918 cm^{-1} , linked to the formation of crystals [200, 201]. FTIR analyses were performed until 60 days since it was enough to evidence the evolution of the crystallinity. Moreover, after 60 days exposure to T/UV, T/RH and T/UV/RH conditions, films exhibit the same M_n as those of 60 days aged plates, reported in **p.90**. Visually, films exposed to T/UV, T/RH and T/UV/RH conditions show the same behavior as the plates (**p.86**).

FTIR results obtained for PLA before and after ageing are presented in **Figure 48**. For the three spectra, peak observed at 950 cm^{-1} corresponds to the $\delta_{\text{asym}}\text{CH}_3 + \nu\text{C-C}$. The one at 918 cm^{-1} is linked to the rCH_3 . Peaks at 870 cm^{-1} , 755 cm^{-1} and 694 cm^{-1} correspond to $\nu\text{C-COO}$, $\delta\text{C=O}$ and νCH , respectively.

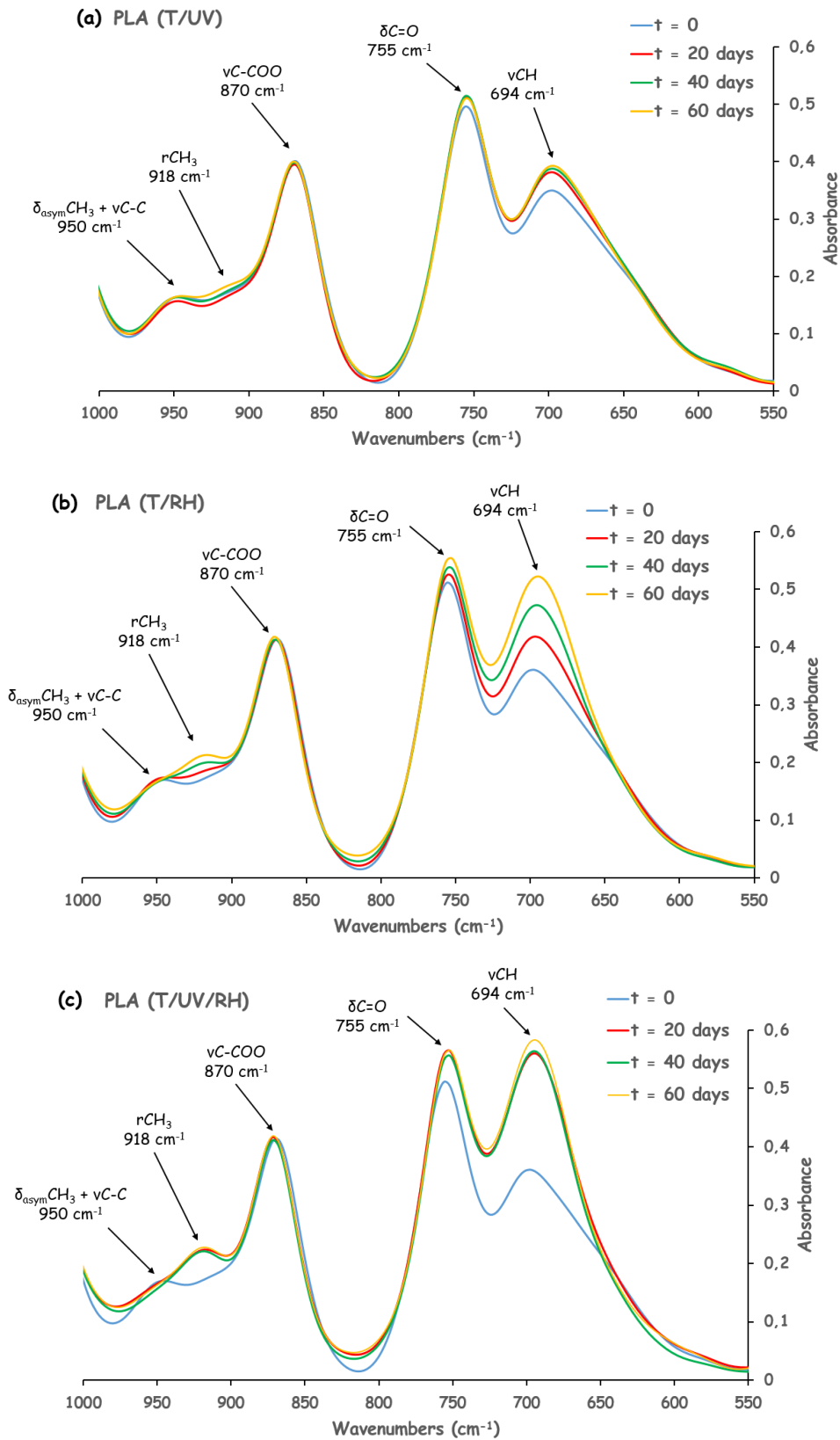


Figure 48: FTIR spectra as a function of ageing time for PLA aged under T/UV (a), T/RH (b) and T/UV/RH (c).

It is obvious that during ageing, the intensity of the band at 950 cm^{-1} decreases, whereas the one at 918 cm^{-1} increases, confirming the evolution from an amorphous phase to a crystalline one. Moreover, the intensity of the two bands at 694 and 755 cm^{-1} increases too, referring to the formation of new crystals in the polymer. This phenomenon quickly appears when PLA is aged under T/UV/RH compared to T/RH and T/UV. However, in the case of T/UV exposure, the formation of crystalline phase seems to be very low. These results are in accordance with the ones reported by DSC where crystallinity is enhanced by 14.3%, 23.6% and 52.9% after 125 days exposure to T/UV, T/RH and T/UV/RH, respectively.

The $r\text{CH}_3$ mode at 918 cm^{-1} is assigned to the 10_3 helix conformation of the α -form crystals [30, 65, 161]. This can demonstrate that during ageing the PLA used in this study crystallizes into α -form. However, this FTIR characteristic band is also present in the spectrum of α' -form crystal [161, 202]. Recently Zhang et al. [202, 203] evidenced the existence of an α' crystal form, considered as a distorted α -form, with a 10_3 helix conformation but with a different lateral arrangement than the one of the α form [161]. In order to determine in which crystalline form PLA crystallizes during ageing, XRD experiments were performed.

The wide-angle X-ray diffraction (WAXD) patterns obtained by XRD (**Figure 49**) show that unaged PLA and PLA exposed to T/UV present a typical amorphous profile. Due to the relatively low crystallinity of this PLA (i.e. 6.5%, **Table 14**), the characteristic diffraction peaks of crystallized PLA are not observed. In the case of T/UV exposure, XRD corroborates the weak formation of crystals related to the band observed at 918 cm^{-1} by FTIR. However, new diffraction peaks appear at $2\theta = 16.6^\circ$ and 18.8° after ageing under T/RH and T/UV/RH conditions, with peaks of higher intensity for this last condition. This can be explained by an increase in crystallinity and the formation of new crystals structure. According to literature [202, 203], reflection observed at $2\theta = 16.6^\circ$ and 18.8° in the WAXD profiles of aged PLAs is typically characteristic of α' -form crystals. Indeed, in presence of α -form crystals, reflections at $2\theta = 16.6^\circ$ and 18.8° are also observed but with additional ones including $2\theta = 12.5^\circ$, 14.8° , 22.5° , 27.3° and 29.2° .

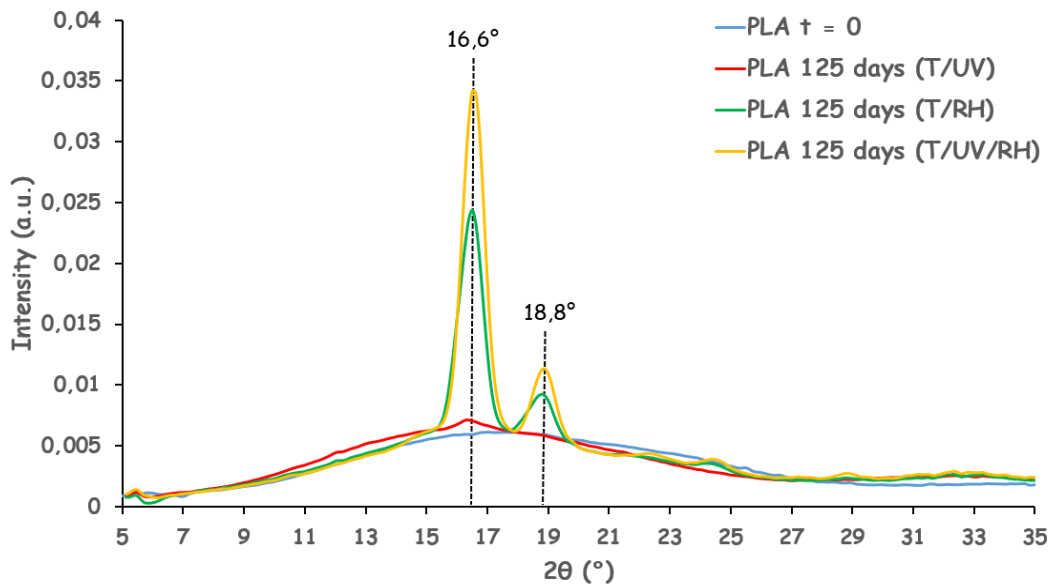


Figure 49: WAXD patterns of PLA obtained by XRD, before (●) and after 60 of ageing under T/UV (●), T/RH (●) and T/UV/RH (●).

In accordance with studies published on the crystallization behavior of PLA during ageing [5, 29, 38, 127], it was demonstrated by DSC, FTIR and XRD that exposure to T/UV, T/RH and T/UV/RH conditions has a direct influence on the crystallization of PLA. Indeed, an increase in crystallinity occurs during ageing, with the formation of α' -form crystals. These phenomena depend on the ageing conditions: whereas it is quite obvious for PLA aged under T/UV/RH and T/RH conditions, the crystallinity is only slightly increased when exposed to T/UV conditions and no formation of new crystalline structures is evidenced. Indeed, the degradation of the material under T/UV exposure is certainly not sufficient after 125 days to achieve high crystallinity and α' -form crystals structure. Hence, the impact of ageing on crystallization is more important when PLA is aged under T/UV/RH, followed by T/RH and T/UV, respectively. This increase in crystallization can be explained by the following mechanisms:

- When submitted to hydrolysis, the amorphous phases of PLA are more susceptible to be degraded than crystalline phases, leading to an increase in crystallinity. In fact, chain scissions occurring in amorphous phase of PLA produce low molecular chains which can integrate crystalline phase if they have sufficient mobility. Indeed, they can rearrange easier and thus giving crystallites leading to a weakening of the system. Thus, an increase in crystallinity of the material occurs. This phenomenon is well known in literature and called “chemi-crystallization” [5, 29, 38].
- Literature reports that when submitted to photo-oxidation, on the contrary to hydrolysis, PLA chains are photodegradable in both crystalline and amorphous regions. Although PLA chains are photodegradable even in crystalline regions, their photo-degradability is higher in the amorphous regions [27, 204]. This is why as well as during hydrolysis, it leads to an increase in crystallinity of PLA. However, it appears that the increase of crystallinity is much lower than in the case of T/RH

exposure. As reported by Fayolle et al. [204], one possibility to explain this difference is that radiochemical events occurring into the crystalline phase induce a decrease of the crystallinity ratio which can compensate, at least partially, the effect of chemi-crystallization. However, in presence of oxygen, the radiochemical yield of crystal destruction is low compared to the crystallization yield, so crystallization is observable. Another assumption to explain this difference is that the kinetics of degradation and thus of crystallization of PLA is lower in the case of T/UV compared to T/RH exposure.

- The combination between T/UV/RH leads to a faster degradation of the material and thus the chemi-crystallization effect is more significant, explaining the higher crystallization after 125 days of ageing compared to T/UV and T/RH exposure.

2.4. Conclusion

It has been demonstrated in this part that ageing affects PLA during its service lifetime. In fact, external stimuli applied on the material such as temperature, UV light or relative humidity have a direct influence on the physico-chemical properties of the material. Indeed, it was highlighted that during ageing:

- The molecular mass (M_n) of the material decreases
- The thermal stability decreases certainly due to the formation of thermally weak bonds during ageing.
- Both T_g and T_m of PLA decrease and this phenomenon occurs from a critical molecular mass around 20000 g/mol
- An increase in crystallinity is observed associated to the formation of α' -form crystals
- These phenomena depend on the ageing conditions. Indeed, the impacts of ageing are even more important for PLA aged under T/UV/RH compared to T/RH and T/UV.

These effects of ageing on the physico-chemical properties are in adequacy with the wide range of papers related to the ageing of PLA [29, 31, 33-35, 38, 121, 123, 153, 157-160, 162]. However, while the effects of ageing have been evidenced, mechanisms of degradation from which these phenomena arise, have to be elucidated. Especially because many different mechanisms have been proposed all over the years depending on the ageing conditions and duration. In this way, the next part of this chapter is dedicated to the understanding of mechanisms of degradation occurring during exposure to T/UV, T/RH and T/UV/RH.

3. Elucidation of the mechanisms of degradation

Depending on the external stimuli applied, many different types of mechanisms can cause degradation of PLA. Whereas literature reveals that hydrolysis is the main phenomenon occurring in presence of water [5, 29, 31, 38, 52, 121, 123, 125, 153, 160, 161], researches dealing with the photo-degradation mechanism of PLA are more contrasted. Indeed, photo-degradation is reported to occur via two distinct mechanisms which are (i) a Norrish II mechanism [27, 32, 33, 158, 159] and (ii) a radical mechanism [28, 29, 34, 35, 39]. In this regard, this section will investigate mechanisms occurring during ageing under T/UV, T/RH and T/UV/RH exposure.

3.1. Degradation under T/RH exposure

FTIR analyses were performed on thin films of PLA along exposure to T/RH in order to identify structural changes occurring during ageing (**Figure 50**). These investigations were performed at a resolution of 32 cm^{-1} . The spectra are classified into four distinct regions, corresponding to specific bands assignment: -OH stretch (3655 and 3671 cm^{-1} , **Figure 50 (a)**), -CH stretch (2877 , 2946 and 2997 cm^{-1} , **Figure 50 (b)**), -C=O ester carbonyl (1762 cm^{-1} , **Figure 50 (c)**), -OH bend (1060 cm^{-1}), -C-O stretch (1093 , 1130 , 1211 cm^{-1}), and -C=O bend (1257 cm^{-1}) and -CH- deformation (1367 , 1454 cm^{-1}) in **Figure 50 (d)**.

These four regions as well as the one between 1560 to 1680 cm^{-1} , corresponding to carboxylate ions (COO^-) (**Figure 50 (e)**), were chosen to follow PLA degradation versus ageing duration. In the -OH region (**Figure 50 (a)**), an increase in hydroxyl absorption is observed as function of ageing. In the case of the -C-H- stretch (**Figure 50 (b)**) no significant changes are observed between virgin and degraded samples. It appears that the band at 1762 cm^{-1} as well as the bands in the range 1090 - 1300 cm^{-1} are decreased during ageing. Indeed, those corresponding to -C=O and -C-O stretching ester respectively shift towards lower wavelength in range 1090 - 1300 cm^{-1} attributed to -C-O- stretching alcohol. One can notice the apparition of a new peak around 1630 cm^{-1} when PLA is aged (**Figure 50 (e)**), corresponding to carboxylate (COO^-), which can result from the hydrolysis of PLA ester bond [31]. A decrease of -OH band at 1060 cm^{-1} is also observed (**Figure 50 (d)**).

Confirming literature [5, 29, 31, 38, 52, 121, 123, 125, 153, 160, 161], observations done by FTIR analyses show that the degradation mechanism of PLA exposed to T/RH conditions is predominantly driven by an hydrolysis of ester linkage, which is accelerated by temperature (**Figure 51**) [29, 205]. As long as the polymer is exposed to this external stimulus, it absorbs water, resulting in hydrolysis of ester linkages and breaking down of long macromolecular chains. Thus, as previously described, this leads to the decrease of both molecular mass and thermal properties of the material, but also to an increase in the crystallinity of the polymer due to a "chemi-crystallization" process [5, 26, 38].

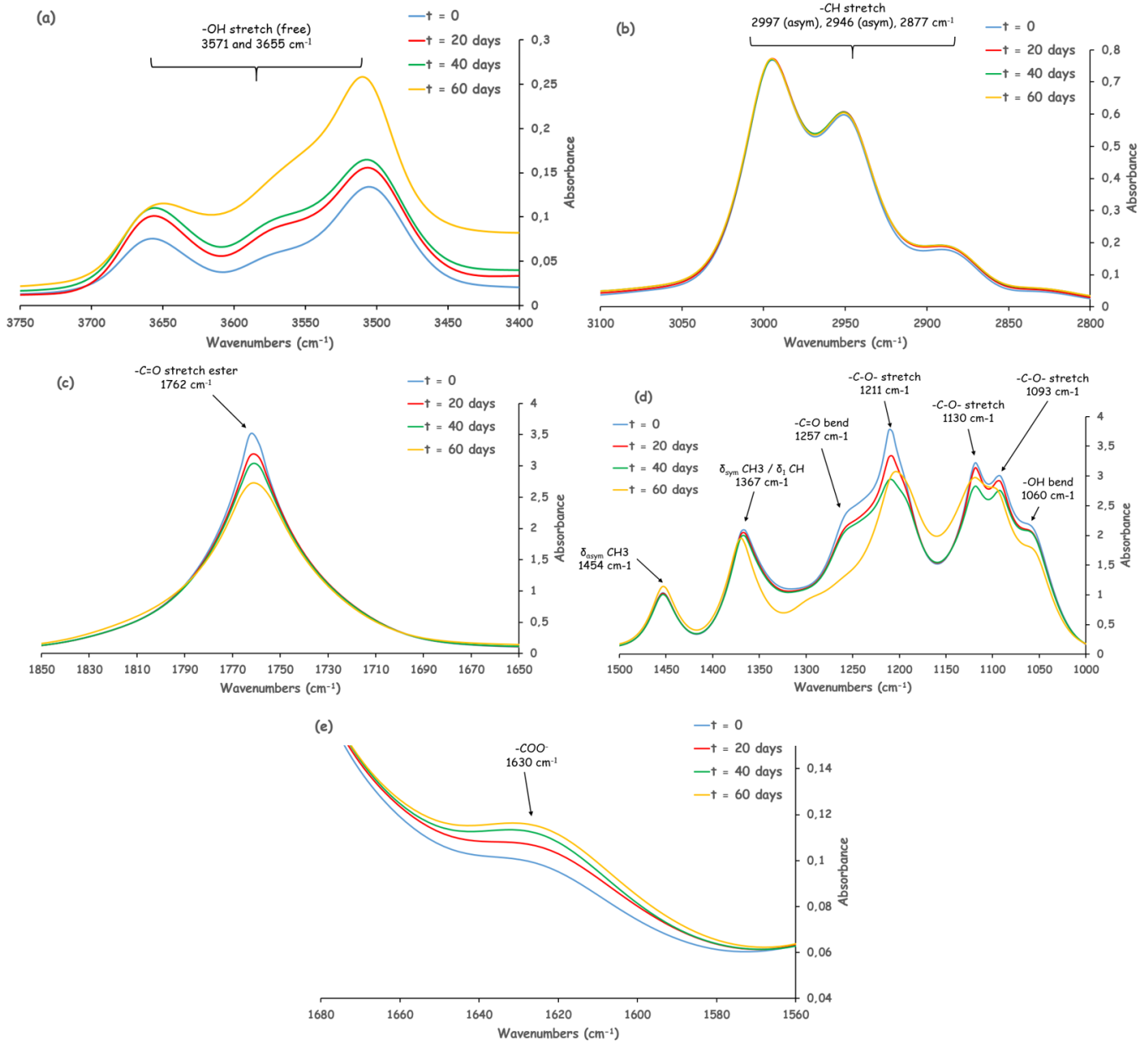


Figure 50: FTIR spectra of PLA before and after various ageing durations under T/RH conditions.

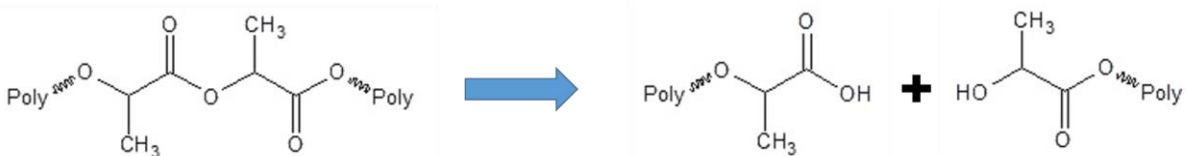


Figure 51: degradation of PLA by hydrolysis under T/RH exposure.

The hydrolysis of PLA has been reported to take place mainly in the bulk of the material rather than on the surface and has been assumed as an autocatalytic process when temperature increases [25, 123, 147, 148, 150, 152]. This phenomenon leads to random chain scission responsible for the decrease of the molecular mass of PLA. As previously reported in

Chapter I (p.52), autocatalysis occurs when the reaction product is itself the catalyst for the same reaction. In the case of PLA, carboxylic acid chains formed in the bulk during the degradation facilitate autocatalysis in the heart of the sample [152]. Moreover, the hydrolytic chain cleavage is known to proceed preferentially in amorphous regions, which, as previously explained, play a role on the crystallization of the polymer along ageing [5, 29, 38].

3.2. Degradation under T/UV and T/UV/RH exposure.

The effects of UV light on the degradation of PLA have been widely studied over the years [27-29, 32-35, 157-159]. Until now, two photo-degradation mechanisms of PLA have been evidenced, i.e. the Norrish II mechanism and a radical mechanism. These mechanisms depend on the UV irradiation wavelength. Indeed, Norrish II occurs when PLA is exposed to UV-rays under 300 nm whereas radical mechanism occurs in the range of 300 to 400 nm. In this study, PLA based materials are exposed to UV-rays in the range 300-400 nm, and thus the Norrish II mechanism does not seem to be the most probable one. Hence, the next part will investigate mainly the radical mechanism.

The radical mechanism involves the abstraction of a tertiary hydrogen from PLA chain, leading to the formation of radical species [34, 35]. Hence two techniques were investigated to prove the existence of this mechanism: Electron Paramagnetic Resonance Spectroscopy (EPR) and FTIR. EPR is known to be one of the most effective technique to detect and identify free radicals generated by a chemical system during UV irradiation. Secondly, FTIR was performed to identify secondary products formed during PLA irradiation.

3.2.1. Identification of radical species

EPR was firstly used to identify the radical species formed during exposure of PLA under T/UV and T/UV/RH conditions. The EPR spectrum displayed in **Figure 52** results from the irradiation of virgin PLA at room temperature in the range 300 to 400 nm. The measurements were carried out in situ while the sample was irradiated. This spectrum shows that the signal is centered at an effective g value of 2.0063, which is typical of carbon radical species close to an oxygen heteroatom [206, 207]. Moreover, the 4 lines splitting of the signal seem to indicate the presence of a biradical specie [208, 209].

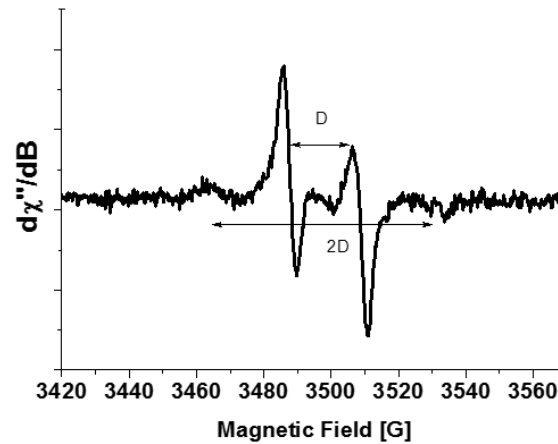


Figure 52: EPR spectrum of PLA irradiated with wavelengths between 300 and 400 nm at room temperature.

EPR analyses performed on PLA suggest that PLA degradation proceeds via a radical mechanism. In fact, it was demonstrated the formation of a carbon biradical specie when exposed to UV-rays in the range 300 to 400 nm. According to the EPR results and literature [28, 34, 35] the biradical formed can be schematized as depicted in **Figure 53**.

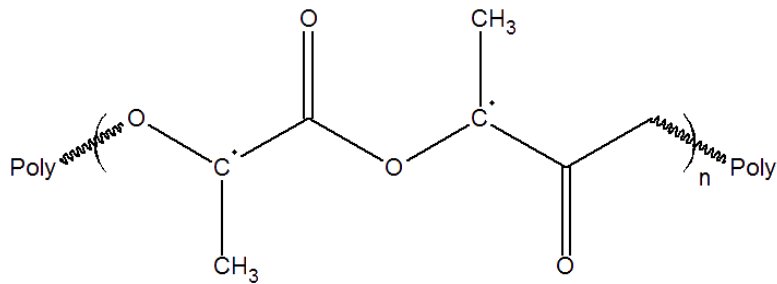


Figure 53: Biradical specie observed by EPR for PLA.

Researches have been already led by Babanalbandi et al. [207], focusing on the effect of gamma irradiation on polylactic acid by EPR. However, contrary to this study, they reported the formation of a monoradical when exposed to gamma irradiation (wavelength < 0.01 nm). Indeed, due to the gamma irradiation, C-C bonds were broken, leading to the formation of monoradical species. Irradiation in the range of 300 to 400 nm is not able to break C-C bonds, thus explaining why only biradicals are observed.

In order to study the influence of temperature on UV ageing, kinetic evolution of the formation of biradical species as a function of temperature was considered (**Figure 54**).

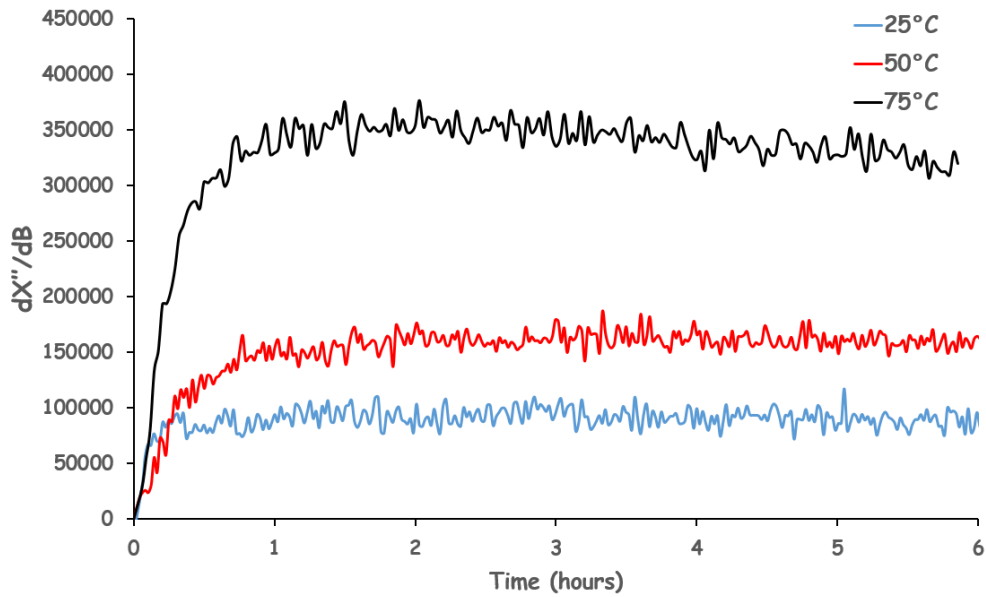


Figure 54: Kinetic evolution of EPR signal for PLA as a function of temperature, 25°C (●), 50°C (●) and 75°C (●).

These curves show that the number of biradical species formed under photochemical ageing is maximum at 75°C and decreases when temperature decreases. These data from EPR signal as a function of temperature were used to determine the activation energy (E_a) needed to initiate the formation of biradical species. This approach is based on an Arrhenius law. Indeed, a linear relation ($R^2=0.98$) is noted between $\ln(dX''/dB)$ and the inverse of temperature (**Figure 55**), suggesting that these coefficients follow an Arrhenius law (**Equation 32**):

$$(dX''/dB) = (dX''/dB)_0 \exp\left(-\frac{E_a}{RT}\right)$$

Equation 32

Where dX''/dB can be assigned to the susceptibility of radical formation, $(dX''/dB)_0$ is the pre-exponential factor, E_a is the activation energy in J/mol, R is the universal gas constant in $J.K^{-1}.mol^{-1}$ and T is the temperature in Kelvin (K).

The activation energy (E_a) is obtained from the slope of the linear fitting of $\ln(dX''/dB)$ versus T^{-1} and is estimated at 20 kJ/mol. The pre-exponential factor is equal to 3.4×10^8 . There is actually no literature dealing with the activation energy of radical formation in PLA. Indeed, the Arrhenius approach is not widespread in the study of radical formation kinetics by EPR. However, few published values are available concerning the E_a of water diffusion coefficient into PLA from 40 to 80 kJ/mol [123, 210] or E_a of thermal degradation from 72 to 125 kJ/mol [127, 166, 211]. Even if it is not comparable, the E_a determined in this study is very low compared to the literature values. It appears that PLA is highly sensitive to photo-degradation

because of its small value of E_a . These investigations demonstrate that temperature promotes the activation of radicals.

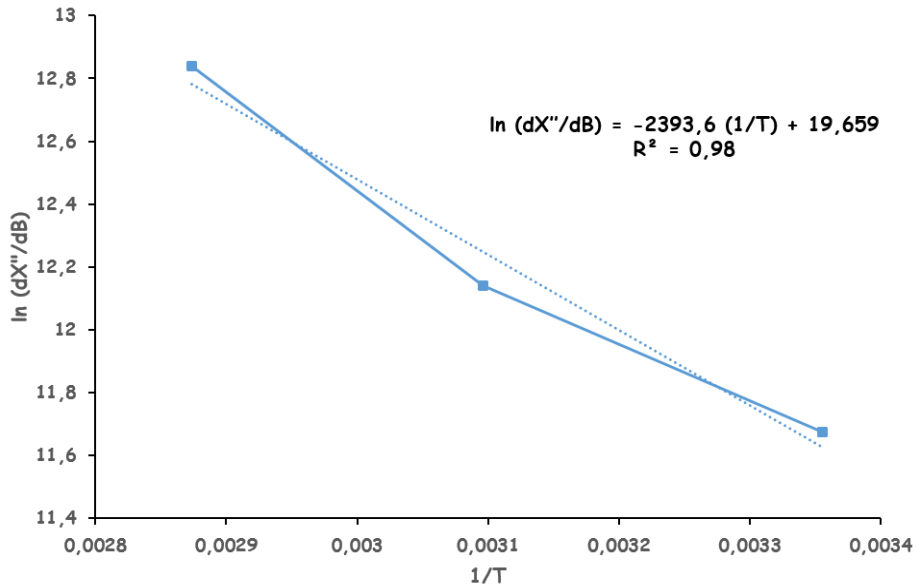


Figure 55: Identification of the activation energy of biradical formation in PLA for different temperatures.

In order to study the distribution of radicals during UV irradiation, EPR imaging experiments (**Figure 56**) were realized on pellets of PLA under irradiation (300 – 400 nm). The pictures show the formation and migration of the biradical species from the bulk to the whole sample.

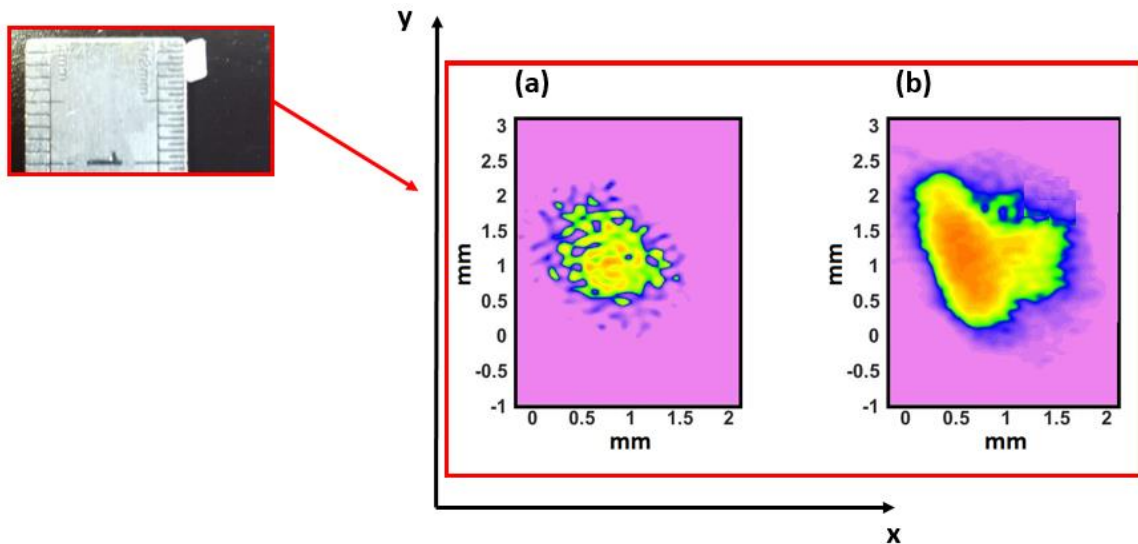


Figure 56: 2D YZ EPR imaging of PLA 50°C under irradiation at 30 min (a) and 4 hours (b). Intensity of color represents the local spin concentration from blue (min) to red (max).

After 30 min irradiation (**Figure 56 (a)**), it appears that micro domains of 50-100 μm are preliminary formed at the center of the PLA sample. These domains extent to whole sample

when irradiation duration increases, with a migration of radicals observed along the X and Y axes (**Figure 56 (b)**). These results are in accordance with literature [159].

The degradation mechanism of PLA samples exposed to both UV-rays and relative humidity is relatively difficult to understand. In fact, there is no practical way to identify which one of these two constraints catalyzes the other one. In order to estimate the additional influence of relative humidity, kinetic evolution of the formation of biradical species as a function of ageing exposure to T/UV/RH was studied at 50°C (**Figure 57**) and compared to results obtained for T/UV exposure.

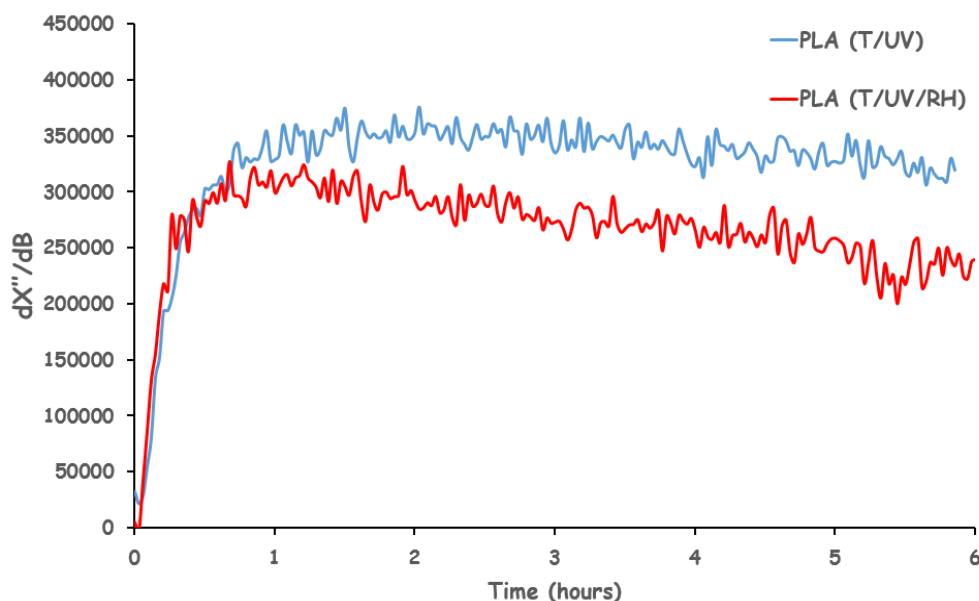


Figure 57: Kinetic evolution of EPR signal for PLA as a function of ageing exposure, T/UV (●) or T/UV/RH (●) at 50°C.

This graph shows that the formation of radicals under T/UV increases during the first hour of irradiation and then reaches a plateau till the end of irradiation. However, it appears that the amount of radicals formed under T/UV/RH exposure is smaller than that under T/UV conditions. The maximum amount of radicals formed is rapidly reached. One assumption to explain this phenomenon is that hydrolysis and radical mechanism occur simultaneously during T/UV/RH exposure. In this case, less radicals are formed because hydrolysis can disrupt their formation by degrading PLA, thus forming secondary products sooner. Hence, the combination between hydrolysis and UV-degradation is more detrimental for PLA lifetime.

FTIR analyses were then performed in order to identify the secondary products formed during exposure to T/UV and T/UV/RH. Hence the next section is dedicated to these investigations.

3.2.2. Secondary products formed during degradation

FTIR analyses were performed at a resolution of 32 cm^{-1} , on thin films of PLA after various durations of exposure to T/UV and T/UV/RH, in order to identify secondary products formed during irradiation of PLA (**Figure 58**).

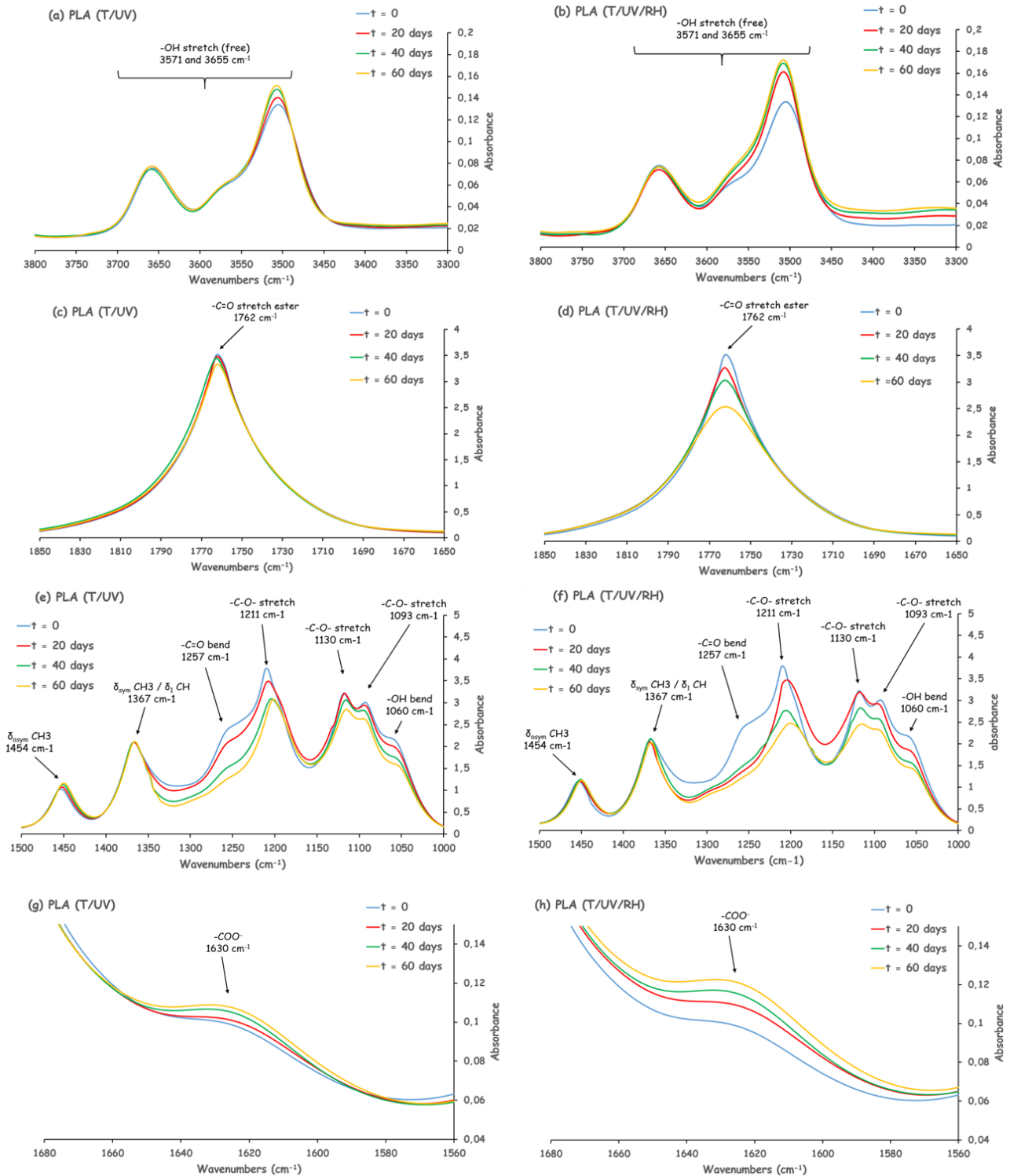


Figure 58: FTIR spectra ($\times 32\text{ cm}^{-1}$) of PLA before and after ageing under T/UV and T/UV/RH as a function of ageing time.

Spectra are classified into four regions, which correspond to the peaks assigned to the following bands: -OH stretch (3655 and 3671 cm^{-1} , (**Figure 58 (a) and (b)**), -C=O ester carbonyl (1762 cm^{-1} , (**Figure 58 (c) and (d)**), -OH bend (1060 cm^{-1}), -C-O stretch (1093 , 1130 and 1211 cm^{-1}), -C=O bend (1257 cm^{-1}) and -CH-/CH₃ deformation (1367 , 1454 cm^{-1}) in **Figure 58 (e) and (f)**, -COO⁻ carboxylate (1630 cm^{-1}) in **Figure 58 (g) and (h)**. These peaks assignments and corresponding positions are given in **Table 1 (p.29)**.

It is clearly observed in **Figure 58 (a) and (b)** that T/UV and T/UV/RH exposure lead to an increase in hydroxyl absorption between 3400 to 3750 cm^{-1} , which can correspond to products of degradation such as hydroperoxides or alcohols [34]. The higher intensity absorption reported after ageing for T/UV/RH exposure (**Figure 58 (b)**) compared to T/UV (**Figure 58 (a)**) suggests that the combination of both humidity and UV enhances the degradation of PLA due to a synergistic effect. The band at 1762 cm^{-1} corresponding to -C=O stretching ester slightly decreases when PLA is aged under T/UV exposure (**Figure 58 (c)**). As for hydroxyl bands, the decrease of the -C=O band is even more pronounced when PLA is aged under T/UV/RH (**Figure 58 (d)**). In the range 1000 - 1300 cm^{-1} (**Figure 58 (e) and (f)**), -C=O (1257 cm^{-1}) and -OH (1060 cm^{-1}) bends are also decreasing along ageing time whatever ageing conditions. Evolution of bands of -C-O- stretching ester in the range of 1093 - 1211 cm^{-1} shows that the bands are decreased and shifted towards lower wavelength after exposure to T/UV and T/UV/RH conditions, corresponding to -C-O- stretching alcohol and carboxylic acid. The increase in carboxylate (COO⁻) observe as a function of ageing at 1630 cm^{-1} (**Figure 58 (g) and (h)**) tends to confirm the formation of carboxylic acid during T/UV and T/UV/RH exposure. Furthermore, this phenomenon is even more pronounced for PLA aged under T/UV/RH conditions. These observations confirm that both radical mechanisms and hydrolysis occur when PLA is exposed to T/UV/RH conditions and their combined action enhances the degradation of PLA compared to T/UV and T/RH exposure.

Generally, the photo-degradation of PLA via a radical mechanism induces the formation of anhydride groups [34, 35, 39]. However, at a resolution of 32 cm^{-1} these chemical compounds were not observed. Hence, in order to evidence their presence, FTIR analyses were also performed at a resolution of 2 cm^{-1} . The analyses of PLA photo-oxidized under both T/UV and T/UV/RH show the formation of a band with a maximum at 1845 cm^{-1} (**Figure 59 (a) and (b)**), attributed to the formation of anhydride groups [34, 35, 39]. The intensity of this band increases versus exposure duration for both ageing tests (**Table 15**). However, it appears that the intensity of the anhydride band increases faster when PLA is exposed to T/UV compared to T/UV/RH conditions. The intensity of the band increases by 0.08 after 60 days under T/UV exposure compared to 0.03 under T/UV/RH exposure. In fact, due to the presence of water under T/UV/RH exposure, anhydrides can be easily decomposed into carboxylic acid by hydrolysis [34], which corroborate FTIR results previously reported.

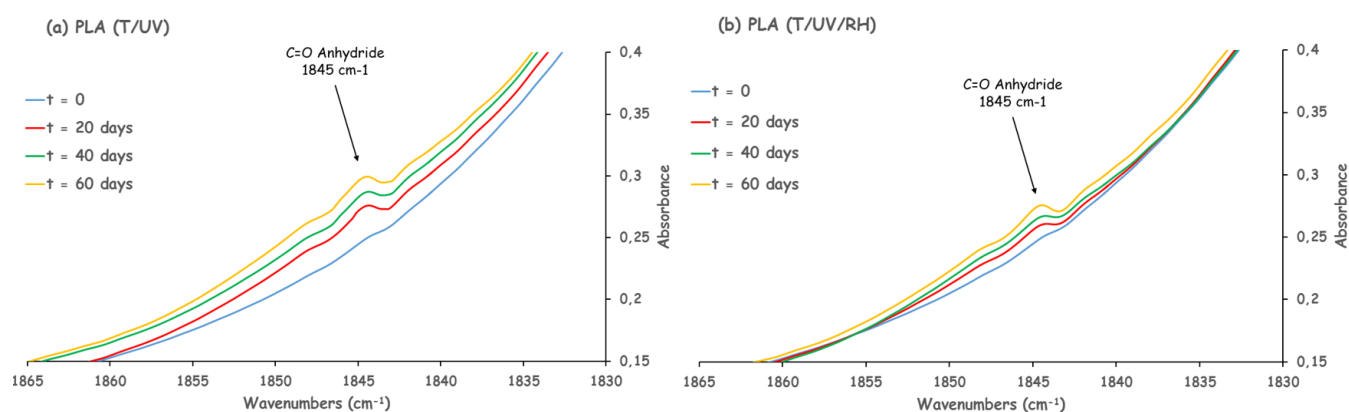


Figure 59: FTIR spectra ($\times 2 \text{ cm}^{-1}$) of PLA before and after ageing under T/UV and T/UV/RH as function of ageing time.

Table 15: Evolution of the band at 1845 cm^{-1} of PLA before and after ageing under T/UV and T/UV/RH as a function of ageing time.

Ageing duration (days)	Abs 1845 cm^{-1} (T/UV)	Abs 1845 cm^{-1} (T/UV/RH)
0	0.24	0.24
20	0.27 (+0.03)	0.25 (+0.01)
40	0.30 (+0.06)	0.26 (+0.02)
60	0.32 (+0.08)	0.27 (0.03)

The presence of the anhydrides was also confirmed by exposing the unaged and 60 days photo-oxidized films (T/UV and T/UV/RH) to ammonia (NH_3) saturated atmosphere for 3 hours. Indeed it is known that the reaction of NH_3 with anhydride leads to the formation of ammonium carboxylates and amide groups [34, 35]. FTIR analysis (resolution 2 cm^{-1} , **Figure 60**) shows that the intensity of the absorption band at 1845 cm^{-1} decreases after NH_3 treatment whereas new bands appear at 1600 cm^{-1} and 1675 cm^{-1} . According to literature [34, 35], these modifications indicate a reaction between photoproducts (e.g. anhydrides) and NH_3 and prove the formation of both amide groups and ammonium carboxylate ions (**Figure 35, p.80**).

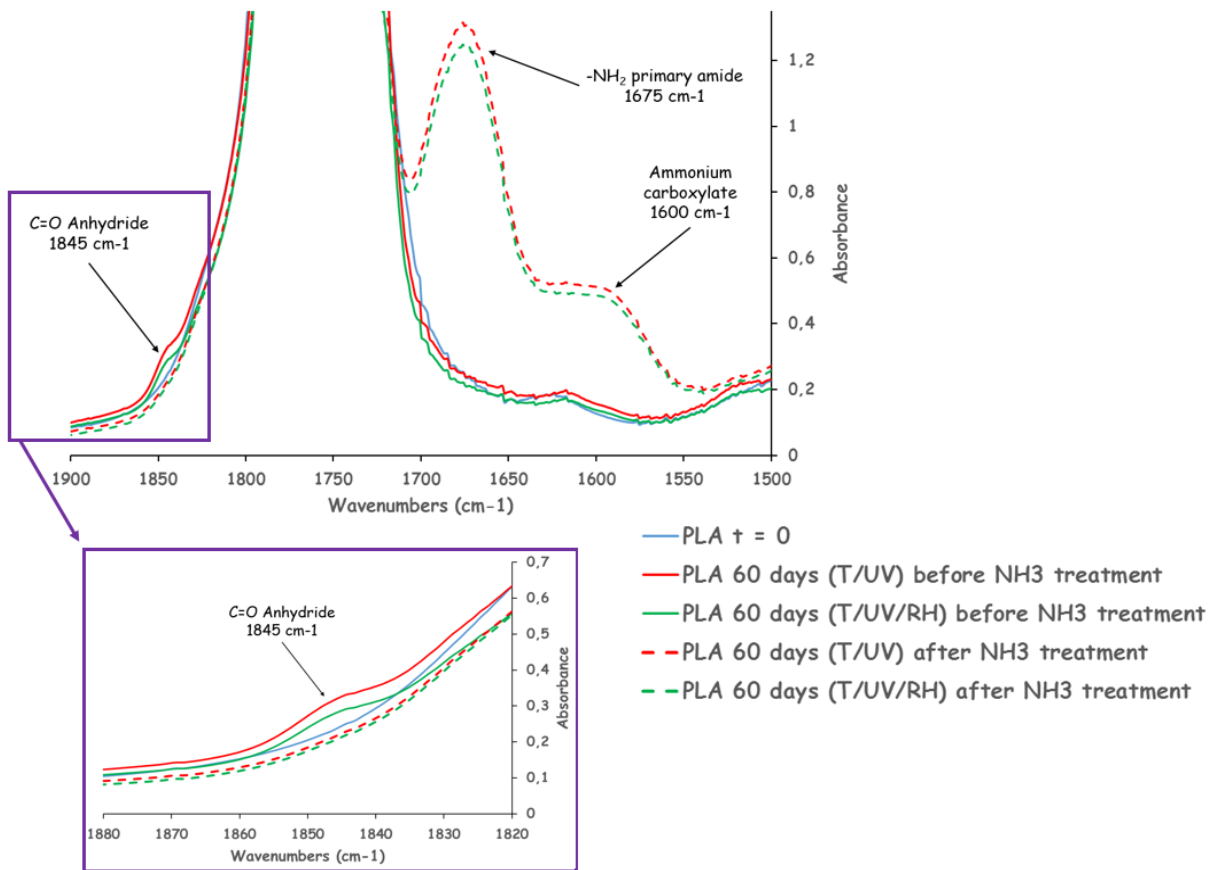


Figure 60: FTIR spectra ($\times 2 \text{ cm}^{-1}$) of 60 days aged PLA films to T/UV and T/UV/RH, before and after treatment with NH₃.

EPR and FTIR allow elucidating the degradation mechanism of PLA under UV irradiation: a radical mechanism. Degradation is accelerated in presence of temperature and relative humidity. This mechanism leads to the formation of secondary products such as anhydrides. According to literature [28, 29, 34, 35, 39, 212] and experiments done in this study, a summarizing mechanism of degradation is proposed in **Figure 61**.

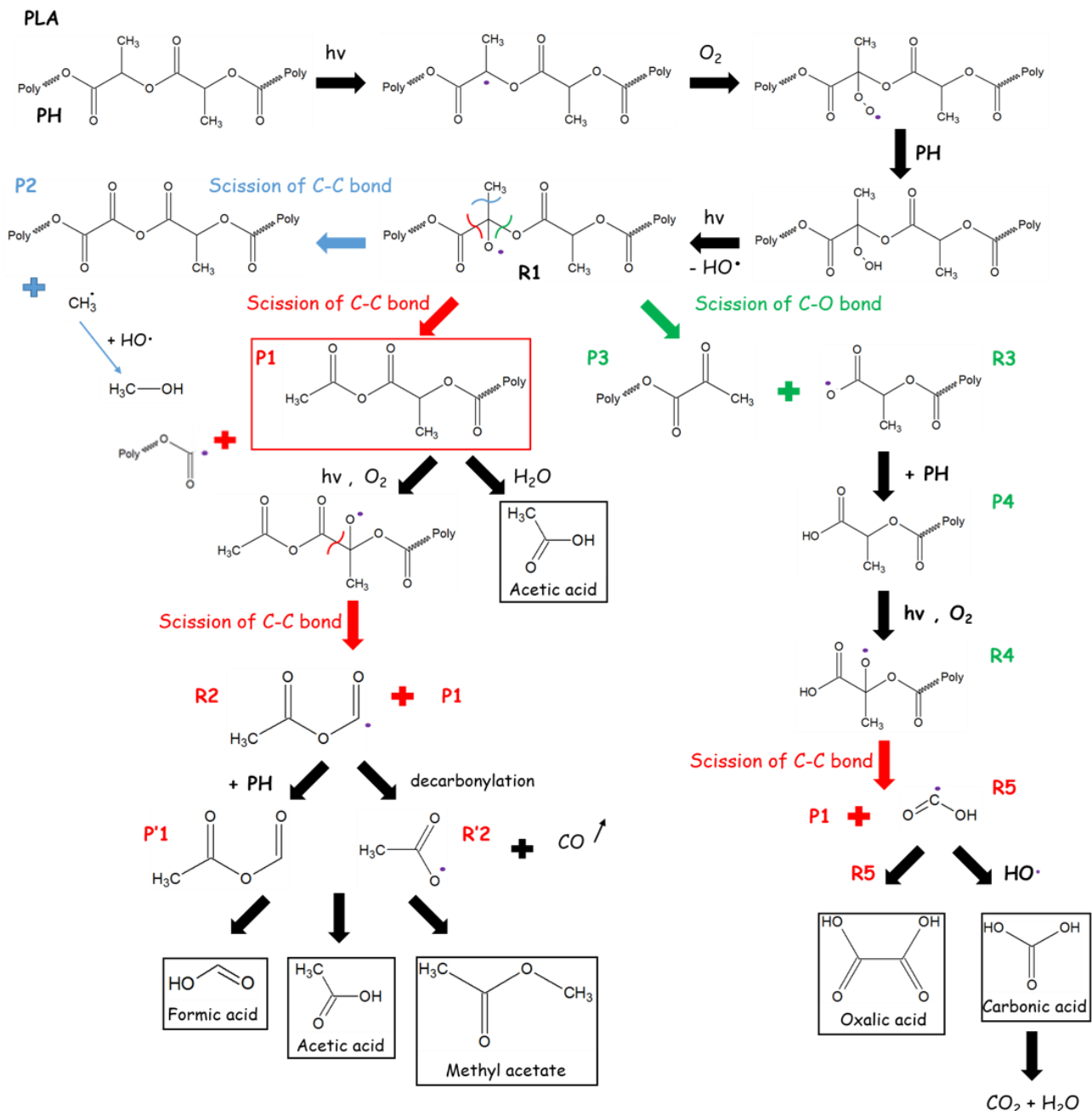


Figure 61: Proposed photo-oxidative mechanism of degradation for PLA, in presence of water.

The mechanism is as follows: due to the action of UV, hydrogen is removed from the PLA chain, leading to the formation of radical species. Then, oxygen reacts with the radical leading to the formation of hydroperoxides. Photolysis of the hydroperoxides forms radicals (R1) that can further evolve by β -scission into three different species: two possible C-C bond scissions leading to P1 and P2 , and one scission of C-O bond leading to P3 . Considering the stability of these different fragments and FTIR analyses previously reported, the most probable β -scission appears to be P1 , leading to the formation of anhydride groups. In presence of water, the formation of anhydrides is disturbed because they can be easily hydrolyzed into carboxylic

acid such as acetic acid. The presence of an acidic medium, evidenced with a pH paper and the characteristic odor of acetic acid reported during ageing makes this assumption reasonable. P1 and P3 products can then further evolve thanks to the action of UV, dioxygen, water and scission of C-C bond to finally yield formic, acetic, oxalic and carbonic acids, as well as methyl acetate. As previously, pH paper allowed evidencing the acidity of the medium. Moreover, the characteristic odors of both acetic acid and methyl acetate were reported during ageing. There is certainly the formation of other products due to the action of combined water and UV during T/UV/RH ageing test but for now, no investigations such as pyrolysis GC/MS were led to determine which ones. Of course, when temperature increases in the medium, the degradation of the material is accelerated, and even more when water is present.

The UV degradation of PLA has been demonstrated to mainly take place in the bulk of the material rather than on the surface. Molecular mass investigations evidenced an autocatalytic process in the presence of UV-rays, leading to random chain scission responsible of the decrease of the molecular mass. Both thermal properties and crystallinity are slightly affected under UV-rays exposure, except in combination with relative humidity. Indeed, the degradation via radical mechanism is enhanced in presence of relative humidity. The combination of both UV and RH leads to a synergistic effect between hydrolysis and radical degradation. Thus, the impacts of ageing are even more important compared to T/UV and T/RH, explaining the higher degradation level of PLA when aged under T/UV/RH conditions.

4. Conclusion

Chapter III was dedicated to effects of different kinds of ageing conditions on neat PLA. The investigations led on (i) the impacts of ageing on the physico-chemical properties and (ii) the mechanisms of degradation are in accordance with the literature [29, 31, 33-35, 38, 121, 123, 153, 157-160, 162].

The appearance of cracks and holes at the surface of the plates, as well as a bleaching of PLA samples was visually reported after 60 days of ageing. An influence of the ageing conditions on the physico-chemical properties of PLA was identified. In fact, it was highlighted that:

- The molecular mass (M_n) of PLA decreases due to a random chain scission
- The thermal stability slightly decreases under T/UV exposure, but this decrease is much more obvious under T/RH and T/UV/RH exposure.
- When exposed to T/UV/RH conditions, both T_g and T_m of PLA decrease and this phenomenon occurs from a critical molecular mass of 20000 g/mol. In the case of T/UV and T/RH exposure, both T_g and T_m are only slightly affected because the critical molecular mass is still not reached after 125 days.
- Due to a “chemi-crystallization” phenomenon, an increase in crystallinity is observed during ageing, associated to the formation of α' -form crystals. These

latter are not observed under T/UV exposure. Hence, the rate of degradation/crystallization is certainly lower than under T/RH and T/UV/RH exposure explaining why crystals are not observed during T/UV ageing.

- After 125 days exposure, the combination between T, UV and RH appears to be the more drastic for lifetime of PLA, due to a synergistic effect. Hence, according to literature and to our different experiments it is evidence that the effect of $T/UV/RH > T/RH > T/UV$.

In any cases, the degradation of PLA has been reported to take place in the bulk of the material rather than on the surface, assuming an autocatalytic process. However, the mechanism of degradation depends on the exposure conditions:

- Under T/RH exposure, PLA is degraded predominantly by hydrolysis of ester bonds. This phenomenon is even more pronounced when temperature increases. Long macromolecular chains are breaking down as long as PLA is exposed to T/RH.
- Under T/UV exposure, PLA is degraded via a radical mechanism. In presence of UV-rays, radicals are formed and evolved into secondary products, reducing the macromolecular chains into smaller unit.
- Under T/UV/RH exposure, it is reported that the combination between UV-rays and RH creates a synergistic effect. Indeed, both hydrolysis and radical mechanism occur during exposure and thus enhance the degradation of the material compared to T/UV and T/RH exposure. However, it is quite difficult for now to determine which of the two phenomena is predominant (i.e. hydrolysis or radical mechanism).
- In any exposure conditions, the temperature increase enhances the degradation of PLA.
- It appears that EPR is an innovative technique to investigate the mechanism of degradation of polymers. Indeed, it offers new perspectives on both mechanistic and kinetic points in the field of photo-degradation of polymers.

Since the mechanisms of degradation of neat PLA were elucidated, it is of interest to investigate the impact of FR fillers when PLA based formulations are aged. Hence, in chapter IV, the influence of FR additives on the physico properties of PLA and ageing behavior will be analyzed in details.

Chapter IV: Influence of flame retardants additives on the ageing of PLA

In this chapter, the influence of the addition of flame retardants (i.e. Melamine, APP and Cloisite 30B) on (i) the physico-chemical properties, (ii) the ageing behavior and (iii) the mechanisms of degradation of the PLA matrix is investigated. Hence, two formulations are studied and compared: FR-PLA, containing APP and Melamine, and FR-PLA-C30B, containing APP, Melamine and Cloisite C30B.

The ageing mechanism of PLA under T/UV, T/RH and T/UV/RH conditions has been investigated and elucidated in chapter III. To fire retard PLA, Melamine, APP and Cloisite 30B are incorporated in the polymer matrix, leading to an intumescent system [12]. However, even if the impact of organoclays on the ageing of PLA has already been studied [32, 34, 37, 39, 162, 213], the impact of FR fillers on the ageing behavior of PLA has never been investigated. This study is of primary importance to predict the lifetime of the FR-PLA and FR-PLA-C30B intumescent systems for potential use in everyday life. In this way, the following part is dedicated to the impact of ageing on the morphology of FR-PLAs.

1. Impact of ageing on the morphology of FR-PLAs

1.1. Visual observations

The numerical pictures of PLA and both FR-PLAs plates taken before ageing (**Figure 62**) show a color change of the material when FR additives are incorporated into the PLA matrix. In fact, whereas PLA (**Figure 62 (a)**) is almost transparent, FR-PLA (**Figure 62 (b)**) and FR-PLA-C30B (**Figure 62 (c)**) samples tend to a cream color. This color change was quantified by $L^*a^*b^*$ (**Appendix 1, p.220**). Indeed, the combination between L^* , b^* and ΔE values obtained during ageing confirm the creamy color observed when FR are incorporated into PLA.

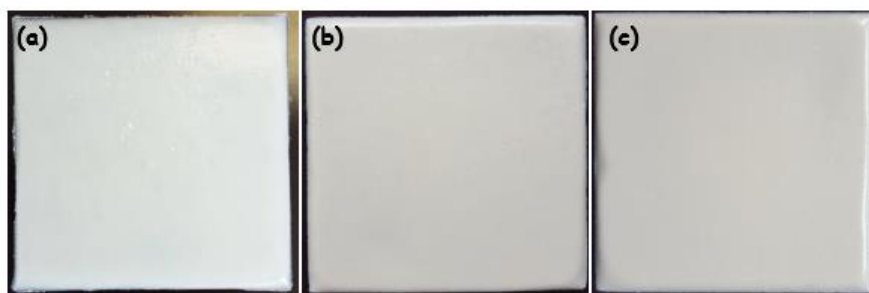


Figure 62: numerical pictures of PLA (a), FR-PLA (b) and FR-PLA-C30B (c) plates before ageing.

Then, in order to evaluate the impact of T/UV, T/RH and T/UV/RH ageing conditions on both FR-PLAs, visual evaluation was also done all along the experiments, as long as possible before the samples degrade (this is why the observation times are different depending on samples). The numerical pictures taken before and after ageing under T/UV, T/RH and T/UV/RH conditions are shown in **Figure 63** and **Figure 64** for FR-PLA and FR-PLA-C30B, respectively. Compare to raw PLA, the main difference is the formation of a rough white layer as well as holes and fractures at the surface of both FR-PLAs plates during ageing: these phenomena are reported after 28 days ageing under T/RH exposure (**Figure 63 (c)** and **Figure 64 (c)**). Regarding (**Figure 63 (d)** and **Figure 64 (d)**), similar phenomena are observed for both FR-PLA and FR-PLA-C30B plates after only 6 days ageing under T/UV/RH conditions. On the contrary, it appears that after 60 days ageing under T/UV, only a laundering of FR-PLA and FR-PLA-C30B occurs ((**Figure 63 (b)** and **Figure 64 (b)**). The laundering and the white layer formed during ageing were also evidence and quantified using $L^*a^*b^*$ device (**Appendix 2, p.221**).

According to the color space of CIE lab system, the increase in ΔE and L^* values confirm the color change during ageing and the tendency for laundering.

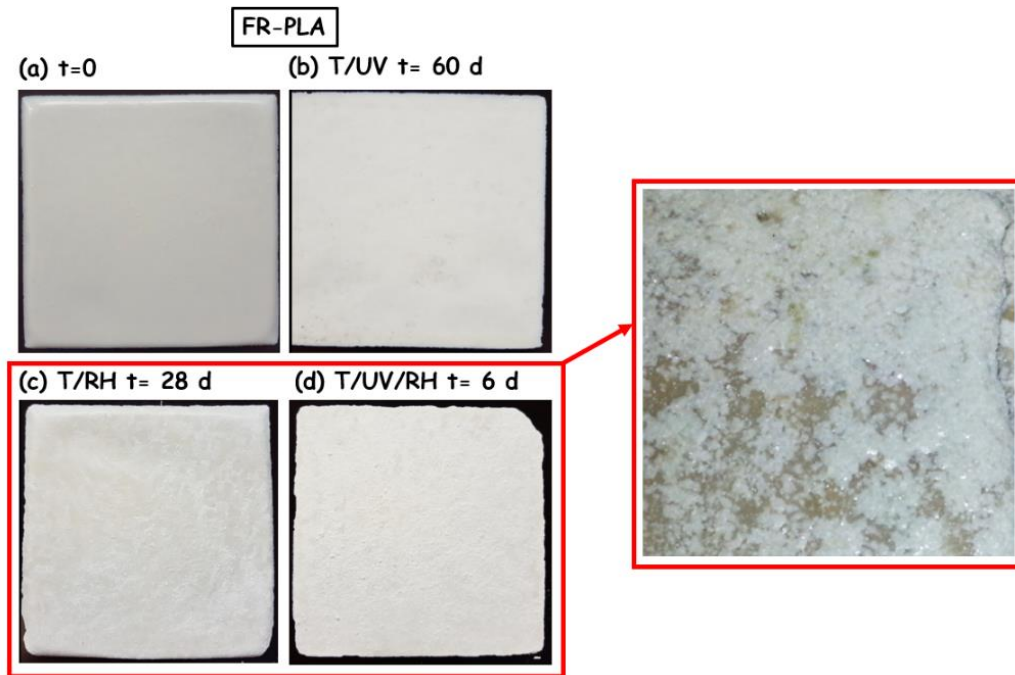


Figure 63: Visual evaluation as a function of ageing for FR-PLA 0 d (a), 60 d T/UV (b), 28 d T/RH (c) and 6 d T/UV/RH (d).

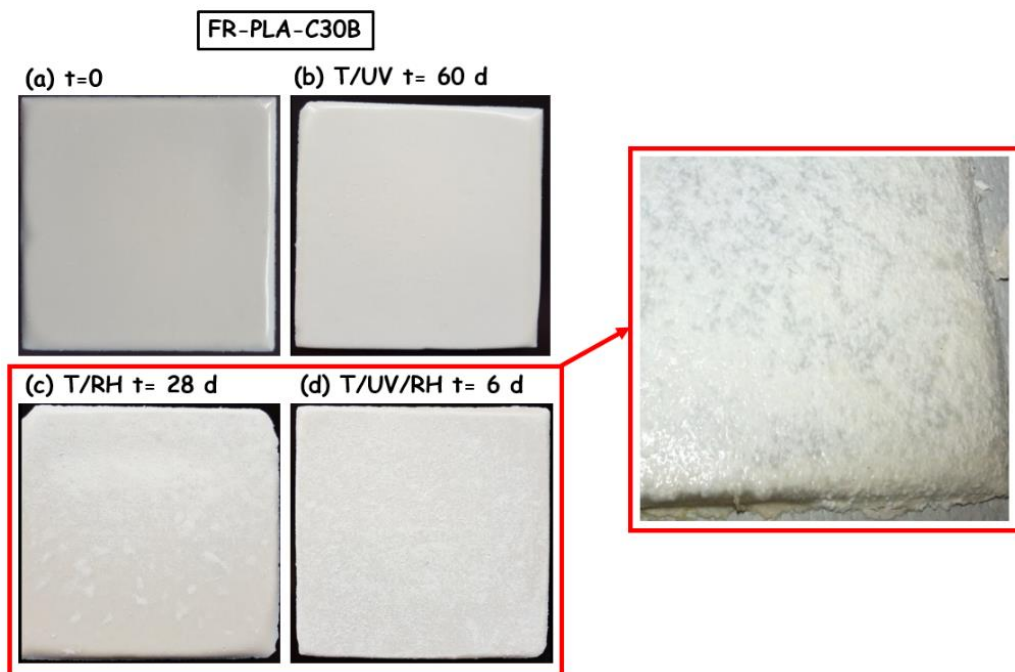


Figure 64: Visual evaluation as a function of ageing for FR-PLA-C30B 0 d (a), 60 d T/UV (b), 28 d T/RH (c) and 6 d T/UV/RH (d).

Focusing on ageing in presence of humidity (i.e. T/RH and T/UV/RH), it appears that FR-PLA and FR-PLA-C30B are completely disintegrated into powder form (**Figure 65**) after 35 days and 10 days under T/RH and T/UV/RH exposure, respectively.

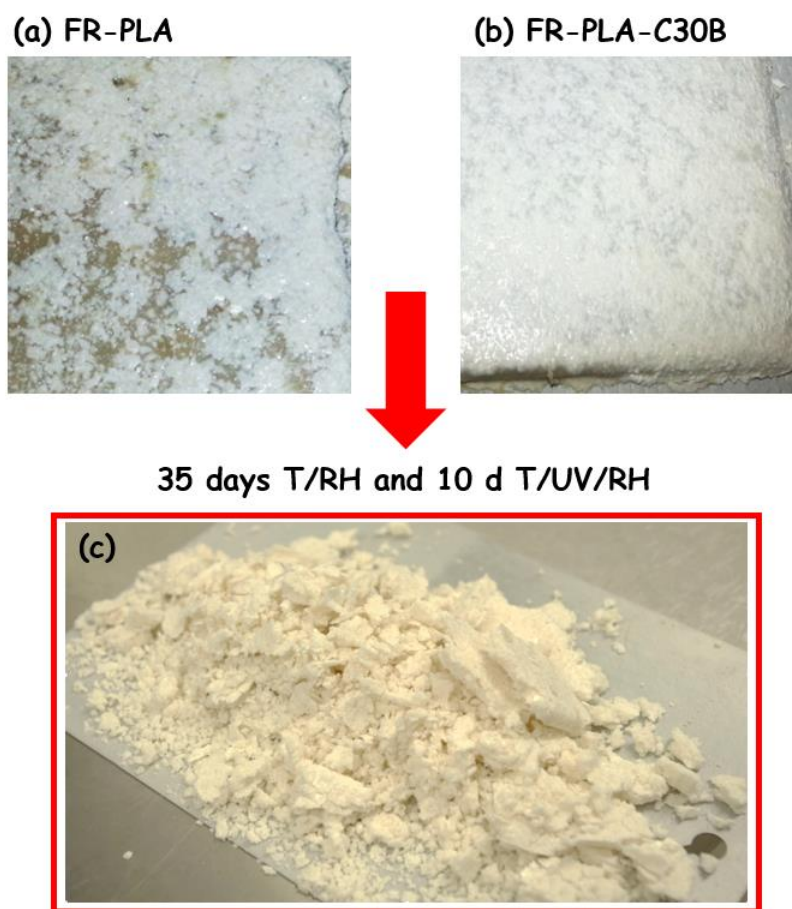


Figure 65: Visual evaluation of FR-PLA (a) and FR-PLA-C30B (b) until disintegration into powder (c).

These observations demonstrate that the presence of FR fillers leads to new phenomena that were not observed in the case of virgin PLA (**p.86**), in particular, the formation of this rough white layer at the surface of FR materials which appears very fast when UV and humidity are combined.

In order to investigate in more detail these surface modifications, scanning electron microscopy (SEM) analyses were performed on FR-PLA and FR-PLA-C30B plates before and after ageing.

1.2. Surface morphology of FR-PLAs after ageing

Scanning electron microscopy (SEM) was used to observe the holes, fractures and white spots at the surface of aged FR-PLA (**Figure 66**) and FR-PLA-C30B (**Figure 67**).

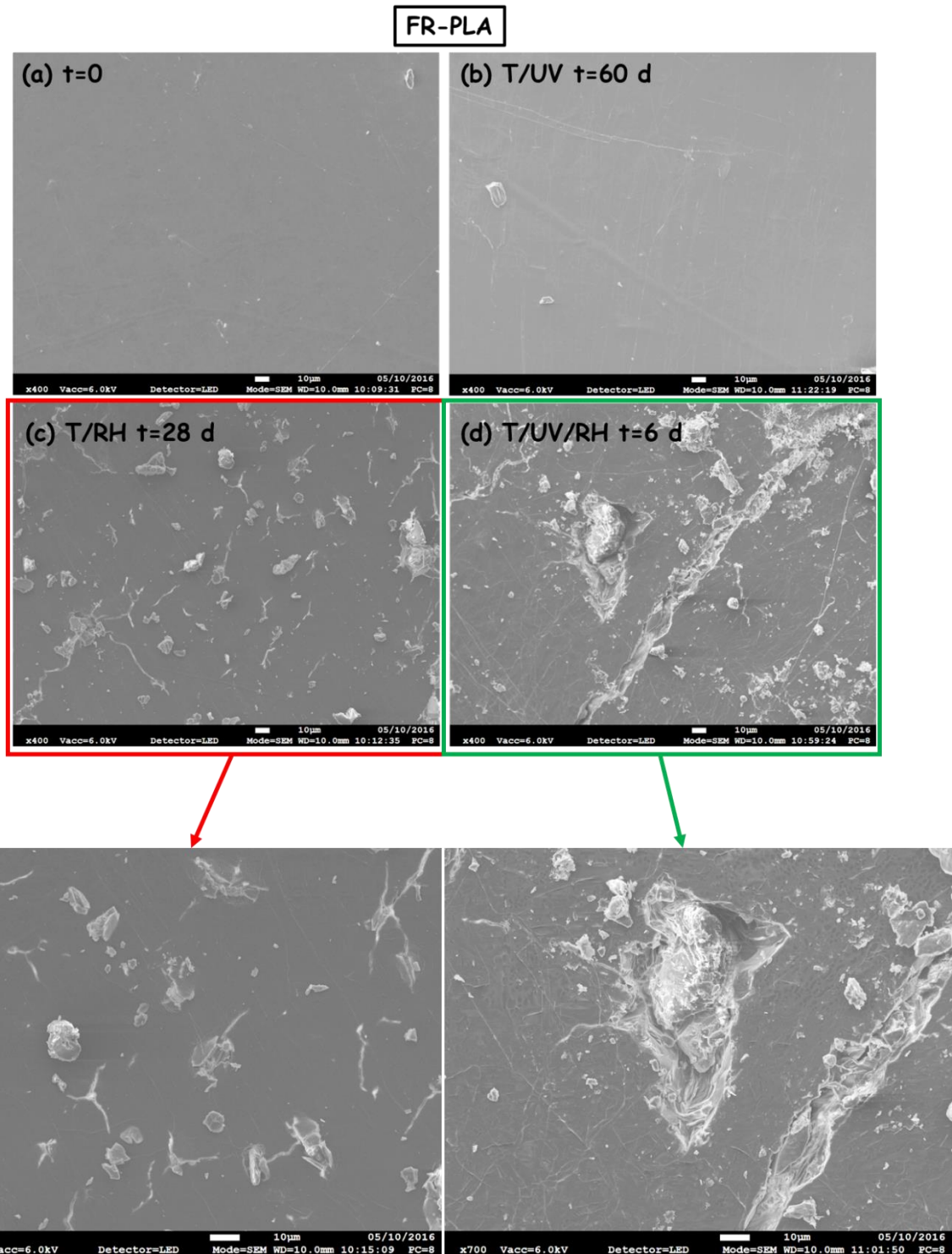


Figure 66: SEM pictures obtained for unaged FR-PLA (a), 60 d T/UV (b), 28 d T/RH (c) and 6 d T/UV/RH (d).

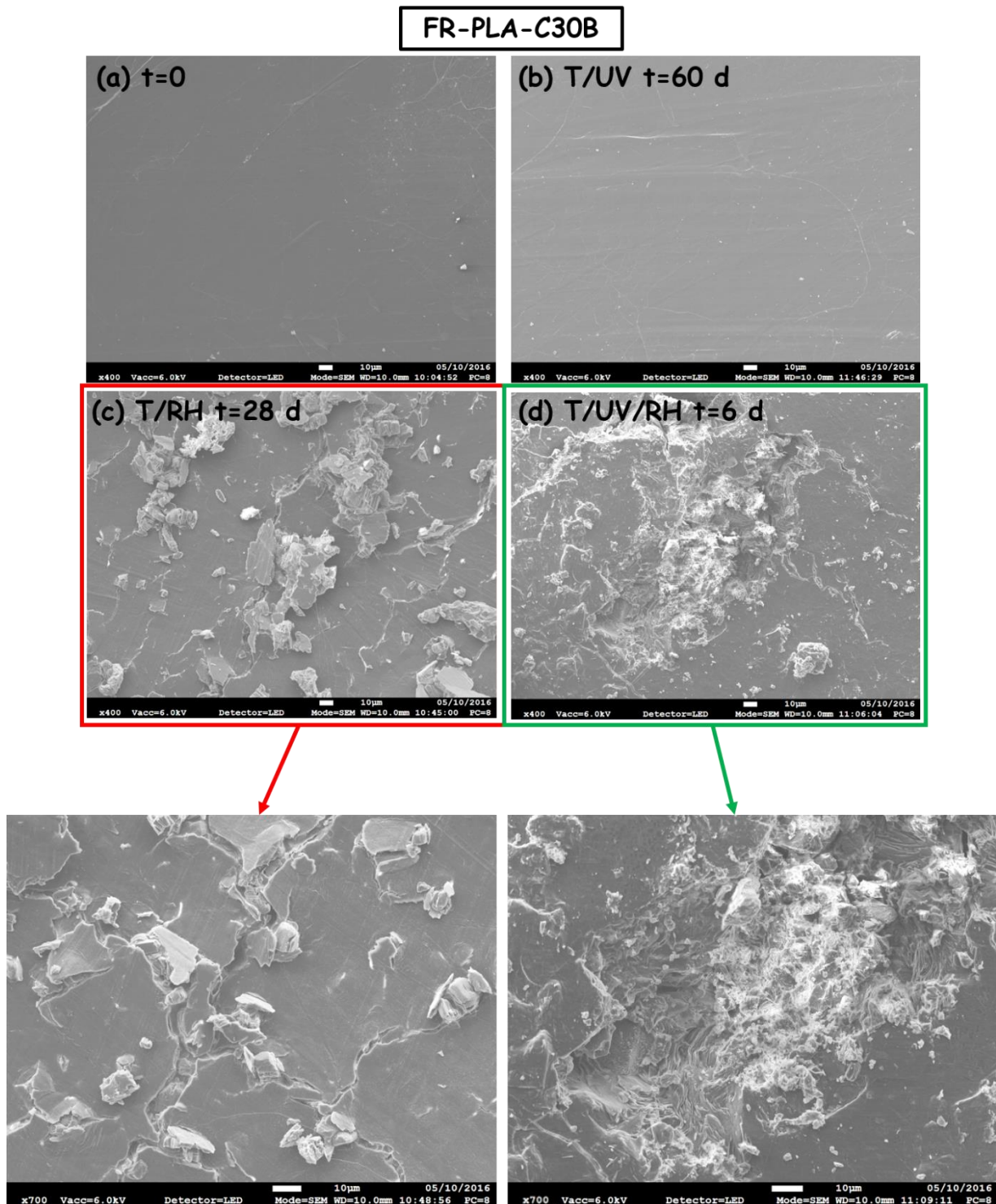


Figure 67: SEM pictures obtained for unaged FR-PLA-C30B (a), 60 d T/UV (b), 28 d T/RH (c) and 6 d T/UV/RH (d).

It appears that the surfaces of FR-PLA and FR-PLA-C30B are relatively smooth before ageing (**Figure 66 (a)** and **Figure 67 (a)**). On the contrary, few cracks are observed after 60 days under T/UV exposure (**Figure 66 (b)** and **Figure 67 (b)**) and impact of ageing is much more pronounced for FR-PLA and FR-PLA-C30B when aged under T/RH and T/UV/RH conditions. Indeed, holes, spots and fractures are observed at the surface of the materials after 28 days

exposure to T/RH conditions (**Figure 66 (c)** and **Figure 67 (c)**). Moreover, phenomena are even more pronounced for FR-PLA-C30B (**Figure 67 (c)**) compared to FR-PLA (**Figure 66 (c)**). It appears that after 6 days under T/UV/RH exposure holes, cracks and spots are more apparent on the surface of both FR-PLAs (**Figure 66 (d)** and **Figure 67 (d)**) and that fillers are less embedded by PLA matrix on the surface. As under T/RH, the degradation seems to be more pronounced for FR-PLA-C30B compare to FR-PLA.

1.3. Conclusion

The visual observations and SEM results reported in this part demonstrate the impact of FR fillers on the ageing of PLA. In fact, only a slight bleaching and cracking were reported for virgin PLA when submitted to T/UV, T/RH and T/UV/RH exposure (**p.86**). However, holes, fractures and a rough white layer appear at the surface of the T/RH and T/UV/RH aged materials until their complete disintegration when FR fillers are incorporated into the PLA matrix. Only the exposure to T/UV conditions appears not to be drastic for visual integrity of FR-PLA and FR-PLA-C30B. Indeed, the material is certainly not sufficiently degraded after 60 days under T/UV exposure. Hence in order to determine the causes of these phenomena, the impact of the addition of fillers on the physico-chemical properties of PLA and their behavior during ageing are investigated in the next part. In particular, molecular mass, thermal properties (i.e. T_g and T_m) and crystallinity are studied into details.

2. Physico-chemical properties of FR-PLAs during ageing

This part investigates the physico-chemical properties of both FR-PLA and FR-PLA-C30B before ageing, in terms of molecular mass (M_n), thermal properties (i.e. T_g , T_m) and crystallinity. The impact of ageing on these physico-chemical properties is then investigated and compared to that of PLA, studied in chapter III. As for PLA, physico-chemical behavior of FR-PLA and FR-PLA-C30B was studied until 125 days under T/UV. However, due to the quick degradation of materials, FR-PLAs were studied until 105 days under T/RH and 90 days under T/UV/RH conditions. Moreover, as FR-PLAs are disintegrated into powder after 10 and 35 days under T/UV/RH and T/RH, respectively, investigations were led using this powder beyond these durations.

2.1. Molecular mass

2.1.1. Impact of fillers on molecular mass of FR-PLAs

The M_n of PLA and FR-PLAs, before ageing, obtained by GPC (**Table 16**) show that when FR fillers are incorporated into PLA, M_n is reduced by 57% and 60% for FR-PLA and FR-PLA-C30B, respectively. However, it appears that the polydispersity index is not affected by the incorporation of FR fillers. Indeed, PI remains stable between 1.8 and 1.9.

Table 16: Number average molecular mass (M_n) of PLA, FR-PLA and FR-PLA-C30B materials.

Material	PLA	FR-PLA	FR-PLA-C30B
M_n (g/mol)	68 000	29 000 (- 57%)	27 000 (- 60%)
PI	1.8	1.9 (+0.1)	1.9 (+0.1)

This M_n decrease is explained by the preparation process of the samples. The incorporation of fillers into PLA via the extrusion process creates mechanical (shear, strain ...) and thermal stresses, decreasing molecular mass of PLA [84, 214-220]. Moreover, due to the presence of fillers, chemical reaction can also occur during extrusion, breaking polymer chains and decreasing M_n . In fact, Melamine and APP contain amine functions that are able to break PLA chains through aminolysis reaction on ester (**Figure 68**) [221-223].

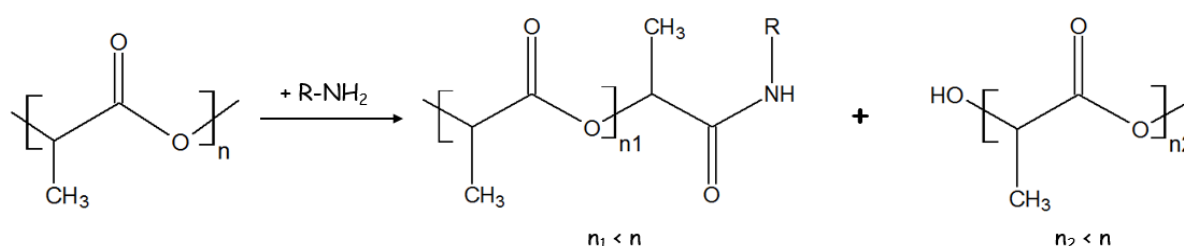


Figure 68: Aminolysis reaction of PLA.

In addition, it is known that the surfactant contained in Cloisite 30B can undergo degradation during the melting process at around 200°C , in presence of residual water, according to Hofmann elimination mechanism (**Figure 69**) [224].

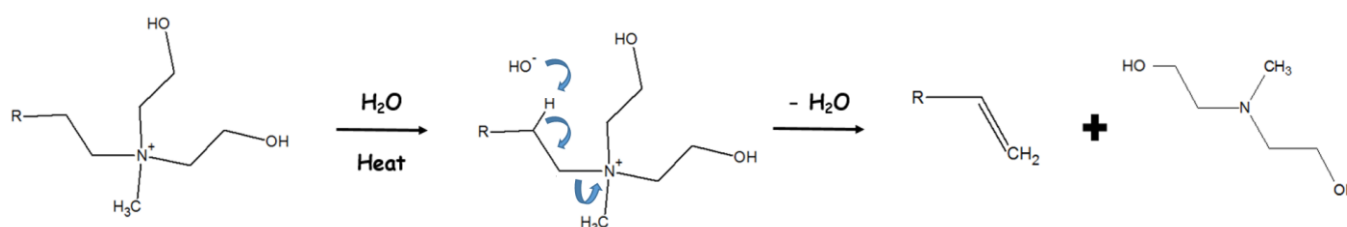


Figure 69: Hofmann elimination reaction on the surfactant of Cloisite 30B.

During Hofmann elimination, the quaternary ammonium salt decomposes into an amine, which can thus be responsible for the acceleration of the polymer decomposition in the initial stage [224-227]. However, due to the temperature used during extrusion process (i.e. 185°C maximum in the zone of incorporation of fillers) and the relatively low loading of organoclays (i.e. 1%), it is doubtful that Hofmann elimination is very meaningful to explain the decrease of M_n in this case. Moreover, considering the measurement uncertainty (i.e. 10%) the decrease of M_n is similar for both FR materials indicating that the 1 wt.-% of organoclays do not particularly impact the M_n of FR materials.

Knowing that M_n of raw PLA is affected by (i) ageing exposure and (ii) the incorporation of FR fillers, it is useful to investigate concerning the impact of ageing on M_n of FR-PLAs.

2.1.2. Impact of ageing on the molecular mass of FR-PLAs

It was previously reported in chapter III (p.90) that the molecular mass of PLA decreases when the exposure duration to T/UV, T/RH and T/UV/RH increases. In order to determine if this phenomenon is also observed in the case of FR-PLAs, GPC analyses were performed during T/UV, T/RH and T/UV/RH exposure. M_n and PI of FR-PLAs as a function of ageing time are compared in **Table 17** to the values obtained for neat PLA. The curves obtained by GPC, plotting M_n as a function of ageing conditions and duration, are presented in **Figure 70**.

Table 17: M_n and PI data as function of ageing of PLA, FR-PLA and FR-PLA-C30B samples aged under T/UV, T/RH and T/UV/RH.

Exposure / time (days)	PLA M_n (g/mol) / PI	FR-PLA M_n (g/mol) / PI	FR-PLA-C30B M_n (g/mol) / PI
0	68 000 / 1.8	29 000 / 1.9	27 000 / 1.9
T/UV 125 d	30 000 (-55%) / 1.7	13 500 (-53%) / 1.8	12 500 (-54%) / 1.9
T/RH 105 d	17 000 (-72%) / 1.7	4 300 (-84%) / 1.8	4 100 (-84%) / 1.8
T/UV/RH 90 d	9 100 (-86%) / 1.8	2 800 (-90%) / 1.8	2 500 (-91%) / 1.9

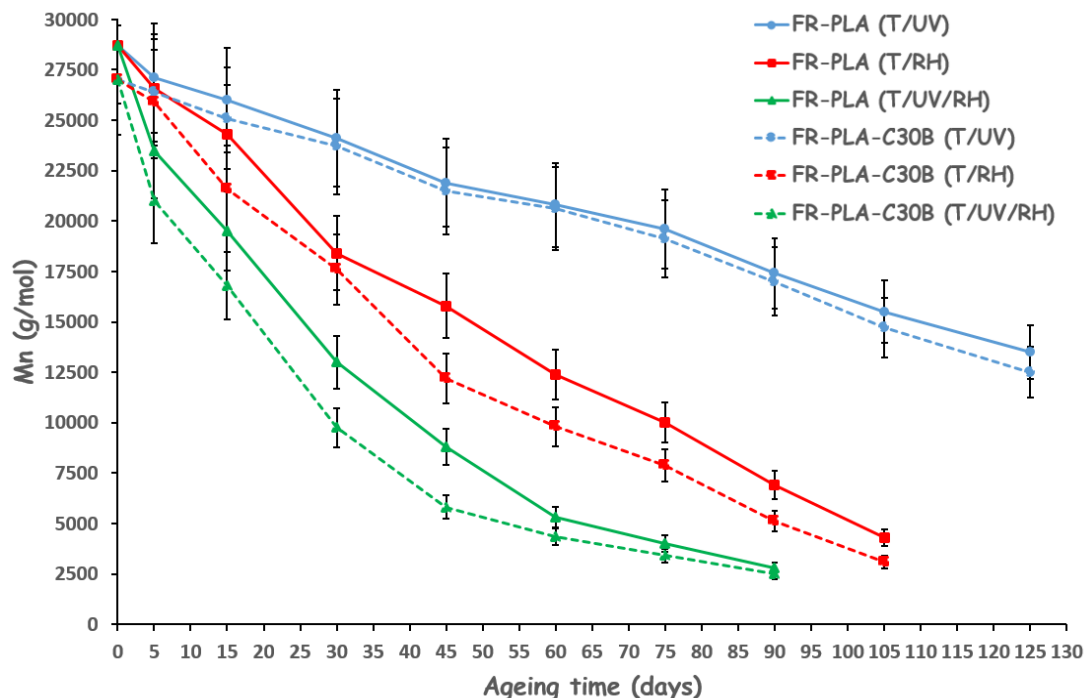


Figure 70: M_n versus ageing time of FR-PLA (a) and FR-PLA-C30B (b) samples aged under T/UV (●), T/RH (■) and T/UV/RH (Δ).

As for virgin PLA, it is evidenced that M_n of FR-PLA and FR-PLA-C30B decreases versus time for all ageing exposure conditions. In fact, regarding FR-PLA, M_n decreases from 29000 g/mol before ageing to 13500 (-53%), 4300 (-84%) and 2800 g/mol (-90%) after 125 days under T/UV, 105 days under T/RH and 90 days under T/UV/RH, respectively. Concerning FR-PLA-C30B, M_n decreases from 27000 g/mol before ageing to 12500 (-54%), 4100 (-84%) and 2500 g/mol (-91%) after 125 days under T/UV, 105 days under T/RH and 90 days under T/UV/RH, respectively. Furthermore, after 6 days of ageing under T/UV/RH and 28 days under T/RH conditions, the M_n of both materials is around 20000 g/mol (**Figure 70**), which corresponds to the appearance of the white layer at the surface of the plates in presence of relative humidity.

As in the case of neat PLA, the drop of M_n suggests that chain scission occurs during ageing of FR-PLAs. Moreover, it seems that M_n of both FR materials decreases at the same rate and that this rate is higher when UV is combined with T and RH compared to T/RH and T/UV. Indeed, after 90 days, M_n is decreased by 90% and 91% under T/UV/RH exposure for FR-PLA and FR-PLA-C30B, respectively. On the contrary, after 90 days exposure to T/RH, M_n is decreased by 75% and 81% for FR-PLA and FR-PLA-C30B, respectively, and by 37% for both materials under T/UV exposure. Moreover, the kinetics of degradation of PLA seems not to be impacted by the presence of FR fillers. As an example, after 90 days under T/UV/RH, M_n of FR-PLAs is reduced by around 90% compared to 86% for neat PLA. These reductions can be considered as similar regarding the measurement uncertainty estimated to 10% and tend to confirm that the degradation rate is similar for PLA and FR-PLAs.

Polydispersity index (PI) of FR-PLA and FR-PLA-C30B is independent of ageing, as it remains stable between 1.8 and 1.9 (**Table 17**). Hence, chain scissions occur randomly along the polymer macromolecules [124, 127, 189].

The number of chain scissions of FR-PLA and FR-PLA-C30B (n_t) as a function of time and ageing conditions (**Figure 71**) shows that whatever the nature of the sample, n_t increases as a function of ageing duration. This phenomenon depends on the ageing conditions: it is even more important for FR-PLAs aged under T/UV/RH conditions than to those submitted to T/RH and T/UV. Moreover, for the same ageing condition, there is no significant difference between FR-PLA and FR-PLA-C30B.

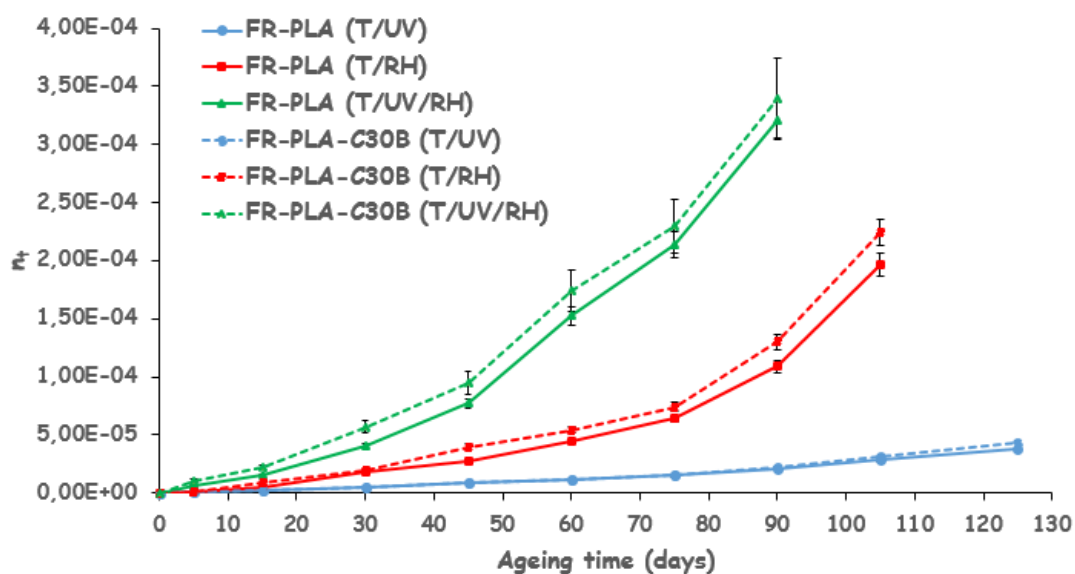


Figure 71: Average number of random chain scissions per unit mass (n_t) for FR-PLA and FR-PLA-C30B as a function of ageing time at different ageing conditions; T/UV (●), T/RH (■) and T/UV/RH (△).

The combination between UV, T and RH accelerates the degradation of FR-PLAs: regarding FR-PLA, under T/UV/RH, n_t is around 3.2×10^{-4} after 90 days against 1.9×10^{-4} and 3.8×10^{-5} after 105 days under T/RH and 125 days under T/UV, respectively. For FR-PLA-C30B, under T/UV/RH, n_t is around 3.6×10^{-4} after 90 days against 2.8×10^{-4} and 4.3×10^{-5} after 105 days under T/RH and 125 days under T/UV, respectively. These results confirm that FR fillers do not disturb the degradation of the materials: (i) the presence of fillers doesn't disturb the chain scission process of PLA and thus (ii) the autocatalytic process still occurs due to the increase of carboxylic acid end groups, as previously reported in chapter III (p.90) [5, 31, 125, 150, 153].

The ageing of FR-PLA and FR-PLA-C30B leads to the decrease of the molecular mass of the material, whatever ageing conditions. However, it appears that the M_n of FR materials reaches lower values after ageing compared to those of PLA. Due to the fact that the degradation rate seems to be the same for unfilled or filled PLAs, the hypothesis is that the already low M_n before ageing of FR-PLA and FR-PLA-C30B is the main cause explaining why such low M_n are reached for FR materials. This also explains why the degradation of FR-PLAs samples is more pronounced compared to unfilled ones. This can also partially explain the phenomena observed at the surface of both FR-PLAs, i.e. appearance of a white layer, when the critical molecular mass (i.e. 20000 g/mol) is reached.

As the impact of fillers on the behavior of the molecular mass during ageing was demonstrated in this section, the next section will investigate the influence of FR fillers on (i) glass transition temperature (T_g) and (ii) melting temperature (T_m) of PLA during ageing, using DSC analyses.

2.2. Thermal properties

2.2.1. Effect of fillers on glass transition and melting temperature

The thermal properties of FR-PLA and FR-PLA-C30B were evaluated by DSC in order to investigate the effect of the incorporation of fillers on the T_g and T_m of materials. The DSC data of FR-PLA and FR-PLA-C30B (**Table 18**) were compared to those of PLA.

Table 18: DSC data of PLA, FR-PLA and FR-PLA-C30B as a function of M_n .

Material name	M_n (g/mol)	T_g (°C)	T_m (°C)
PLA	68000	61.5	160.0
FR-PLA	29000 (-57%)	57.5 (-6.5%)	159.8 (-0.1%)
FR-PLA-C30B	27000 (-60%)	57.4 (-7.0%)	159.2 (-0.5%)

Whereas FR additives do not affect the T_m of materials, it appears that the T_g of FR-PLA and FR-PLA-C30B is somehow lower (loss of 4°C) compared to that of PLA. Incorporation of fillers into a polymer can affect the molecular mobility of the polymer chains due to a plasticizing effect [228-230]: the fillers can increase the local flexibility of the material, thus affecting the free volume of the polymer. Therefore, it can cause the decrease of T_g . On the other hand, the decrease of T_g can also be explained by the degradation of the PLA matrix during extrusion process, which is in accordance with the decrease of M_n observed when FR fillers are incorporated into the material (**p. 125**). Indeed, the molecular mass of a polymer is known to be a parameter affecting T_g [231-235]. In the case of linear polymer such as PLA, the glass transition temperature decreases when the number average molecular mass of the polymer decreases [231, 234-236]. Generally, this dependence can be quantified using the Fox and Flory relationship (cf. **Equation 30, p.94**). In reality, this phenomenon is linked to the concentration of chain ends of the material. Indeed, the increase of chain ends (low M_n) leads to an increase in free volume of the polymer, thus decreasing T_g [231].

As both T_g and T_m of neat PLA are impacted by (i) ageing exposure and (ii) the incorporation of FR fillers, the next section focus on the effect of ageing on thermal properties (T_g and T_m) of FR-PLAs.

2.2.2. Behavior of glass transition and melting temperatures during ageing

The glass transition (T_g) and melting temperatures (T_m) of FR-PLA and FR-PLA-C30B were also evaluated by DSC all along the exposure to T/UV, T/RH and T/UV/RH conditions and compared to those obtained for non-aged materials (**Table 19** and **Table 20** for FR-PLA and FR-PLA-C30B, respectively).

Table 19: DSC data of FR-PLA as a function of M_n and ageing time under T/UV, T/RH and T/UV/RH.

Ageing exposure (days)	T/UV M_n (g/mol)	T/UV T_g (°C)	T/UV T_m (°C)	T/RH M_n (g/mol)	T/RH T_g (°C)	T/RH T_m (°C)	T/UV/RH M_n (g/mol)	T/UV/RH T_g (°C)	T/UV/RH T_m (°C)
0	29000	57.5	159.8	29000	57.5	159.8	29000	57.5	159.8
15	26000 (-9%)	56.4 (-1.1)	158.4 (-1.4)	24300 (-16%)	54.8 (-2.7)	153.3 (-6.5)	17500 (-39%)	50.3 (-7.2)	151.9 (-7.9)
30	24100 (-14%)	56.3 (-1.2)	156.5 (-3.3)	18400 (-34%)	52.8 (-4.7)	150.7 (-9.1)	13000 (-54%)	46.9 (-10.6)	149.4 (-10.4)
45	21900 (-22%)	55.1 (-2.4)	156.3 (-3.5)	15800 (-44%)	50.2 (-7.3)	148.4 (-11.4)	8800 (-69%)	40.7 (-16.8)	140.1 (-19.7)
60	21300 (-26%)	53.9 (-3.6)	155.1 (-4.7)	12400 (-56%)	48.6 (-8.9)	138.5 (-21.3)	5300 (-80%)	29.9 (-27.6)	128.8 (-31)
75	19600 (-30%)	52.8 (-4.7)	154.5 (-5.3)	10000 (-65%)	44.8 (-12.7)	131.7 (-28.1)	4000 (-86%)	25.2 (-32.3)	110.6 (-49.2)
90	17400 (-37%)	50.9 (-6.6)	154.1 (-5.7)	6900 (-75%)	40.8 (-16.7)	120.9 (-38.9)	2800 (-90%)	21.5 (-36)	94.3 (-65.5)
105	15500 (-45%)	49.5 (-8)	153.5 (-6.3)	4300 (-84%)	36.2 (-21.3)	101.1 (-58.7)	-	-	-
125	13500 (-53%)	48.3 (-9.2)	152.5 (-7.3)	-	-	-	-	-	-

Table 20: DSC data of FR-PLA-C30B as a function of M_n and ageing time under T/UV, T/RH and T/UV/RH.

Ageing exposure (days)	T/UV M_n (g/mol)	T/UV T_g (°C)	T/UV T_m (°C)	T/RH M_n (g/mol)	T/RH T_g (°C)	T/RH T_m (°C)	T/UV/RH M_n (g/mol)	T/UV/RH T_g (°C)	T/UV/RH T_m (°C)
0	27000	57.4	159.2	27000	57.4	159.2	27000	57.4	159.2
15	25100 (-7%)	56.2 (-1.2)	157.4 (-1.8)	21600 (-20%)	52.9 (-4.5)	152.0 (-7.2)	15000 (-45%)	43.1 (-14.3)	148.9 (-10.3)
30	23700 (-12%)	55.3 (-2.1)	154.3 (-4.9)	17600 (-35%)	50.4 (-7)	148.9 (-10.3)	9700 (-64%)	40.0 (-17.4)	146.1 (-13.1)
45	21600 (-20%)	55.1 (-2.3)	154.0 (-4.6)	12200 (-55%)	46.6 (-10.8)	145.9 (-13.3)	5800 (-75%)	34.9 (-22.5)	132.8 (-26.4)
60	21100 (-23%)	53.2 (-4.2)	153.3 (-5.9)	9800 (-64%)	39.6 (-17.8)	134.9 (-24.3)	4300 (-84%)	22.5 (-34.9)	115.4 (-43.8)
75	19100 (-29%)	52.3 (-5.1)	152.8 (-6.4)	7900 (-71%)	35.2 (-22.2)	122.7 (-36.5)	3400 (-88%)	16.2 (-41.2)	96.1 (-63.1)
90	17000 (-37%)	49.0 (-8.4)	152.3 (-6.9)	5100 (-81%)	28.9 (-28.5)	107.5 (-51.7)	2500 (-91%)	11.5 (-45.9)	83.9 (-75.3)
105	14700 (-54%)	48.6 (-8.8)	151.3 (-7.9)	4100 (-85%)	23.0 (-33.4)	89.4 (-69.8)	-	-	-
125	12500 (-54%)	46.7 (10.7)	150.0 (-9.2)	-	-	-	-	-	-

Regarding FR-PLA material (**Table 19**, **Figure 72** and **Figure 73**) it is evidenced that both T_g and T_m are affected by ageing under T/UV, T/RH and T/UV/RH conditions. In fact, T_g decreases from 57.5°C to 48.3°C (-9.2°C), 36.2°C (-21.3°C) and 21.5°C (-36°C) after 125 days under T/UV, 105 days under T/RH and 90 days under T/UV/RH exposure, respectively. T_m decreases from 159.8°C to 152.5°C (-7.3°C), 101.1°C (-58.7°C) and 94.3°C (-35.5°C) after 125 days under T/UV, 105 days under T/RH and 90 days under T/UV/RH, respectively.

FR-PLA-C30B (**Table 20**, as well as **Figure 72** and **Figure 73**) exhibits the same behavior as FR-PLA: both T_g and T_m are affected by ageing under T/UV, T/RH and T/UV/RH exposure. Indeed, T_g decreases from 57.4°C to 46.7°C (-10.7°C), 23°C (-33.4°C) and 11.5°C (-39.3°C) after 125 days under T/UV, 105 days under T/RH and 90 days under T/UV/RH, respectively. T_m decreases from 159.2°C to 150°C (-9.2°C), 89.4°C (-69.8°C) and 83.9°C (-75.3°C) after 125 days under T/UV, 105 days under T/RH and 90 days under T/UV/RH, respectively.

These results demonstrate once ageing, that the impact of ageing on T_g and T_m is dependent on the ageing conditions: the decrease of T_g and T_m is more important when samples are exposed to T/UV/RH conditions compared to T/RH and T/UV, respectively.

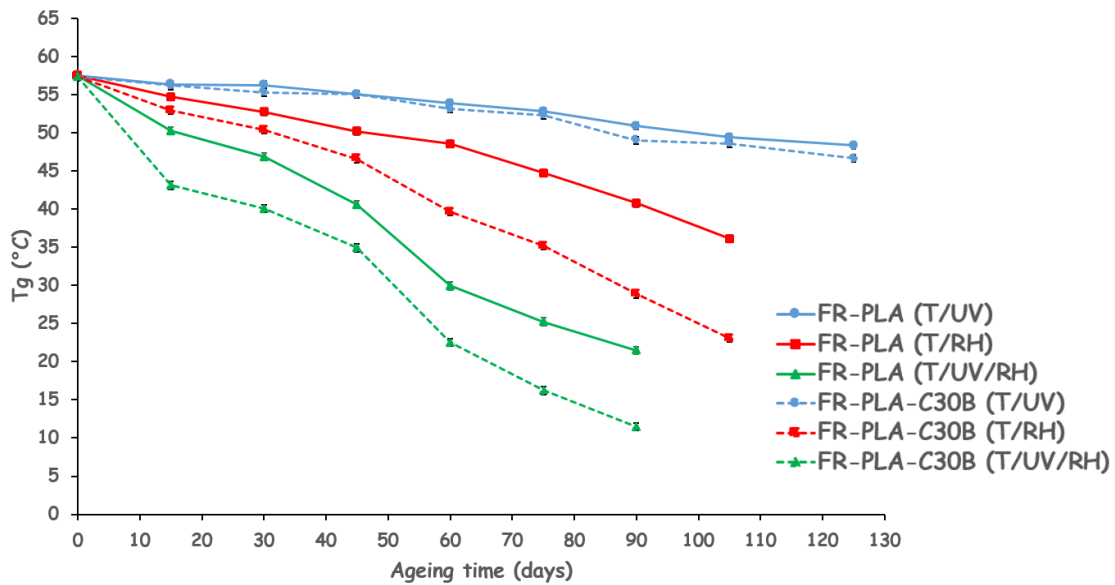


Figure 72: Evolution of glass transition temperature (T_g) of FR-PLA and FR-PLA-C30B as a function of exposure time under T/UV (●), T/RH (■) and T/UV/RH (△).

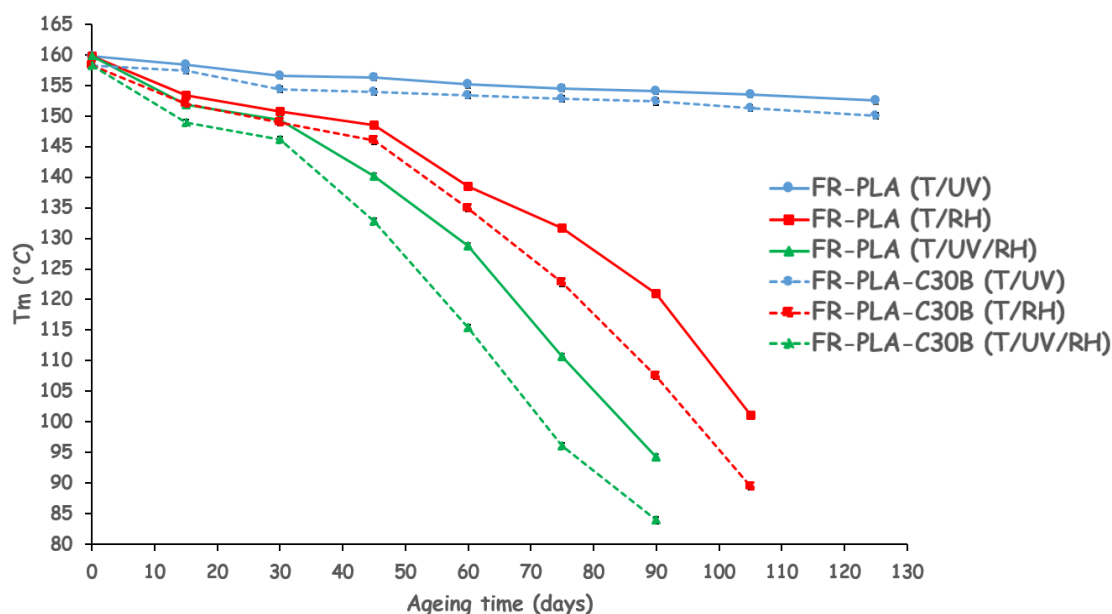


Figure 73: Evolution of melting temperature (T_m) of FR-PLA and FR-PLA-C30B as function of exposure time under T/UV (●), T/RH (■) and T/UV/RH (△).

Moreover, it is quite obvious regarding **Table 19**, **Table 20** and **Figure 74** that the decrease of both T_g and T_m of FR materials is even more important for low molecular masses:

- For FR-PLA: T_g and T_m are 48.3°C and 152.5°C, respectively, for a molecular mass of 13500 g/mol compared to 21.5°C and 94.3°C, respectively, for a molecular mass of 2800 g/mol.
- For FR-PLA-C30B: T_g and T_m are 46.7°C and 150°C, respectively, for a molecular mass of 12500 g/mol compared to 11.5°C and 83.9°C, respectively, for a molecular mass of 2500 g/mol.
- The lower M_n reported during ageing for FR-PLA-C30B compared to FR-PLA can be held responsible for the lower T_g and T_m values observed for this intumescent formulation.

This clearly demonstrates the importance of the molecular mass of FR-PLAs on the behavior of T_g and T_m during ageing (cf. Fox and Flory relationship **Equation 30**, p.94). Regarding the graph plotting T_g as a function of M_n of FR-PLA and FR-PLA-C30B for different ageing exposure conditions and durations (**Figure 74**), it appears that for both formulations T_g is stable at the beginning of the exposure and then decreases when M_n reaches the critical molecular mass (i.e. 20000 g/mol). T_m follows the same evolution as T_g during ageing. The high mobility of the polymer chains due to ageing affects the backbone flexibility and intermolecular interactions, leading to the decrease of T_m [38]. Compared to PLA, the lower M_n before ageing of both FR-PLAs permits to reach quickly the critical M_n from which T_g and T_m start to decrease.

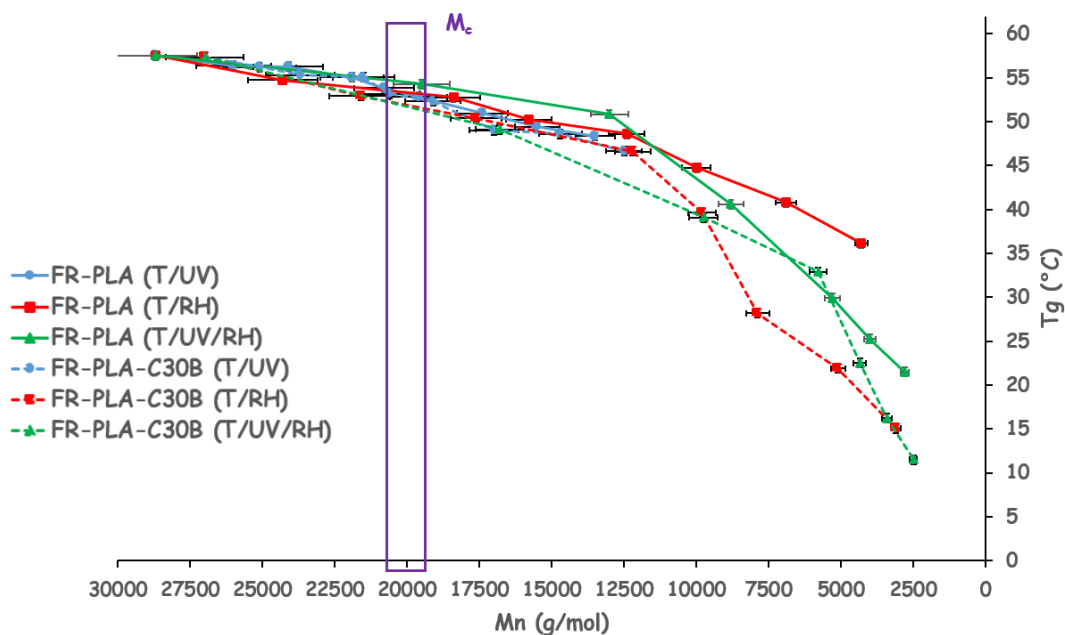


Figure 74: Correlation between the decrease of T_g and M_n of FR-PLA and FR-PLA-C30B as a function of ageing under T/UV (\bullet), T/RH (\blacksquare) and T/UV/RH (\blacktriangle).

It is also observed that whatever ageing conditions, the decrease of both T_g and T_m is more pronounced in the case of FR-PLA-C30B compared to FR-PLA. The most probable explanation is that the lower M_n reported during ageing for FR-PLA-C30B can be held responsible for the lower T_g and T_m values. However, another assumption to explain this phenomenon is that Cloisite 30B catalyzes the degradation of FR-PLA-C30B due to the presence of hydroxyl groups in the structure of the clay [237, 238]. This last hypothesis will be investigated in the next part.

Knowing the behavior of the molecular mass and thermal properties (i.e. T_g and T_m) of FR-PLAs during ageing, the crystallization behavior is the last physico-chemical property to investigate in order to compare the performance of FR-PLAs and PLA during ageing. Hence, the next section is dedicated to the effect of fillers on the crystallization of FR-PLA and FR-PLA-C30B as well as to their behavior during ageing.

2.3. Crystallization behavior

2.3.1. Crystallization compartment of unaged FR-PLAs

The crystallization behavior of FR-PLA and FR-PLA-C30B, studied using DSC, is compared to the one of PLA. Crystallinity (χ) of the different formulations are reported in **Table 21** and were calculated according to **Equation 24** (p.76).

Table 21: Crystallinity (χ) data for PLA, FR-PLA and FR-PLA-C30B as a function of M_n .

Material name	M_n (g/mol)	χ (%)
PLA	68000	6.5
FR-PLA	29000 (-57%)	11.5 (+5)
FR-PLA-C30B	27000 (-60%)	12.5 (+6)

Unfilled PLA is almost amorphous with a relatively low crystallinity of about 6.5%. However, it appears that when fillers are added into PLA, the crystallinity of the material increases, reaching 11.5% and 12.5% for FR-PLA and FR-PLA-C30B, respectively. It seems that Melamine, APP in particular and Cloisite 30B to a less extent, promote the crystallization of the FR-materials. Two assumptions can be made to explain this effect on crystallinity:

- FR fillers act as nucleating agents by promoting the crystallization of the materials [25, 36, 39, 239-242].
- The lower M_n of FR-PLA and FR-PLA-C30B before ageing promotes the crystallization of the materials. Indeed, polymers of low molecular weight can crystallize more easily compared to those of high molecular weight [66, 81, 231, 243-245]. This is probably due to the fact that smaller molecules have a higher mobility and can thus easily form crystals

XRD experiments were performed in order to determine if fillers have an influence on the kind of crystals formed during crystallization (**Figure 75**).

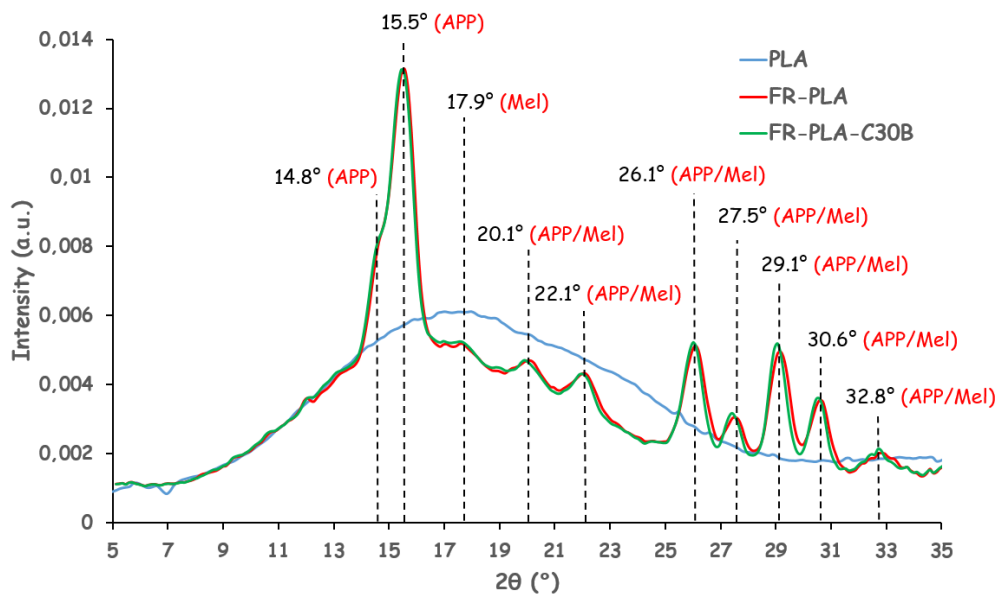


Figure 75: WAXD patterns of PLA (●), FR-PLA (●) and FR-PLA-C30B (●).

PLA presents a typical amorphous WAXD patterns due to its low crystallinity (i.e. 6.5%). FR-PLA and FR-PLA-C30B exhibit similar WAXD patterns. Characteristic diffraction peaks of FR fillers are identified: (i) Melamine peaks at $2\theta = 17.9^\circ, 20.1^\circ, 22.1^\circ, 26.1^\circ, 27.5^\circ, 29.1^\circ, 30.6^\circ$ and 32.8° [246, 247]; (ii) APP peaks at $2\theta = 14.8^\circ, 15.5^\circ, 20.1^\circ, 22.1^\circ, 26.1^\circ, 27.5^\circ, 29.1^\circ, 30.6^\circ$ and 32.8° [248-250]; (iii) The characteristic peak of Cloisite 30B at $2\theta = 5.0^\circ$ [36, 251] is not observed due to the relatively low loading of organoclay (i.e. 1 wt.-%). No characteristic peak of crystallized PLA is observed in the WAXD patterns of the two FR formulations. Indeed, the crystallinity of PLA versus FR fillers is certainly too low to see these peaks and thus it is not possible to determine under which form PLA crystallizes.

2.3.2. Influence of ageing exposure on crystallization behavior of FR-PLAs

The evolution of crystallinity (χ) for FR-PLA and FR-PLA-C30B was then studied as a function of ageing time for T/UV, T/RH and T/UV/RH exposure (**Table 22** and **Table 23** for FR-PLA and FR-PLA-C30B, respectively). Focusing firstly on FR-PLA, results reported in **Table 22** and **Figure 76** plotting the behavior of χ as a function of ageing duration both evidence that crystallinity increases when FR-PLA is exposed to T/UV, T/RH and T/UV/RH. Indeed, χ increases by 11.5% and 43% after 125 days exposure to T/UV and 105 days exposure to T/RH, respectively. However, the most significant increase is observed for FR-PLA aged under T/UV/RH conditions, where a 53.5% increase in crystallinity is achieved after 90 days, corresponding to a χ of 65% and to the lower M_n of the material (i.e. 2800 g/mol).

Table 22: Evolution of Crystallinity for FR-PLA as a function of M_n for different ageing durations under T/UV, T/RH and T/UV/RH exposure.

Ageing time (days)	T/UV M_n (g/mol)	T/UV χ (%)	T/RH M_n (g/mol)	T/RH χ (%)	T/UV/RH M_n (g/mol)	T/UV/RH χ (%)
0	29000	11.5	29000	11.5	29000	11.5
15	26000 (-9%)	14.0 (+2.5)	24300 (-16%)	15 (+4.5)	17500 (-39%)	27.0 (+15.5)
30	24100 (-14%)	16.0 (+4.5)	18400 (-34%)	19.0 (+7.5)	13000 (-54%)	36.0 (+24.5)
45	21900 (-22%)	17.0 (+5.5)	15800 (-44%)	28.0 (+16.5)	8800 (-69%)	43.0 (+31.5)
60	21200 (-26%)	18.0 (+6.5)	12400 (-56%)	31.0 (+19.5)	5300 (-80%)	49.0 (+37.5)
75	19600 (-30%)	20.0 (+8.5)	10000 (-65%)	38.0 (+26.5)	4000 (-86%)	60.0 (+48.5)
90	17400 (-38%)	21.5 (+10)	6900 (-75%)	43.0 (+31.5)	2800 (-90%)	65.0 (+53.5)
105	15500 (-45%)	22.0 (+10.5)	4300 (-85%)	54.5 (+43)	-	-
125	13500 (-52%)	23.0 (+11.5)	-	-	-	-

Regarding FR-PLA-C30B formulation, an increase in crystallinity is also observed (**Table 23** and **Figure 76**). Indeed, χ is enhanced by 14.5% and 52.5% after 125 days exposure to T/UV and 105 days exposure to T/RH, respectively. However, as for FR-PLA, the most significant increase is observed for exposure under T/UV/RH conditions, where an increase in crystallinity of 63.5% is achieved after 90 days, corresponding to a χ of 76%. This value of crystallinity corresponds to the lower M_n observed for the material (i.e. 2500 g/mol) when exposed to T/UV/RH.

Table 23: Evolution of Crystallinity for FR-PLA-C30B as a function of M_n for different ageing duration under T/UV, T/RH and T/UV/RH exposure.

Ageing time (days)	T/UV M_n (g/mol)	T/UV χ (%)	T/RH M_n (g/mol)	T/RH χ (%)	T/UV/RH M_n (g/mol)	T/UV/RH χ (%)
0	27000	12.5	27000	12.5	27000	12.5
15	25100 (-7%)	14.5 (+2)	21600 (-20%)	15.5 (+3)	15000 (-45%)	32.0 (+19.5)
30	23700 (-12%)	18.0 (+5.5)	17600 (-35%)	23.0 (+10.5)	9700 (-64%)	41.0 (+28.5)
45	21500 (-20%)	19 (+6.5)	12200 (-55%)	34 (+21.5)	5800 (-79%)	54.0 (+41.5)
60	20900 (-23%)	21.0 (+8.5)	9800 (-64%)	42 (+29.5)	4300 (-84%)	59.0 (+46.5)
75	19100 (-29%)	22.0 (+9.5)	7900 (-71%)	50 (+37.5)	3400 (-88%)	71.0 (+58.5)
90	17000 (-37%)	23.0 (+10.5)	5100 (-81%)	57 (+44.5)	2500 (-91%)	76.0 (+63.5)
105	14700 (-54%)	26.0 (+13.5)	4100 (-85%)	65 (+52.5)	-	-
125	12500 (-54%)	27.0 (+14.5)	-	-	-	-

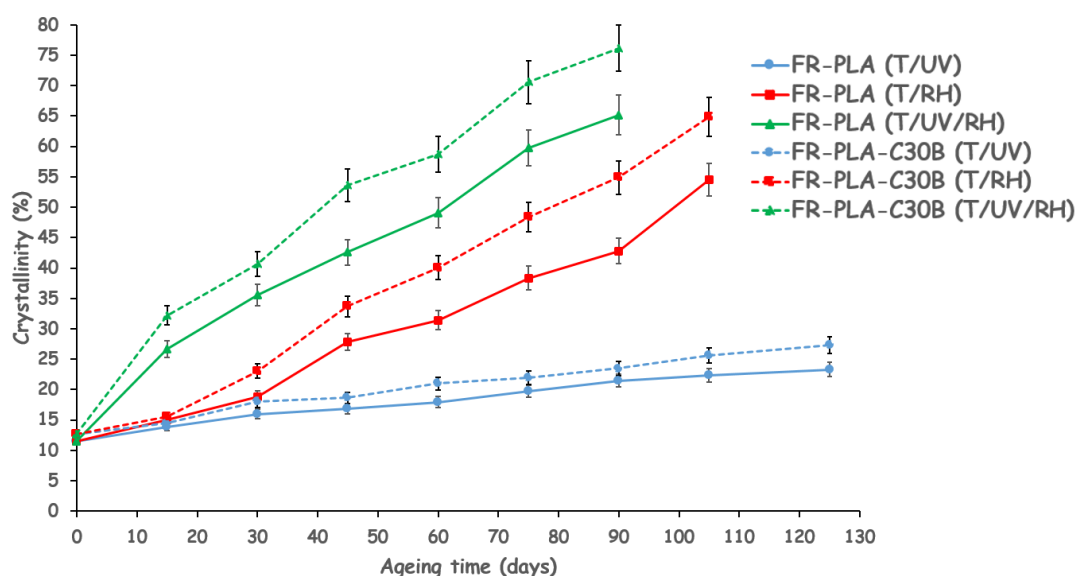


Figure 76: Evolution of crystallinity of FR-PLA (a) and FR-PLA-C30B (b) as a function of ageing time, for T/UV (●), T/RH (■) and T/UV/RH (△) exposure.

These results seem to indicate that the increase in crystallinity is linked to the decrease of the molecular mass, which is in accordance both with literature [5, 27, 29, 38, 204] and the results reported for PLA in chapter III (p.98). Indeed, during degradation, the molecular mass decreases and due to a chemi-crystallization process [5, 27, 29, 38, 204] the crystallinity increases. It is also observed that the increase in crystallinity is more pronounced for FR-PLA-C30B than for FR-PLA (Table 22 and Table 23). In fact, χ increases by 53.5% and 63.5% for FR-PLA and FR-PLA-C30B after 90 days exposure to T/UV/RH, respectively. This phenomenon can be explained by the lower M_n reached by FR-PLA-C30B during ageing. Indeed, when plotting crystallinity as a function of M_n for FR-PLA and FR-PLA-C30B (Figure 77) it appears that the lower the M_n , the higher the crystallinity: for example, after 105 days exposure to T/RH χ reaches 54.5% and 65% when M_n is 4300 and 4100 g/mol for FR-PLA and FR-PLA-C30B,

respectively. On the other hand, it is possible that organoclays acts as strong nucleating agents, altering the materials crystallization behavior during ageing by promoting the crystallization of FR-PLA-C30B [25, 38, 39].

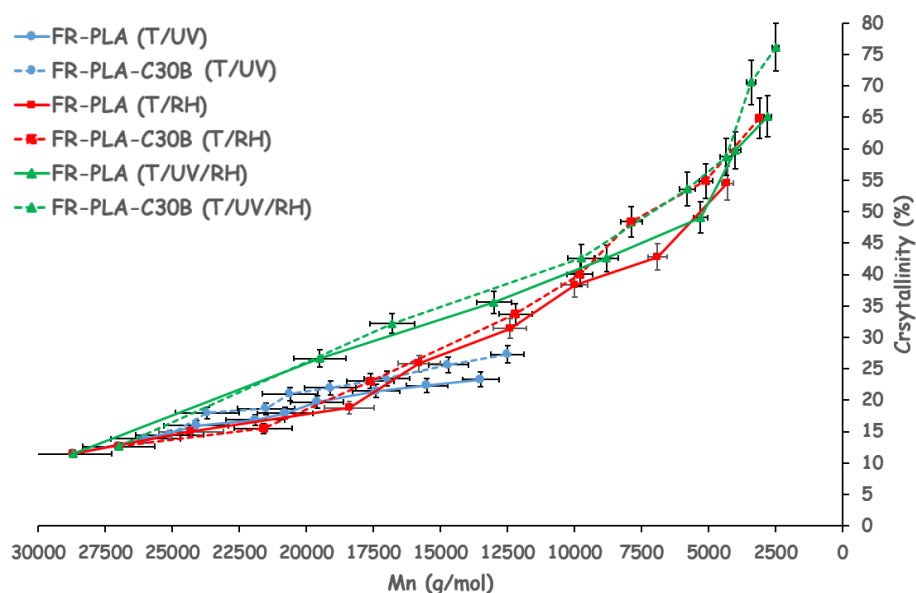


Figure 77: Correlation between the decrease of crystallinity and M_n of FR-PLA and FR-PLA-C30B as a function of ageing under T/UV (\bullet), T/RH (\blacksquare) and T/UV/RH (Δ).

It was previously demonstrated that the increase in crystallinity of PLA during ageing is linked to the formation of α' -form crystals (p.98). Hence, XRD was performed to identify if the presence of FR fillers change the nature of crystals formed during ageing exposure. The WAXD patterns obtained by XRD for unaged and 60 days aged FR-PLA and FR-PLA-C30B under T/UV, T/RH and T/UV/RH conditions are shown in **Figure 78**. Before ageing, both FR-PLA and FR-PLA-C30B exhibit the characteristic diffraction peaks of Melamine and APP that have been previously reported (p.135). Even if these peaks are also observed for both materials after 60 days ageing, the appearance of two new diffraction peaks is observed for both FR-PLAs. These two new peaks that appear at $2\theta = 16.6^\circ$ and 18.8° are characteristic of α' -form crystals of PLA [202, 203]. As for PLA, no additional peaks characteristic of α -form crystals are observed during ageing at $2\theta = 12.5^\circ$, 14.8° , 22.5° , 27.3° and 29.2° .

The two α' -form characteristic peaks show higher intensity for materials exposed to T/UV/RH conditions compared to those exposed to T/RH and T/UV. Moreover, regarding one kind of exposure, the intensities of α' -form crystals peaks are higher for FR-PLA-C30B compared to FR-PLA. This is in accordance with the evolution of the crystallinity observed by DSC.

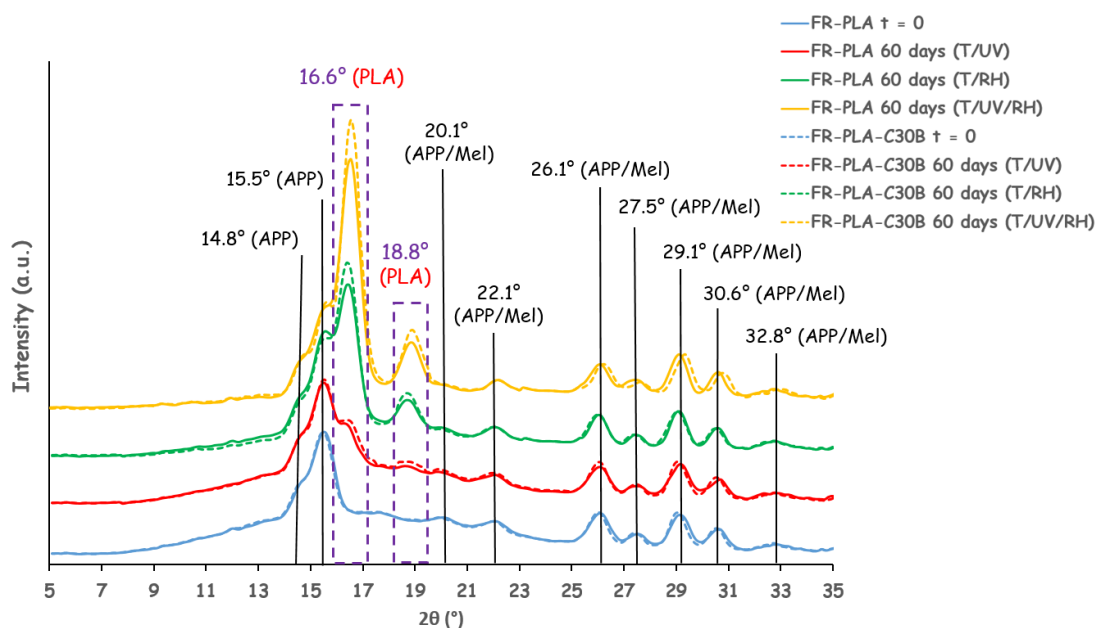


Figure 78: WAXD patterns of FR-PLA and FR-PLA-C30B obtained by XRD, before (●) and after 60 of ageing under T/UV (●), T/RH (●) and T/UV/RH (●).

DSC and XRD analyses both evidence the increase in crystallinity when FR-PLA and FR-PLA-C30B are exposed to T/UV, T/RH and T/UV/RH conditions. As for PLA, α' -form crystals appear during ageing which formation is linked to (i) the decrease of M_n and (ii) chemi-crystallization process occurring during ageing. This means that presence of FR fillers doesn't impact the nature of crystal formed during ageing. The lower M_n of FR-PLAs before ageing and the nucleating effect of fillers promote the crystallization of both FR materials. Moreover, the lower M_n of FR-PLA-C30B during ageing, compared to the one of FR-PLA, leads to a material of higher crystallinity for the same ageing period.

2.4. Conclusion

It has been demonstrated in this part that the incorporation of FR additives (i.e. Melamine, APP and C30B) impact the physico-chemical properties of PLA at two different levels: (i) before and (ii) after ageing of the materials.

Indeed, even before ageing these FR additives can modify some properties of PLA:

- The incorporation of fillers reduces the molecular mass of PLA, due to physical and/or chemical processes.
- The molecular mass is known to be a parameter affecting T_g . Thus the decrease of M_n can be held responsible for the decrease of T_g observed when PLA is filled with FR fillers. Moreover, the plasticizing effect of fillers can also be a reasonable assumption to explain the lower T_g of FR-PLAs.
- As well as T_g , the crystallinity is also dependent on the molecular mass of the material. Thus, the lower M_n of FR-PLA and FR-PLA-C30B before ageing

promotes the crystallization of the materials, explaining why the crystallinity of FR-PLAs are higher than those of PLA. In addition, the nucleating character of FR fillers can slightly promotes the crystallization of the materials

Secondly, it was also reported that effects of ageing are more pronounced when FR fillers are incorporated into the PLA matrix:

- Voids, fractures and a white layer are observed at the surface of FR-PLAs until their complete disintegration when exposed to T/RH and T/UV/RH conditions. These phenomena are observed when $M_c (\pm 20000 \text{ g/mol})$ is reached.
- Only the 60 days exposure to T/UV appear not to be too damaging for the visual integrity of FR-PLA and FR-PLA-C30B. In fact, after 60 days M_c is still not reached.
- As for neat PLA, it was evidenced that the molecular mass of FR-PLA and FR-PLA-C30B decreases when exposed to T/UV, T/RH and T/UV/RH conditions.
- The behavior of the molecular mass has a direct impact on the physico-chemical properties of FR materials during ageing. Indeed, the decrease of M_n leads to a decrease in both T_g and T_m as well as an increase in crystallinity.
- Due to the lower M_n of FR-PLAs before ageing, FR-PLA and FR-PLA-C30B reach more rapidly the critical molecular mass ($M_c \pm 20000 \text{ g/mol}$) from which the material starts to disaggregate and to lose its thermal properties. Thus explaining why FR-PLAs are more degraded after 125 days of ageing compared to PLA.

Hence, it is obvious that FR fillers impact PLA before and after ageing. Furthermore, the molecular mass appears to be a key parameter in the durability of PLA and FR-PLAs as it governs the structural integrity as well as the behavior of thermal properties and crystallinity during ageing. However, while the mechanisms of degradation of neat PLA have been elucidated in the previous chapter (**p.104**), the impact of the addition of fillers on the mechanisms of degradation of PLA still has to be investigated. This is why the next part of this chapter is dedicated to the understanding of the impact of fillers on the mechanisms of degradation occurring during exposure to T/UV, T/RH and T/UV/RH.

3. Mechanisms of degradation of PLA in presence of fillers

Literature as well as our previous investigations have demonstrated that mechanism of degradation of PLA depends on the kind of accelerated ageing conditions (Chapter III, **p.104**) [5, 27-29, 31-35, 38, 39, 52, 121, 123, 125, 153, 158-161]. In fact, when exposed to T/RH, hydrolysis is the predominant mechanism. On the contrary, under T/UV and T/UV/RH, it was reported that PLA is degraded via a radical mechanism, which is in competition with hydrolysis in the case of T/UV/RH. Objective of the following part is to determine if flame retardant additives influence the mechanisms of degradation of PLA.

3.1. Surface chemical analysis of aged FR materials

Chemical surface analyses of the layer formed at the surface of both FR-PLAs (before and after T/RH and T/UV/RH conditions) have been carried out by electron probe micro analysis (EPMA) X-Ray mappings (1 μm^3 diffusion volume) and X-Ray photoelectron spectroscopy (XPS) experiments (few μm^3 diffusion volume).

EPMA X-Ray mappings were carried out to characterize the surface of FR-PLA and FR-PLA-C30B plates, looking at (i) nitrogen, present in both Melamine and APP, (ii) phosphorus, characteristic of APP and (iii) silicon, characteristic of Cloisite 30B. The evolution of nitrogen and phosphorus concentrations at the surface of FR-PLA plates (**Figure 79**) is reported before ageing and after 60 days under T/UV ($M_n \pm 21300$ g/mol), 28 days under T/RH ($M_n \pm 20000$ g/mol) and 6 days under T/UV/RH exposure ($M_n \pm 20000$ g/mol). Whereas no significant evolution is noticed concerning FR-PLA aged under T/UV (**Figure 79 (b)**), pictures indicate that the concentrations of nitrogen and phosphorus increase slightly at the surface of the plate after 28 days exposure to (T/RH) (**Figure 79 (c)**) compared to unaged material (**Figure 79 (a)**). This phenomenon is even more obvious (in particular for phosphorus) at the surface of plates aged for 6 days under T/UV/RH (**Figure 79 (d)**).

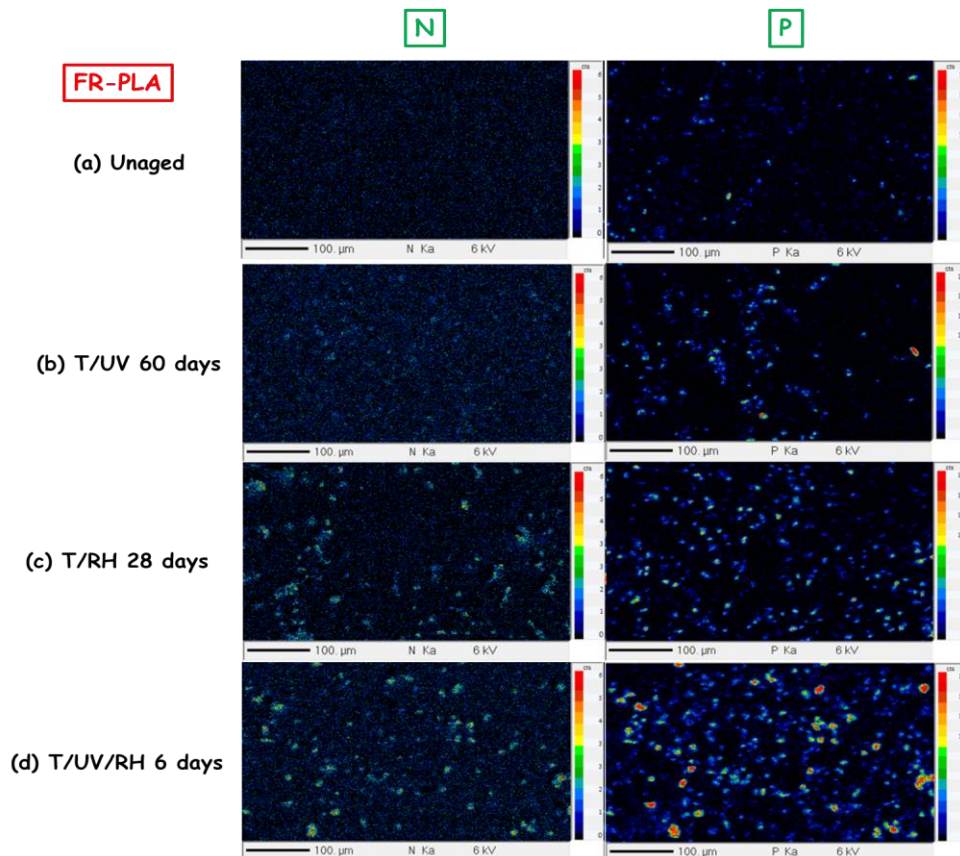


Figure 79: EPMA pictures for unaged (a), 60 d T/UV (b), 28 d T/RH (c) and 6 d T/UV/RH (d) aged FR-PLA.

Regarding FR-PLA-C30B, the X-Ray mappings of silicon, nitrogen and phosphorus (**Figure 80**) are reported before and after 60 days under T/UV ($M_n \pm 21100$ g/mol), 28 days under T/RH ($M_n \pm 20000$ g/mol) and 6 days under T/UV/RH exposure ($M_n \pm 20000$ g/mol). As well as for FR-PLA, no significant evolution is noticed concerning FR-PLA-C30B aged under T/UV condition (**Figure 80 (b)**). Pictures after 28 days exposure to T/RH show that the concentrations of silicon, nitrogen and phosphorus increase at the surface of the plates (**Figure 80 (c)**) compared to the unaged FR-PLA-C30B (**Figure 80 (a)**). This increase in fillers concentration at the surface of the plates is quite obvious after 6 days exposure to T/UV/RH (**Figure 80 (d)**) and much more visible than the one for FR-PLA (**Figure 79 (d)**).

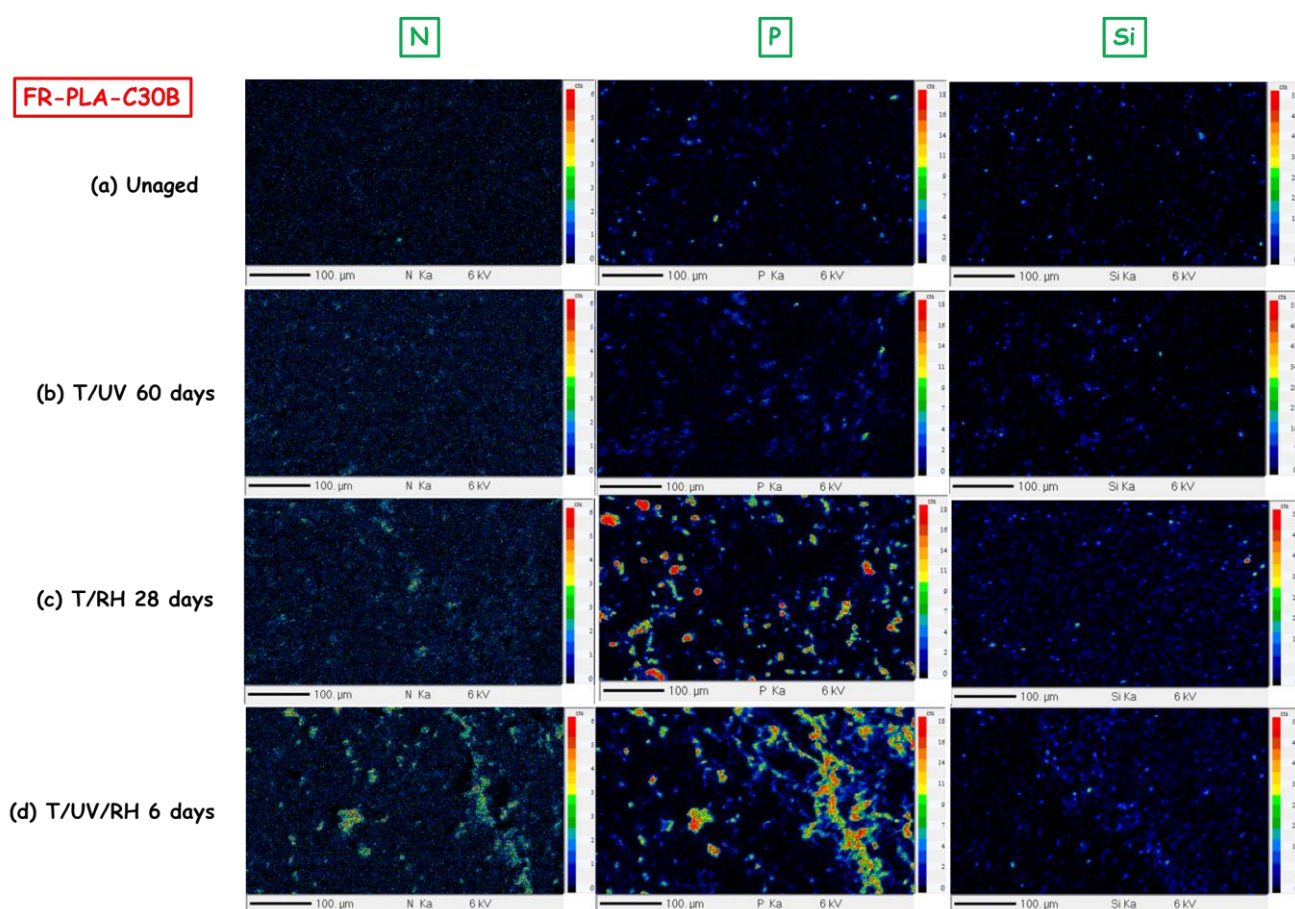


Figure 80: EPMA pictures for unaged (a), 60 d T/UV (b), 28 d T/RH (c) and 6 d T/UV/RH (d) aged FR-PLA-C30B.

These X-Ray mappings confirm that when the critical molecular mass (± 20000 g/mol) is reached, the combination of water and FR fillers leads to the formation of the white layer observed at the surface of aged FR-PLAs (cf. **p.122**). Moreover, this effect is enhanced by UV exposure. The layer is composed of nitrogen, phosphorus and silicon which are characteristic elements of FR fillers incorporated into the PLA matrix (i.e. Melamine, APP and Cloisite 30B).

In addition to EPMA analysis, X-Ray photoelectron spectroscopy was also performed on FR-PLA and FR-PLA-C30B plates before and after 60 days exposure to T/UV, 28 days to T/RH and

6 days to T/UV/RH conditions. The atomic percentages (At %) of carbon (C), oxygen (O), nitrogen (N), phosphorus (P) and silicon (Si) at the extreme surface of FR-PLAs plates were then quantified (**Table 24** and **Table 25** for FR-PLA and FR-PLA-C30B, respectively). Whereas the concentration of carbon decreases at the surface of aged materials when exposed to T/UV, T/RH and T/UV/RH conditions, it appears that the concentration of oxygen, nitrogen, phosphorus and silicon increases. As an example, C % at the surface of the plates is decreased by 17.6% and 22.7% for FR-PLA and FR-PLA-C30B, respectively, after 6 days exposure to T/UV/RH conditions. Meanwhile, (i) O % increases by 13.8 and 17.9%, (ii) P % increases by 2.5% and 2.7%, (iii) N % is increased by 1.8% and 2.1% for FR-PLA and FR-PLA-C30B, respectively and (iv) Si % reaches 0.8 % for FR-PLA-C30B after 6 days exposure to T/UV/RH conditions.

Table 24: At % on the surface of FR PLA determined by XPS as a function of ageing.

Ageing (type/days)	C 1s (At %)	O 1s (At %)	N 1s (At %)	P 2p (At %)
0	83.4	16.2	0.4	-
T/UV 60 d	78.9 (-4.5)	19.5 (+3.3)	0.7 (+0.3)	0.9
T/RH 28 d	67.4 (-16)	29.4 (+13.2)	1.4 (+1)	1.8
T/UV/RH 6 d	65.8 (-17.6)	30 (+13.8)	1.8 (+1.4)	2.5

Table 25: At % on the surface of FR PLA-C30B determined by XPS as a function of ageing.

Ageing (type/days)	C 1s (At %)	O 1s (At %)	N 1s (At %)	P 2p (At %)	Si 2p (At %)
0	83.9	15.1	0.8	0.2	-
T/UV 60 d	77.5 (-6.4)	20 (+4.9)	1.3 (+0.5)	1.2 (+1)	-
T/RH 28 d	65 (-18.9)	30.9 (+15.8)	1.7 (+0.9)	2 (+1.8)	0.4
T/UV/RH 6 d	61.2 (-22.7)	33 (+17.9)	2.1 (+1.3)	2.9 (+2.7)	0.8

These results, which demonstrate the higher concentration of nitrogen, phosphorus and silicon at the surface of aged materials are in accordance with the observations done by EPMA X-Ray mappings. It also appears that relative humidity exposure increases the concentration of fillers at the surface of aged samples. Hence, the role of fillers during hydrolysis is investigated in the next section.

3.2. Role FR additives during hydrolysis

3.2.1. Hydrolysis of flame retardant additives

Whereas the presence of water was evidenced to play a key role during the formation of the white layer during ageing, it is not clear if this layer corresponds to FR fillers on the surface or to secondary products due to their degradation (hydrolysis). Hence, in order to identify

structural changes of additives during ageing in presence of relative humidity, Melamine, APP and Cloisite 30B were exposed to T/RH atmosphere for 125 days. FTIR-ATR analyses were performed on powder all along the exposure to T/RH.

Firstly, focusing on Melamine (**Figure 81**), the spectra can be classified into different regions, which correspond to the following bands assignment [252, 253]: -N-H (primary amine), stretching and bending from 2800 cm^{-1} to 3500 cm^{-1} , -N-H (primary amine) stretching located at 1650 cm^{-1} , C=N ring vibration observed at 1546 cm^{-1} , -C-N triazine stretching and bending at 1460 cm^{-1} , 1430 cm^{-1} and 1020 cm^{-1} and C=N bending of triazine ring located at 800 cm^{-1} . These characteristics peaks are also observed after 60 and 125 days of exposure to T/RH with no appearance of new peaks, indicating that Melamine is not hydrolyzed in Ammeline, Ammelide or Cyanuric acid in these relative humidity conditions [254-256].

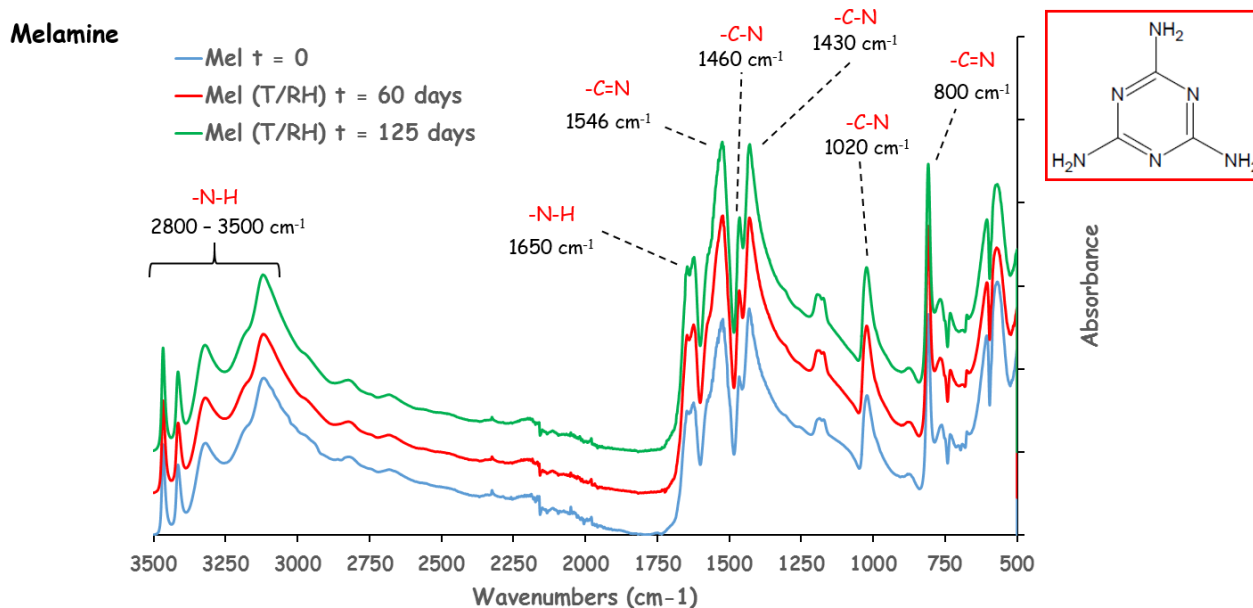


Figure 81: FTIR spectra (ATR) of Melamine as function of ageing exposure under T/RH.

Spectra of APP before ageing and after 60 days and 125 days exposure to T/RH conditions are shown in **Figure 82**. APP like many other polyphosphates is known to be sensitive to hydrolysis [257-260]. In fact, APP is initially water insoluble and becomes soluble when its molecular weight decreases, thus leading to the formation of polyphosphoric acid (**Figure 83**) [175]. However, in our study, it seems that APP is not hydrolyzed (**Figure 82**), as similar characteristics peaks of APP are observed [261, 262] before and after ageing: -N-H (primary amine) bending from 2800 cm^{-1} to 3200 cm^{-1} , NH_4^+ located at 1710 cm^{-1} , 1670 cm^{-1} and 1470 cm^{-1} , -P=O bands identified at 1240 cm^{-1} , the region between 800 cm^{-1} and 1100 cm^{-1} is assigned to asymmetric and symmetric vibration of P-O. The peak located at 795 cm^{-1} is assigned to P-O-P bands and should decrease during hydrolysis, which is not the case here. Moreover, the characteristic peaks of polyphosphoric acid [259, 260], i.e. -OH in the range of $3200-3600\text{ cm}^{-1}$ and -P-OH at 898 cm^{-1} are not observed.

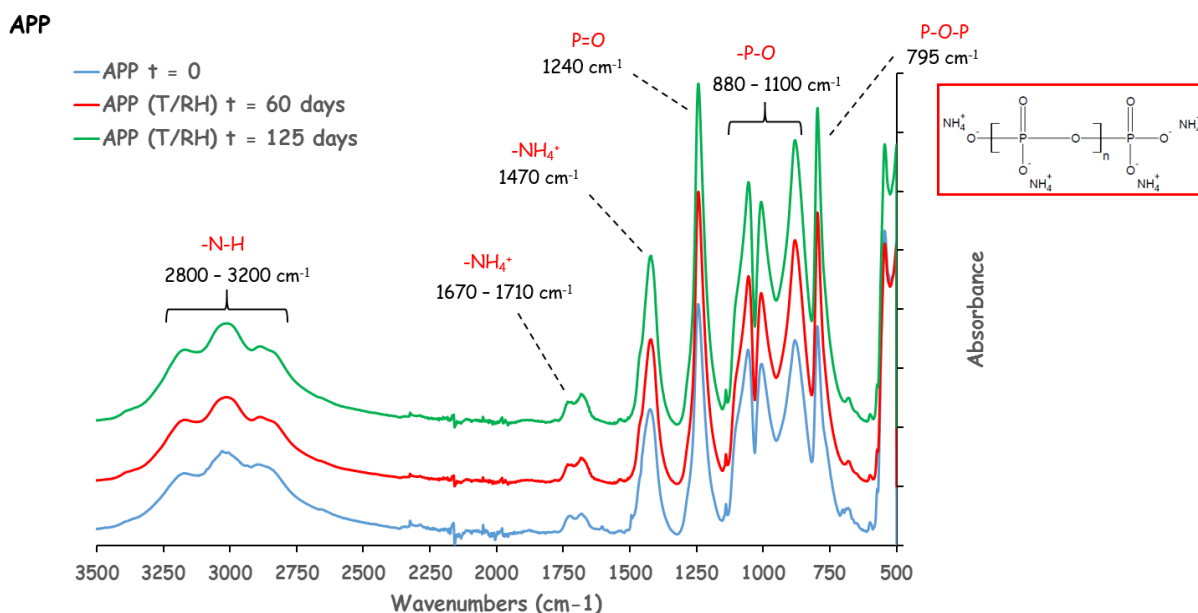


Figure 82: FTIR spectra (ATR) of APP as function of ageing exposure under T/RH.

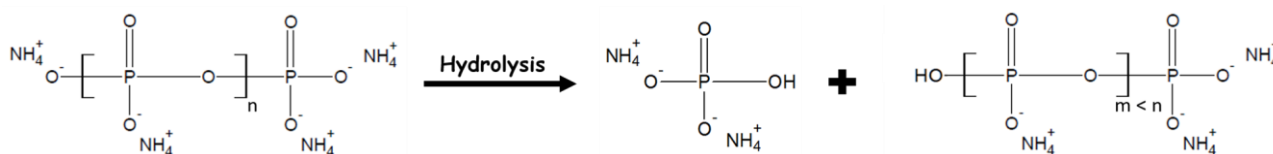


Figure 83: Hydrolysis reaction of APP, according to Chen et al. [175].

As it is quite difficult to distinguish -P-O-P- and -P-OH or -N-H and -OH regions in FTIR, ³¹P solid state NMR analyses were carried out on FR-PLA and FR-PLA-C30B to support the FTIR results. Experiments were performed before ageing, on APP after 105 days exposure to T/RH and on the white layer collected on the surface after 28 days exposure to T/RH conditions and 6 days exposure to T/UV/RH conditions (**Figure 84**). Whereas APP generally shows two peaks located at -22 and -24 ppm, corresponding to a well crystallized structure with Q₂ phosphorus units contained in polyphosphate chains, the APP spectrum depicted in **Figure 84(a)** and **(b)** exhibits one single band located at -22 ppm (P-O-P links, here in polyphosphates) [258, 263]. Moreover, this spectrum shows an amorphization due to the form of the band. Before ageing, both FR-PLA and FR-PLA-C30B exhibit this single band at -22 ppm. After 28 days of ageing under T/RH and 6 days under T/UV/RH, APP is also visible on the white layer formed on FR-PLA and FR-PLA-C30B and the two peaks characteristic of Q₂ units of polyphosphoric acid (H⁺ substituting NH₄⁺) located at -25 and -27 ppm [258] are not observed (**Figure 84 (a)** and **(b)**). This tendency is confirmed by the spectrum of APP exposed 105 days to T/RH ageing, where only the band at -22 ppm is observed. Hence, this tends to confirm that (i) APP is not degraded or very partially, explaining why polyphosphoric acid is not detected and that (ii) FR fillers are found at the surface of FR-PLA plates after ageing. It is possible that after 125 days of ageing APP is still not sufficiently degraded to observe its hydrolysis.

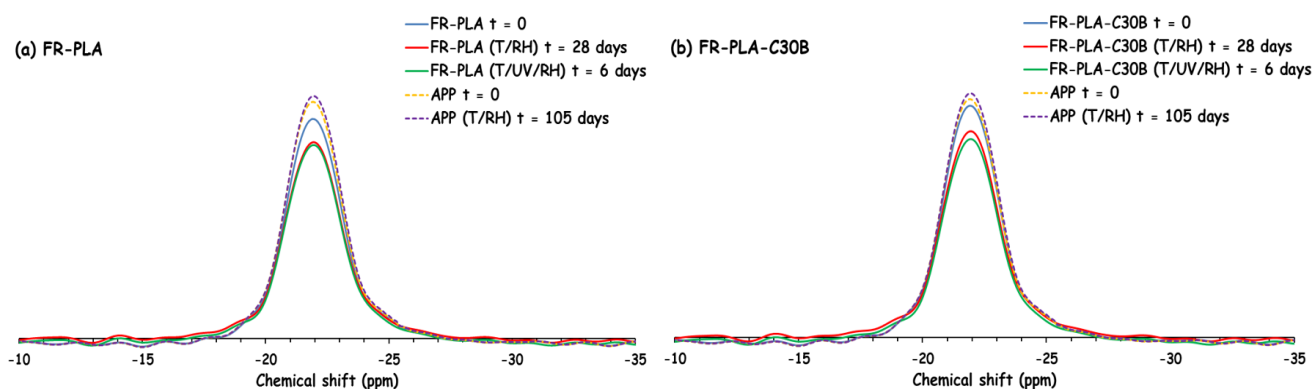


Figure 84: ^{31}P Solid-state NMR spectra of FR-PLA (a) and FR-PLA-C30B (b) before and after 105 days and 90 days exposure to T/RH and T/UV/RH conditions, respectively.

FTIR spectra of Cloisite 30B before and after 60 days and 125 days exposure to T/RH conditions are shown in **Figure 85**. Characteristic peaks of this organomodified montmorillonite [264, 265] are similar before and after ageing: -OH structural hydroxyl group stretching at 3610 cm^{-1} , -C-H asymmetric and symmetric stretching at 2920 cm^{-1} and 2850 cm^{-1} , respectively. The band located at 1610 cm^{-1} can be attributed to -C-OH deformation, the one at 1120 cm^{-1} corresponds to Si-O stretching. The bands in the range of 880 to 980 cm^{-1} correspond to Al-FeOH deformation and the band located at 790 cm^{-1} is also attributed to Si-O stretching. Some papers report the catalytic effect of Cloisite 30B on the degradation of polymers due to the structure of the clay [237, 238]. However, (i) the behavior of the clay reported by FTIR during ageing and (ii) previous results concerning the evolution of the physico-chemical properties of FR-PLAs (**p.125**) seem to indicate that these clays do not accelerate the hydrolysis of PLA.

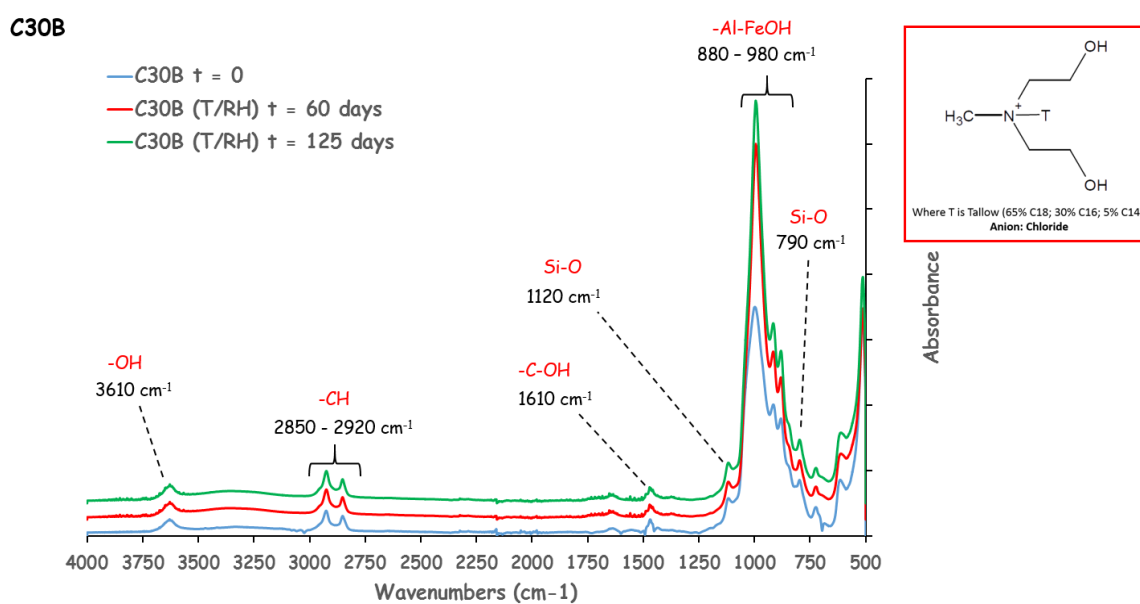


Figure 85: FTIR spectra (ATR) of Cloisite 30B as function of ageing exposure under T/RH.

Moreover, even if the results are not presented, a parallel study (**Appendix 3, p.221**) was also led during this work concerning the effect of the type of nanoparticle on the hydrolytic degradation of flame retarded PLA. In fact, literature reveals that the hydrophilic character of clays, due to the type of surfactant, can enhance or not the degradation rate of PLA [25, 37, 38]. Hence, three kinds of Cloisite, i.e. 20A, 30B and Na⁺ (hydrophilic character of C-Na⁺ > C-30B > C-20A) were incorporated into FR-PLA materials and then aged for 60 days under T/RH conditions. The formation of voids, fractures and of a white layer was reported after 28 days ageing for each formulation. Moreover, physico-chemical properties of the materials were studied and it appears that the molecular mass, T_g, T_m and crystallinity of the three materials exhibit the same behavior during ageing, whatever the formulation. All these results seem to indicate that the hydrophilic character of organoclays does not play a particular role during the degradation of the PLA matrix.

The behavior of FR fillers during ageing was confirmed by FTIR spectra recorded for FR-PLAs during exposure to T/RH and T/UV/RH conditions (**Appendix 4, p. 226**). As it was reported that FR fillers are not degraded (or partially in the case of APP) during ageing in presence of RH, it is confirmed that the white layer formed at the surface of FR materials during RH exposure is mainly composed of Melamine, APP and C30B in the case of FR-PLA-C30B. However, it is still not so obvious to determine if (i) the flame retardant additives migrate through the PLA matrix during ageing or if (ii) fillers are just more accessible at the surface due to the degradation of the matrix (both chain mobility and structural integrity of the material are no longer sufficient to maintain the cohesion between fillers and polymer matrix).

3.2.2. Evaluation of the migration of flame retardant additives

In order to assess the possible migration of FR fillers to the surface of FR-PLAs, SEM and EPMA analysis were carried out. Cross section SEM analyses have been performed on FR-PLA-C30B exposed for 28 days to T/RH (**Figure 86 (a)**) and 6 days to T/UV/RH conditions (**Figure 86 (b)**). Fillers seem to be uniformly dispersed in the PLA matrix with no migration during ageing. Thus, to validate this assumption, EPMA analyses were also performed on these samples.

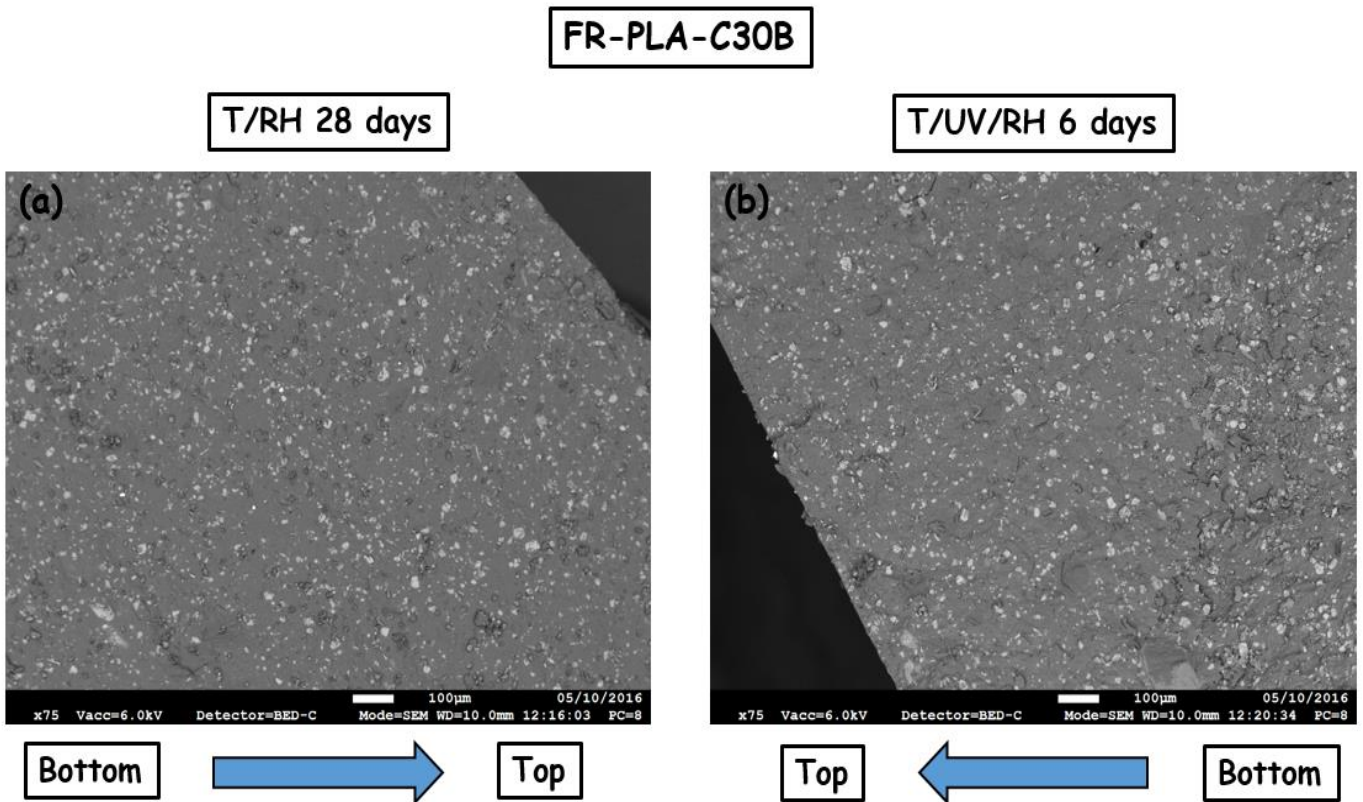


Figure 86: SEM pictures in cross section obtained for FR-PLA-C30B aged 28 days under T/RH (a) and 6 days under T/UV/RH (b).

Cross section EPMA X-Ray mappings performed on FR-PLA-C30B aged for 28 days under T/RH and 6 days under T/UV/RH conditions are reported in **Figure 87**. Mappings in nitrogen, phosphorus and silicon contained in T/RH aged (**Figure 87 (a)**) and T/UV/RH aged FR-PLA-C30B (**Figure 87 (b)**) corroborate the assumption that fillers do not migrate to the surface of the plates during ageing. In fact, for both materials, the concentration of nitrogen, phosphorus and silicon is quite the same from the bottom to the top of the plates. The high concentration of fillers on the surface of FR-PLAs is certainly related to the fact that fillers are more accessible, which is confirmed by SEM pictures (**Figure 88**). In fact, SEM picture of FR-PLA-C30B exposed for 28 days to T/RH conditions reveals that APP particles are clearly visible and not completely embedded in the PLA matrix anymore.

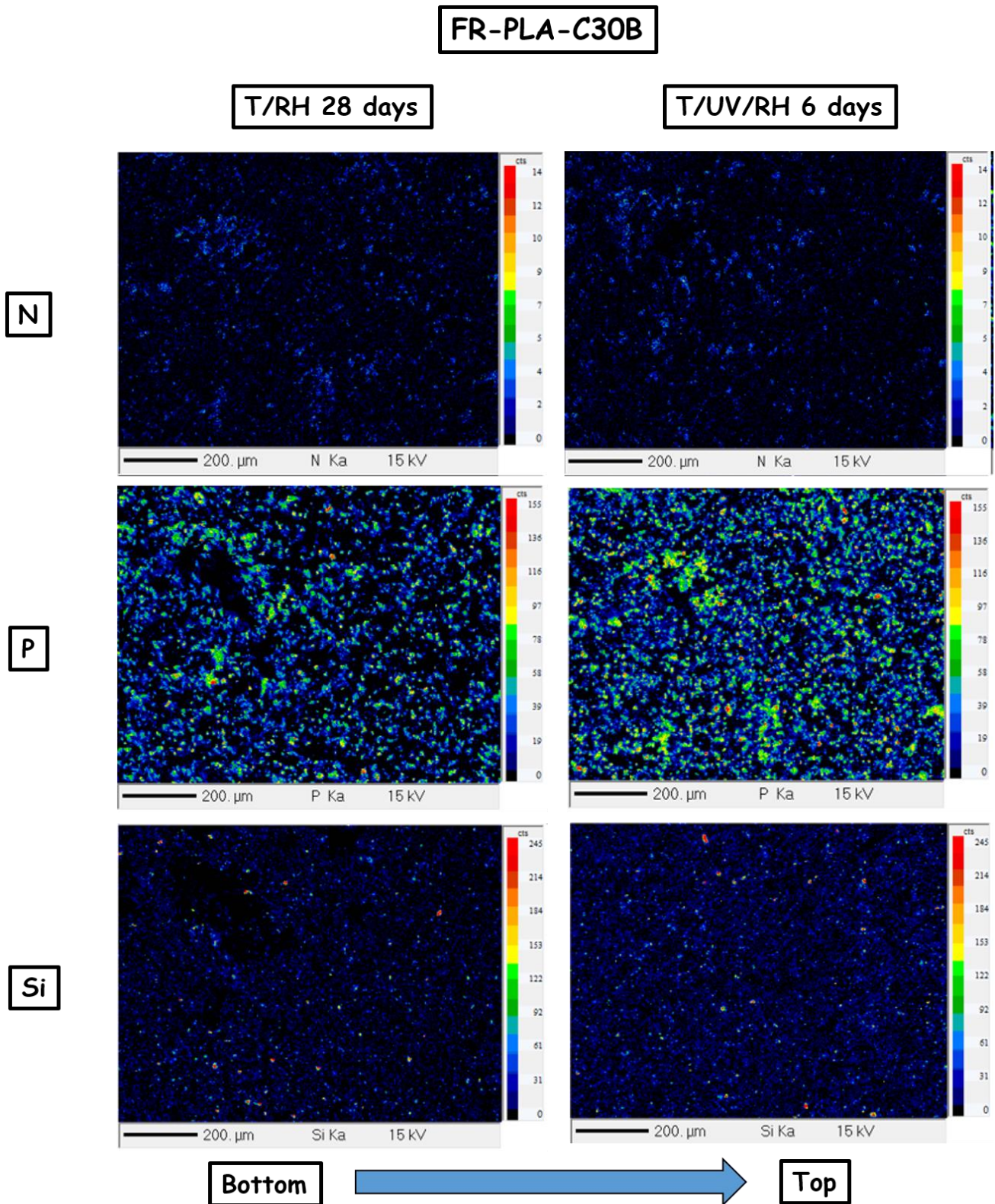


Figure 87: EPMA pictures in cross section for FR-PLA-C30B aged 28 days under T/RH and 6 days under T/UV/RH conditions.

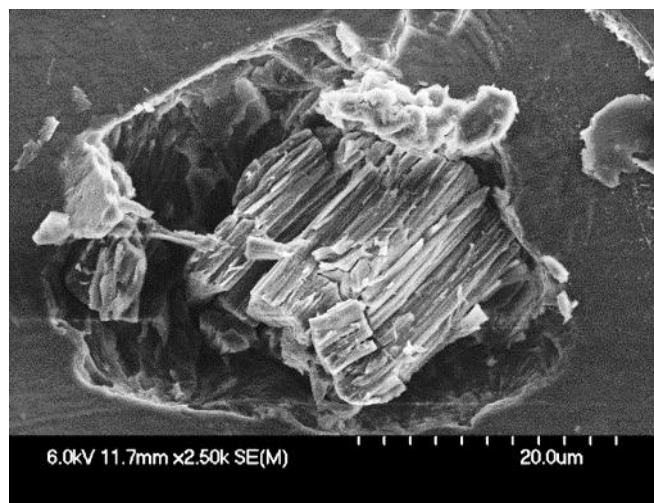


Figure 88: SEM pictures obtained for FR-PLA-C30B after 28 days exposure to T/RH.

As previously demonstrated (p.104), the hydrolytic degradation of PLA starts from the bulk of the material. Investigations led during this chapter reveal that in presence of FR additives, small voids, fractures and a layer composed of FR fillers appear at the surface of the formulations exposed to RH. Moreover, those fillers such as APP are clearly visible and are not completely embedded in the PLA matrix anymore. To explain these phenomena, the impact of FR fillers on the hydrolysis of PLA can thus be described as follow:

- The M_n of FR materials is lower than the one of PLA before ageing, due to the incorporation of fillers into the polymer matrix.
- This lower M_n before ageing allows reaching more rapidly the critical molecular mass from which the materials starts to disaggregate and to lose its properties (T_g , T_m , ...), explaining why FR-PLAs are more degraded compared to PLA.
- When the critical molecular mass (M_c) is reached during degradation, both chain mobility and structural integrity of the material are no longer sufficient to maintain the cohesion between fillers and polymer matrix. Moreover, it seems that hydrolysis of PLA occurs at the interface between polymer matrix and fillers. This can be explained by accumulation of water at this interface due to the hydrophilic character of clays and APP [25, 38, 266]. Indeed, it is possible that these fillers attract water, resulting in a higher local water concentration, increasing the degradation of the PLA matrix. Additives are thus more accessible at the surface, leading to the formation of a layer composed of Melamine, APP and C30B (in the case of FR-PLA-C30B) until complete disintegration of the material into powder.
- On the other hand, it is possible that APP is partially hydrolyzed (even if results suggest otherwise) [175, 258, 267] and thus explaining why particles are not completely embedded in the PLA matrix anymore.

As for neat PLA, investigations led on the ageing of FR-PLAs show that the combination of T, UV and RH is more drastic compared to sole T and RH exposure. In fact, whereas FR-PLAs

disintegrate into powder after 35 days exposure to T/RH, they need only 10 days when exposed to T/UV/RH. This demonstrates the synergistic effect of the combination between UV and RH on the degradation of FR-PLAs. The next step consists in elucidating the degradation mechanism of FR-PLAs exposed to UV rays and to understand the role of fillers during such a degradation.

3.3. Impact of FR additives during UV irradiation of PLA

It was demonstrated in chapter III (p.106) that UV degradation of PLA proceeds via a radical mechanism. This latter leads to the formation of secondary products such as anhydrides, alcohols or carboxylic acid until the complete degradation of PLA. The objective is now to determine the impact of FR fillers on UV degradation of PLA.

Since the UV irradiation of PLA leads to the formation of biradical species, EPR experiments were led both on PLA and FR-PLAs in order to study the kinetics of formation of these radicals when FR fillers are incorporated into the PLA matrix (**Figure 89**). EPR spectra recorded at 50°C for the three materials clearly show that less radicals are formed during UV irradiation when FR fillers are incorporated into the materials. Indeed, whereas the sensitivity of radicals' formation is around 300000 for PLA after 6 hours of exposure, it is only around 125000 for both FR-PLAs. Hence, it appears that the incorporation of flame retardant additives into PLA matrix has a direct impact on the photo-oxidation of PLA. However, the presence of Cloisite 30B into FR-PLA-C30B formulation does not seem to impact the formation of radical species compared to FR-PLA.

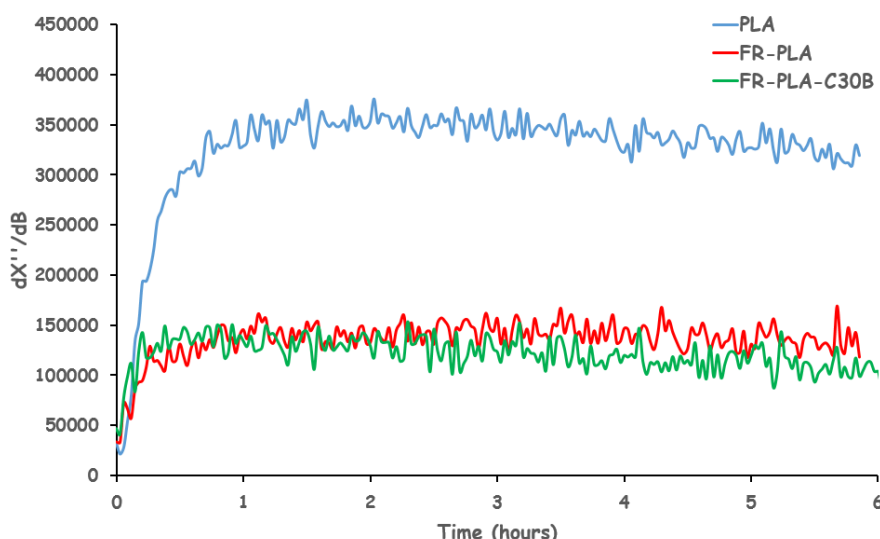


Figure 89: Kinetic evolution of EPR signal as a function of time, for PLA (●), FR-PLA (●) and FR-PLA-C30B (●).

To support these results, 2D hyperfine sub-level correlation (2D HYSORE, **Appendix 5, p.228**) measurements were performed on PLA (**Figure 90**) and both FR-PLAs (**Figure 91**) at 50°C. Neat PLA (**Figure 90**) shows a typical spectrum of the polylactide structure. In fact, the

spectrum shows a ^1H pattern centered at 14.5 MHz corresponding to CH_3 with two protons coupled at respectively 10 MHz and 18 MHz corresponding to CH . At low frequency region, a weak coupling with ^{13}C of 2 MHz (CH_3) and one at 5 MHz (CH) can also be observed.

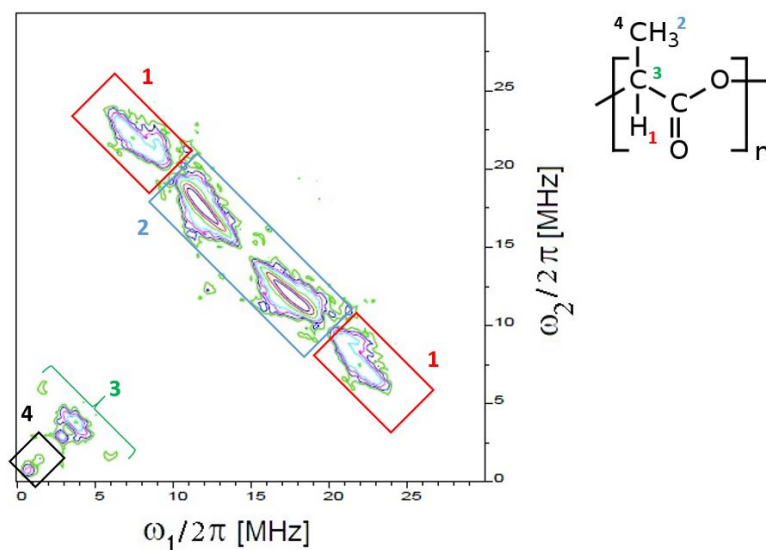


Figure 90: 2D HYSORE recorded at 50°C for PLA.

Focusing on the 2D HYSORE experiments carried out for FR-PLA and FR-PLA-C30B, the two materials exhibit the same spectrum. Thus only FR-PLA-C30B is reported in **Figure 91**. The CH protons of PLA at 10 and 18 MHz are not further observed. The second change occurs in the ^{13}C region with a coupling of one carbon at 4 MHz and two carbons of PLA coupled at 2 MHz (CH_3) and 5 MHz (CH). Additionally, a weak coupling of 1.8 MHz with ^{14}N and 6 MHz with ^{31}P is observed at Larmor frequency of 2.6 MHz.

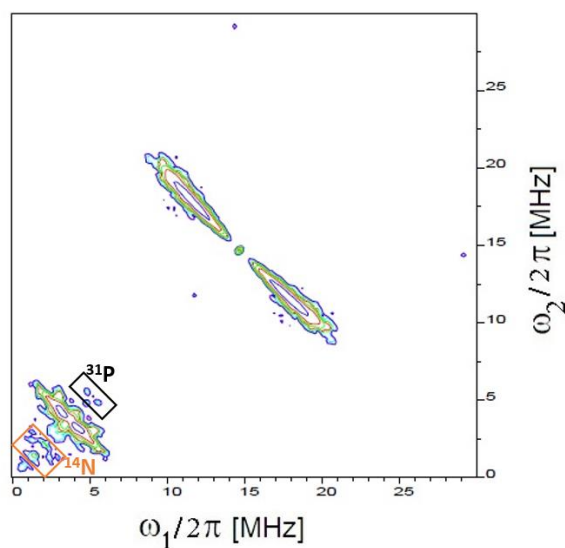


Figure 91: 2D HYSORE recorded at 50°C for FR-PLA and FR-PLA-C30B.

These results suggest an interaction between fillers and PLA that disrupts the formation of radical species. In fact, it is possible that fillers inhibit and stabilize the formation of radicals, thus preventing radical mobility. Some authors have already reported this kind of phenomenon, particularly in presence of Melamine (as UV absorber) and organoclays [47, 48, 268-270]. The presence of FR-fillers in FR-PLAs can attenuate the light absorption (UV penetration) within the polymer matrix, preventing the material from degradation. Moreover, FR-fillers can avoid oxygen diffusivity in the mass of a specimen, thus leading to a starvation of oxygen in the core of the material. The mobility of radicals created during irradiation is thus reduced.

The effect of the combination between UV-rays and relative humidity during exposure of PLA to T/UV/RH was previously elucidated (**p.106**). It was reported that in presence of water, hydrolysis and radical mechanism occur simultaneously, reducing the amount of radicals formed. Indeed, hydrolysis can disrupt their formation by degrading PLA, thus forming secondary products sooner. In order to estimate the additional influence of relative humidity during ageing of FR-PLA and FR-PLA-C30B, kinetic study of the formation of radical species for both FR-PLAs as a function of exposure to T/UV/RH was carried out by EPR (**Figure 92**) and compared to the results obtained for sole T/UV exposure.

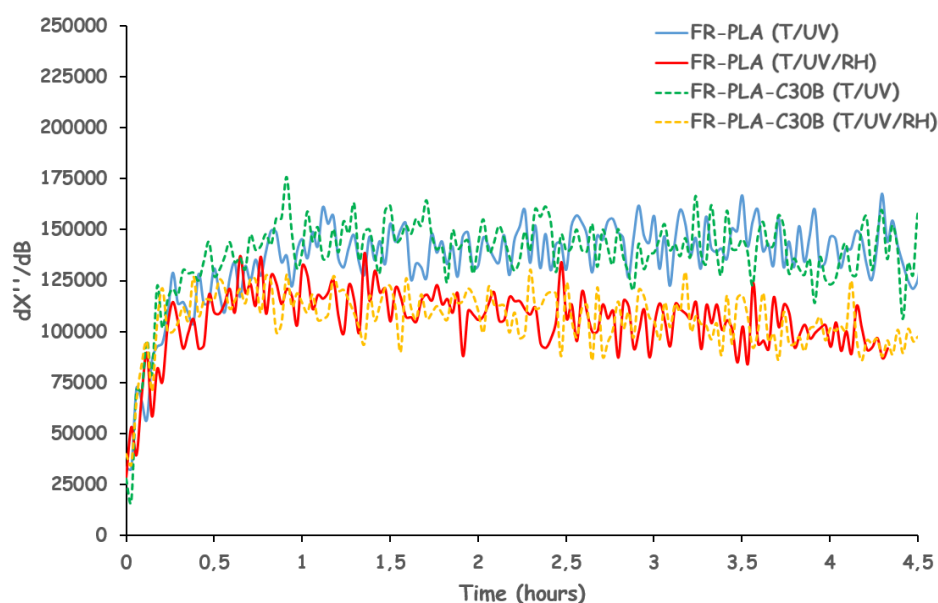


Figure 92: Kinetic evolution of EPR signal for FR-PLA and FR-PLA-C30B, as a function of ageing exposure to T/UV (●) or T/UV/RH (●) at 50°C.

As for PLA, this graph shows that the same quantity of radicals is susceptible to be formed for both kinds of exposure until approximately half an hour of irradiation. The quantity of radicals then formed under T/UV exposure is higher than that formed under T/UV/RH conditions. As in the case of neat PLA, UV and water are in competition during degradation. Indeed, hydrolysis and radical mechanism occur simultaneously during exposure to T/UV/RH, secondary products are thus formed sooner and can be easily decomposed. As expected, the

presence of relative humidity enhances the degradation of FR-PLAs due to the combination between hydrolysis and radical mechanism. Whereas fillers protect the material against UV degradation, the lower M_n of both FR-PLA and FR-PLA-C30B before ageing is responsible for the more pronounced degradation of the formulations.

The impact of FR fillers on the UV degradation of PLA can be summarized as follow:

- The M_n of FR materials are lower than those of PLA before ageing, due to the incorporation of fillers into the polymer matrix.
- FR additives protect the material against UV degradation, thus limiting radical formation and mobility. This also explains why T/UV exposure is less drastic compared to T/RH
- The exposure to T/UV/RH appears to be the most detrimental for both FR-PLAs. Indeed, the degradation of the material is enhanced as hydrolysis and UV mechanism occur simultaneously.
- For a given kind of exposure, the lower M_n before ageing of FR-PLAs is responsible for the sooner degradation than the one of neat PLA. Indeed, the critical molecular mass from which the FR-materials start to disaggregate and lose their properties is reached more rapidly.

4. Conclusion

Chapter IV was dedicated to the study of the impact of fillers on the ageing of PLA. It was demonstrated that FR fillers impact PLA at three different levels: (i) before ageing, (ii) during ageing and (iii) on the mechanism of degradation.

Even before ageing, it was showed that the incorporation of FR additives impact the different properties of PLA:

- The most obvious effect is the reduction of the molecular mass of around 60% when fillers are incorporated due to physical and/or chemical process (mechanical shear, thermal stress, aminolysis ...)
- T_g is decreased due to the M_n decrease and/or plasticizing effect of fillers
- Crystallinity is increased due to the lower M_n and/or nucleating character of fillers

It has been evidenced that both kinds of ageing exposure and flame retardant additives have a direct impact on the ageing of PLA (**Figure 93**). The effects of ageing are indeed more pronounced when FR fillers are incorporated into the PLA matrix:

- Whereas only slight bleaching and cracking are observed for virgin PLA, voids, fractures and a white layer appear at the surface of the T/RH and T/UV/RH aged FR-PLAs when the critical molecular mass (M_c) of 20000 g/mol is reached (**Figure 93**).

- FR-PLAs are completely disintegrated into powder after 10 and 35 days of exposure to T/UV/RH and T/RH conditions, respectively. Only the exposure to T/UV appears not to be drastic for the visual integrity of FR-PLA and FR-PLA-C30B as the critical molecular mass is still not reached ($M_{n0} > M_{n1} > M_c$) (Figure 93).
- The causes of these phenomena can be explained by the evolution of physico-chemical properties of the materials during ageing. Indeed, the decrease of the M_n has a direct impact on the behavior of T_g , T_m and crystallinity (decrease of T_g and T_m and increase in crystallinity).
- The most important point is that due to the already low molecular mass of FR-PLAs before ageing (M_i), these materials reach more rapidly the critical molecular mass, thus explaining the faster degradation of the materials. As well as for unfilled PLA, T/UV/RH exposure conditions are the most drastic conditions for the ageing of FR materials followed by T/RH and T/UV (Figure 93).

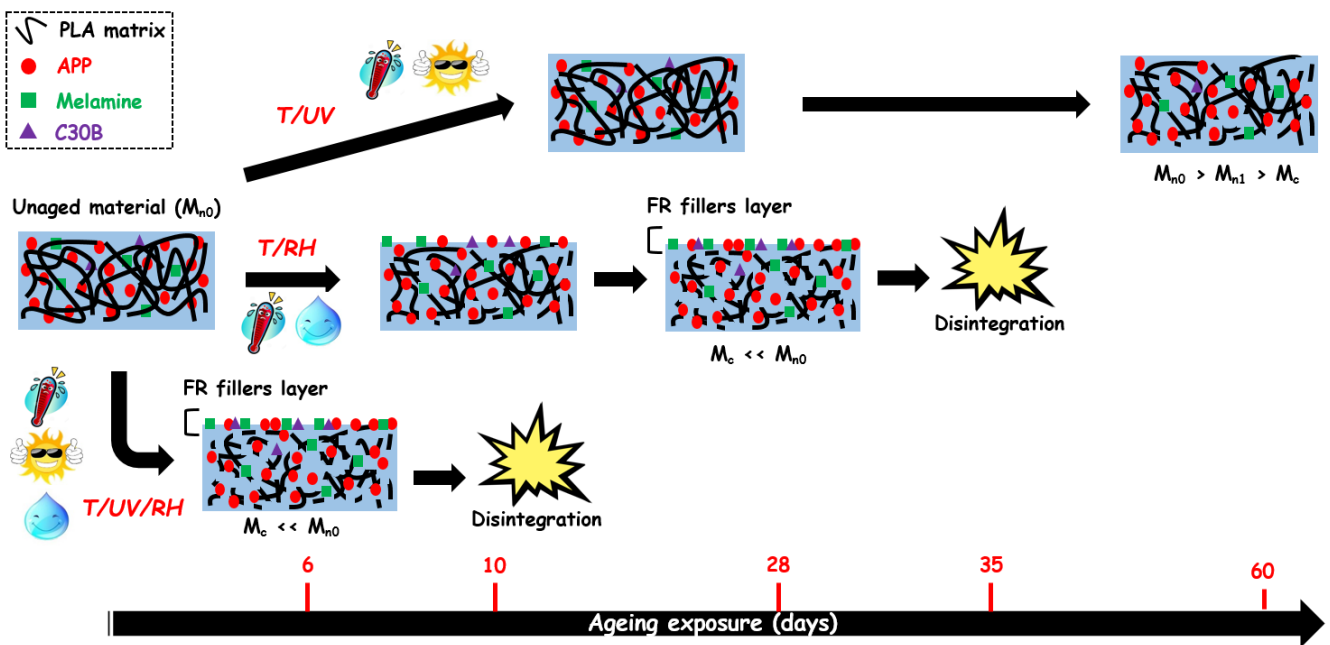


Figure 93: Schematic representation of the effect of fillers and ageing exposure on the degradation of FR-PLA-C30B.

It was then demonstrated that the incorporation of FR fillers has a direct impact on the hydrolysis and radical mechanism during degradation:

- FR fillers protect the material against UV degradation, thus limiting the formation of radical species and of secondary degradation products.
- In presence of water the critical molecular mass (M_c) is quickly reached, at the expense of the cohesion between filler and polymer matrix. Hydrolysis of FR-PLAs occurs at the interface between matrix and fillers. This is certainly due to an

accumulation of water between the fillers-matrix interface, thus leading to the formation of a layer composed of Melamine, APP and C30B (in the case of FR-PLA-C30B) at the surface of FR-PLAs (**Figure 93**).

- The potential hydrolysis of APP could also explain why particles are not completely embedded in the PLA matrix anymore.
- As demonstrated in the case of virgin PLA, combination between T, UV and RH enhances the degradation of both FR-PLAs due to hydrolysis and radical mechanism that occur simultaneously.

Finally, the faster degradation of FR-PLAs compared to the one of PLA is explained by the lower molecular mass of FR-PLAs before ageing, demonstrating that molecular mass is a crucial parameter for PLA and FR-PLAs as it governs the other properties of the material (T_g , T_m , crystallinity ...) and its durability.

The main goal of incorporating FR fillers into PLA is to improve its flame retardant properties. The impact of these fillers on the mechanisms of degradation and properties of PLA without and with ageing has been studied in this last chapter. It is now necessary to determine and understand the effect of ageing on the fire properties of our materials. Hence, the chapter V is dedicated to the fire retardancy of PLA and a special attention will be given to the impact of ageing on the fire properties of materials.

Chapter V: Impact of ageing on the flame retardant properties of FR-PLAs

Melamine, APP and Cloisite 30B were incorporated into PLA to increase its flame retardant properties. In the first part of this chapter, the flame retardant properties of PLA and both FR-PLAs are examined and the mechanism of intumescence is reminded. However, these properties must be kept for the lifetime of the product designed, this is why impact of ageing on FR properties is of primary importance. The second part of this chapter is thus dedicated to the study of impact of ageing on the FR properties of PLA and FR-PLAs. In regards to literature, this work is the first fundamental study on this topic.

1. Flame retardant performances of FR-PLAs

The two flame retarded materials studied in our work (i.e. FR-PLA and FR-PLA-C30B) have been developed during previous researches carried out in our lab [12]. The aim of the project was to develop and optimize an intumescent polylactide exhibiting a non-burning behavior upon heating. The intumescent mechanism as well as FR properties of such materials have already been elucidated [12, 24, 61]. However, it is necessary to evaluate the thermal and fire properties of our own formulations, before investigating their behavior during ageing. Hence, this part is focused on the study of the thermal stability and flame retardant properties of PLA and both FR-PLAs using TGA, MLC and LOI. Furthermore, the FR mechanism of action of the intumescent PLAs will be reminded.

1.1. Thermal stability of FR-PLAs

Previous researches have demonstrated that the intumescent mechanism mainly takes place in condensed phase [61]. Hence, thermal stability plays a fundamental role in the mechanism of protection. In this way, the thermal stability of our FR-PLAs was studied using TGA, and compared to that of neat PLA.

Data collected from the TGAs of PLA and FR-PLAs are reported in **Table 26**. The onset temperature ($T_{10\%}$) corresponding to 10 wt.-% degradation of each material, the temperatures corresponding to its maximum rates of degradation (DTG) and the residual weight obtained at 800°C are considered in these tables. The thermal stability of pure compounds, already investigated by Fontaine et al. [12], is reported in **Appendix 6, p.229**.

Table 26: TGA data (10°C/min under air) obtained for PLA, FR-PLA and FR-PLA-C30B.

Material name	M_n (g/mol)	$T_{10\%}$ (°C)	Max DTG ₁ (°C)	Max DTG ₂ (°C)	Max DTG ₃ (°C)	Residual weight (wt.-%) at 800°C
PLA	68000	332	358	-	-	0
FR-PLA	29000 (-57%)	312 (-20)	346 (-12)	555	730	9.5
FR-PLA-C30B	27000 (-60%)	308 (-24)	343 (-15)	560	740	12

The TGA curves obtained for PLA (**Figure 94**) show that the polymer decomposes in one step from 280°C with a maximum of degradation at 358°C with no residue left at 800°C.

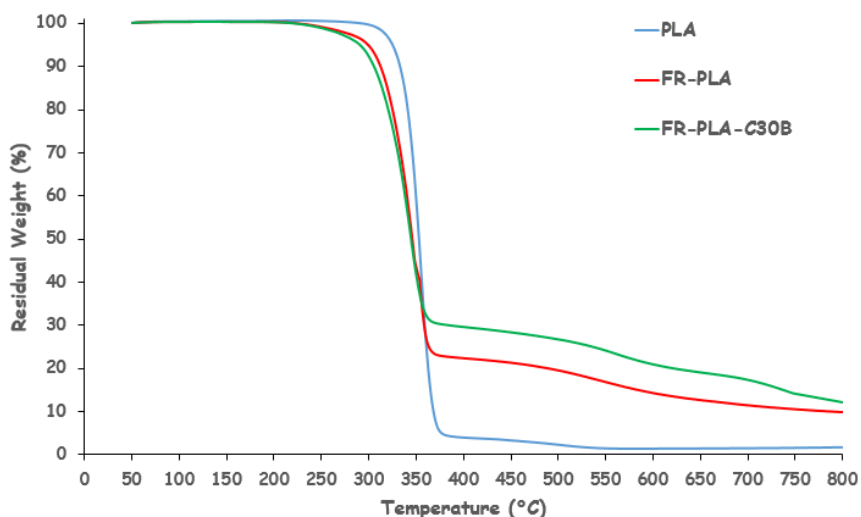


Figure 94: TGA curves of PLA (●), FR-PLA (●) and FR-PLA-C30B (●) under air flow at 10°C/min.

FR-PLA and FR-PLA-C30B degrade in three steps (**Figure 94**). For FR-PLA, the first degradation step occurs between 250°C and 400°C with 70% weight loss. The second step occurs between 400°C and 650°C with 15% weight loss. The last one starts from 650°C until 750°C with 9.5 wt.-% residue at 800°C. The TGA curve of FR-PLA-C30B is similar to that of FR-PLA until 400°C. However, a significant difference is observed after 400°C. Indeed, after 400°C, FR-PLA-C30B degrades by forming a larger amount of stable residue, resulting in a final residue of 12 wt.-% against 9.5 wt.-% for FR-PLA. The different compounds interact together (chemical reaction and/or physical interaction, lower M_n of FR-PLAs), leading to a thermal degradation of the PLA matrix at lower temperature in a first time [12, 61] ($T_{10\%}$ is 312°C and 308°C for FR-PLA and FR-PLA-C30B, respectively, against 332°C for PLA) but in a second time, FR additives lead to a thermal stabilization of PLA with higher residues at the end of the experiment. The destabilization is similar for both FR-PLAs, but stabilizing effect is more important in the case of FR-PLA-C30B. Indeed, nanoparticles in PLA/Melamine/APP formulations can stabilize the intumescent char [12, 24, 61]. C30B acts as a reinforcing agent of the intumescent coating, allowing to increase its efficiency.

1.2. Reaction to fire

1.2.1. Behavior under mass loss cone calorimeter (MLC)

The aim of incorporating flame retardant fillers was to design a PLA with excellent fire retardant properties (i.e. FR-PLA and FR-PLA-C30B). In order to investigate the fire retardant properties of such materials, the mass loss cone calorimeter (MLC) is one of the well established tools, providing data on the surface ignition and penetrative burning of a material. Hence, the heat release rate (HRR) of the two intumescent formulations was measured by MLC and compared to unfilled PLA (**Figure 95** and **Table 27**).

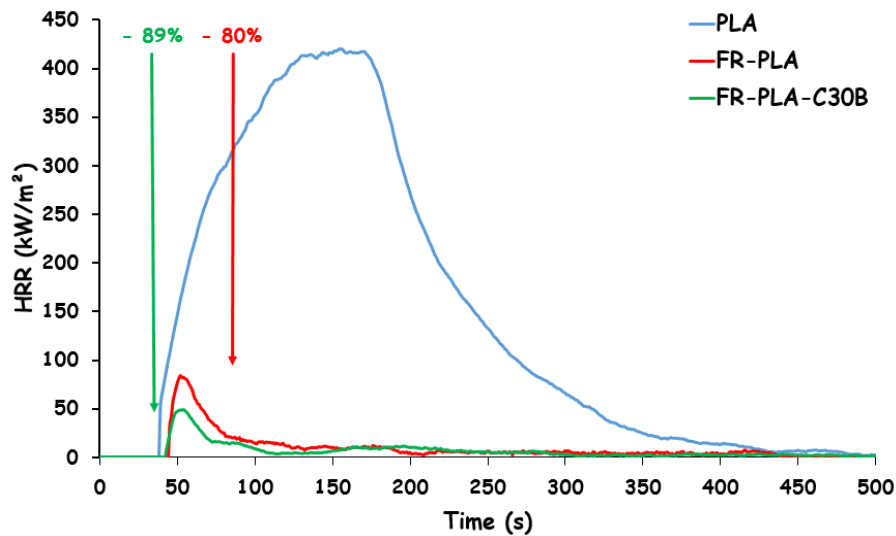


Figure 95: HRR curves as a function of time of PLA (●), FR-PLA (●) and FR-PLA-C30B (●).

Table 27: MLC values obtained for PLA, FR-PLA and FR-PLA-C30B.

Material name	Time to ignition (s)	pHRR (kW/m ²)	THR (MJ/m ²)
PLA	39	420	72.0
FR-PLA	45 (+6)	82 (-80%)	4.8 (-93%)
FR-PLA-C30B	43 (+4)	48 (-89%)	3.1 (-96%)

The virgin PLA ignites 39 s after the beginning of the experiment and reaches a peak of heat release rate (pHRR) of 420 kW/m² with a total heat release (THR) of 72 MJ/m². For both FR-PLAs, an intumescent char is obtained (**Figure 96**) and in all the cases the addition of fillers decreases both pHRR and THR compared to the neat PLA.

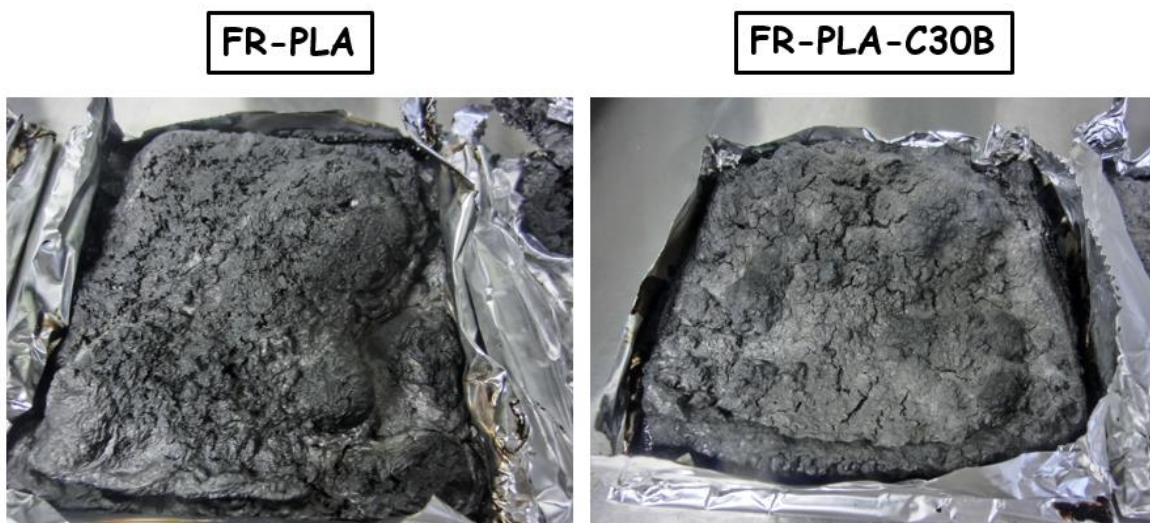


Figure 96: Char residues of FR-PLA and FR-PLA-C30B.

Indeed, pHRR reaches 82 kW/m^2 (-80%) and 48 kW/m^2 (-89%) and THR reaches 4.8 MJ/m^2 (-93%) and 3.1 MJ/m^2 (-96%) for FR-PLA and FR-PLA-C30B, respectively. However, it appears that the time to ignition is similar to that of unfilled PLA (39 s for PLA compared to 45 s and 43 s for FR-PLA and FR-PLA-C30B, respectively). These results indicate that the intumescent shield developed by FR-PLA and FR-PLA-C30B when exposed to a radiative heat flux is very efficient, leading to an important decrease of both pHRR and THR. Concerning the char residues (**Figure 97**), it seems that the one of FR-PLA-C30B is more compact and cohesive, but less expanded than the one of FR-PLA. Moreover, whereas few flames were observed at the surface of FR-PLA during MLC experiment, FR-PLA-C30B exhibits a non-burning behavior, confirming that C30B acts as a good synergist for intumescent PLA [12, 24, 61].

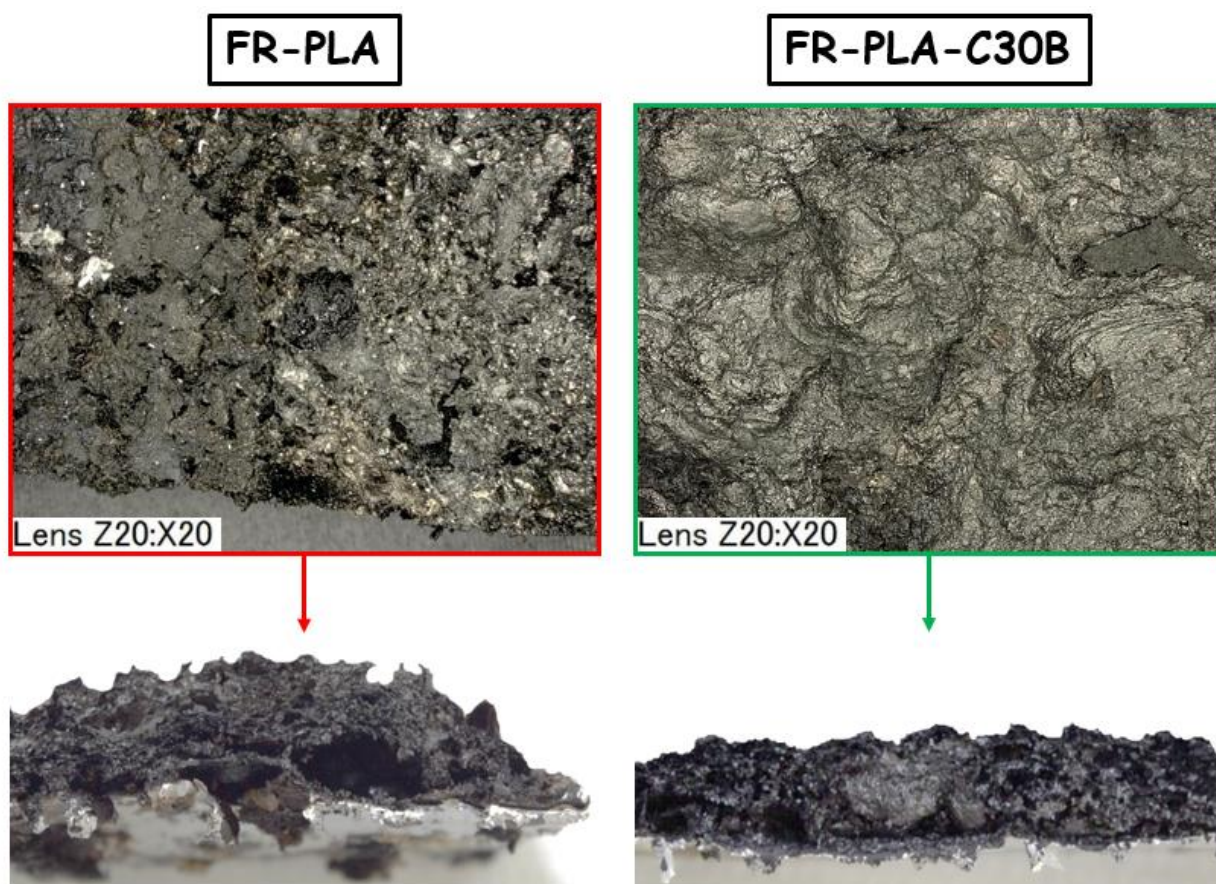


Figure 97: Digital microscopy pictures and cross section of char residues of FR-PLA and FR-PLA-C30B.

MLC results demonstrate that the intumescent char formed under radiative heat flux plays an impressive protective role, with strong reductions of HRR and THR. The addition of a low percentage (1 wt.-%) of nanoparticles such as C30B improves further the efficiency of the protection by decreasing the pHRR by 89% compared to PLA. Regarding these results, we also investigated the flammability of PLA and FR-PLAs using limiting oxygen index (LOI).

1.2.2. Limiting oxygen index (LOI) test results

Flammability is one of the most important characteristics of materials in the field of flame retardancy. In fact, when a material exhibits good performances during flammability scenario, it should limit propagation of flames during a real fire. Limiting oxygen index (LOI) is one of the scenarios commonly used to evaluate the flammability of a material. The results obtained for PLA and both FR-PLAs are presented in **Table 28**.

Table 28: LOI values of PLA, FR-PLA and FR-PLA-C30B.

Material name	LOI (vol.-%)
PLA	20
FR-PLA	50 (+30)
FR-PLA-C30B	56 (+36)

The results obtained show that the combination of Melamine and APP in PLA provides very high LOI values. LOI of FR-PLA reaches 50 vol.-% compared to 20 vol.-% for unfilled PLA. Moreover, the incorporation of C30B into FR-PLA-C30B allows an increase of LOI values to 56 vol.-% due to the intumescent phenomenon. Intumescent PLAs exhibit high LOI values compared to the unfilled PLA, which demonstrate their lower flammability compared to PLA and proves the efficiency of FR fillers. In addition, these results show once again that organoclay (C30B) has a synergistic effect with APP and Melamine when only a small amount is incorporated into FR-PLA.

1.3. Mechanism of action of FR-PLAs

Previous researches reported by Fontaine et al. [24] and Gallos et al [61] have elucidated the mechanism of action of the intumescent FR-PLA and FR-PLA-C30B. Indeed, the combination between Melamine and APP into PLA (i.e. FR-PLA) leads to the formation of an intumescent structure that is able to enhance the fire properties of the material during fire scenarios. It is reported that PLA is thermally degraded in order to form aromatic and aliphatic carbonyl compounds in the condensed phase. Other compounds such as lactide, carbon dioxide, ester and aldehyde are released in the gas phase. APP is reported to be thermally degraded by chain scission mechanisms forming phosphates. These latter present an acidic character and react with the carbonyl compounds in the condensed phase. Phosphates also permit the development of an intumescent phenomenon when combined with Melamine (**Figure 98**).

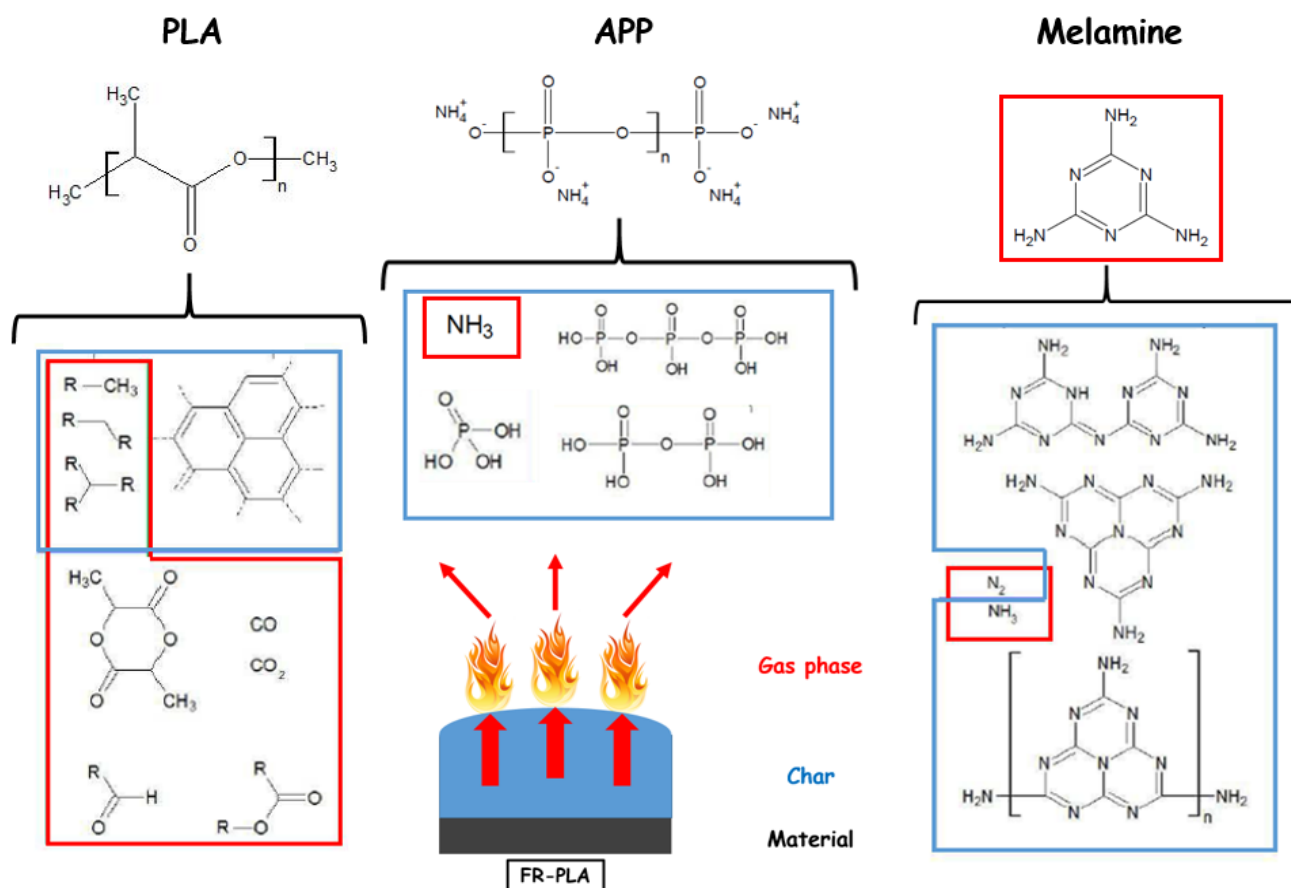


Figure 98: Intumescent mechanism, adapted from Gallos et al [61].

Viscosity of polymers during burning is a key point to control the development of intumescent barriers [271]. Gallos et al. [61] reported that the viscosity of the FR-PLA upon heating is adequate to lead to the formation of this intumescent thermal barrier. The addition of Cloisite 30B allows increasing the viscosity of the blend and this increase is enough to significantly impact the swelling kinetics. Indeed, both swelling rate and expansion of the char of FR-PLA-C30B are decreased compared to FR-PLA. MLC and LOI results reveal that FR-PLA-C30B exhibits better fire performances compared to FR-PLA. Indeed, whereas FR-PLA presents flames at the surface of the char when exposed to the radiative heat flux, FR-PLA-C30B presents a non-burning behavior. Flames are extinguished 10 s maximum after ignition. This is due to the fact that the structure of the two chars of FR-PLA and FR-PLA-C30B is different, thus the release of gases is also different (**Figure 99**).

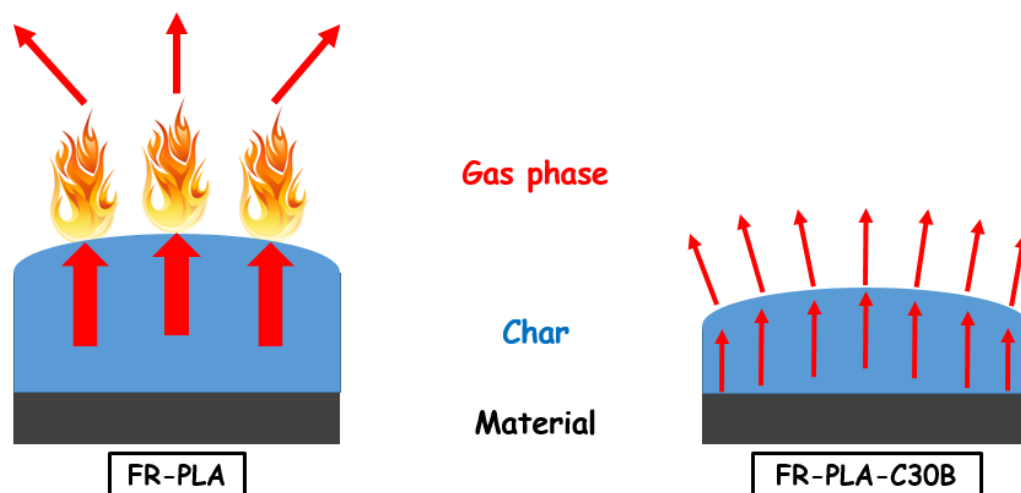


Figure 99: Release of gas through the char of FR-PLA and FR-PLA-C30B, adapted from Gallos et al [61].

In the clay containing formulation, C30B reacts with APP and forms aluminophosphate species [24, 61]. These species can thermally stabilize the structure of the char, allowing to obtain a more cohesive char. The role played by the clay in the improvement of the FR performances can be summarized as follows: the Cloisite 30B permits to obtain a better protection by an intumescent and more insulating char (less swelling but lower temperature). The char also limits the “fuel” release due to its better cohesion. This limitation of fuel release is a consequence of the diminution of the HRR since there is less fuel to feed the flame and the sporadic flames observed extinguish spontaneously and quickly. This intumescent PLA becomes then nonflammable.

1.4. Conclusion

In conclusion, the combination of APP and Melamine is an effective method to improve the fire properties of PLA and to obtain a thermal shield via an intumescent phenomenon. The combination of FR-PLA with nanoparticles such as Cloisite 30B permits to obtain a synergistic effect which enhances the efficiency of the intumescent PLA process. Indeed, the organomodified montmorillonite should increase the viscosity of the formulations which plays a key role on the swelling kinetic and reacts with APP to form aluminophosphates contributing to the modification of the char structure. These differences in terms of structure lead to a more cohesive char. More homogeneous combustible gases are liberated at the surface of the char, reducing their local concentration and preventing their combustion, while maintaining the protection efficiency in terms of thermal isolation. As the mechanism of intumescence of our FR materials as well their associated fire performances have been evidenced, the next part is dedicated to the effect of ageing on the thermal stability and the reaction to fire of PLA and both FR-PLAs.

2. Thermal stability and flame retardant properties after ageing

In this part, the effect of T/UV, T/RH and T/UV/RH ageing on the thermal stability of FR-PLA and FR-PLA-C30B is investigated. Moreover, fire retardant properties (MLC and LOI) of PLA and both FR-PLAs are examined all along the exposure to T/UV, T/RH and T/UV/RH conditions. Finally, the influence of ageing on the mode of action of flame retarded materials will be studied.

One may notice that it was not possible to perform LOI and MLC measurements after 35 days and 10 days ageing under T/RH and T/UV/RH, respectively, as the materials were completely disintegrated into powder. Thus, the fire performances of FR-PLAs have been evaluated until 60 days ($M_n \pm 21300$ g/mol), 28 days ($M_n \pm 20000$ g/mol) and 6 days ($M_n \pm 20000$ g/mol) exposure to T/UV, T/RH and T/UV/RH conditions, respectively.

2.1. Effect of ageing on thermal stability of FR-PLAs

As well as for neat PLA in chapter III (p.93), the thermal stability of FR-PLAs as a function of ageing conditions was evaluated using TGA. Data obtained are reported in **Table 29** and **Table 30** for FR-PLA and FR-PLA-C30B, respectively. The onset temperature ($T_{10\%}$), corresponding to 10 wt.-% degradation of the material, the temperatures corresponding to its maximum rates of degradation (DTG), and the residual weight obtained at 800°C are considered in these tables.

Table 29: TGA data (10°C/min under air) obtained after ageing of FR-PLA exposed to T/UV, T/RH and T/UV/RH conditions.

Exposure / time (days)	M_n (g/mol)	$T_{10\%}$ (°C)	Max DTG ₁ (°C)	Max DTG ₂ (°C)	Max DTG ₃ (°C)	Residual weight (wt.-%) at 800°C
0	29000	312	346	555	730	9.5
T/UV 125 d	13 500 (-53%)	304 (-8)	345 (-1)	557 (+2)	732 (+2)	9.7 (+0.2)
T/RH 105 d	4 300 (-84%)	297 (-15)	333 (-13)	555	729 (-1)	9.0 (-0.5)
T/UV/RH 90 d	2 800 (-90%)	277 (-35)	325 (-21)	556 (+1)	732 (+2)	9.5

Table 30: TGA data (10°C/min under air) obtained after ageing of FR-PLA-C30B exposed to T/UV, T/RH and T/UV/RH conditions.

Exposure / time (days)	M _n (g/mol)	T _{10%} (°C)	Max DTG ₁ (°C)	Max DTG ₂ (°C)	Max DTG ₃ (°C)	Residual weight (wt.-%) at 800°C
0	27000	308	343	560	740	12
T/UV 125 d	12 500 (-54%)	305 (-3)	340 (-3)	561 (+1)	740	12.5 (+0.5)
T/RH 105 d	4 100 (-84%)	295 (-13)	327 (-16)	561 (+1)	742 (+2)	13.0 (+1)
T/UV/RH 90 d	2 500 (-91%)	258 (-50)	311 (-32)	562 (+2)	742 (+2)	13.0 (+1)

As well as unaged materials, aged FR-PLAs (**Figure 100 (a) and (b)**) degrade in three steps and lead to a residue at 800°C. However, as for neat PLA (**p.93**), the onset temperature of degradation of both FR-PLAs decreases upon heating. Indeed, T_{10%} of FR-PLA (i) decreases from 312°C before ageing to 304°C, 297°C and 277°C after 125 days exposure to T/UV, 105 days to T/RH and 90 days to T/UV/RH conditions, respectively. For FR-PLA-C30B (ii), T_{10%} decreases from 308°C before ageing to 305°C, 295°C and 258°C after 125 days exposure to T/UV, 105 days to T/RH and 90 days to T/UV/RH conditions, respectively.

Same phenomenon is reported concerning the behavior of DTG₁. In fact, DTG₁ of FR-PLA (i) decreases from 346°C before ageing to 345°C, 333°C and 325°C after 125 days exposure to T/UV, 105 days to T/RH and 90 days to T/UV/RH conditions, respectively. DTG₁ of FR-PLA-C30B (ii) decreases from 343°C before ageing to 340°C, 327°C and 311°C after 125 days exposure to T/UV, 105 days to T/RH and 90 days to T/UV/RH conditions, respectively. However, it appears that whatever the kind of ageing exposure, DTG₂ and DTG₃ remain similar after ageing for both materials. Indeed, DTG₂ is 555°C ± 2°C and 560°C ± 2°C for FR-PLA and FR-PLA-C30B, respectively, whereas DTG₃ is 730°C ± 2°C and 740°C ± 2°C for FR-PLA and FR-PLA-C30B, respectively.

The residue left at 800°C is quite similar for FR-PLA and FR-PLA-C30B after ageing: whatever the kind of ageing exposure it is around 9 wt.-% ± 0.5 wt.-% for FR-PLA and 12 wt.-% ± 1 wt.-% for FR-PLA-C30B. One can notice that like unaged materials, the final residue of FR-PLA-C30B is higher than that of FR-PLA after ageing.

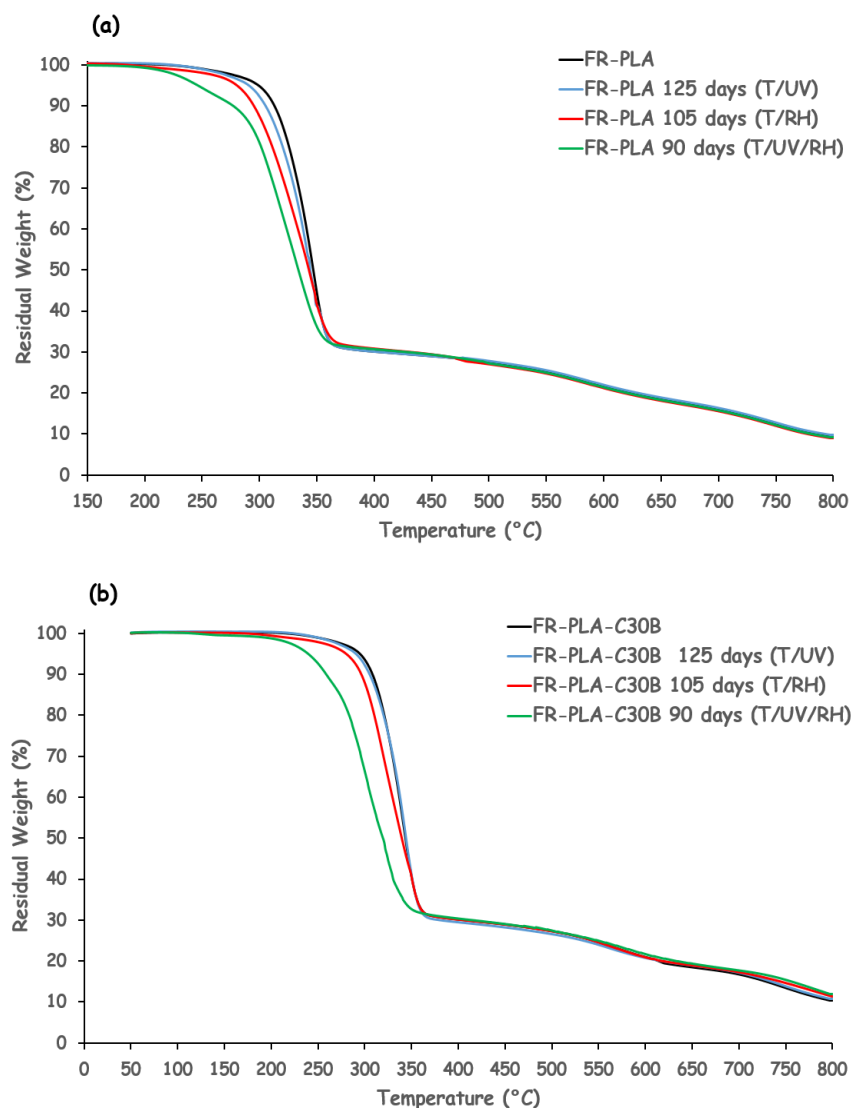


Figure 100: TGA curves as function of time for FR-PLA (a) and FR-PLA-C30B (b), before ageing (●), 125 days T/UV (●), 105 days T/RH (●) and 60 days T/UV/RH (●) exposure.

All these results indicate that the thermal stability of FR-PLAs materials is impacted during ageing. The decrease of $T_{10\%}$ and $DTGA_1$, which correspond to the degradation of PLA, suggests the formation of thermally weak bond (e.g. hydroperoxides, carboxylic acids and peroxides) during the ageing exposure of the PLA matrix (chapter III, p.93). These ones can quickly initiate the thermal degradation and then decrease the thermal stability of PLA [174, 190-192], explaining the behavior of both $T_{10\%}$ and $DTGA_1$. On the other hand, knowing that $DTGA_2$ and $DTGA_3$ are linked to the presence of FR fillers into FR-PLAs, their behavior reported during ageing seems to indicate that FR fillers are not affected by ageing, which is in accordance with observations previously reported in chapter IV (p.141).

Theoretical TGA curves of FR-PLA and FR-PLA-C30B calculated according to **Equation 23** demonstrate that the residues obtained at 800°C are mainly due to the presence of FR fillers into the PLA matrix (**Table 31**). Indeed, whereas no residue is left at 800°C for neat PLA, the residues obtained by TGA experiment are 9.5 wt. % and 12 wt. % at 800°C for FR-PLA and FR-

PLA-C30B, respectively. These values are close to the theoretical ones of 9.1 wt. % and 11.5 wt. % calculated for FR-PLA and FR-PLA-C30B, respectively.

Table 31: Comparison between theoretical and experimental residual weight (wt. %) obtained at 800°C for FR-PLA and FR-PLA-C30B.

Formulation name	Residual weight (wt.-%) at 800°C
FR-PLA (theo)	9.1
FR-PLA (exp)	9.5 (+0.4)
FR-PLA-C30B (theo)	11.5
FR-PLA-C30B (exp)	12 (+0.5)

Thus, if the residue left at 800°C is mainly due to the presence of FR fillers, and considering that only PLA matrix is affected by ageing, it is quite obvious that this residue does not change during ageing. Hence, the limitation of fuel release due to the insulating char is still efficient and the thermal protection is thus maintained during ageing.

As the effect of ageing on the thermal stability of intumescent PLAs is now evidenced, the next section is dedicated to the effect of ageing on the fire performances of the materials studied, in particular thanks to LOI test.

2.2. Limiting Oxygen Index (LOI) test results after ageing

The impact of ageing on flame retardancy of PLA was firstly assessed by LOI test. The values obtained are summarized in **Table 32**, **Table 33** and **Table 34** for PLA, FR-PLA and FR-PLA-C30B, respectively.

Table 32: LOI ranking of PLA as a function of exposure to T/UV, T/RH and T/UV/RH conditions.

Ageing time (days)	LOI (vol.-%) T/UV	LOI (vol.-%) T/RH	LOI (vol.-%) T/UV/RH
PLA			
0	20	20	20
3	20	20	20
6	20	20	20
28	20	20	20
60	20	20	20

Table 33: LOI ranking of FR-PLA as a function of exposure to T/UV, T/RH and T/UV/RH conditions. The (+x) are calculated using the unaged formulation as reference.

Ageing time (days)	LOI (vol.-%) T/UV	LOI (vol.-%) T/RH	LOI (vol.-%) T/UV/RH
FR-PLA			
0	50	50	50
3	50	50	57 (+7)
6	50	52 (+2)	60 (+10)
28	52 (+2)	59 (+9)	-
60	54 (+4)	-	-

Table 34: LOI ranking of FR-PLA-C30B as a function of exposure to T/UV, T/RH and T/UV/RH conditions. The (+x) are calculated using the unaged formulation as reference.

Ageing time (days)	LOI (vol.-%) T/UV	LOI (vol.-%) T/RH	LOI (vol.-%) T/UV/RH
FR-PLA-C30B			
0	56	56	56
3	56	56	64 (+8)
6	56	58 (+2)	67 (+11)
28	58 (+2)	67 (+11)	-
60	60 (+4)	-	-

Results show that whatever the kind of exposure, ageing does not impact the LOI value of unfilled PLA which remains at 20 vol.-% (**Table 32**). However, regarding FR-PLA (**Table 33**) and FR-PLA-C30B (**Table 34**), LOI values surprisingly increase when the formulations are exposed to T/UV, T/RH and T/UV/RH conditions:

- Under exposure to T/UV: LOI increases by 4 vol.-% for both FR-PLAs after 60 days, from 50 to 54 vol.-% for FR-PLA and from 56 to 60 vol.-% for FR-PLA-C30B.
- Under exposure to T/RH: LOI reaches 59 vol.-% (+9) and 67 vol.-% (+11) after 28 days for FR-PLA and FR-PLA-C30B, respectively.
- Under exposure to T/UV/RH: LOI rises by 10 vol.-% and 11 vol.-% to reach 60 and 67 vol.-% after 6 days for FR-PLA and FR-PLA-C30B, respectively.

It appears that during ageing, the LOI values of FR-PLA and FR-PLA-C30B surprisingly increase. This increase clearly depends on the ageing conditions: it is more important for ageing under T/UV/RH conditions than for T/RH and T/UV exposure. In fact, as an example, LOI of FR-PLA-C30B slightly increases until 60 vol.-% after 60 days exposure to T/UV, whereas it reaches 67 vol.-% after 28 days exposure to T/RH or only 6 days to T/UV/RH conditions.

It is noteworthy that a change in behavior of FR-PLA and FR-PLA-C30B is reported during LOI tests (**Figure 101**). Indeed, it appears that the charring effect decreases, while dripping occurs when ageing exposure time increases. Nevertheless, this behavior is more noticeable for materials aged under T/UV/RH conditions compared to T/RH and T/UV.

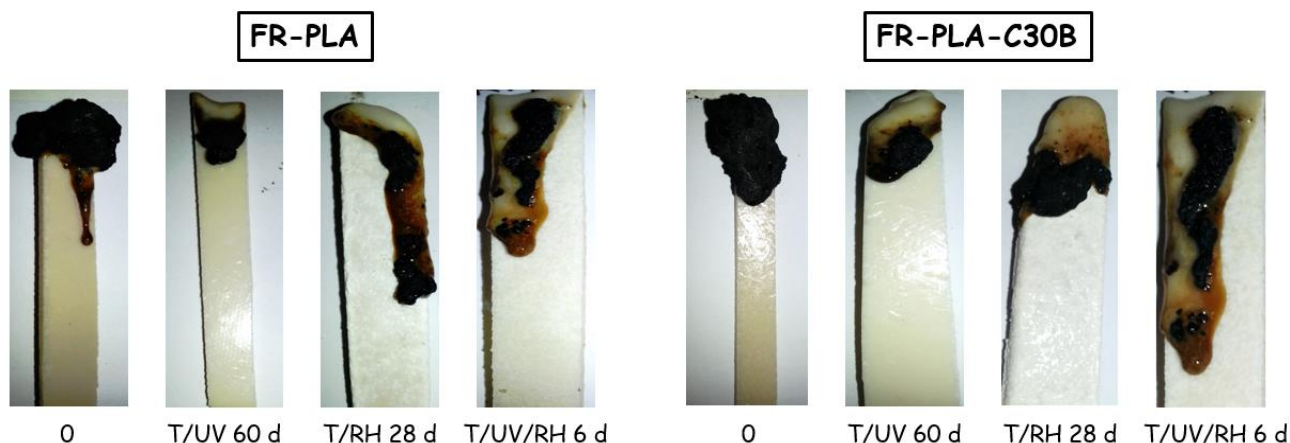


Figure 101: Evolution of the behavior of LOI samples of FR-PLA and FR-PLA-C30B as a function of ageing exposure to T/UV, T/RH and T/UV/RH conditions.

These investigations demonstrate that ageing has a positive effect on LOI values, by reducing the flammability. This phenomenon is certainly due to a “runaway effect”. Indeed, the combustible material escapes from the flame by dripping phenomenon which stops the flaming of the samples. In order to better understand this phenomenon, the behavior of the viscosity of materials during ageing was investigated. As mentioned previously, ageing leads to a decrease of the molecular mass. The decrease in M_n of a polymer is known to usually lead to a decrease in the viscosity of the material [272] and this parameter is an important factor that impacts the general fire retardant behavior of a material, particularly on LOI test [50, 61, 102, 273, 274]. In this aim, melt flow indexer (MFI) was performed on FR-PLAs before and all along ageing exposure.

2.3. Viscosity of FR-PLAs

MFI was performed in order to investigate the changes in viscosity of FR-PLAs during ageing. Indeed, the dynamic viscosity is known to be inversely proportional to MFI (viscosity decreases when MFI increases) [272, 275]. Data obtained are reported in **Table 35** and **Table 36** for FR-PLA and FR-PLA-C30B, respectively.

Table 35: Viscosity data obtained for FR-PLA exposed to T/UV, T/RH and T/UV/RH conditions.

Ageing time (days) FR-PLA	(T/UV) M _n (g/mol)	(T/UV) Viscosity (Pa/s)	(T/RH) M _n (g/mol)	(T/RH) Viscosity (Pa/s)	(T/UV/RH) M _n (g/mol)	(T/UV/RH) Viscosity (Pa/s)
0	29000	1240	29000	1240	29000	1240
7	27100 (-3%)	1100 (-11%)	25800 (-11%)	750 (-40%)	21500 (-23%)	400 (-68%)
14	26000 (-10%)	910 (-27%)	21300 (-24%)	370 (-70%)	17500 (-39%)	120 (-90%)
21	25300 (-13%)	720 (-42%)	18400 (-37%)	160 (-87%)	-	-
30	24100 (-17%)	460 (-63%)	-	-	-	-

Table 36: Viscosity data obtained for FR-PLA-C30B exposed to T/UV, T/RH and T/UV/RH conditions.

Ageing time (days) FR-PLA-C30B	(T/UV) M _n (g/mol)	(T/UV) Viscosity (Pa/s)	(T/RH) M _n (g/mol)	(T/RH) Viscosity (Pa/s)	(T/UV/RH) M _n (g/mol)	(T/UV/RH) Viscosity (Pa/s)
0	27000	2010	27000	2010	27000	2010
7	26000 (-4%)	1600 (-20%)	24800 (-8%)	1000 (-49%)	22300 (-18%)	600 (-70%)
14	25100 (-7%)	1300 (-35%)	21200 (-22%)	450 (-78%)	15000 (-45%)	100 (-95%)
21	24500 (-10%)	800 (-60%)	15400 (-43%)	110 (-94%)	-	-
30	21800 (-19%)	430 (-79%)	-	-	-	-

One can firstly notice that the dynamic viscosity of FR-PLA-C30B is higher than that of FR-PLA before ageing, thus even if the M_n is lower. As already reported (**p.164**), this is due to the incorporation of organomodified montmorillonite into the material [24, 61]. Generally, intercalation, exfoliation and dispersion of clays in a polymer matrix can display an increase in viscosity [276-281]. In order to evaluate the dispersion of organoclays in our materials, transmission electron microscopy (TEM) analyses were thus performed on FR-PLA-C30B. It appears that FR-PLA-C30B is constituted of many big agglomerates of clay platelets with width superior to 0.5 μm (**Figure 102 (a)**). However, the material also present platelets of smaller size with width of 200 nm (**Figure 102 (b)**). Due to their length and width, these agglomerates are of intermediate size between micrometrical and nanometrical fillers. Indeed, although these agglomerates have a dimension lower than one micron, they have a shape factor

relatively low compared to the one that can be obtained when clay platelets are well exfoliated.

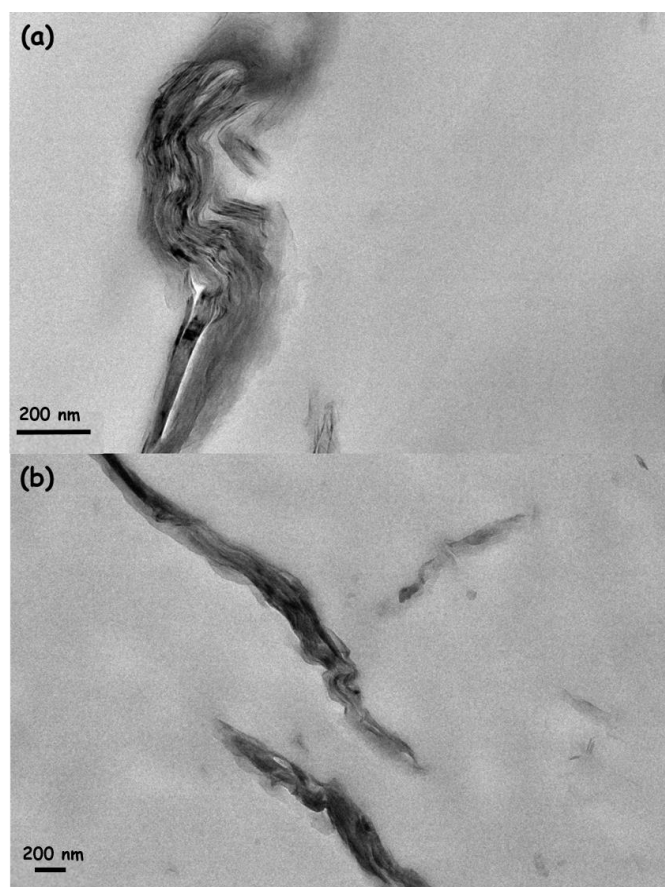


Figure 102: TEM pictures of big (a) and small (b) agglomerates of Cloisite 30B in FR-PLA-C30B.

FR-PLA-C30B contains different sizes of agglomerates of Cloisite 30B but no isolated platelets. Thus, the organoclay is not well dispersed and FR-PLA-C30B is not a nanocomposite but a microcomposite. Nevertheless, this state of dispersion seems to be enough to display an increase in viscosity of the FR-PLA-C30B material compared to FR-PLA.

The dynamic viscosity of FR-PLA and FR-PLA-C30B appears to be dependent on the ageing exposure time (**Figure 103 (a)**) and on the molecular mass of the material (**Figure 103 (b)**). Indeed, the viscosity decreases when ageing exposure increases (M_n decreases) whatever ageing conditions:

- Under T/UV, the dynamic viscosity decreases from 1240 Pa/s ($M_n = 29000$ g/mol) and 2010 Pa/s ($M_n = 27000$ g/mol) to 460 Pa/s ($M_n = 24100$ g/mol) and 430 Pa/s ($M_n = 21800$ g/mol) after 30 days for FR-PLA and FR-PLA-C30B, respectively.
- Under T/RH, the dynamic viscosity reaches 160 Pa/s ($M_n = 18400$ g/mol) and 110 Pa/s ($M_n = 15400$ g/mol) after 21 days for FR-PLA and FR-PLA-C30B, respectively.

- Under T/UV/RH the most noticeable decrease of viscosity is observed. Indeed, it decreases to 120 Pa/s ($M_n = 17500$ g/mol) and 100 Pa/s ($M_n = 15000$ g/mol) after only 14 days for FR-PLA and FR-PLA-C30B, respectively.

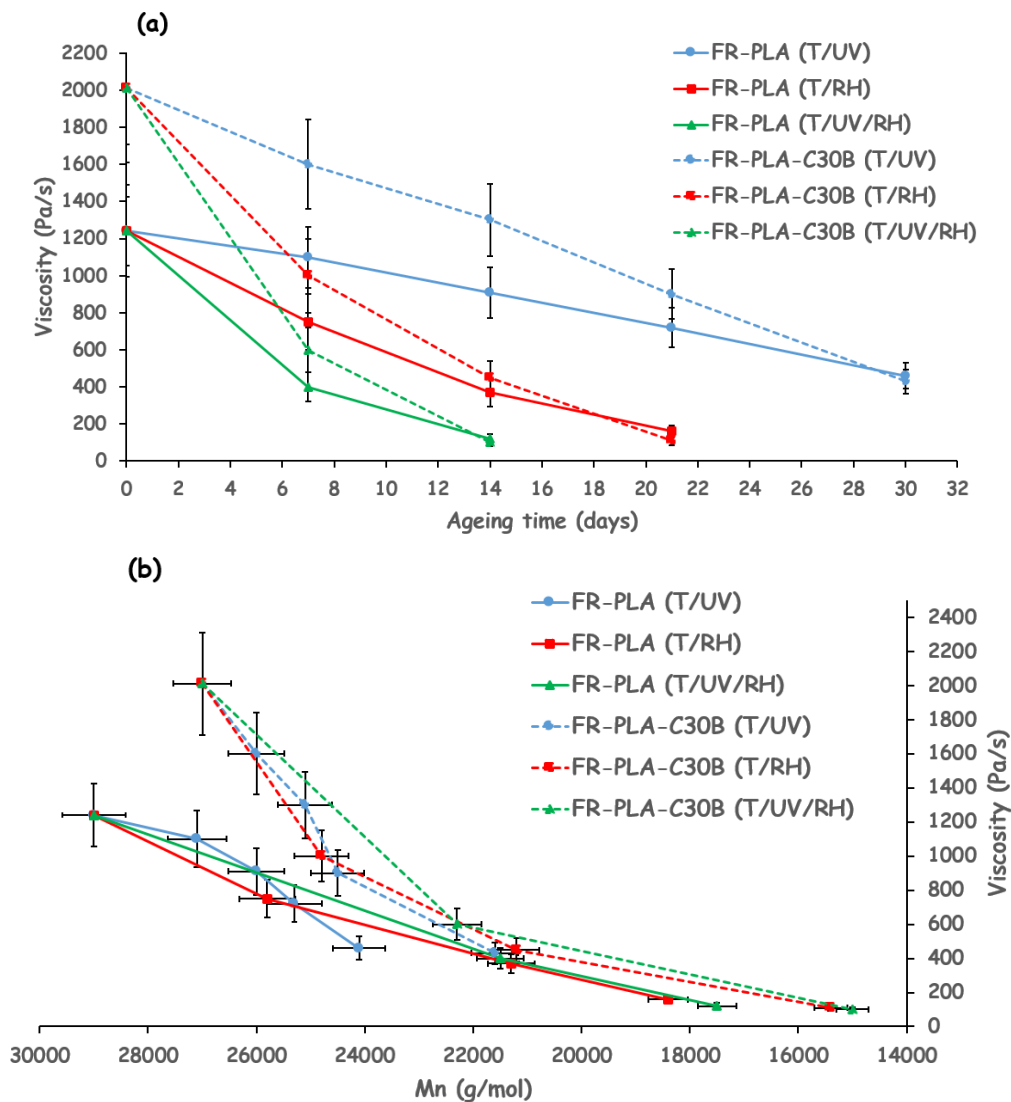


Figure 103: Evolution of viscosity of FR-PLA and FR-PLA-C30B as a function of ageing exposure to T/UV (●), T/RH (■) and T/UV/RH (△) conditions (a) and molecular mass (b).

As for the molecular mass (p.90 and p.127), the decrease of viscosity is more important when materials are aged under T/UV/RH compared to T/RH and T/UV conditions: after 14 days ageing, the dynamic viscosity is only 100 Pa/s for FR-PLA-C30B aged under T/UV/RH, compared to 450 Pa/s and 1300 Pa/s for T/RH and T/UV exposure, respectively.

Hence, the decrease in viscosity observed during ageing is responsible for the “runaway effect” previously described. This one thus leads to an increase in LOI values for both FR-PLAs during ageing. Knowing the impact of ageing on the LOI performance of our materials, it is now useful to study its impact on MLC performances. The next section is then dedicated to these investigations.

2.4. Mass loss cone performances after ageing

As demonstrated in the last part (p.160), the use of Melamine, APP and organoclay (C30B) leads to the development of an efficient intumescent shield protecting PLA against fire. It is suitable to keep these performances during the lifetime of the material. Thus, MLC properties of PLAs were examined as a function of ageing in order to evaluate the impact of T/UV, T/RH and T/UV/RH exposure on the flame retardancy.

MLC measurements were performed until 60 days for PLA under each exposure conditions (Table 37 and Figure 104). As for LOI test, results depicted for PLA show that whatever the kind of exposure, ageing does not impact the MLC performances. Indeed the time to ignition (TTI) as well as both pHRR and THR remain unchanged. Indeed, TTI is around $39 \text{ s} \pm 4 \text{ s}$, pHRR is $420 \pm 2\%$ and THR is $72 \pm 6\%$. Whereas the physico-chemical properties (M_n , T_g , T_m and crystallinity) of unfilled PLA are impacted during ageing, the LOI and MLC results demonstrate that the fire performances of the material remain unchanged.

Table 37: MLC values obtained for PLA as a function of exposure to T/UV, T/RH and T/UV/RH conditions.

PLA	M_n (g/mol)	Time to ignition (s)	pHRR (kW/m ²)	THR (MJ/m ²)
t = 0	68000	39	420	72.0
T/UV t= 60 days	47000 (-31%)	43 (+4)	424 (+2%)	71.1 (-2%)
T/RH t = 60 days	34200 (-50%)	41 (+2)	422 (+1%)	69.4 (-4%)
T/UV/RH t = 60 days	21500 (-68%)	38 (-1)	416 (-1%)	67.7 (-6%)

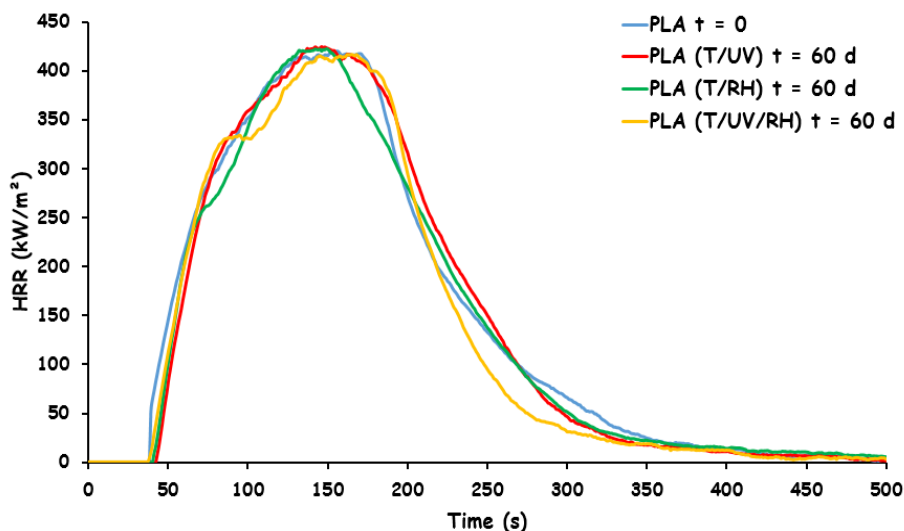


Figure 104: RHR curves of unaged PLA (●) and 60 days exposure to T/UV (●), T/RH (●) and T/UV/RH (●) conditions.

Focusing on the two intumescent PLAs, measurements were performed until 6, 28 and 60 days under T/UV/RH, T/RH and T/UV, respectively. MLC data obtained for FR-PLA are

reported in **Table 38** and **Figure 105**. Contrary to LOI it seems that MLC performances are not impacted during ageing. Indeed, TTI is 45 s for unaged material and remains quite similar after ageing. The pHRR remains at 82 kW/m² after 60 days ageing to T/UV and decreases to 81 kW/m² (-2%) and 79 kW/m² (-4%) after 28 days under T/RH and 6 days under T/UV/RH conditions, respectively. The only difference is observed for the THR which is decreased by 33%, 34% and 55% to reach 2.9 MJ/m², 2.8 MJ/m² and 1.9 MJ/m² after 60 days under T/UV, 28 days under T/RH and 6 days under T/UV/RH, respectively. However, due to the relatively low values of THR and the limits of the MLC device, the decrease of THR cannot be considered as significant.

Table 38: MLC values obtained for FR-PLA as a function of exposure to T/UV, T/RH and T/UV/RH conditions.

FR-PLA	Mn (g/mol)	Time to ignition (s)	pHRR (kW/m ²)	THR (MJ/m ²)
t = 0	29000	45	82	4.8
T/UV t= 60 days	21300 (-26%)	43 (-2)	82	2.9 (-33%)
T/RH t = 28 days	20000 (-30%)	45	81 (-2%)	2.8 (-34%)
T/UV/RH t = 6 days	20000 (-30%)	43 (-2)	79 (-4%)	1.9 (-55%)

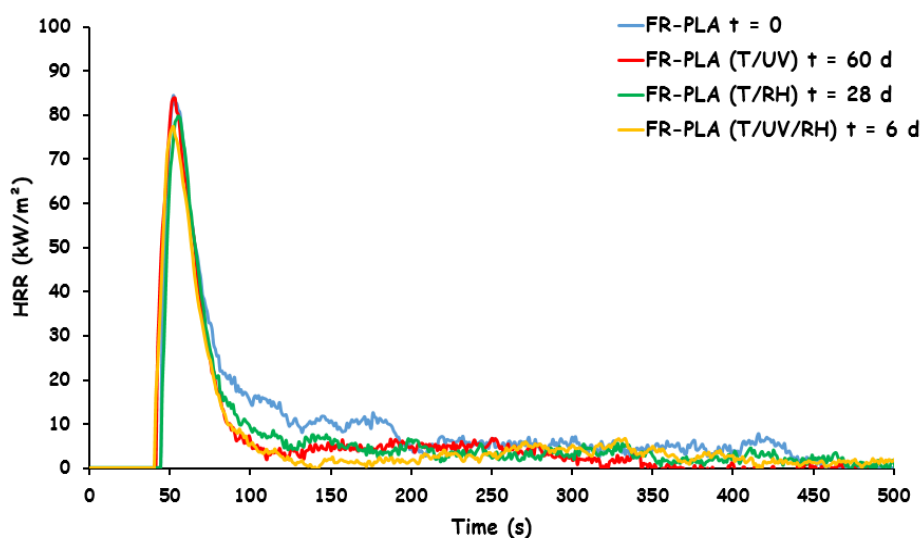


Figure 105: RHR curves of unaged FR-PLA (●) and 60 days exposure to T/UV (●), T/RH (●) and T/UV/RH (●) conditions.

The FR-PLA-C30B formulation shows the same behavior as FR-PLA (**Table 39** and **Figure 106**). Indeed, The TTI which is 43 s before ageing reaches 46 s, 45s and 44s after 60 days under T/UV, 28 days under T/RH and 6 days under T/UV/RH, respectively. Thus, the TTI can be considered as unchanged after ageing. The pHRR of the material is slightly decreased during ageing but is in the experimental error of 10%. Indeed, pHRR is 48 kW/m² before ageing and reaches 47 kW/m² (-2%), 46 kW/m² (-3%) and 43 kW/m² (-8%) after 60 days under T/UV, 28 days under T/RH and 6 days under T/UV/RH, respectively. As well as for FR-PLA, the THR is

reported to decrease during ageing, from 3.1 MJ/m² before ageing to 1.9 MJ/m² (-36%), 1.8 MJ/m² (-42%) and 1.1 MJ/m² (-63%) after 60 days under T/UV, 28 days under T/RH and 6 days under T/UV/RH, respectively. However, due to the relatively low values of THR and the limits of the MLC device, the decrease of THR cannot be considered as significant.

Table 39: MLC values obtained for FR-PLA-C30B as a function of exposure to T/UV, T/RH and T/UV/RH conditions.

FR-PLA-C30B	M _n (g/mol)	Time to ignition (s)	pHRR (kW/m ²)	THR (MJ/m ²)
t = 0	27000	43	48	3.1
T/UV t= 60 days	21100 (-23%)	46 (+3)	47 (-2%)	1.9 (-36%)
T/RH t = 28 days	20000 (-26%)	45 (+2)	46 (-3%)	1.8 (-42%)
T/UV/RH t = 6 days	20000 (-26%)	44 (+1)	43 (-8%)	1.1 (-63%)

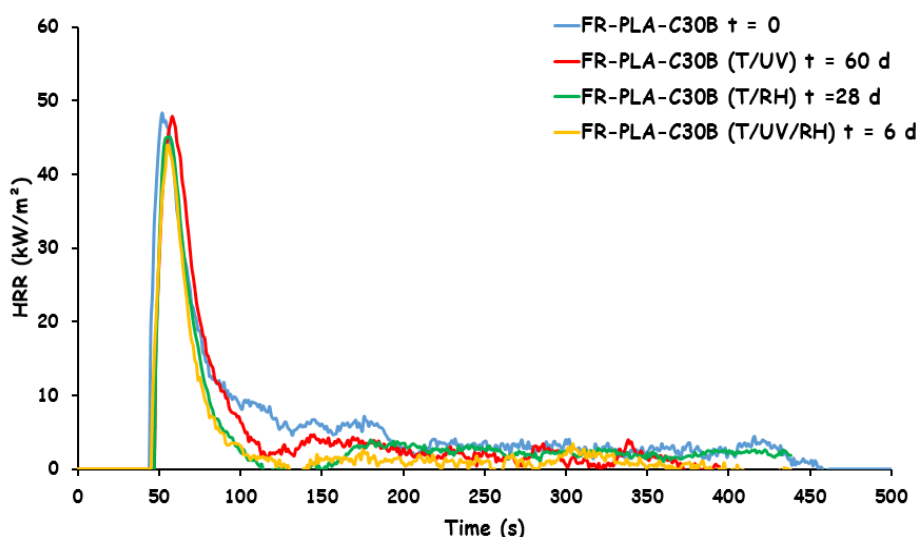


Figure 106: RHR curves of unaged FR-PLA-C30B (●) and 60 days exposure to T/UV (●), T/RH (●) and T/UV/RH (●) conditions.

Considering the experimental error and the low values obtained in terms of pHRR and THR, no significant changes in MLC performances were evidenced after ageing for FR-PLAs loaded at 30wt.-%. Hence, even if ageing has a direct impact on the physico-chemical properties of FR-PLAs, it appears that it does not affect fire performances of such materials measured by MLC. It was thus decided to investigate the impact of ageing on the MLC performances of a less effective system. Hence, PLAs filled at 20 wt.-% FR loading were investigated. In fact, the MLC performances of a less effective system may be affected during ageing exposure.

2.5. Mass loss cone behavior of FR-PLAs loaded at 20 wt.-%.

This study was led on two FR-PLAs filled with 20 wt.-% of FR fillers in the same ratio as for the formulations at 30 wt.-%. The composition and names of these two formulations are reported in chapter II (Table 7, p.70). FR-PLA-20% and FR-PLA-C30B-20% were aged under

T/UV/RH condition since this latter was previously reported to be the more drastic for PLA materials (**p.106** and **p.152**), thus the effects of ageing should be quickly observed.

As FR-PLA-20% and FR-PLA-C30B-20% were completely disintegrated into powder after 28 days, MLC investigations were led on both materials before ageing, after 17 and 22 days of exposure to T/UV/RH conditions. Indeed, after 17 days the M_c is reached and the high concentrated FR layer is formed at the surface of the plates. As expected, FR-PLA-20% (**Table 40** and **Figure 107**) exhibits lower fire properties than FR-PLA-30% before ageing, pHRR and THR are 186 kW/m^2 and 46.3 MJ/m^2 , respectively, compared to 82 kW/m^2 and 4.8 MJ/m^2 for the FR-PLA-30%. Regarding their fire properties after ageing, it appears that the TTI which is $88 \text{ s} \pm 2 \text{ s}$ all along the exposure is quite stable for the FR-PLA-20%. The THR is surprisingly decreased by 20% and 30% after 17 days and 22 days exposure. Same phenomenon is observed for the pHRR which is 186 kW/m^2 before ageing and reaches 124 kW/m^2 (-33%) and 94 kW/m^2 (-48%) after 17 days and 22 days of ageing, respectively. These results obtained show that MLC fire performances of the FR-PLA-20% material are clearly improved after ageing.

Table 40: MLC values obtained for FR-PLA-20% as a function of exposure time to T/UV/RH conditions.

FR-PLA-20%	Time to ignition (s)	pHRR (kW/m^2)	THR (MJ/m^2)
t = 0	88	186	46.3
T/UV/RH t= 17 days	90 (+2)	124 (-33%)	37.5 (-20%)
T/UV/RH t = 22 days	86 (-2)	94 (-48%)	32.5 (-30%)

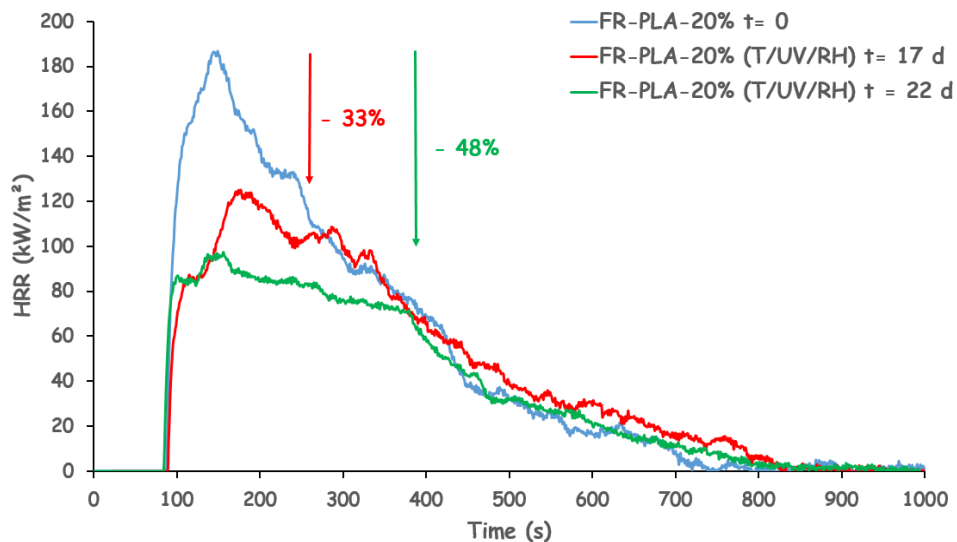


Figure 107: RHR curves of unaged FR-PLA-20% (●), 17 days (●) and 22 days (●) aged under T/UV/RH conditions.

As well as in the case of FR-PLA, FR-PLA-C30B-30% presents higher fire performances compared to FR-PLA-C30B-20% (**Table 41** and **Figure 108**). Whereas pHRR and THR are 48 kW/m² and 3.1 MJ/m² for FR-PLA-C30B-30%, they respectively reach 88 kW/m² and 11.6 MJ/m² for FR-PLA-C30B-20%. Focusing on the performances of FR-PLA-C30B-20% after ageing, the TTI remains unchanged until 22 days exposure. Indeed, TTI is 92 s ± 3 s. Furthermore, the pHRR decreases after ageing from 88 kW/m² to 65 kW/m² (-26%) and 51 kW/m² (-42%) after 17 and 22 days exposure to T/UV/RH, respectively. The same trend is observed for THR which is reduced from 11.6 MJ/m² to 8.9 MJ/m² (-23%) and 7.6 (-35%) after 17 and 22 days exposure, respectively. Like FR-PLA-20%, the behavior of FR-PLA-C30B-20% demonstrates that MLC fire performances are improved after ageing.

Table 41: MLC values obtained for FR-PLA-C30B-20% as a function of exposure time to T/UV/RH conditions.

FR-PLA-C30B-20%	Time to ignition (s)	pHRR (kW/m ²)	THR (MJ/m ²)
t = 0	92	88	11.6
T/UV/RH t= 17 days	93 (+1)	65 (-26%)	8.9 (-23%)
T/UV/RH t = 22 days	95 (+3)	51 (-42%)	7.6 (-35%)

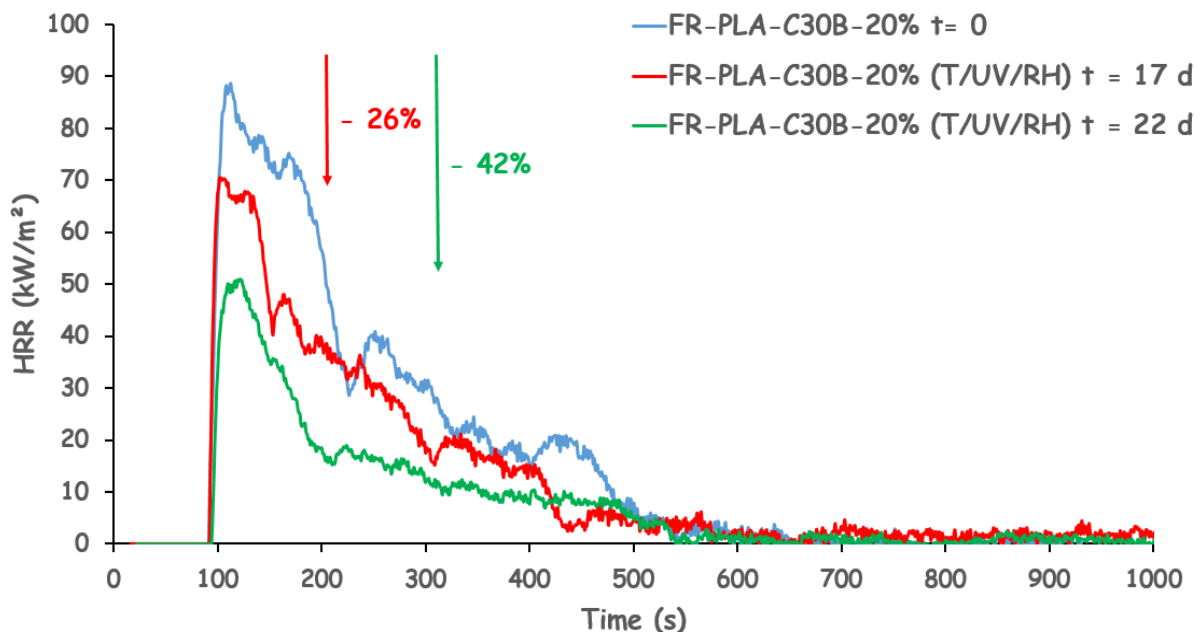


Figure 108: RHR curves of unaged FR-PLA-C30B-20% (●), 18 days (●) and 22 days (●) aged under T/UV/RH conditions.

The study led on FR-PLAs loaded at 20 wt.-% show that MLC performances are enhanced during ageing. A reduction of pHRR and THR along with unchanged TTI is observed. Moreover, a change in intumescent behavior is reported when samples are aged. Indeed, during the experiments, the thermal shield was observed to be formed sooner, with a higher swelling, resulting in a more expanded char. The cross section of the chars obtained after MLC

measurements were thus analyzed by digital microscopy. The expansion of the char as a function of ageing exposure to T/UV/RH is reported in **Figure 109** and **Figure 110** for FR-PLAs-20%. The thickness of the char was measured on three different chars of FR-PLA-20% and FR-PLA-C30B-20%.

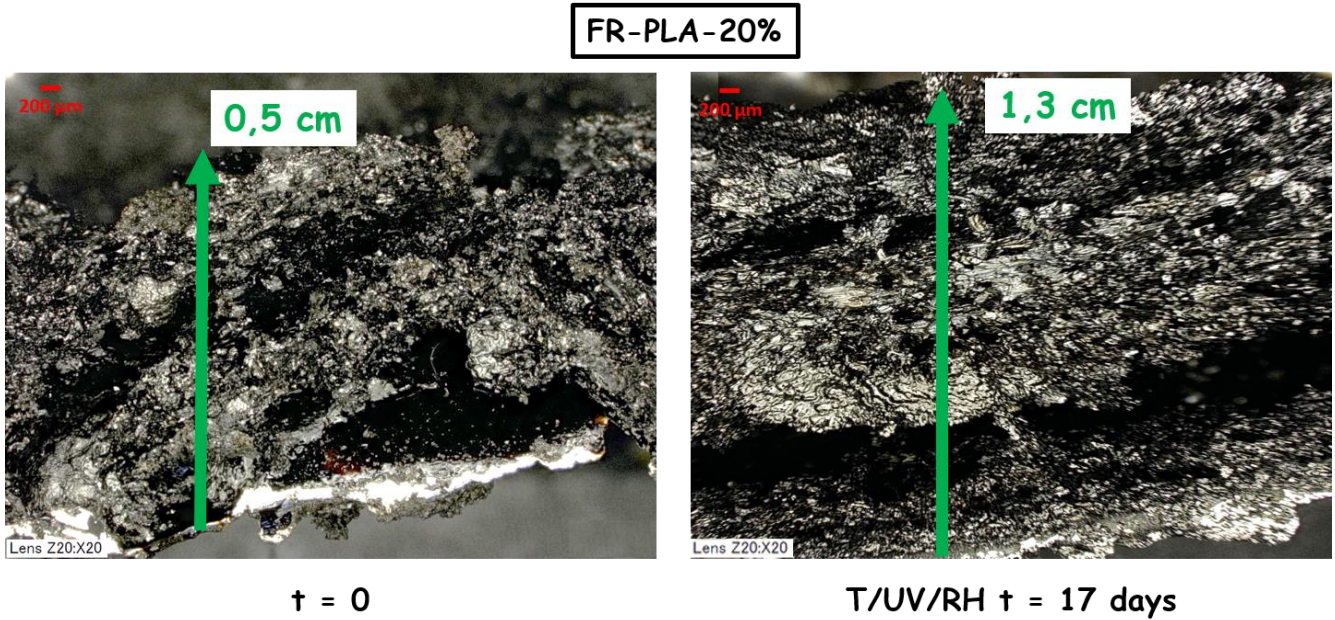


Figure 109: Evolution of the char expansion of FR-PLA-20% as a function of ageing under T/UV/RH exposure.

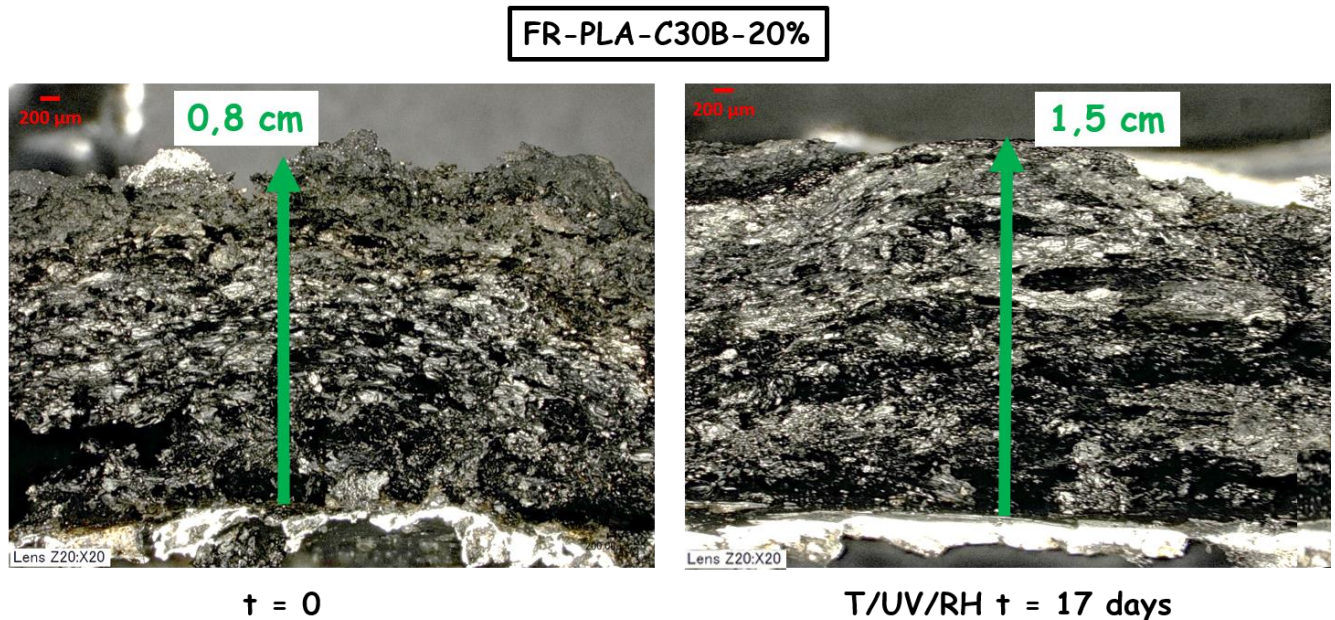


Figure 110: Evolution of the char expansion of FR-PLA-C30B-20% as a function of ageing under T/UV/RH exposure.

The thickness of FR-PLA-20% char (**Figure 109**) is 0.5 cm before ageing and reaches 1.3 cm after 17 days exposure to T/UV/RH. Moreover, the thickness of the FR-PLA-C30B-20% char (**Figure 110**) is 0.8 cm before ageing and grows up to 1.5 cm after 17 days exposure to T/UV/RH. These observations confirm the higher expansion of the char after ageing, for both FR-PLA and FR-PLA-C30B filled at 20 wt.-%.

Knowing the positive impact of ageing on the thermal protection of intumescent PLA, it is of interest to understand how ageing can improve the MLC performances. For this purpose, investigations were led on the molecular mass of FR-PLAs loaded at 20 wt.-%.

2.6. Molecular mass of FR-PLAs loaded at 20 wt.-%

The change in molecular mass of FR-PLAs-20% was studied as a function of ageing exposure to T/UV/RH and compared to FR-PLA and FR-PLA-C30B filled at 30 wt.-% (**Table 42** and **Figure 111**). The first observation is that before ageing, the M_n of FR-PLAs-20% is higher than that of FR-PLAs-30%. Indeed, M_n of FR-PLA-20% and FR-PLA-C30B-20% are 32500 g/mol and 31000 g/mol, respectively, compared to 29000 g/mol for FR-PLA-30% and 27000 g/mol for FR-PLA-C30B-30%. Hence the incorporation of 20 wt.-% of fillers is less impacting for the molecular mass compared to the incorporation of 30 wt.-%.

Table 42: M_n data of FR-PLAs-20% and FR-PLAs-30% as a function of ageing exposure to T/UV/RH conditions.

Exposure time (days)	FR-PLA-20%	FR-PLA-30%	FR-PLA-C30B-20%	FR-PLA-C30B-30%
0	32500	29000	31000	27000
5	27900 (-14%)	23500 (-17%)	26000 (-16%)	21000 (-20%)
15	21000 (-35%)	17500 (-38%)	20200 (-35%)	15000 (-40%)
30	16500 (-49%)	13000 (-53%)	15300 (-51%)	9750 (-60%)
45	11000 (-67%)	8800 (-69%)	9250 (-70%)	5800 (-75%)

Furthermore, as for FR-PLAs-30%, the exposure to T/UV/RH conditions leads to the decrease of the molecular mass of both intumescent materials. Indeed, M_n of FR-PLA-20% decreases from 32500 to 11000 g/mol (-67%) whereas for FR-PLA-C30B-20% it decreases from 31000 to 9250 g/mol (-70%) after 45 days exposure to T/UV/RH conditions. Considering the experimental error of 10%, one can notice that the M_n of FR-PLAs-20% and FR-PLAs-30% decreases at the same rate. M_n decreases by 67% and 70% for FR-PLA-20% and FR-PLA-C30B-20%, respectively compared to 68% and 75% for FR-PLA-30% and FR-PLA-C30B-30%, respectively, after 45 days exposure to T/UV/RH. However, due to the higher M_n of FR-PLAs-20% before ageing, compared to that of FR-PLAs-30%, more time is required to reach the critical molecular mass ($M_c = 20000$ g/mol) from which the material starts to disaggregate. This explains why the materials need 17 days to reach the critical M_n compared to 6 days for PLAs filled at 30 wt.-% loading.

As previously reported in chapter IV (p.120 and p.127), when the critical molecular mass is reached, a high concentrated FR layer appears at the surface of the materials. In the case of intumescent FR-PLAs-20%, this layer is formed after 17 days when M_n reaches the M_c of 20000 g/mol (the complete disintegration of the plates occurs after 28 days approximately). This phenomenon is in accordance with the improvement of MLC performances reported in this section.

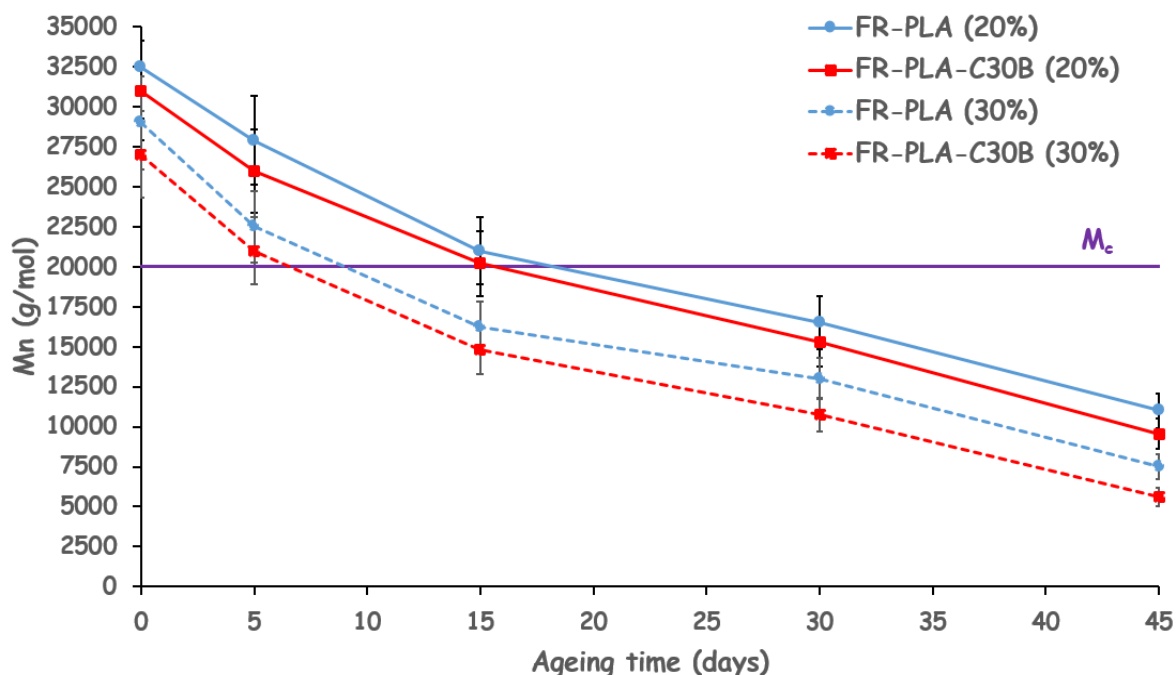


Figure 111: M_n versus ageing time of FR-PLA 20% and 30% (●) and FR-PLA-C30B (●) 20% and 30% materials aged under T/UV/RH conditions.

All along the different investigations led during our work, some phenomena were evidenced both in terms of physico-chemical properties or fire performances after ageing:

- The decrease of the molecular mass of FR-PLAs when exposed to artificial accelerated ageing (T/UV, T/RH and T/UV/RH).
- The decrease of thermal stability of FR-PLAs as a function of ageing exposure.
- When the critical molecular mass (M_c) is reached, a high concentrated FR layer is formed at the surface of the materials.
- In terms of fire performances, a reduction of pHRR and THR is observed along ageing exposure.
- A change of the intumescent behavior is reported when samples are aged. Indeed, it was observed that the intumescent shield is formed sooner accompanied by a higher expansion of the char.

According to these different observations a simple mechanism can be proposed to explain the impact of ageing on the MLC performances (**Figure 112**):

- The decrease of the molecular mass occurring during ageing of FR-PLAs impacts the dynamics of molecular chains. In fact, ageing can increase the mobility of the chains and have an effect on the strength of polymer bonds. The degradation of the polymer matrix could lead to the formation of new or more reactive species that can initiate quicker the thermal degradation of the polymer [174, 190-192] (**Figure 112 (a)**).
- The decrease of both pHRR and THR is observed from the moment when the critical molecular mass (M_c) is reached. Thus, when the high concentrated FR layer is formed at the surface of the material, i.e. when FR fillers are more readily available on the surface (**Figure 112 (a)**).
- It is thus possible that the more reactive species formed during PLA degradation and fillers layer formed at the surface of FR-PLAs both promote the intumescent mechanism. Thus, when exposed to the radiative heat flux of the MLC, PLA and fillers can quickly react, thus promoting the intumescent mechanism. The insulative barrier is formed sooner and both pHRR and THR are decreased (**Figure 112 (b)**).
- On the other hand if more reactive species are formed during ageing, they are able to react with fillers in the condensed phase. Thus explaining the higher expansion of the char reported during MLC test and demonstrating that the polymer itself participate to its own protection.
- Hence, it seems that ageing promotes the intumescence mechanism through the kinetics of formation of the protective shield.
- However, further investigations are still needed as to prove our different assumptions and in particular determine if the mechanism of intumescence itself is modified during ageing. Hence it will be possible to evidence a complete mechanism of action in terms of MLC fire performances of aged FR-PLAs.

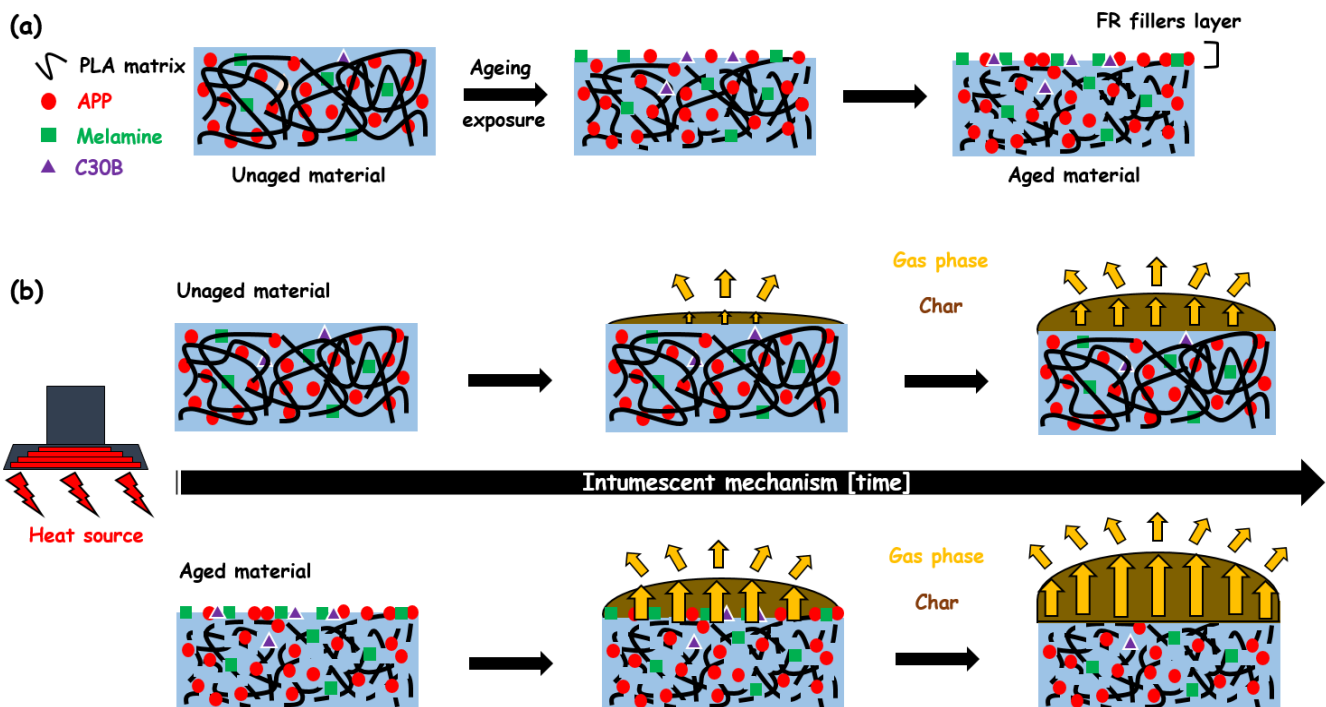


Figure 112: Schematic representation of the effect of ageing on the intumescent mechanism of FR-PLA-C30B-20%.

In the case of FR-PLA and FR-PLA-C30B filled at 30 wt.-% loading, the MLC performances remain similar after ageing maybe because the two intumescent formulations already exhibit very high fire performances before the formation of the FR concentrated layer at the surface. On the other hand, the values of pHRR and THR obtained during the experiments are very low, thus considering the limits of measurements of the MLC device no effect of ageing can be considered. One possibility to avoid this problem is to increase the heat flux of the MLC device. Indeed, whereas our experiments were performed at 35 kW/m², by increasing the heat flux until 50 or 75 kW/m², it should be possible to obtain higher values of THR and pHRR and thus evidence the effect of ageing on the MLC performances of FR-PLAs-30%.

3. Conclusion

In Chapter V, the fire properties of intumescent PLAs as well as their behavior during ageing were studied. Firstly, it was confirmed that the incorporation of fillers such as Melamine and APP allows the development of an efficient intumescent system improving the fire performances of PLA [12, 24, 61]. Moreover, the addition of nanoparticles (i.e. Cloisite 30B) shows a synergistic effect enhancing the protection by intumescence, with a more insulating char that limits the “fuel” release due to its better cohesion, thus decreasing pHRR and THR.

In the second part, flame retardant properties of PLA and FR-PLAs after ageing were investigated under T/UV, T/RH and T/UV/RH conditions. During ageing it appears that flame retardant properties of virgin PLA are not modified until 60 days of ageing and thus whatever the kind of exposure. However, concerning FR-PLA and FR-PLA-C30B, investigations led for LOI

and MLC tests reveal that ageing impacts the flame retardancy of intumescent PLAs. It was demonstrated that the LOI of FR-PLAs increases during ageing. The increase of LOI was reported to be higher in the case of T/UV/RH exposure compared to T/RH then T/UV conditions. Action mechanism was found to be due to a “runaway effect”. Indeed, during ageing, the degradation of the material leads to a decrease in viscosity of the system. This phenomenon creates a “runaway effect”, which permits to the combustible material to escape from the flame by dripping, thus, leading to the increase in the LOI values for both FR-PLAs.

Furthermore, ageing was reported to have no effect on the fire performances observed by MLC for PLA and FR-PLAs. Even before ageing the two intumescent PLAs exhibit very high fire performances (very low pHRR and THR), due to the optimization of the formulation. Thus the effect of ageing on the MLC performances cannot be observed for these formulations at 35 kW/m².

However, by studying a less effective intumescent PLAs (i.e. FR-PLA-20% and FR-PLA-C30B-20%) it was found that ageing improves the MLC performances at 35 kW/m², by decreasing both pHRR and THR, whereas TTI remains stable. The degradation of the materials during ageing is responsible for these surprising performance. Indeed, the enhanced degradation of FR-PLAs (the high decrease of molecular mass) can lead to the formation of new or more reactive products and of a concentrated layer of nitrogen and phosphorus (also Cloisite 30B in the case of FR-PLA-C30B formulations) at the surface of the sample (**p.120, p.142**). Both phenomena promote the kinetics of intumescence through the development of a more efficient shield when the material is exposed to a heat source, favoring the intumescent phenomenon and enhancing the flame retardancy of the materials.

Investigations reported during this work demonstrate that physico-chemical properties (M_n , viscosity ...) and FR fillers both play an important part in the improvement of fire properties during ageing. It is obvious that the molecular mass plays a crucial role in the durability of intumescent PLAs. Indeed it is mainly responsible for the behavior of the other physico-chemical properties (viscosity, T_g , T_m , thermal stability, crystallinity ...) and thus indirectly to the formation of a high concentrated FR layer at the surface of the materials during ageing. Hence, the degradation level of the materials governs the molecular mass and thus the behavior of the physico-chemical properties and fire performances during FR-PLAs lifetime.

General conclusion

PLA is nowadays the first commodity biodegradable polymer produced from annually renewable resources. It is a potential good candidate for replacement of traditional petroleum derived polymeric materials. Indeed PLA is relatively cheap and has some remarkable properties that make it suitable for various applications such as packaging, textile or transportation like automobile. However, to be used in certain sectors (e.g. automobile), PLA has to be flame retarded and its flame retardant properties as well as its properties of use must be kept for the product lifetime. Literature review revealed that the interest for flame retarded PLA kept growing these past few years. Indeed, many conventional flame retardants which can be combined with nanoparticles (metal hydroxides, phosphorus-containing compounds, halogenated and nitrogenated compounds, organoclays ...) are generally incorporated with efficiency into PLA matrix, to design flame retardant formulations. However, regardless of its interesting properties, PLA is known to be extremely sensitive to its environment of use, impacting the lifetime of the material. Ageing generally leads to the degradation of the material via various phenomena (e.g. hydrolysis, thermo-degradation, photo-degradation ...). Ageing which is detrimental for the integrity of the material over time can also affect the durability of the flame retardancy. The aim of this PhD was to evaluate the effect of ageing on the lifetime of flame retarded PLAs.

In this context, the first purpose of this work was to evidence the impact of ageing on neat PLA, a commercially available grade used in this study. Indeed, the understanding of the behavior of neat PLA during ageing was of primary importance to apprehend the ageing of flame retarded PLAs. The ageing of the material was carried out under three different accelerated ageing tests under T/UV, T/RH and T/UV/RH exposure. The physico-chemical properties (M_n , T_g , T_m , thermal stability, crystallinity) and visual appearance of PLA during ageing were assessed by a various number of techniques, such as GPC, DSC, TGA, XRD, FTIR, digital microscopy, SEM and $L^*a^*b^*$. This step of characterization permitted to correlate the effects of ageing with the ones already reported in literature. Indeed, it was found that ageing has a direct influence on the physico-chemical properties of the material by decreasing M_n , T_g , T_m and thermal stability of PLA. On the contrary, the crystallinity of the material increased. Visually, cracks, holes and a bleaching of the material were reported during ageing. It was reported that these phenomena depend on the ageing conditions, as the impacts of ageing are even more important for PLA aged under T/UV/RH compared to T/RH and T/UV. The influence of flame retardant additives on the ageing of PLA was then studied. Both visual and physico-chemical characterizations performed during exposure revealed that flame retardant additives have a direct impact on the ageing of PLA. Indeed, the effects of ageing appeared to be more pronounced when FR fillers are incorporated into the PLA matrix. Even if cracks and holes are also observed during ageing of FR-PLAs, the formation of a white layer was evidenced at the surface of the T/RH and T/UV/RH aged materials when a critical molecular mass of 20000 g/mol is reached. Moreover, it appeared that both FR-PLA and FR-PLA-C30B were surprisingly disintegrated into powder after 10 and 35 days of exposure to T/UV/RH and T/RH conditions, respectively. On the contrary, after 60 days, the exposure to T/UV appeared not to be drastic for the visual integrity of FR-PLAs as it was demonstrated that the M_c was still

not reached. The different characterization techniques used all along the ageing exposure (GPC, DSC, XRD, FTIR ...) suggested that these phenomena can be explained by the evolution of physico-chemical properties of the materials. The impacts of ageing on the physico-chemical properties of FR-PLAs were found to be similar to those reported for neat PLA (decrease of M_n , T_g , T_m , increase in crystallinity ...). However, the already low molecular mass before ageing explained why FR-PLAs reached quickly the M_c (20000 g/mol) and thus the faster degradation of FR materials. This proved that the molecular mass is a crucial parameter for polymers as it governs most of the physico-chemical properties of the material (T_g , T_m , crystallinity ...) and thus its durability.

Strategically, it was also fundamental to elucidate the mechanisms of degradation occurring during T/UV, T/RH and T/UV/RH exposure. Especially as many different mechanisms have been proposed all over the years depending on the ageing conditions and duration. It was evidenced that the degradation of neat PLA takes place in the bulk of the material assuming an autocatalytic process, but mechanism of degradation depends on the exposure conditions. FTIR evidenced that hydrolysis is the predominant phenomenon occurring during T/RH exposure, whereas under T/UV, EPR experiments revealed that PLA is degraded via a radical mechanism. On the other hand, the increase in temperature was reported to be responsible for a faster degradation. The combination between UV-rays and RH creates a synergistic effect under T/UV/RH exposure. Both hydrolysis and radical mechanism occur simultaneously, accelerating the degradation of the polymer matrix. However, only few studies reported in literature deal with the exposure to T/UV/RH conditions and it is quite difficult up to now to determine which of the two phenomena is predominant. In presence of FR fillers, EPR experiments indicated that FR fillers protect the material against UV and O_2 penetration. On the contrary, hydrolysis mechanism appeared to be modified when FR fillers are incorporated into the PLA matrix. Indeed, in presence of FR fillers, hydrolysis seems to occur at the interface between matrix and fillers, certainly due to an accumulation of water. As a consequence the formation of the white layer composed of Melamine, APP and C30B (in the case of FR-PLA-C30B) at the surface of FR-PLAs. Moreover, the partial hydrolysis of APP could also be held responsible for this phenomenon, explaining why APP particles are not completely embedded in the PLA matrix anymore. During this work, the use of the EPR device was revealed to be an innovative technique to use, as it offers new perspectives on both mechanistic and kinetics points in the field of photo-degradation of polymers.

The main goal of incorporating FR fillers into PLA was to improve its flame retarded properties. Knowing the impact of fillers on the physico-chemical properties and mechanisms of degradation of PLA, it was thus crucial to investigate the durability of the flame retardant properties. It was firstly demonstrated that the incorporation of FR fillers (i.e. Melamine and APP) permitted the development of an efficient intumescent system improving the fire performances of PLA. Furthermore, the addition of nanoparticles (i.e. Cloisite 30B) showed a synergistic effect. The intumescence of the system was enhanced, with a more insulating and a more cohesive char. After ageing, it was showed that the fire performances of neat PLA

remained similar whereas those of FR-PLAs were improved, especially in LOI test. Indeed, it was demonstrated that the LOI of FR-PLAs increases during ageing due to a “runaway effect”. Due to the already very high fire performances before ageing, ageing was reported to have no effect on the fire performances observed by MLC for FR-PLAs filled at 30 wt.-%. However, it was demonstrated that ageing improves the MLC performances of a less effective intumescent PLA (i.e. FR-PLA-20% and FR-PLA-C30B-20%) by decreasing both pHRR and THR. The degradation of the matrix during ageing and the high concentrated FR layer formed at the surface of the materials were held responsible for this surprising behavior. They both accelerate the kinetics of intumescence, thus promoting the development of a more efficient shield able to enhance the flame retardancy of the materials. This demonstrates the key role of ageing in the behavior and the durability of flame retardancy during lifetime of FR-PLAs.

This PhD aimed to evidence the impact of ageing on the durability of a flame retardant system, based on PLA. It was shown that PLA is a very promising polymer in the field of flame retardancy, even if it is extremely sensitive to its environment of use. It was demonstrated that both FR fillers and physico-chemical properties (especially the molecular mass) play an important role in the improvement of fire properties during ageing. This could be used as a basis for further work, dealing with the ageing of flame retarded polymers

Outlook

As many topics were approached in this manuscript, many outlook emerged along the dissertation: optimization of extrusion process, mechanistic outlook, kinetics degradation, modelling...

The first and obvious outlook is related to the molecular mass of FR-PLAs. In this manuscript, it was evidenced that the molecular mass is a crucial parameter for the durability of the material. It could be interesting to limit the decrease of M_n during the extrusion process of FR-PLAs (chain extender, master batch...), as to study PLA and FR-PLAs with similar molecular mass. Hence, avoiding the effect of the molecular mass on degradation of FR-PLAs, it would be possible to focus solely on the contribution of FR fillers on the ageing of the intumescent materials.

Most papers dealing with ageing of polymers, especially PLA, demonstrate the effect of ageing on the mechanical properties of the material. The mechanical properties of a polymer involve its behavior under stress. These properties are essential when considering how a polymer can be used. Hence, the impact of the addition of FR fillers on the mechanical properties of PLA (using tensile tests, dynamic mechanical analysis...) should be studied as well as their behavior under exposure to T/UV, T/RH and T/UV/RH exposure.

In terms of mechanistic approach, it was reported in this manuscript that PLA is mainly degraded into carboxylic acids, such as formic acid, acetic acid, oxalic acid... During this work, the use of pH paper and the identification of their characteristic odor were the only way to evidence these products. However, the pyrolysis – gas chromatography - mass spectroscopy (Py-GC/MS) is a chemical analysis that could evidence the secondary products formed during the degradation of PLA. Indeed, Py-GC/MS is a method of thermal decomposition in which smaller molecules produced can be separated by gas chromatography and detected using mass spectrometry. Hence, it is a useful techniques for the identification of chemical species. As already reported, electron paramagnetic resonance (EPR) is another innovative technique that should be further used in order to study the kinetics and mechanism of degradation of polymeric materials. Most papers focusing on the photo-degradation of polymers, especially PLA, suggest mechanism of degradation based on FTIR investigations. However, this technique should be coupled with EPR in order to elucidate the intermediate mechanisms (radicals) occurring during photo-degradation and not only evidence the final products. Moreover, EPR is an appropriate technique as to evidence the role of FR fillers during photo-degradation of FR-PLAs. Indeed, this could be interesting to further investigate the protective role of FR fillers during photo-degradation of FR-PLAs. Thus determining how FR fillers prevent the degradation of PLA and evidencing the mechanism of protection.

In the field of fire testing, it has been reported that the MLC performances of FR-PLAs filled at 30 wt.-% loading remain similar after ageing, maybe because the two intumescent formulations already exhibit very high fire performances before ageing. Hence, the values of pHRR and THR obtained during the experiments are very low, thus considering the limits of measurements of the MLC device no effect of ageing can be considered. The question raised

from these results is “*Could that be possible to avoid the limitation of the MLC device?*”. For instance, one possibility could be to increase the heat flux of the MLC device. Indeed, whereas our experiments were performed at 35 kW/m², by increasing the heat flux until 50 or 75 kW/m², it should be possible to obtain higher values of THR and pHRR and thus evidence the effect of ageing on the MLC performances of FR-PLAs-30%. This phenomenon have been demonstrated in the case of neat PLA (**Figure 113** and **Table 43**).

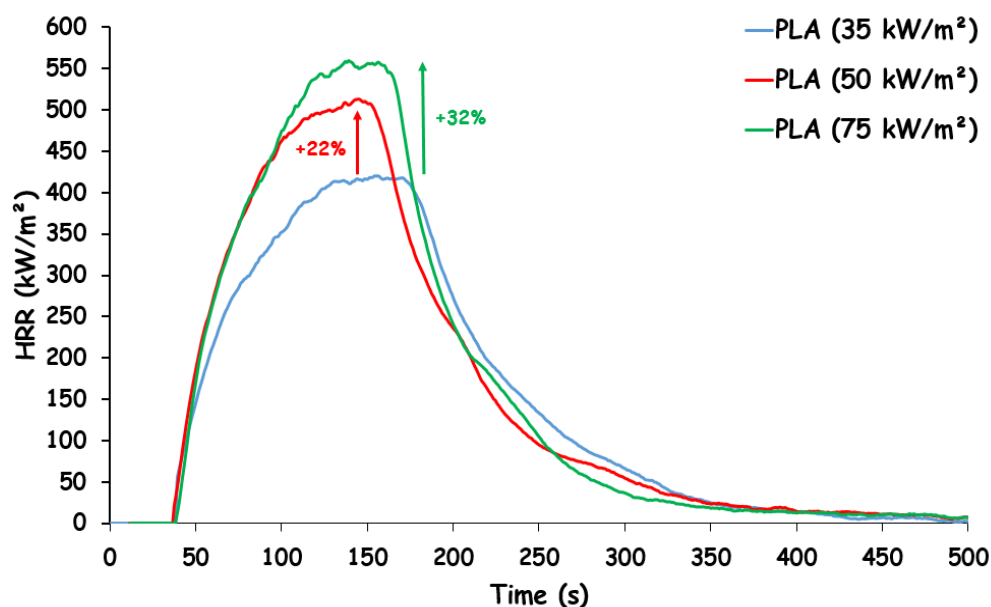


Figure 113: RHR curves as a function of time of PLA at 35 kW/m²(●), 50 kW/m² (●) and 75 kW/m² (●).

Table 43: MLC values obtained for PLA at 35 kW/m², 50 kW/m² and 75 kW/m².

Heat flux (kW/m ²)	Time to ignition (s)	pHRR (kW/m ²)	THR (MJ/m ²)
35	39	420.0	72.0
50	37 (-2)	513.0 (+22%)	80 (+11%)
75	40 (+1)	557.0 (+32%)	82 (+14%)

Indeed, at 35 kW/m², pHRR and THR of PLA are 420 kW/m² and 72 MJ/m², respectively. By increasing the heat flux until 50 kW/m², pHRR and THR reach 513 kW/m² (+22%) and 80 MJ/m² (+12%), respectively. For an external heat flux of 75 kW/m², pHRR and THR of PLA are increased until 557 kW/m² (+32%) and 82 MJ/m² (+14%). Finally, it was shown that during MLC experiment, the intumescent shield of aged FR-PLAs is formed sooner, with a higher swelling, resulting in a more expanded char. In this manuscript, no investigations were led on the structure of the chars during ageing. Knowing the role of the char structure on the intumescent mechanism of FR-PLAs [12, 24], more studies should be led on this topic. Using techniques such as 3D X-Ray tomography or rheometer, it could be interesting to study the structure, the porosity and the resistance of the char before and after ageing, in order to

understand the role of the char in the improvement of fire performances during ageing. In general, more investigations are needed to evidence if ageing impacts the intumescent mechanism itself or if it only plays on the kinetics of intumescence.

Some issues still exist to design long term commercially applications for flame retarded PLA systems, as addressed in this Ph.D work, but the current efforts will probably help to resolve them. In particular all the methods developed and the key parameters detailed in this Ph.D work are really required to go further in the research on the ageing of flame retarded systems.

List of figures, tables and equations

List of Figures

Figure 1: World plastic production from 1950 to 2012 [1, 2].	18
Figure 2: Global production capacities of bioplastics in 2014 (by material type) [4].	19
Figure 3: Evolution of number of publications versus time with keyword “flame retardancy” and “PLA” (Scifinder Sept 2016).	20
Figure 4: Synthesis of PLA from L- and D-lactic acids, adapted from Lim et al. [52].	25
Figure 5: Poly(lactic acid) structure.	26
Figure 6: The stereoisomers of lactic acid.	26
Figure 7: Chemical structures of L,L-, L,D- and D,D-lactides [5].	27
Figure 8: Stereocomplex of PLLA and PDLA [61].	27
Figure 9: PDLLA multiblocks as function of D and L content, adapted from Kakuta et al. [60].	27
Figure 10: Transmission percentage versus wavelength for PLA, PS, LDPE, PET and cellophane films, adapted from Auras et al. [5].	28
Figure 11: FTIR (ATR) spectrum of PLA in the range 500 to 4000 cm^{-1} .	29
Figure 12: Glass transition temperatures for PLAs of different L-contents as a function of molecular weight, adapted from Dorgan et al. [67].	30
Figure 13: Peak melting temperature of PLA as a function of % meso-lactide [52]. (o) represents values reported by Witzke [71]; (●) represents values reported by Hartmann [72].	31
Figure 14: DSC thermograms of water quenched, air-annealed (cooled from 220°C to ambient temperature in 5 min), and full-annealed (cooled from 220°C to ambient temperature in 105 min) PLLA samples. DSC scans were performed at a heating rate of 10°C/min, adapted from Sarasua et al. [77].	33
Figure 15: DSC scans for 1.5% D-lactide PLA samples cooled from the melt at 10K/min and then reheated at different heating rates from 30 to 0.3 K/min, adapted from Pyda et al. [78].	34
Figure 16: DSC scans at 20 K/min for PLA with 1.5% (PLA-L), 8.1% (PLA-M) and 16.4% (PLA-H) D-isomers. All samples were cooled quickly from the melt and isothermally crystallized at 145°C for 15h. The quenched PLA-L sample was cooled similarly from the melt but did not undergo the 15 h isothermal crystallization, adapted from Pyda et al. [78].	34
Figure 17: Combustion of a polymer [90].	37
Figure 18: Main chemical ageing factors and consequences on polymeric materials.	44
Figure 19: General degradation mechanisms, adapted from Beyler, at al. [124].	45
Figure 20: Norrish I and II mechanisms.	48
Figure 21: simplified photo-oxidation cycle of polymers, adapted from Yousif et al [129].	49
Figure 22: Example of hydrolysis of polyether.	53
Figure 23: Illustration of the hydrolytic mechanisms: (a) surface erosion, (b) bulk erosion without autocatalysis, and (c) bulk erosion with autocatalysis, adapted from Viera et al. [150].	54

Figure 24: Norrish II mechanism for PLA photo-degradation: (a) PLA chain under UV irradiation, (b) photophysical excitation and (c) oxidation/scission reactions in PLA chains, adapted from Belbachir et al. [33].	56
Figure 25: Photo-degradation (radical oxidation) process of irradiated PLA: hydroperoxides chain propagation and formation of anhydrides by photolysis of hydroperoxides, adapted from Gardette et al. [35].	57
Figure 26: Hydrolysis of PLA.	58
Figure 27: Biodegradation of PLA in 60°C, adapted from Auras et al. [5].	58
Figure 28: Thermal degradation mechanism of PLA, adapted from McNeill et al. [166].	59
Figure 29: Thermo Scientific extruder.	70
Figure 30: Humidity chamber test HCP 108.	72
Figure 31: Q-LAB, QUV/spray weathering chamber.	72
Figure 32: Temperature/time ramp used for the DSC analysis.	75
Figure 33: color space of CIE Lab system.	76
Figure 34: Melt flow Index tester.	78
Figure 35: Reaction of anhydride with ammonia.	80
Figure 36: Schematic representation of mass loss calorimeter.	83
Figure 37: Experimental set-up of the LOI test.	84
Figure 38: Pictures of PLA at 0 d (a), 60 d T/UV (b), 60 d T/RH (c) and 60 d T/UV/RH (d) exposure.	86
Figure 39: Digital microscopy pictures of unaged PLA (a), 60 d T/UV (b), 60 d T/RH (c) and 60 d T/UV/RH (d).	87
Figure 40: SEM pictures obtained for unaged PLA (a), 60 d aged under T/UV (b), T/RH (c) and T/UV/RH (d) conditions.	88
Figure 41: M_n (a) and polydispersity index PI (b) versus ageing time of PLA samples aged under T/UV (●), T/RH (▪) and T/UV/RH (Δ) conditions.	91
Figure 42: Average number of random chain scissions per unit mass (n_t) for PLA as function of ageing time for different ageing conditions; T/UV (●), T/RH (▪) and T/UV/RH (Δ).	92
Figure 43: TGA curves as a function of time for unaged PLA (-), T/UV (-), T/RH (-) and T/UV/RH (-) 125 days aged (10°C/min under air).	93
Figure 44: Evolution of glass transition temperature (T_g) of PLA as a function of exposure to T/UV (●), T/RH (▪) and T/UV/RH (Δ) conditions.	95
Figure 45: Evolution of melting temperature (T_m) of PLA as a function of exposure to T/UV (●), T/RH (▪) and T/UV/RH (Δ) conditions.	95
Figure 46: T_g as a function of M_n for PLA aged under T/UV (●), T/RH (▪) and T/UV/RH (Δ) exposure.	96
Figure 47: Evolution of crystallinity of PLA as a function of ageing time, for T/UV (●), T/RH (▪) and T/UV/RH (Δ) exposure.	99
Figure 48: FTIR spectra as a function of ageing time for PLA aged under T/UV (a), T/RH (b) and T/UV/RH (c).	100

Figure 49: WAXD patterns of PLA obtained by XRD, before (●) and after 60 of ageing under T/UV (●), T/RH (●) and T/UV/RH (●).....	102
Figure 50: FTIR spectra of PLA before and after various ageing durations under T/RH conditions.....	105
Figure 51: degradation of PLA by hydrolysis under T/RH exposure.	105
Figure 52: EPR spectrum of PLA irradiated with wavelengths between 300 and 400 nm at room temperature.	107
Figure 53: Biradical specie observed by EPR for PLA.	107
Figure 54: Kinetic evolution of EPR signal for PLA as a function of temperature, 25°C (●), 50°C (●) and 75°C (●).	108
Figure 55: Identification of the activation energy of biradical formation in PLA for different temperatures.....	109
Figure 56: 2D YZ EPR imaging of PLA 50°C under irradiation at 30 min (a) and 4 hours (b). Intensity of color represents the local spin concentration from blue (min) to red (max).....	109
Figure 57: Kinetic evolution of EPR signal for PLA as a function of ageing exposure, T/UV (●) or T/UV/RH (●) at 50°C.....	110
Figure 58: FTIR spectra ($\times 32 \text{ cm}^{-1}$) of PLA before and after ageing under T/UV and T/UV/RH as a function of ageing time.	111
Figure 59: FTIR spectra ($\times 2 \text{ cm}^{-1}$) of PLA before and after ageing under T/UV and T/UV/RH as a function of ageing time.	113
Figure 60: FTIR spectra ($\times 2 \text{ cm}^{-1}$) of 60 days aged PLA films to T/UV and T/UV/RH, before and after treatment with NH_3	114
Figure 61: Proposed photo-oxidative mechanism of degradation for PLA, in presence of water.	115
Figure 62: numerical pictures of PLA (a), FR-PLA (b) and FR-PLA-C30B (c) plates before ageing.	120
Figure 63: Visual evaluation as a function of ageing for FR-PLA 0 d (a), 60 d T/UV (b), 28 d T/RH (c) and 6 d T/UV/RH (d).	121
Figure 64: Visual evaluation as a function of ageing for FR-PLA-C30B 0 d (a), 60 d T/UV (b), 28 d T/RH (c) and 6 d T/UV/RH (d).	121
Figure 65: Visual evaluation of FR-PLA (a) and FR-PLA-C30B (b) until disintegration into powder (c).	122
Figure 66: SEM pictures obtained for unaged FR-PLA (a), 60 d T/UV (b), 28 d T/RH (c) and 6 d T/UV/RH (d).	123
Figure 67: SEM pictures obtained for unaged FR-PLA-C30B (a), 60 d T/UV (b), 28 d T/RH (c) and 6 d T/UV/RH (d).	124
Figure 68: Aminolysis reaction of PLA.	126
Figure 69: Hofmann elimination reaction on the surfactant of Cloisite 30B.	126
Figure 70: M_n versus ageing time of FR-PLA (a) and FR-PLA-C30B (b) samples aged under T/UV (●), T/RH (■) and T/UV/RH (Δ).	127

Figure 71: Average number of random chain scissions per unit mass (n_t) for FR-PLA and FR-PLA-C30B as a function of ageing time at different ageing conditions; T/UV (●), T/RH (■) and T/UV/RH (Δ).....	129
Figure 72: Evolution of glass transition temperature (T_g) of FR-PLA and FR-PLA-C30B as a function of exposure time under T/UV (●), T/RH (■) and T/UV/RH (Δ).	133
Figure 73: Evolution of melting temperature (T_m) of FR-PLA and FR-PLA-C30B as function of exposure time under T/UV (●), T/RH (■) and T/UV/RH (Δ).	134
Figure 74: Correlation between the decrease of T_g and M_n of FR-PLA and FR-PLA-C30B as a function of ageing under T/UV (●), T/RH (■) and T/UV/RH (Δ).	135
Figure 75: WAXD patterns of PLA (●), FR-PLA (●) and FR-PLA-C30B (●).	136
Figure 76: Evolution of crystallinity of FR-PLA (a) and FR-PLA-C30B (b) as a function of ageing time, for T/UV (●), T/RH (■) and T/UV/RH (Δ) exposure.	138
Figure 77: Correlation between the decrease of crystallinity and M_n of FR-PLA and FR-PLA-C30B as a function of ageing under T/UV (●), T/RH (■) and T/UV/RH (Δ).....	139
Figure 78: WAXD patterns of FR-PLA and FR-PLA-C30B obtained by XRD, before (●) and after 60 of ageing under T/UV (●), T/RH (●) and T/UV/RH (●).	140
Figure 79: EPMA pictures for unaged (a), 60 d T/UV (b), 28 d T/RH (c) and 6 d T/UV/RH (d) aged FR-PLA.....	142
Figure 80: EPMA pictures for unaged (a), 60 d T/UV (b), 28 d T/RH (c) and 6 d T/UV/RH (d) aged FR-PLA-C30B.	143
Figure 81: FTIR spectra (ATR) of Melamine as function of ageing exposure under T/RH.	145
Figure 82: FTIR spectra (ATR) of APP as function of ageing exposure under T/RH.	146
Figure 83: Hydrolysis reaction of APP, according to Chen et al. [175].	146
Figure 84: ^{31}P Solid-state NMR spectra of FR-PLA (a) and FR-PLA-C30B (b) before and after 105 days and 90 days exposure to T/RH and T/UV/RH conditions, respectively.	147
Figure 85: FTIR spectra (ATR) of Cloisite 30B as function of ageing exposure under T/RH... ..	147
Figure 86: SEM pictures in cross section obtained for FR-PLA-C30B aged 28 days under T/RH (a) and 6 days under T/UV/RH (b).	149
Figure 87: EPMA pictures in cross section for FR-PLA-C30B aged 28 days under T/RH and 6 days under T/UV/RH conditions.....	150
Figure 88: SEM pictures obtained for FR-PLA-C30B after 28 days exposure to T/RH.	151
Figure 89: Kinetic evolution of EPR signal as a function of time, for PLA (●), FR-PLA (●) and FR-PLA-C30B (●).	152
Figure 90: 2D HYSORE recorded at 50°C for PLA.	153
Figure 91: 2D HYSORE recorded at 50°C for FR-PLA and FR-PLA-C30B.	153
Figure 92: Kinetic evolution of EPR signal for FR-PLA and FR-PLA-C30B, as a function of ageing exposure to T/UV (●) or T/UV/RH (●) at 50°C.	154
Figure 93: Schematic representation of the effect of fillers and ageing exposure on the degradation of FR-PLA-C30B.	156
Figure 94: TGA curves of PLA (●), FR-PLA (●) and FR-PLA-C30B (●) under air flow at 10°C/min.	161

Figure 95: RHR curves as a function of time of PLA (●), FR-PLA (●) and FR-PLA-C30B (●)....	162
Figure 96: Char residues of FR-PLA and FR-PLA-C30B.....	162
Figure 97: Digital microscopy pictures and cross section of char residues of FR-PLA and FR-PLA-C30B.	163
Figure 98: Intumescent mechanism, adapted from Gallos et al [61].	165
Figure 99: Release of gas through the char of FR-PLA and FR-PLA-C30B, adapted from Gallos et al [61].	166
Figure 100: TGA curves as function of time for FR-PLA (a) and FR-PLA-C30B (b), before ageing (●), 125 days T/UV (●), 105 days T/RH (●) and 60 days T/UV/RH (●) exposure.	169
Figure 101: Evolution of the behavior of LOI samples of FR-PLA and FR-PLA-C30B as a function of ageing exposure to T/UV, T/RH and T/UV/RH conditions.....	172
Figure 102: TEM pictures of big (a) and small (b) agglomerates of Cloisite 30B in FR-PLA-C30B.....	174
Figure 103: Evolution of viscosity of FR-PLA and FR-PLA-C30B as a function of ageing exposure to T/UV (●), T/RH (■) and T/UV/RH (Δ) conditions (a) and molecular mass (b)....	175
Figure 104: RHR curves of unaged PLA (●) and 60 days exposure to T/UV (●), T/RH (●) and T/UV/RH (●) conditions.....	176
Figure 105: RHR curves of unaged FR-PLA (●) and 60 days exposure to T/UV (●), T/RH (●) and T/UV/RH (●) conditions.....	177
Figure 106: RHR curves of unaged FR-PLA-C30B (●) and 60 days exposure to T/UV (●), T/RH (●) and T/UV/RH (●) conditions.	178
Figure 107: RHR curves of unaged FR-PLA-20% (●), 17 days (●) and 22 days (●) aged under T/UV/RH conditions.....	179
Figure 108: RHR curves of unaged FR-PLA-C30B-20% (●), 18 days (●) and 22 days (●) aged under T/UV/RH conditions.....	180
Figure 109: Evolution of the char expansion of FR-PLA-20% as a function of ageing under T/UV/RH exposure.	181
Figure 110: Evolution of the char expansion of FR-PLA-C30B-20% as a function of ageing under T/UV/RH exposure.....	181
Figure 111: M_n versus ageing time of FR-PLA 20% and 30% (●) and FR-PLA-C30B (●) 20% and 30% materials aged under T/UV/RH conditions.	183
Figure 112: Schematic representation of the effect of ageing on the intumescent mechanism of FR-PLA-C30B-20%.....	185
Figure 113: RHR curves as a function of time of PLA at 35 kW/m ² (●), 50 kW/m ² (●) and 75 kW/m ² (●).....	193
Figure 114: FR-PLA-C20A (a), FR-PLA-C30B (b) and FR-PLA-CNa ⁺ (c) plates aged 28 days under T/RH conditions.....	222
Figure 115: M_n versus ageing time of FR-PLA-C20A (●), FR-PLA-C30B (■) and FR-PLA-C30B (Δ) samples aged under T/RH conditions.	223
Figure 116: Evolution of glass transition temperature (T_g) of FR-PLA-C20A (●), FR-PLA-C30B (■) and FR-PLA-CNa ⁺ (Δ) as a function of exposure time under T/RH conditions.	224

Figure 117: Evolution of melting temperature (T_m) of FR-PLA-C20A (●), FR-PLA-C30B (▪) and FR-PLA-CNa ⁺ (Δ) as a function of exposure time under T/RH conditions.	224
Figure 118: Evolution of crystallinity of FR-PLA-C20A (●), FR-PLA-C30B (▪) and FR-PLA-CNa ⁺ (Δ) as a function of ageing time under T/RH conditions.	225
Figure 119: FTIR (ATR) spectra of PLA, FR-PLA, FR-PLA 105 days (T/RH) and FR-PLA 90 days (T/UV/RH) in the range of 600 to 3600 cm^{-1}	226
Figure 120: FTIR (ATR) spectra of PLA, FR-PLA-C30B, FR-PLA-C30B 105 days (T/RH) and FR-PLA-C30B 90 days (T/UV/RH) in the range of 600 to 3600 cm^{-1}	227
Figure 121: Example of 2D HYSCORE microwave pulses.	228
Figure 122: 2D HYSCORE spectrum of a coat standard sample.	228
Figure 123: TGA curves of pure compounds, PLA (●), Mel (●), APP (●) and C30B (●) under air flow at 10°C/min.	229
Figure 124: DTG of pure compounds, PLA (●), Mel (●), APP (●) and C30B (●) under air flow at 10°C/min.	230

List of Tables

Table 1: Infrared spectroscopy data for PLA.....	29
Table 2: Unit cell parameters for PLLA and stereocomplex crystals [5].	32
Table 3: PLA mechanical properties compared to those of most common polymers used in commodity applications [83].....	35
Table 4: Properties of Ingeo PLA 4032D.....	68
Table 5: Summary of additives used.	69
Table 6: Composition and name of the formulations PLA, FR-PLA, FR-PLA-C30B at 30 wt.-% loading.	70
Table 7: Composition and name of the formulations FR-PLA, FR-PLA-C30B at 20 wt.-% loading.	70
Table 8: Temperature profile of the extruder from hopper to die.....	70
Table 9: Conditions in accelerated weathering chambers for T/UV and T/UV/RH ageing.....	73
Table 10: L*a*b* values of unaged and 60 days aged PLA under T/UV, T/RH and T/UV/RH conditions.....	89
Table 11: M _n and polydispersity index (PI) data as a function of ageing of PLA exposed to T/UV, T/RH and T/UV/RH conditions.	90
Table 12: TGA data (10°C/min under air) obtained after ageing of PLA exposed to T/UV, T/RH and T/UV/RH conditions.	93
Table 13: DSC data of PLA reported as a function of ageing exposure to T/UV, T/RH and T/UV/RH conditions.....	94
Table 14: Crystallinity of PLA as a function of ageing duration under T/UV, T/RH and T/UV/RH exposure.....	98
Table 15: Evolution of the band at 1845 cm ⁻¹ of PLA before and after ageing under T/UV and T/UV/RH as a function of ageing time.	113
Table 16: Number average molecular mass (M _n) of PLA, FR-PLA and FR-PLA-C30B materials.	126
Table 17: M _n and PI data as function of ageing of PLA, FR-PLA and FR-PLA-C30B samples aged under T/UV, T/RH and T/UV/RH.	127
Table 18: DSC data of PLA, FR-PLA and FR-PLA-C30B as a function of M _n	130
Table 19: DSC data of FR-PLA as a function of M _n and ageing time under T/UV, T/RH and T/UV/RH.	131
Table 20: DSC data of FR-PLA-C30B as a function of M _n and ageing time under T/UV, T/RH and T/UV/RH.	132
Table 21: Crystallinity (χ) data for PLA, FR-PLA and FR-PLA-C30B as a function of M _n	136
Table 22: Evolution of Crystallinity for FR-PLA as a function of M _n for different ageing durations under T/UV, T/RH and T/UV/RH exposure.	137
Table 23: Evolution of Crystallinity for FR-PLA-C30B as a function of M _n for different ageing duration under T/UV, T/RH and T/UV/RH exposure.....	138
Table 24: At % on the surface of FR PLA determined by XPS as a function of ageing.	144

Table 25: At % on the surface of FR PLA-C30B determined by XPS as a function of ageing..	144
Table 26: TGA data (10°C/min under air) obtained for PLA, FR-PLA and FR-PLA-C30B.....	160
Table 27: MLC values obtained for PLA, FR-PLA and FR-PLA-C30B.....	162
Table 28: LOI values of PLA, FR-PLA and FR-PLA-C30B.	164
Table 29: TGA data (10°C/min under air) obtained after ageing of FR-PLA exposed to T/UV, T/RH and T/UV/RH conditions.	167
Table 30: TGA data (10°C/min under air) obtained after ageing of FR-PLA-C30B exposed to T/UV, T/RH and T/UV/RH conditions.	168
Table 31: Comparison between theoretical and experimental residual weight (wt. %) obtained at 800°C for FR-PLA and FR-PLA-C30B.	170
Table 32: LOI ranking of PLA as a function of exposure to T/UV, T/RH and T/UV/RH conditions.....	170
Table 33: LOI ranking of FR-PLA as a function of exposure to T/UV, T/RH and T/UV/RH conditions. The (+x) are calculated using the unaged formulation as reference.	171
Table 34: LOI ranking of FR-PLA-C30B as a function of exposure to T/UV, T/RH and T/UV/RH conditions. The (+x) are calculated using the unaged formulation as reference.	171
Table 35: Viscosity data obtained for FR-PLA exposed to T/UV, T/RH and T/UV/RH conditions.	173
Table 36: Viscosity data obtained for FR-PLA-C30B exposed to T/UV, T/RH and T/UV/RH conditions.....	173
Table 37: MLC values obtained for PLA as a function of exposure to T/UV, T/RH and T/UV/RH conditions.....	176
Table 38: MLC values obtained for FR-PLA as a function of exposure to T/UV, T/RH and T/UV/RH conditions.....	177
Table 39: MLC values obtained for FR-PLA-C30B as a function of exposure to T/UV, T/RH and T/UV/RH conditions.....	178
Table 40: MLC values obtained for FR-PLA-20% as a function of exposure time to T/UV/RH conditions.....	179
Table 41: MLC values obtained for FR-PLA-C30B-20% as a function of exposure time to T/UV/RH conditions.....	180
Table 42: M_n data of FR-PLAs-20% and FR-PLAs-30% as a function of ageing exposure to T/UV/RH conditions.....	182
Table 43: MLC values obtained for PLA at 35 kW/m ² , 50 kW/m ² and 75 kW/m ²	193
Table 44: $L^*a^*b^*$ values of PLA, FR-PLA and FR-PLA-C30B.	220
Table 45: $L^*a^*b^*$ values of unaged and aged FR-PLA under T/UV, T/RH and T/UV/RH conditions.	221
Table 46: $L^*a^*b^*$ values of unaged and aged FR-PLA-C30B under T/UV, T/RH and T/UV/RH conditions.....	221

List of equations

Equation 1	31
Equation 2	31
Equation 3	33
Equation 4	47
Equation 5	47
Equation 6	47
Equation 7	47
Equation 8	48
Equation 9	49
Equation 10	49
Equation 11	49
Equation 12	49
Equation 13	50
Equation 14	50
Equation 15	50
Equation 16	51
Equation 17	51
Equation 18	52
Equation 19	52
Equation 20	52
Equation 21	52
Equation 22	52
Equation 23	75
Equation 24	76
Equation 25	77
Equation 26	78
Equation 27	79
Equation 28	81
Equation 29	84
Equation 30	96
Equation 31	97
Equation 32	108

References

1. PlasticsEurope. *Plastics - the Facts 2014/2015 An analysis of European plastics production, demand and waste data*. 2014 [cited 2015 06-2015]; Available from: <http://www.plasticseurope.fr/>.
2. PlasticsEurope. *Plastics - the Facts 2013 - An analysis of European plastics production demand and waste data*. 2013 [cited 2015 06-2015]; Available from: <http://www.plasticseurope.fr/>.
3. Shen, L., Haufe J, Patel M K, *Product overview and market projection of emerging bio-based plastics*. Copernicus Institute for Sustainable Development and Innovation, Utrecht University, 2009.
4. EuropeanBioplastics. *Global production capacities of bioplastics 2015* [cited 2016 02-2016]; Available from: <http://www.european-bioplastics.org/>.
5. Auras, R., Harte B, Selke S, *An overview of polylactides as packaging materials*. Macromolecular Bioscience, 2004. **4**(9): p. 835-864.
6. Association, N.F.P. *Fires in the US*. 2013 [cited 2016 04-2016]; Available from: <http://www.nfpa.org/news-and-research/fire-statistics-and-reports/fire-statistics/fires-in-the-us>.
7. Levchik, S., V., Weil E D, *Flame retardancy of thermoplastic polyesters—a review of the recent literature*. Polymer International, 2005. **54**(1): p. 11-35.
8. Bourbigot, S., Fontaine G, *Flame retardancy of polylactide: an overview*. Polymer Chemistry, 2010. **1**(9): p. 1413-1422.
9. Réti, C., Casetta M, Duquesne S, Bourbigot S, Delobel R, *Flammability properties of intumescent PLA including starch and lignin*. Polymers for Advanced Technologies, 2008. **19**(6): p. 628-635.
10. Bourbigot, S., Duquesne S, Fontaine G, Bellayer S, Turf T, Samyn F, *Characterization and reaction to fire of polymer nanocomposites with and without conventional flame retardants*. Molecular Crystals and Liquid Crystals, 2008. **486**: p. 325.
11. Solarski, S., Ferreira M, Devaux E, Fontaine G, Bachelet P, Bourbigot S., et al, *Designing polylactide/clay nanocomposites for textile applications: effect of processing conditions, spinning and characterization*. Journal of Applied Polymer Science, 2008. **109**: p. 841.
12. Fontaine, G., Bourbigot S, *Intumescent polylactide : A nonflammable material*. Journal of Applied Polymer Science, 2009. **113**(2009): p. 3860-3865.
13. Nishida, H., Fan Y, Mori T, Oyagi N, Shirai Y, Endo T, *Feedstock recycling of flame-resisting poly(lactic acid)/aluminum hydroxide composite to L,L-lactide*. Industrial & Engineering Chemistry Research, 2005. **44**: p. 1433-1437.
14. Yanagisawa, T., Kiuchi Y, Iji M, *Enhanced flame retardancy of polylactic acid with aluminium tri-hydroxide and phenolic resins*. Kobunshi Ronbunshu, 2009. **66**(49-54).
15. Kubokawa, H., Ohta M, Hatakeyama T, *Flame-retarding of polylactide fabrics*. Sen'i gakkaiishi, 1999. **55**: p. 290-297.
16. Kimura, K., Horikoshi Y, *Bio-based polymers*. Fujitsu Scientific and Technical Journal, 2005(41): p. 173-180.
17. Kubokawa, H., Komatsu H, *Flammability and thermal decomposition behavior of polylactide - cellulose union cloths*. Sen'i gakkaiishi, 2000. **56**: p. 497-500.
18. Kubokawa, H., Hatakeyama T, *Thermal decomposition behavior of polylactide fabrics treated with flame retardants*. Sen'i gakkaiishi, 1999. **55**: p. 349-355.
19. Isitman, N., A., Dogan M, Bayramli E, Kaynak C, *The role of nanoparticle geometry in flame retardancy of polylactide nanocomposites containing aluminium phosphinate*. Polymer Degradation and Stability, 2012. **97**(8): p. 1285-1296.
20. Bourbigot, S., Fontaine G, Duquesne S, Delobel R, *PLA nanocomposites: quantification of clay nanodispersion and reaction to fire*. International Journal of nanotechnology, 2008. **5**: p. 683-692.

21. Kashiwagi, T., Du F, Douglas J F, Winey K I, Harris R H, Shields J R, *Nanoparticle networks reduce the flammability of polymer nanocomposites*. *Nature Materials*, 2005. **4**(12): p. 928-933.
22. Murariu, M., Dechief A L, Bonnaud L, Paint Y, Gallos A, Fontaine G, Bourbigot S, Dubois P, *The production and properties of polylactide composites filled with expanded graphite*. *Polymer Degradation and Stability*, 2010. **95**(5): p. 889-900.
23. Shumao, L., Jie R, Hua Y, Tao Y, Weizhong Y, *Influence of ammonium polyphosphate on the flame retardancy and mechanical properties of ramie fiber-reinforced poly(lactic acid) biocomposites*. *Polymer International*, 2010. **59**(2): p. 242-248.
24. Fontaine, G., Gallos A, Bourbigot S, *Role of montmorillonite for enhancing fire retardancy of intumescent PLA*. *Fire Safety Science*, 2014. **11**: p. 808-820.
25. Fukushima, K., Tabuani D, Dottori M, Armentano I, Kenny J M, Camino G, *Effect of temperature and nanoparticle type on hydrolytic degradation of poly(lactic acid) nanocomposites*. *Polymer Degradation and Stability*, 2011. **96**(12): p. 2120-2129.
26. Ho, K., Pometto A L, Hinz P N, *Effects of temperature and relative humidity on polylactic acid plastic degradation*. *Journal of Environmental Polymer Degradation*, 1999. **7**(2): p. 83-92.
27. Tsuji, H., Echizen Y, Nishimura Y, *Photodegradation of biodegradable polyesters: A comprehensive study on poly(l-lactide) and poly(ε-caprolactone)*. *Polymer Degradation and Stability*, 2006. **91**(5): p. 1128-1137.
28. Janorkar, A.V., Metters A T, Hirt D E, *Degradation of poly(L-lactide) films under ultraviolet-induced photografting and sterilization conditions*. *Journal of Applied Polymer Science*, 2007. **106**(2): p. 1042-1047.
29. Copinet, A., Bertrand C, Govindin S, Coma V, Couturier Y, *Effects of ultraviolet light (315 nm), temperature and relative humidity on the degradation of polylactic acid plastic films*. *Chemosphere*, 2004. **55**(5): p. 763-773.
30. Badia, J., D., Santonja-Blasco L, Martinez-Felipe A, Ribes-Greus A, *Hygrothermal ageing of reprocessed polylactide*. *Polym. Degrad. Stab.*, 2012. **97**(Copyright (C) 2013 American Chemical Society (ACS). All Rights Reserved.): p. 1881-1890.
31. Sambha'a, E.L., Lallam A, Jada A, *Effect of hydrothermal polylactic acid degradation on polymer molecular weight and surface properties*. *Journal of Polymers and the Environment*, 2010. **18**(4): p. 532-538.
32. Zaidi, L., Kaci M, Bruzaud S, Bourmaud A, Grohens Y, *Effect of natural weather on the structure and properties of polylactide/Cloisite 30B nanocomposites*. *Polymer Degradation and Stability*, 2010. **95**(9): p. 1751-1758.
33. Belbachir, S., Zaïri F, Ayoub G, Maschke U, Naït-Abdelaziz M, Gloaguen J M, Benguediab M, Lefebvre J M, *Modelling of photodegradation effect on elastic-viscoplastic behaviour of amorphous polylactic acid films*. *Journal of the Mechanics and Physics of Solids*, 2010. **58**(2): p. 241-255.
34. Bocchini, S., Fukushima K, Di Blasio A, Fina A, Frache A, Geobaldo F, *Polylactic acid and polylactic acid-based nanocomposite photooxidation*. *Biomacromolecules*, 2010. **11**(11): p. 2919-2926.
35. Gardette, M., Thérias S, Gardette J L, Murariu M, Dubois P, *Photooxidation of polylactide/calcium sulphate composites*. *Polymer Degradation and Stability*, 2011. **96**(4): p. 616-623.
36. Fukushima, K., Tabuani D, Camino G, *Poly(lactic acid)/clay nanocomposites: effect of nature and content of clay on morphology, thermal and thermo-mechanical properties*. *Materials Science and Engineering: C*, 2012. **32**(7): p. 1790-1795.
37. Paul, M.A., Delcourt C, Alexandre M, Degée P, Monteverde F, Dubois P., *Polylactide/montmorillonite nanocomposites: study of the hydrolytic degradation*. *Polymer Degradation and Stability*, 2005. **87**(3): p. 535-542.
38. Zhou, Q., Xanthos M, *Nanoclay and crystallinity effects on the hydrolytic degradation of polylactides*. *Polymer Degradation and Stability*, 2008. **93**(8): p. 1450-1459.

39. Araujo, A., Botelho G L, Silva M, Machado A V, *UV Stability of Poly(Lactic Acid) Nanocomposites*. Journal of Materials Science and Engineering, 2012. **B(3 (2))**: p. 75-83.
40. Vahabi, H., Sonnier R, Ferry L, *Effects of ageing on the fire behaviour of flame-retarded polymers: a review*. Polymer International, 2015. **64(3)**: p. 313-328.
41. Inata, H., Maki I, Ishikawa T, Takeda K, *Diffusion of additives and deterioration with passage of time in polypropylene*. Journal of Applied Polymer Science, 2006. **99**: p. 2152-2162.
42. Colonna, S., Cuttica F, Frache A, *Aging of EVA/organically modified clay: Effect on dispersion, distribution and combustion behavior*. Polymer Degradation and Stability, 2014. **107**: p. 184-187.
43. Oztekin, E., S., Crowley S B, Lyon R E, Stoliarov S I, Patel P, Hull T R, *Sources of variability in fire test data: A case study on poly(aryl ether ether ketone) (PEEK)*. Combustion and Flame, 2012. **159(4)**: p. 1720-1731.
44. Levchik, S.V., Bright D A, Alessio G R, Dashevsky S, *New halogen-free fire retardant for engineering plastic applications*. Journal of Vinyl and Additive Technology, 2001. **7(2)**: p. 98-103.
45. Sinturel, C., Philippart JL, Lemaire J, Gardette JL, *Photooxidation of fire retarded polypropylene. I. Photoageing in accelerated conditions*. European Polymer Journal, 1999. **35(10)**: p. 1773-1781.
46. Sinturel, C., Lemaire J, Gardette JL, *Photooxidation of fire retarded polypropylene: III. Mechanism of HAS inactivation*. European Polymer Journal, 2000. **36(7)**: p. 1431-1443.
47. Diagne, M., Guèye M, Vidal L, Tidjani A, *Thermal stability and fire retardant performance of photo-oxidized nanocomposites of polypropylene-graft-maleic anhydride/clay*. Polymer Degradation and Stability, 2005. **89(3)**: p. 418-426.
48. Diagne, M., Gueye M, Dasilva A, Vidal L, Tidjani A, *The effect of photo-oxidation on thermal and fire retardancy of polypropylene nanocomposites*. Journal of Materials Science, 2006. **41**: p. 7005-7010.
49. Reti, C., Casetta M, Duquesne S, Bourbigot S, Delobel R, *Flammability properties of intumescent PLA including strach and lignin*. Polymers for Advanced Technologies, 2008. **19**: p. 173.
50. Bourbigot, S., Le Bras M, Duquesne S, Rochery M, *Recent advances for intumescent polymers*. Macromolecular Materials and Engineering, 2004. **289(6)**: p. 499-511.
51. Bourbigot, S., Fontaine G, Gallos A, Bellayer S, *Reactive extrusion of PLA and of PLA/carbon nanotubes nanocomposite: processing, characterization and flame retardancy*. Polymers for Advanced Technologies, 2011. **22(1)**: p. 30-37.
52. Lim, L.T., Auras R, Rubino M, *Processing technologies for poly(lactic acid)*. Progress in Polymer Science, 2008. **33(8)**: p. 820-852.
53. Kricheldorf, H., R., Kraiser-Saunders I, Jurgens C, Wolter D, *Poly lactides synthesis, characterization and medical application*. Macromolecular Symposia, 1996. **103(85)**.
54. Hyon, S., H., Jamshidi K, Ikada Y, *Synthesis of poly lactides with different molecular weights*. Biomaterials, 1997. **18(22)**: p. 1503-1508.
55. Kaihara, S., Matsumura S, Mikos A G, Fisher J P, *Synthesis of poly(L-lactide) and polyglycolide by ring-opening polymerization*. Nat. Protocols, 2007. **2(11)**: p. 2767-2771.
56. Dubois, P., Degee P, Jerome R, Teyssie P, *Macromolecular engineering of polylactones and polylactides. 8. Ring-opening polymerization of ϵ -caprolactone initiated by primary amines and trialkylaluminum*. Macromolecules, 1992. **25(10)**: p. 2614-2618.
57. Miyamoto, T., Inagaki H, *The stereocomplex formation in poly(methyl methacrylate) and the stereospecific solymerization of Its monomer*. Polym J, 1970. **1(1)**: p. 46-54.
58. Fukuzawa, T., Uematsu I, Uematsu Y, *Physical properties of mixtures of poly(γ -benzyl-L-glutamate) and poly(γ -benzyl-D-glutamte)*. Polymer Journal, 1974. **6(6)**: p. 537-541.
59. Ikada, Y., Jamshidi K, Tsuji H, Hyon S H, *Stereocomplex formation between enantiomeric poly(lactides)*. Macromolecules, 1987. **20**: p. 904-906.
60. Kakuta, M., Hirata M, Kimura Y, *Stereoblock polylactides as high-performance bio-based polymers*. Polymer Reviews, 2009. **49:2**: p. 107-140.

61. Gallos, A., *Poly lactides stéréocomplexés et ignifugés : Élaboration par extrusion réactive et caractérisations*, 2011, Ph.D. Thesis, Université Lille 1, Sciences et Technologies. p. 221.
62. Nakayama, N., Hayashi T, *Preparation and characterization of poly(l-lactic acid)/TiO₂ nanoparticle nanocomposite films with high transparency and efficient photodegradability*. *Polymer Degradation and Stability*, 2007. **92**(7): p. 1255-1264.
63. Bocchini, S., Frache A, *Comparative Study of Filler Influence on Poly lactide Photooxidation*. *eXPRESS Polymer Letters*, 2013. **7**(5): p. 431-442.
64. Garlotta, D., *A literature review of poly(lactic acid)*. *Journal of Polymers and the Environment*, 2001. **9**(2): p. 63-84.
65. Kister, G., Cassanas G, Vert M, *Effects of morphology, conformation and configuration on the IR and Raman spectra of various poly(lactic acid)s*. *Polymer*, 1998. **39**(2): p. 267-273.
66. Drumright, R., E., Gruber P R, Henton D E, *Poly lactic acid technology*. *Advanced Materials*, 2000. **12**(23): p. 1841-1846.
67. Dorgan, J.R., Janzen J, Clayton M P, Hait S B, Knauss D M, *Melt rheology of variable L-content poly(lactic acid)*. *Journal of Rheology*, 2005. **49**(3): p. 607-619.
68. Jamshidi, K., Hyon S H, Okada Y, *Thermal characterizaton of poly lactides*. *Polymer*, 1988. **29**(2229).
69. Celli, A., Scandola M, *Thermal properties and physical ageing of poly (l-lactic acid)*. *Polymer*, 1992. **33**(13): p. 2699-2703.
70. Cai, H., Dave V, Gross R A, McCarthy S P, *Effects of physical aging, crystallinity, and orientation on the enzymatic degradation of poly(lactic acid)*. *Journal of Polymer Science Part B: Polymer Physics*, 1996. **34**(16): p. 2701-2708.
71. Witzke, D.R., *Introduction to properties, engineering, and prospects of poly lactide polymers*. PhD thesis. East Lansing, MI: Michigan State University, 1997.
72. Hartmann, M.H., *High molecular weight poly lactic acid polymers*, in *Biopolymers from Renewable Resources*, D.L. Kaplan, Editor 1998, Springer Berlin Heidelberg: Berlin, Heidelberg. p. 367-411.
73. Hoogsteen, W., Postema A R, Pennings A J, Ten Brinke G, Zugenmaier P, *Crystal structure, conformation and morphology of solution-spun poly(L-lactide) fibers*. *Macromolecules*, 1990. **23**(2): p. 634-642.
74. Sasaki, S., Asakura T, *Helix distortion and crystal structure of the α -form of poly(l-lactide)*. *Macromolecules*, 2003. **36**(22): p. 8385-8390.
75. Cartier, L., Okihara T, Ikada Y, Tsuji H, Puiggali J, Lot B, *Epitaxial crystallization and crystalline polymorphism of poly lactides*. *Polymer*, 2000. **41**(25): p. 8909-8919.
76. Tsuji, H., Ikada Y, *Properties and morphologies of poly(l-lactide): 1. Annealing condition effects on properties and morphologies of poly(l-lactide)*. *Polymer*, 1995. **36**(14): p. 2709-2716.
77. Sarasua, J.R., Arraiza A L, Balerdi P, Maiza I, *Crystallinity and mechanical properties of optically pure poly lactides and their blends*. *Polymer Engineering & Science*, 2005. **45**(5): p. 745-753.
78. Pyda, M., Bopp R C, Wunderlich B, *Heat capacity of poly(lactic acid)*. *The Journal of Chemical Thermodynamics*, 2004. **36**(9): p. 731-742.
79. Kolstad, J.J., *Crystallization kinetics of poly(L-lactide-co-meso-lactide)*. *Journal of Applied Polymer Science*, 1996. **62**(7): p. 1079-1091.
80. Kishore, K.V.R., *Nucleation parameters for polymer crystallization from non-isothermal thermal analysis*. *Colloid and Polymer Science*, 1988. **266**(11): p. 999-1002.
81. Kishore, K., Vasanthakumari R, Pennings A J, *Crystallization kinetics of poly(l-lactic acid)*. *Polymer*, 1983. **24**(2): p. 175-178.
82. Perego, G., Cella D, Bastioli C, *Effect of molecular weight and crystallinity on poly(lactic acid) mechanical properties*. *Journal of Applied Polymer Science*, 1996. **59**: p. 37-43.
83. Liu, H., Zhang J, *Research progress in toughening modification of poly(lactic acid)*. *Journal of Polymer Science Part B: Polymer Physics*, 2011. **49**(15): p. 1051-1083.

84. Al-Itry, R., Lamnawar K, Maazouz A, *Improvement of thermal stability, rheological and mechanical properties of PLA, PBAT and their blends by reactive extrusion with functionalized epoxy*. *Polymer Degradation and Stability*, 2012. **97**(10): p. 1898-1914.
85. Yang, S.L., Wu Z H, Yang W, Yang M B, *Thermal and mechanical properties of chemical crosslinked polylactide (PLA)*. *Polymer Testing*, 2008. **27**(8): p. 957-963.
86. Montse, C.H., Del Valle S, Hentges E, Bleuët P, Lacroix D, Planell J A, *Mechanical and structural characterisation of completely degradable polylactic acid/calcium phosphate glass scaffolds*. *Biomaterials*, 2007. **28**(30): p. 4429-4438.
87. Laoutid, F., Bonnaud L, Alexandre M, Lopez-Cuesta J M, Dubois Ph, *New prospects in flame retardant polymer materials: From fundamentals to nanocomposites*. *Materials Science and Engineering: R: Reports*, 2009. **63**(3): p. 100-125.
88. Vovelle, C., Delfau J L, *Combustion des plastiques*. *Technique de l'Ingénieur*, 1997.
89. Bourbigot, S., Delobel R, Duquesne S, *Comportement au feu des composites*. *Technique de l'Ingénieur*, 2006.
90. European_Flame_Retardants_Association, *How do flame retardants work ?* 2006.
91. Müller, M., *Systemic approach of the synergism in flame retarded intumescent polyurethanes*, 2012, Ph.D. Thesis, Université Lille 1, Sciences et Technologies. p. 268.
92. Wang, H., Wang Q, Huang Z, Shi W, *Synthesis and thermal degradation behaviors of hyperbranched polyphosphate*. *Polymer Degradation and Stability*, 2007. **92**(10): p. 1788-1794.
93. Price, D., Pyrah K, Hull T R, Milnes G J, Ebdon J R, Hunt B J, Joseph P, *Flame retardance of poly(methyl methacrylate) modified with phosphorus-containing compounds*. *Polymer Degradation and Stability*, 2002. **77**(2): p. 227-233.
94. Lammers, M., Klop E A, Northolt M G, Sikkema D J, *Mechanical properties and structural transitions in the new rigid-rod polymer fibre PIPD ('M5') during the manufacturing process*. *Polymer*, 1998. **39**(24): p. 5999-6005.
95. Cheng, T., W., Chiu J P, *Fire-resistant geopolymers produced by granulated blast furnace slag*. *Minerals Engineering*, 2003. **16**(3): p. 205-210.
96. Wang, G., Yang J, *Influences of expandable graphite modified by polyethylene glycol on fire protection of waterborne intumescent fire resistive coating*. *Surface and Coatings Technology*, 2010. **204**(21–22): p. 3599-3605.
97. Wang, Z., Han E, Ke W, *An investigation into fire protection and water resistance of intumescent nano-coatings*. *Surface and Coatings Technology*, 2006. **201**(3–4): p. 1528-1535.
98. Duquesne, S., Magnet S, Jama C, Delobel R, *Intumescent paints: fire protective coatings for metallic substrates*. *Surface and Coatings Technology*, 2004. **180–181**: p. 302-307.
99. Gardelle, B., Duquesne S, Vandereecken P, Bellayer S, Bourbigot S, *Resistance to fire of curable silicone/expandable graphite based coating: Effect of the catalyst*. *European Polymer Journal*, 2013. **49**(8): p. 2031-2041.
100. Jimenez, M., Duquesne S, Bourbigot S, *Intumescent fire protective coating: Toward a better understanding of their mechanism of action*. *Thermochimica Acta*, 2006. **449**(1–2): p. 16-26.
101. Bourbigot, S., Le Bras M, Leeuwendal R, Shen K K, Schubert D, *Recent advances in the use of zinc borates in flame retardancy of EVA*. *Polymer Degradation and Stability*, 1999. **64**(3): p. 419-425.
102. Bourbigot, S., Duquesne S, *Fire retardant polymers: recent developments and opportunities*. *Journal of Materials Chemistry*, 2007. **17**(22): p. 2283-2300.
103. Morgan, A., B., Wilkie C A, *Fire retardancy of polymeric materials*. CRC Press, Taylor and Francis Group, 2010.
104. Troitzsch, J., *Plastics flammability handbook*. Munich, Carl Hanser Verlag Munich, 2004.
105. Lewin, M., *Unsolved problems and unanswered questions in flame retardance of polymers*. *Polymer Degradation and Stability*, 2005. **88**(1): p. 13-19.
106. Alexandre, M., Dubois P, *Polymer-layered silicate nanocomposites: preparation, properties and uses of a new class of materials*. *Materials Science and Engineering: R: Reports*, 2000. **28**(1–2): p. 1-63.

107. Sinha Ray, S., Okamoto M, *Biodegradable polylactide and its nanocomposites: opening a new dimension for plastics and composites*. Macromolecular Rapid Communications, 2003. **24**(14): p. 815-840.
108. Bourbigot, S., Vanderhart D L, Gilman J W, Bellayer S, Stretz H, Paul D R, *Solid state NMR characterization and flammability of styrene-acrylonitrile copolymer montmorillonite nanocomposite*. Polymer, 2004. **45**(22): p. 7627-7638.
109. Zheng, X., Wilkie C A, *Nanocomposites based on poly (ϵ -caprolactone) (PCL)/clay hybrid: polystyrene, high impact polystyrene, ABS, polypropylene and polyethylene*. Polymer Degradation and Stability, 2003. **82**(3): p. 441-450.
110. Kashiwagi, T., Grulke E, Hilding J, Harris R, Awad W, Douglas J, *Thermal degradation and flammability properties of poly(propylene)/carbon nanotube composites*. Macromolecular Rapid Communications, 2002. **23**(13): p. 761-765.
111. Wang, S., Tambraparni M, Qiu J, Tipton J, Dean D, *Thermal expansion of graphene composites*. Macromolecules, 2009. **42**(14): p. 5251-5255.
112. Steurer, P., Wissert R, Thomann R, Mülhaupt R, *Functionalized graphenes and thermoplastic nanocomposites based upon expanded graphite oxide*. Macromolecular Rapid Communications, 2009. **30**(4-5): p. 316-327.
113. Vandersall, H., J., *Intumescent coating systems, their development and chemistry*. Journal of Fire Flammability, 1971. **2**: p. 97-140.
114. Bourbigot, S., Le Bras M, Delobel R, *Carbonization mechanisms resulting from intumescence association with the ammonium polyphosphate-pentaerythritol fire retardant system*. Carbon, 1993. **31**(8): p. 1219-1230.
115. Bourbigot, S., Le Bras M, Delobel R, Decressain R, Amoureux, J P, *Synergistic effect of zeolite in an intumescence process: study of the carbonaceous structures using solid-state NMR*. Journal of the Chemical Society, Faraday Transactions, 1996. **92**: p. 149-158.
116. Bourbigot, S., Le Bras M, Dabrowski F, Gilman J W, Kashiwagi T, *PA-6 clay nanocomposite hybrid as char forming agent in intumescent formulations*. Fire and Materials, 2000. **24**(4): p. 201-208.
117. White, J.R., *Polymer ageing: physics, chemistry or engineering? Time to reflect*. Comptes Rendus Chimie, 2006. **9**(11-12): p. 1396-1408.
118. Bonten, C., Berlich R, *Aging and chemical resistance*. Hanser Verlag, 2001.
119. Pillai, S., K., Sinha Ray S, Scriba M, Ojijo V, Hato M J, *Morphological and thermal properties of photodegradable biocomposite films*. Journal of Applied Polymer Science, 2013. **129**(1): p. 362-370.
120. Zuo, X., Shao H, Zhang D, Hao Z, Guo J, *Effects of thermal-oxidative aging on the flammability and thermal-oxidative degradation kinetics of tris(tribromophenyl) cyanurate flame retardant PA6/LGF composites*. Polymer Degradation and Stability, 2013. **98**(12): p. 2774-2783.
121. Gil-Castell, O., Badia J D, Kittikorn T, Strömberg E, Martínez-Felipe A, Ek M, Karlsson S, Ribes-Greus A, *Hydrothermal ageing of polylactide/sisal biocomposites. Studies of water absorption behaviour and physico-chemical performance*. Polymer Degradation and Stability, 2014. **108**: p. 212-222.
122. Perry, M., C., Vail M A, Devries K L, *Effect of NO_x environments and stress on degradation of mechanical properties of Kevlar 49 and nylon 6*. Polymer Engineering & Science, 1995. **35**(5): p. 411-418.
123. Deroiné, M., Le Duigou A, Corre Y M, Le Gac P Y, Davies P, César G, Bruzaud S, *Accelerated ageing of polylactide in aqueous environments: Comparative study between distilled water and seawater*. Polymer Degradation and Stability, 2014. **108**: p. 319-329.
124. Beyler, C.L., Hirschler M M, *Thermal decomposition of polymers*. SFPE Handbook of Fire Protection Engineering 2, Section 1, Chapter 7, 2002: p. 111-131.
125. Singh, B., Sharma N, *Mechanistic implications of plastic degradation*. Polym Degrad Stab, 2008. **93**: p. 561 - 584.

126. Azapagic, A., Emsley A, Hamerton I, *Polymers: The environment and sustainable development*. 2003.
127. Rasselet, D., Ruellan A, Guinault A, Miquelard-Garnier G, Sollogoub C, Fayolle B, *Oxidative degradation of polylactide (PLA) and its effects on physical and mechanical properties*. European Polymer Journal, 2014. **50**(0): p. 109-116.
128. Le Duigou, A., Davies P, Baley C, *Seawater ageing of flax/poly(lactic acid) biocomposites*. Polymer Degradation and Stability, 2009. **94**(7): p. 1151-1162.
129. Yousif, E., Haddad R, *Photodegradation and photostabilization of polymers, especially polystyrene: review*. SpringerPlus, 2013. **2**(1): p. 398.
130. Martin, J.W., Chin J W, Nguyen T, *Reciprocity law experiments in polymeric photodegradation: a critical review*. Progress in Organic Coatings, 2003. **47**(3-4): p. 292-311.
131. Hamid, S.H., Prichard W H, *Mathematical modeling of weather-induced degradation of polymer properties*. Journal of Applied Polymer Science, 1991. **43**(4): p. 651-678.
132. Andrady, A.L., Pegram J E, Tropsha Y, *changes in carbonyl index and average molecular weight on embrittlement of enhanced photo-degradable polyethylene*. J Environ Degrad Polym, 1993. **1**: p. 171-179.
133. Rånby, B., *Photodegradation and photo-oxidation of synthetic polymers*. Journal of Analytical and Applied Pyrolysis, 1989. **15**(0): p. 237-247.
134. Jensen, J.P.T., Kops J., *Photochemical degradation of blends of polystyrene and poly(2,6 - dimethyl-1,4-phenylene oxide)*. Journal of Polymer Science: Polymer Chemistry Edition, 1980. **18**(8): p. 2737-2746.
135. Sheldrick, G.E., Vogl O, *Induced photodegradation of styrene polymers: A survey*. Polymer Engineering & Science, 1976. **16**(2): p. 65-73.
136. Weiss, P., *The effects of hostile environments on coatings and plastics*. Journal of Polymer Science: Polymer Letters Edition, 1984. **22**(5): p. 296-296.
137. Ito, M., Nagai K, *Degradation issues of polymer materials used in railway field*. Polymer Degradation and Stability, 2008. **93**(10): p. 1723-1735.
138. Feldman, D., *Polymer weathering: photo-oxidation*. Journal of Polymers and the Environment, 2002. **10**(4): p. 163-173.
139. Davidson, R., S., Goodwin D, Fournier de Violet P, *The mechanism of the norrish type II reaction of α -keto-acids and esters*. Tetrahedron Letters, 1981. **22**(26): p. 2485-2486.
140. Wang, Z., *Norrish type I reaction*, in *Comprehensive Organic Name Reactions and Reagents 2010*, John Wiley & Sons, Inc.
141. Rabek, J., F, *Mechanism of photophysical process and photochemical reaction in polymers*. John Wiley and Sons, New York, 1987.
142. Zhou, Q., Xanthos M, *Nanosize and microsize clay effects on the kinetics of the thermal degradation of polylactides*. Polymer Degradation and Stability, 2009. **94**(3): p. 327-338.
143. Taylor, D., R, *Mechanistic aspects of the effects of stress on the rates of photochemical degradation reactions in polymers*. Journal of Macromolecular Science, Part C: Polymer Reviews, 2004. **44**(4): p. 351 - 388.
144. Pizzi, A., Mittal K L, *Handbook of adhesive technology, revised and expanded*. CRC Press, 2003: p. 1036.
145. Murata, K., Hirano Y, Sakata Y, Azhar-Uddin MD, *Basic study on a continuous flow reactor for thermal degradation of polymers*. Journal of Analytical and Applied Pyrolysis, 2002. **65**(1): p. 71-90.
146. Soto-Oviedo, M.A., Lehrle R S, Parsons I W, De Paoli M A, *Thermal degradation mechanism and rate constants of the thermal degradation of poly(epichlorohydrin-co-ethylene oxide), deduced from pyrolysis-GC-MS studies*. Polymer Degradation and Stability, 2003. **81**(3): p. 463-472.
147. Engineer, C., Parikh J, Raval A, *Review on hydrolytic degradation behavior of biodegradable polymers from controlled drug delivery system*. Trends Biomaterials and Artificial Organs, 2011. **25**(2): p. 79-85.

148. Hofmann, D., Entrialgo-Castaño, M., Kratz, K., Lendlein, A., *Knowledge-based approach towards hydrolytic degradation of polymer-based biomaterials*. *Advanced Materials*, 2009. **21**(32-33): p. 3237-3245.
149. Göpferich, A., Tessmar J, *Polyanhydride degradation and erosion*. *Advanced Drug Delivery Reviews*, 2002. **54**(7): p. 911-931.
150. Viera, A., C., Viera J C, Ferra J M, Magalhaes F D, Guedes R M, Marques A T, *Mechanical study of PLA–PCL fibers during in vitro degradation*. *Journal of the Mechanical Behavior of Biomedical Materials*, 2011. **4**(3): p. 451-460.
151. Siparsky, G., L., Voorhees K J, Miao F, *Hydrolysis of polylactic acid (PLA) and polycaprolactone (PCL) in aqueous acetonitrile solutions: autocatalysis*. *Journal of environmental polymer degradation*, 1998. **6**(1): p. 31-41.
152. Göpferich, A., *Mechanisms of polymer degradation and erosion*. *Biomaterials*, 1996. **17**(2): p. 103-114.
153. Li, S., Vert M., *Biodegradation of aliphatic polyesters*, in *Degradable Polymers 2002*, Springer Netherlands. p. 71-131.
154. Lucas, N., Bienaime C, Belloy C, Queneudec M, Silvestre F, Nava-Saucedo J E, *Polymer biodegradation: Mechanisms and estimation techniques – A review*. *Chemosphere*, 2008. **73**(4): p. 429-442.
155. Katarzyna, L., Lewandowicz G, *Polymer biodegradation and biodegradable polymers – a review* *Polish Journal of Environmental Studies*, 2010. **19**(2): p. 255 - 266.
156. Palmisano, A., C., Pettigrew C A, *Biodegradability of plastics*. *BioScience*, 1992. **42**(9): p. 680 - 685.
157. Ho, K., L, G., Pometto A L, *Effects of electron-beam irradiation and ultraviolet light (365 nm) on polylactic acid plastic films*. *Journal of environmental polymer degradation*, 1999. **7**(2): p. 93-100.
158. Sato, S., Ono M, Yamauchi J, Kanehashi S, Ito H, Matsumoto S, Iwai Y, Matsumoto H, Nagai K, *Effects of irradiation with vacuum ultraviolet xenon excimer lamp at 172 nm on water vapor transport through poly(lactic acid) membranes*. *Desalination*, 2012. **287**: p. 290-300.
159. Tsuji, H., Echizen Y, Nishimura Y, Saha S K, *Photodegradation of poly(L-lactic acid): Effects of photosensitizer*. *Macromolecular Materials and Engineering*, 2005. **290**(12): p. 1192-1203.
160. Gorrasi, G., Pantani R, *Effect of PLA grades and morphologies on hydrolytic degradation at composting temperature: Assessment of structural modification and kinetic parameters*. *Polymer Degradation and Stability*, 2013. **98**(5): p. 1006-1014.
161. Pan, P., Inoue, Y, *Polymorphism and isomorphism in biodegradable polyesters*. *Progress in Polymer Science*, 2009. **34**(7): p. 605-640.
162. Stloukal, P., Kalendova A, Mattausch H, Laske S, Holzer C, Koutny M, *The influence of a hydrolysis-inhibiting additive on the degradation and biodegradation of PLA and its nanocomposites*. *Polymer Testing*, 2015. **41**: p. 124-132.
163. Rasmussen, K., Grampp G, Van Eesbeek M, Rohr T, *Thermal and UV degradation of polymer films studied in situ with ESR spectroscopy*. *ACS Appl. Mater. Interfaces*, 2010. **2**(Copyright (C) 2013 American Chemical Society (ACS). All Rights Reserved.): p. 1879-1883.
164. Badía, J., D., Strömberg E, Ribes-Greus A, Karlsson S, *Assessing the MALDI-TOF MS sample preparation procedure to analyze the influence of thermo-oxidative ageing and thermo-mechanical degradation on poly (Lactide)*. *European Polymer Journal*, 2011. **47**(7): p. 1416-1428.
165. Kopinke, F.D., Remmler, M., Mackenzie, K., *Thermal decomposition of biodegradable polyesters—II. Poly(lactic acid)*. *Polymer Degradation and Stability*, 1996. **53**(3): p. 329-342.
166. McNeill, I., C., Leiper H A, *Degradation studies of some polyesters and polycarbonates—2. Polylactide: Degradation under isothermal conditions, thermal degradation mechanism and photolysis of the polymer*. *Polymer Degradation and Stability*, 1985. **11**(4): p. 309-326.
167. Speranza, V., De Meo A, Pantani R, *Thermal and hydrolytic degradation kinetics of PLA in the molten state*. *Polymer Degradation and Stability*, (0).

168. Kashiwagi, T., Shields JR, Harris RH, Davis RD, *Flame-retardant mechanism of silica: Effects of resin molecular weight*. Journal of Applied Polymer Science, 2003. **87**(9): p. 1541-1553.
169. Kashiwagi, T., Mu M, Winey K, Cipriano B, Raghavan S, Pack S, rafailovich M, Yang Y, Grulke E, Shields J, Harris R, Douglas R, *Relation between the viscoelastic and flammability properties of polymer nanocomposites*. Polymer, 2008. **49**: p. 4358-4368.
170. Carpentier, F., Bourbigot S, Le Bras M, Delobel R, *Rheological investigations in fire retardancy: application to ethylene–vinyl-acetate copolymer–magnesium hydroxide/zinc borate formulations*. Polymer International, 2000. **49**(10): p. 1216-1221.
171. Batistella, M., Otazaghine B, Sonnier R, Caro-Bretelle AS, Petter C, Lopez-Cuesta JM, *Fire retardancy of ethylene vinyl acetate/ultrafine kaolinite composites*. Polymer Degradation and Stability, 2014. **100**: p. 54-62.
172. Chantegraille, D., Morlat-Therias S, Gardette, JL, *Photochemical behaviour of fire-retarded polymers*. Polymer Degradation and Stability, 2010. **95**(3): p. 274-277.
173. Lonkar, S., P., Therias S, Capera N, Leroux F, Gardette JL, *Photo-oxidation of polypropylene/layered double hydroxide nanocomposites: Influence of intralamellar cations*. European Polymer Journal, 2010. **46**: p. 1456-1464.
174. Tidjani, A., Wilkie C A, *Photo-oxidation of polymeric-inorganic nanocomposites: chemical, thermal stability and fire retardancy investigations*. Polymer Degradation and Stability, 2001. **74**(1): p. 33-37.
175. Chen, D., Li J, Rena J, *Combustion properties and transference behavior of ultrafine microencapsulated ammonium polyphosphate in ramie fabric-reinforced poly(L-lactic acid) biocomposites*. Polymer International, 2011. **60**: p. 599-606.
176. Almeras, X., Le Bras M, Hornsby P, Bourbigot S, Marosi G, Anna P, Delobel R, *Artificial weathering and recycling effect on intumescent polypropylene based blends*. Journal of Fire Sciences, 2004. **22**(2): p. 143-161.
177. Larché, J., F., Gallot G, Boudiaf-Lomri L, Poulard C, Duemmler I, Meyer M, *Evidence of surface accumulation of fillers during the photo-oxidation of flame retardant ATH filled EVA used for cable applications*. Polymer Degradation and Stability, 2014. **103**: p. 63-68.
178. El Hage, R., Viretto A, Sonnier R, Ferry L, Lopez-Cuesta JM, *Flame retardancy of ethylene vinyl acetate (EVA) using new aluminum-based fillers*. Polymer Degradation and Stability, 2014. **108**: p. 56-67.
179. Wang, L., L., Wang Y C, Li G Q, *Experimental study of hydrothermal aging effects on insulative properties of intumescent coating for steel elements*. Fire Safety Journal, 2013. **55**(0): p. 168-181.
180. ISO-4589-2:1996, *Plastics -- Determination of burning behaviour by oxygen index -- Part 2: Ambient-temperature test*, 1996.
181. ISO-13927:2001, *Plastics -- Simple heat release test using a conical radiant heater and thermopile detector*, 2001.
182. ISO-4892-3:2013, *Methods of exposure to laboratory light sources -- Part 3: Fluorescent UV lamps*, 2013.
183. Ghoreishian, S., Badii K, Norouzi M, Malek K, *Effect of cold plasma pre-treatment on photocatalytic activity of 3D fabric loaded with nano-photocatalysts: Response surface methodology*. Applied Surface Science, 2016. **365**: p. 252-262.
184. Colleoni, C., Massafra M R, Migani V, Rosace G, *Dendrimer finishing influence on CO/PES blended fabrics color assessment*. Journal of Applied Polymer Science, 2011. **120**(4): p. 2122-2129.
185. Kowalski, A., Duda A, Penczek S, *Polymerization of L,L-Lactide initiated by aluminum isopropoxide trimer or tetramer*. Macromolecules, 1998. **31**(7): p. 2114-2122.
186. Foulc, M., P., Bergeret A, Ferry L, lenny P, Crespy A, *Study of hygrothermal ageing of glass fibre reinforced PET composites*. Polymer Degradation and Stability, 2005. **89**(3): p. 461-470.
187. ISO-1133:2005, *Plastics -- Determination of the melt mass-flow rate (MFR) and the melt volume-flow rate (MVR) of thermoplastics*, 2005.

References

188. Feller, R.L., *Accelerated ageing: Photochemical and thermal aspects* 1994: Marina del Rey, CA : Getty Conservation Institute, 1994.
189. Keles, H., Naylor A, Clegg F, Sammon C, *Investigation of factors influencing the hydrolytic degradation of single PLGA microparticles*. *Polymer Degradation and Stability*, 2015. **119**: p. 228-241.
190. Manring, E., L., Blume R C, Simonsick J, Adelman D J, *Thermal degradation of Poly(2,2-dialkyl-3-hydroxypropionic acid). 2. Thermal degradation initiated by random scission* *Macromolecules*, 1992. **25**: p. 4863-4870.
191. Grassie, N., McNeill I C, *Thermal degradation of polymethacrylonitrile. Part V. The mechanism of the initiation step in coloration reactions*. *Journal of polymer science*, 1959. **39**(135): p. 211-222.
192. de Oliveira, H., P., Rieumont J, Nogueiras C, Souza D, Sanchez R, *Thermal degradation behavior of a carboxylic acid-terminated amphiphilic block copolymer poly(ethylene)-b-poly(ethylene oxide)*. *Journal of Thermal Analysis and Calorimetry*, 2011. **103**(2): p. 443-451.
193. Dobkowski, Z., *Determination of critical molecular weight for entangled macromolecules using the tensile strength data*. *Rheologica Acta*, 1995. **34**(6): p. 578-585.
194. Cho, K., S., Ahn K H, Lee S J, *Simple method for determining the critical molecular weight from the loss modulus*. *Journal of Polymer Science Part B: Polymer Physics*, 2004. **42**(14): p. 2724-2729.
195. Lyu, S., Untereker D, *Degradability of polymers for implantable biomedical devices*. *International Journal of Molecular Sciences*, 2009. **10**(9): p. 4033-4065.
196. Dorgan, J., R., *Rheology of Poly(Lactic Acid)*, in *Poly(Lactic Acid)* 2010, John Wiley & Sons, Inc. p. 125-139.
197. Inkinen, S., Hakkarainen M, Albertsson AC, Södergård A, *From lactic acid to poly(lactic acid) (PLA): Characterization and analysis of PLA and its precursors*. *Biomacromolecules*, 2011. **12**(3): p. 523-532.
198. Stloukal, P., Pekařová S, Kalendova A, Mattausch H, Laske S, Holzer C, Chitu L, Bodner S, Maier G, Slouf M, Koutny M, *Kinetics and mechanism of the biodegradation of PLA/clay nanocomposites during thermophilic phase of composting process*. *Waste Management*, 2015. **42**: p. 31-40.
199. Rathi, S., Coughlin E, Hsu S, Golub C, Ling G, Tzivanis M, *Maintaining structural stability of poly(lactic acid): effects of multifunctional epoxy based reactive oligomers*. *Polymers*, 2014. **6**(4): p. 1232.
200. Liu, X., Zou Y, Li W, Cao G, Chen W, *Kinetics of thermo-oxidative and thermal degradation of poly(D,L-lactide) (PDLLA) at processing temperature*. *Polymer Degradation and Stability*, 2006. **91**(12): p. 3259-3265.
201. Meaurio, E., López-Rodríguez N, Sarasua J R, *Infrared Spectrum of Poly(l-lactide): Application to Crystallinity Studies*. *Macromolecules*, 2006. **39**(26): p. 9291-9301.
202. Zhang, J., Duan Y, Sato H, Tsuji H, Noda I, Yan S, Ozaki Y, *Crystal modifications and thermal behavior of poly(l-lactic acid) revealed by infrared spectroscopy*. *Macromolecules*, 2005. **38**(19): p. 8012-8021.
203. Zhang, J., Tashiro K, Tsuji H, Domb A J, *Disorder-to-order phase transition and multiple melting behavior of poly(l-lactide) investigated by simultaneous measurements of WAXD and DSC*. *Macromolecules*, 2008. **41**(4): p. 1352-1357.
204. Fayolle, B., Richaud E, Colin X, Verdu J, *Review: degradation-induced embrittlement in semi-crystalline polymers having their amorphous phase in rubbery state*. *Journal of Materials Science*, 2008. **43**(22): p. 6999-7012.
205. Torres, A., Li S M, Roussos S, Vert M, *Degradation of L- and DL-lactic acid oligomers in the presence of Fusarium moniliforme and Pseudomonas putida*. *Journal of environmental polymer degradation*, 1996. **4**(4): p. 213-223.
206. McCain, D., C., Hayden D W, *Theory of electron spin g-values for carbonyl radicals*. *Journal of Magnetic Resonance (1969)*, 1973. **12**(3): p. 312-330.

207. Babanalbandi, A., Hill D J T, O'Donnell J H, Pomery P J and A. Whittaker, *An electron spin resonance study on γ -irradiated poly(l-lactic acid) and poly(d,l-lactic acid)*. *Polymer Degradation and Stability*, 1995. **50**(3): p. 297-304.
208. Laurent, B., Roskosz M, Remusat L, Leroux H, Vezin H, Depecker C, *Isotopic and structural signature of experimentally irradiated organic matter*. *Geochimica et Cosmochimica Acta*, 2014. **142**: p. 522-534.
209. Laurent, B., Roskosz M, Remusat L, Robert F, Leroux H, Vezin H, Depecker C, Nuns N, Lefebvre JM, *The deuterium/hydrogen distribution in chondritic organic matter attests to early ionizing irradiation*. *Nat Commun*, 2015. **6**.
210. Codari, F., Lazzari S, Soos M, Storti G, Morbidelli M, Moscatelli D, *Kinetics of the hydrolytic degradation of poly(lactic acid)*. *Polymer Degradation and Stability*, 2012. **97**(11): p. 2460-2466.
211. Gupta, M., C., Deshmukh V G, *Thermal oxidative degradation of poly-lactic acid*. *Colloid and Polymer Science*, 1982. **260**(3): p. 308-311.
212. Bussiere, P.O., *Etude des mécanismes de phototransformation des polymères au cours du vieillissement photochimique oxydatif: de l'échelle moléculaire à l'échelle macroscopique*, in *Institut de Chimie de Clérmont-Ferrand 2012*, Ecole nationale Supérieure de Chimie de Clermont-Ferrand. p. 164.
213. Cevdet, K., Burcu S, *Accelerated weathering performance of polylactide and its montmorillonite nanocomposite*. *Applied Clay Science*, 2016. **121–122**: p. 86-94.
214. Liu, X., Wang T, Chow LC, Yang M, Mitchell JW, *Effects of inorganic fillers on the thermal and mechanical properties of poly(lactic acid)*. *International Journal of Polymer Science*, 2014. **2014**: p. 8.
215. Capone, C., Di-Landro L, Inzoli F, Penco M, Sartore L, *Thermal and mechanical degradation during polymer extrusion processing*. *Polymer Engineering & Science*, 2007. **47**(11): p. 1813-1819.
216. El'darov, E., G., Mamedov F V, Gol'dberg V M, Zaikov G E, *A kinetic model of polymer degradation during extrusion*. *Polymer Degradation and Stability*, 1996. **51**(3): p. 271-279.
217. Pielichowski, K., Njuguna J, *Thermal degradation of polymeric materials 2005*: Rapra Technology Limited.
218. Vera-Sorroche, J., Kelly A L, Brown E C, Gough T, Abeykoon C, Coates P D, Deng J, Li K, Harkin-Jones E, Price M, *The effect of melt viscosity on thermal efficiency for single screw extrusion of HDPE*. *Chemical Engineering Research and Design*, 2014. **92**(11): p. 2404-2412.
219. González-González, V., A., Neira-Velázquez G, Angulo-Sánchez J L, *Polypropylene chain scissions and molecular weight changes in multiple extrusion*. *Polymer Degradation and Stability*, 1998. **60**(1): p. 33-42.
220. Goetze, K., P., Porter R S, *Extrusion degradation of a high molecular weight polystyrene*. *Journal of Polymer Science Part C: Polymer Symposia*, 1971. **35**(1): p. 189-200.
221. Hong, Y., Gao C, Xie Y, Gong Y, Shen J, *Collagen-coated polylactide microspheres as chondrocyte microcarriers*. *Biomaterials*, 2005. **26**: p. 6305-6313.
222. Rangelov, M., A., Petrova G P, Yomtova V M, Vayssilov G N, *Catalytic role of vicinal OH in ester aminolysis: proton shuttle versus hydrogen bond stabilization*. *The Journal of Organic Chemistry*, 2010. **75**(20): p. 6782-6792.
223. Vakhitova, L.N., Taran N A, Lapushkin M P, Drizhd V L, Lakhtarenko N V, Popov A F, *Solid-phase aminolysis in the ammonium polyphosphate– pentaerythritol–amine system*. *Theoretical and Experimental Chemistry*, 2012. **48**(3): p. 176-181.
224. Leszczyńska, A., Njugunab J, Pielichowska K, Banerjee JR, *Polymer/montmorillonite nanocomposites with improved thermal properties. Part II: Thermal stability of montmorillonite nanocomposites based on different polymeric matrixes*. *Thermochimica Acta*, 2007. **454**(1): p. 1-22.
225. Zheng, X., Gilbert, M., *An investigation into the thermal stability of PVC/montmorillonite composites*. *Journal of Vinyl and Additive Technology*, 2011. **17**(2): p. 77-84.

226. Isfahani, A.P., Mehrabzadeh M, Morshedian J, *The effects of processing and using different types of clay on the mechanical, thermal and rheological properties of high-impact polystyrene nanocomposites*. Polymer Journal, 2013. **45**(3): p. 346-353.
227. Romanzini, D., Piroli V, Frache A, Zattera A J, Amico S C, *Sodium montmorillonite modified with methacryloxy and vinylsilanes: Influence of silylation on the morphology of clay/unsaturated polyester nanocomposites*. Applied Clay Science, 2015. **114**: p. 550-557.
228. Lewitus, D., McCarthy S, Ophir A, Kenig S, *The effect of nanoclays on the properties of PLLA-modified polymers part 1: mechanical and thermal properties*. Journal of Polymers and the Environment, 2006. **14**(2): p. 171-177.
229. Chieng, B., Ibrahim N, Yunus W, Hussein M, *Poly(lactic acid)/Poly(ethylene glycol) polymer nanocomposites: Effects of graphene nanoplatelets*. Polymers, 2014. **6**(1): p. 93.
230. Shi, X., Zhang G, Vu-Phuong T, Lazzeri A, *Synergistic effects of nucleating agents and plasticizers on the crystallization behavior of poly(lactic acid)*. Molecules, 2015. **20**: p. 1579-1593.
231. Oudet, C., *Polymères: structure et propriétés, introduction*1994: Masson.
232. Blanchard, L., P., Hesse J, Lal-Malhotra S, *Effect of Molecular Weight on Glass Transition by Differential Scanning Calorimetry*. Canadian Journal of Chemistry, 1974. **52**(18): p. 3170-3175.
233. Tadlaoui, K., Pietrasanta Y, Michel A, Verney V, *Influence of molecular weight on the glass transition temperature and the melt rheological behaviour of methyl methacrylate telomers*. Polymer, 1991. **32**(12): p. 2234-2237.
234. Omelczuk, M., O., McGinity J W, *The influence of polymer glass transition temperature and molecular weight on drug release from tablets containing poly(DL-lactic acid)*. Pharmaceutical Research, 1992. **9**(1): p. 26-32.
235. Narladkar, A., Balnois E, Vignaud G, Grohens Y, Bardeau J F, *Morphology and glass transition of thin polylactic acid films*. Polymer Engineering & Science, 2008. **48**(9): p. 1655-1660.
236. Montserrat, S., Colomer P, *The effect of the molecular weight on the glass transition temperature in amorphous poly(ethylene terephthalate)*. Polymer Bulletin, 1984. **12**(2): p. 173-180.
237. Fukushima, K., Abbate C, Tabuani D, Gennari M, Camino G, *Biodegradation of poly(lactic acid) and its nanocomposites*. Polymer Degradation and Stability, 2009. **94**(10): p. 1646-1655.
238. Sinha Ray, S., Yamada K, Okamoto M, Ueda K, *New polylactide-layered silicate nanocomposites. 2. Concurrent improvements of material properties, biodegradability and melt rheology*. Polymer, 2003. **44**(3): p. 857-66.
239. Marosi, G., Anna P, Balogh I, Bertalan G, Tohl A, Maatoug M A, *Thermoanalytical study of nucleating effects in polypropylene composites*. Journal of thermal analysis, 1997. **48**(4): p. 717-726.
240. Krikorian, V., Pochan D J, *Unusual crystallization behavior of organoclay reinforced poly(L-lactic acid) nanocomposites*. Macromolecules, 2004. **37**: p. 6480-6491.
241. Qian, J., Zhu L, Zhang J, Whitehouse R S, *Comparison of different nucleating agents on crystallization of poly(3-hydroxybutyrate-co-3-hydroxyvalerates)*. Journal of Polymer Science Part B: Polymer Physics, 2007. **45**(13): p. 1564-1577.
242. Ujhelyiova, A., Slobodova M, Ryba J, Borsig E, Vencelova P, *The effect of inorganic nanoadditives on the thermal, mechanical and UV radiation barrier properties of polypropylene fibres*. Open Journal of Organic Polymer Materials, 2012. **2**: p. 9.
243. Gopalan, M., R., Mandelkern L, *Effect of crystallization temperature and molecular weight on the melting temperature of linear polyethylene*. The Journal of Physical Chemistry, 1967. **71**(12): p. 3833-3841.
244. Stack, G., M., Mandelkern L, Voigt-Martin I G, *Crystallization, melting, and morphology of low molecular weight polyethylene fractions*. Macromolecules, 1984. **17**(3): p. 321-331.
245. Tin-Sin, L., Rahmat A R, Rahman W A W A, *Polylactic acid: PLA biopolymer technology and applications*. PDL handbook series2012: Elsevier. 352.
246. Yu, D., L., He J L, Liu Z Y, Xu B, Li D C, Tian Y J, *Phase transformation of melamine at high pressure and temperature*. Journal of Materials Science, 2008. **43**(2): p. 689-695.

References

247. Liao, Y., Zhu S, Ma J, Sun Z, Yin C, Zhu C, Lou X, Zhang D, *Tailoring the morphology of g-C₃N₄ by self-assembly towards high photocatalytic performance*. ChemCatChem, 2014. **6**(12): p. 3419-3425.
248. Levchik, G., F., Levchik S V, Sachok P D, Selevich A F, Lyakhov A S, Lesnikovich A I, *Thermal behaviour of ammonium polyphosphate-inorganic compound mixtures. Part 2. Manganese dioxide*. Thermochimica Acta, 1995. **257**: p. 117-125.
249. Uma, T., Tu H Y, Warth S, *Synthesis and characterization of proton conducting poly phosphate composites*. Journal of Materials Science and Engineering, 2005. **40**: p. 2059-2063.
250. Sherief, M., A., Hanna, A A, Abdelmoaty A S, *Synthesis and characterization of nanosized ammonium polyphosphate*. Canadian Journal of Applied Sciences, 2014. **3**(4): p. 94-99.
251. Sahoo, D., Nayak P L, *Synthesis and characterization of chitosan/cloisite 30B film for controlled release of ofloxacin*. Journal of Applied Polymer Science, 2012. **123**(5): p. 2588-2594.
252. Wang, Y., L., Mebel A M, Chung-Jen W, Chen Y T, Ching-Erh I, Jyh-Chiang j, *IR spectroscopy and theoretical vibrational calculation of the melamine molecule*. Journal of the Chemical Society, Faraday Transactions, 1997. **93**(19): p. 3445-3451.
253. Mircescu, N., E., Oltean M, Chiş V, Leopold N, *FTIR, FT-Raman, SERS and DFT study on melamine*. Vibrational Spectroscopy, 2012. **62**: p. 165-171.
254. Kokotou, M., Thomaidis N, *Behavior and retention models of melamine and its hydrolysis products*. Chromatographia, 2012. **75**(9): p. 457-467.
255. Bernhard, A., Peitz D, Elsener M, Wokaun A, Kröcher O, *Hydrolysis and thermolysis of urea and its decomposition byproducts biuret, cyanuric acid and melamine over anatase TiO₂*. Applied Catalysis B: Environmental, 2012. **115–116**: p. 129-137.
256. Gong, H., Tang S, Zhang T, *Catalytic hydrolysis of waste residue from the melamine process and the kinetics of melamine hydrolysis in NaOH solution*. Reaction Kinetics, Mechanisms and Catalysis, 2016. **118**(2): p. 377-391.
257. Venugopalan, M., V., Prasad R, *Hydrolysis of ammonium polyphosphate in soils under aerobic and anaerobic conditions*. Biology and Fertility of Soils, 1989. **8**(4): p. 325-327.
258. Jimenez, M., Bellayer S, Revel B, Duquesne S, Bourbigot S, *Comprehensive study of the influence of different aging scenarios on the fire protective behavior of an epoxy based intumescent coating*. Ind. Eng. Chem. Res., 2013. **52**: p. 729-743.
259. Arai, Y., Sparks D L, *ATR-FTIR spectroscopic investigation on phosphate adsorption mechanisms at the ferrihydrite-water interface*. Journal of Colloid and Interface Science, 2001. **241**(2): p. 317-326.
260. Rudolph, W., W.,, *Raman- and infrared-spectroscopic investigations of dilute aqueous phosphoric acid solutions*. Dalton Transactions, 2010. **39**(40): p. 9642-9653.
261. Lizheng, S., Kefu C, *Preparation and characterization of ammonium polyphosphate/diatomite composite fillers and assessment of their flame retardant effects on paper*. BioResources, 2014. **9**(2): p. 3104-3116.
262. Shao, Z., Deng C, Tan Y, Yu L, Chen M J, Chen L, Wang Y Z, *Ammonium polyphosphate chemically-modified with ethanolamine as an efficient intumescent flame retardant for polypropylene*. Journal of Materials Chemistry A, 2014. **2**(34): p. 13955-13965.
263. Gérard, C., Fontaine G, Bellayer S, Bourbigot S, *Reaction to fire of an intumescent epoxy resin: Protection mechanisms and synergy*. Polymer Degradation and Stability, 2012. **97**(8): p. 1366-1386.
264. Hadj-Hamou, A., S., Matassi S, Abderrahmane H, Yahiaoui F, *Effect of cloisite 30B on the thermal and tensile behavior of poly(butylene adipate-co-terephthalate)/poly(vinyl chloride) nanoblends*. Polymer Bulletin, 2014. **71**(6): p. 1483-1503.
265. Debasish, S., Nayak P L, *Synthesis and characterization of chitosan/cloisite 30B film for controlled release of ofloxacin*. Journal of Applied Polymer Science, 2012. **123**(5): p. 2588-2594.
266. Martos, J., Osinaga P W R, De-Olivera E, Suita-de-Castro L A, *Hydrolytic degradation of composite resins: Effects on the microhardness*. Materials Research, 2003. **6**(4): p. 599-604.

267. Braun, U., Wachtendorf V, Geburtig A, Bahr H, Schartel B, *Weathering resistance of halogen-free flame retardance in thermoplastics*. *Polymer Degradation and Stability*, 2010. **95**(12): p. 2421-2429.
268. Jahromi, S., Moosheimer U, *Oxygen barrier coatings based on supramolecular assembly of melamine*. *Macromolecules*, 2000. **33**(20): p. 7582-7587.
269. Purser, D., *Fire retardant materials. 3 - Toxicity of fire retardants in relation to life safety and environmental hazards*, in *Fire Retardant Materials 2001*, Woodhead Publishing. p. 69-127.
270. Lahtela, V., Kärki T, *Improving the UV and water-resistance properties of Scots pine (Pinus sylvestris) with impregnation modifiers*. *European Journal of Wood and Wood Products*, 2014. **72**(4): p. 445-452.
271. Gérard, C., *Contribution of nanoparticles to the flame retardancy of epoxy resins*, 2011, Université des sciences et technologies de Lille.
272. Sanches, N., B., Dias M L, Pacheco E B A V, *Comparative techniques for molecular weight evaluation of poly (ethylene terephthalate) (PET)*. *Polymer Testing*, 2005. **24**(6): p. 688-693.
273. Schartel, B., Bartholmai M, Knoll U, *Some comments on the main fire retardancy mechanisms in polymer nanocomposites*. *Polymers for Advanced Technologies*, 2006. **17**(9-10): p. 772-777.
274. Matzen, M., Kandola B, Huth C, Schartel B, *Influence of flame retardants on the melt dripping behaviour of thermoplastic polymers*. *Materials*, 2015. **8**: p. 5621-5646.
275. Dealy, J., M., Wissbrun K F, *Role of rheology in extrusion*, in *Melt Rheology and Its Role in Plastics Processing: Theory and Applications 1999*, Springer Netherlands: Dordrecht. p. 441-490.
276. Mishra, A., K., Mushtaq S, Nando G B, Chattopadhyay S, *Effect of Cloisite and modified Laponite clays on the rheological behavior of TPU–clay nanocomposites*. *Rheologica Acta*, 2010. **49**(8): p. 865-878.
277. Bashir, M., A., *Effect of nanoclay dispersion on the processing of polyester nanocomposites*, in *Department of Mechanical Engineering 2008*, McGill University, Montreal, QC, Canada. p. 118.
278. Huang, X., Lewis S, Brittain W J, Vaia R A., *Synthesis of polycarbonate-layered silicate nanocomposites via cyclic oligomers*. *Macromolecules*, 2000. **33**(6): p. 2000-2004.
279. Ishida, H., Campbell S, Blackwell J, *General approach to nanocomposite preparation*. *Chemistry of Materials*, 2000. **12**(5): p. 1260-1267.
280. Hyun, Y., H., Lim S T, Choi H J, Jhon M S, *Rheology of poly(ethylene oxide)/organoclay nanocomposites*. *Macromolecules*, 2001. **34**(23): p. 8084-8093.
281. Vaia, R., A., Ishii H, Giannelis E P, *Synthesis and properties of two-dimensional nanostructures by direct intercalation of polymer melts in layered silicates*. *Chemistry of Materials*, 1993. **5**(12): p. 1694-1696.
282. Camino, G., Costa L, Trossarelli L, *Study of the mechanism of intumescence in fire retardant polymers. V. Mechanism of formation of gaseous products in the thermal degradation of ammonium polyphosphate*. *Polymer Degradation and Stability*, 1985. **12**: p. 203-212.
283. Bellucci, F., Camino G, Frache A, Sarra A, *Catalytic charring–volatilization competition in organoclay nanocomposites*. *Polymer Degradation and Stability*, 2007. **92**(3): p. 425-436.
284. Xie, W., Gao Z, Pan W P, Hunter D, Singh A, Vaia R, *Thermal degradation chemistry of alkyl quaternary ammonium montmorillonite*. *Chemistry of Materials*, 2001. **13**(9): p. 2979-2990.
285. Xie, W., Xie R, Pan W P, Hunter D, Koene B, Tan L S, Vaia R, *Thermal stability of quaternary phosphonium modified montmorillonites*. *Chemistry of Materials*, 2002. **14**(11): p. 4837-4845.
286. Cervantes-Uc, J., M., Cauich-Rodríguez J V, Vázquez-Torres H, Garfias-Mesías L F, Paul D R, *Thermal degradation of commercially available organoclays studied by TGA–FTIR*. *Thermochimica Acta*, 2007. **457**(1–2): p. 92-102.
287. Solarski-Samyn, F., *Compréhension des procédés d'ignifugation du polyamide 6 : Apport des nanocomposites aux systèmes retardateurs de flamme phosphorés*, 2007, Université des sciences et technologies de Lille.

Appendix

Appendix 1: Quantification of color change for FR-PLAs.

To quantify the color change observed when FR fillers are incorporated into the PLA matrix, $L^*a^*b^*$ measurements (**Table 44**) were performed on all samples (i.e. PLA, FR-PLA and FR-PLA-C30B). L^* corresponds to color position between black and white, a^* the color position between red/magenta and green and b^* the color position between yellow and blue. ΔE corresponds to the differences between PLA and FR-PLAs, calculated according to **Equation 25** (cf. chapter II, p.76).

*Table 44: $L^*a^*b^*$ values of PLA, FR-PLA and FR-PLA-C30B.*

$L^*a^*b^*$ values	PLA	FR-PLA	FR-PLA-C30B
L^*	52	83	76
a^*	-2	0.5	2.5
b^*	-1	12	12
ΔE	-	35	28

Data evidence the color change of PLA when fillers are incorporated into it. L^* increases from 52 for PLA to 83 for FR-PLA and 76 for FR-PLA-C30B. a^* increases by 2.5 and 4.5 for FR-PLA and FR-PLA-C30B, respectively, compare to neat PLA. Finally, b^* increases by 13 for both FR-PLA and FR-PLA-C30B compare to neat PLA. ΔE reaches 35 and 28 for FR-PLA and FR-PLA-C30B, respectively. These results demonstrate that when FR fillers are incorporated the color of PLA material changes: the high L^* value of both FR-PLAs specifies that the materials tend to whiter color and the positive value of b^* for both FR materials indicates a tendency to yellowing. The combination between L^* and b^* values evidence the creamy color observed when FR are incorporated into PLA. a^* cannot be taken into account due to the value close to zero.

Appendix 2: Color changes of FR-PLA and FR-PLA-C30B after ageing

It was demonstrated that when FR-PLA and FR-PLA-C30B are submitted to environmental constraints (i.e. T/UV, T/RH and T/UV/RH conditions), some phenomena are observed on the surface of the materials. Indeed, a laundering of plates is reported when samples are aged under T/UV whereas under T/RH and T/UV/TH, the appearance of a white layer at the surface of the samples is evidenced. Thus $L^*a^*b^*$ measurements were performed in order to quantify the color changes of FR-PLAs before and after ageing (Table 45 and Table 46 for FR-PLA and FR-PLA-C30B, respectively).

Table 45: $L^*a^*b^*$ values of unaged and aged FR-PLA under T/UV, T/RH and T/UV/RH conditions.

$L^*a^*b^*$ values	FR-PLA	FR-PLA T/UV 60 d	FR-PLA T/RH 28 d	FR-PLA T/UV/RH 6 d
L^*	83	86 (+3)	89 (+6)	95 (+12)
a^*	0.5	0.3 (-0.2)	0.2 (-0.3)	0.01 (-0.4)
b^*	12	9 (-3)	8 (-4)	4 (-8)
ΔE	-	4	7	15

Table 46: $L^*a^*b^*$ values of unaged and aged FR-PLA-C30B under T/UV, T/RH and T/UV/RH conditions.

$L^*a^*b^*$ values	FR-PLA-C30B	FR-PLA-C30B T/UV 60 d	FR-PLA-C30B T/RH 28 d	FR-PLA-C30B T/UV/RH 6 d
L^*	76	80 (+4)	84 (+8)	93 (+17)
a^*	2.5	2.5	2 (-0.5)	1.9 (-0.6)
b^*	12	12	11 (-1)	6.5 (-5.5)
ΔE	-	4	8	18

Data obtained by $L^*a^*b^*$ display that when FR-PLA and FR-PLA-C30B are aged, the color of the materials changes. Regarding at first the FR-PLA formulation, ΔE is 4 after 60 days exposure to T/UV and reaches 7 and 15 after 28 days and 6 days exposure to T/RH and T/UV/RH, respectively. For FR-PLA-C30B, ΔE is 4 after 60 days exposure to T/UV and reaches 8 and 18 after 28 days and 6 days exposure to T/RH and T/UV/RH, respectively. The increase in the ΔE demonstrates the alteration of colors during ageing. Moreover, for both materials, it appears that L^* increases as function of ageing time and conditions. This shows that materials become whiter after ageing and corroborates the bleaching phenomenon visually observed. Concerning a^* , it appears that the values does not present significant changes for both FR-formulations. In the case of b^* , the values are decreased as function of ageing time and kind of exposure. Indeed, the higher decrease of b^* for FR-PLA and FR-PLA-C30B is observed when materials are aged under T/UV/RH: b^* is decreased by 8 for FR-PLA and by 5.5 for FR-PLA-C30B after 6 days exposure. The negative tendency value of b^* for both FR materials indicates a propensity for the blue color. For a^* , the close zero value designate neutral colors. $L^*a^*b^*$ results clearly prove the bleaching observed when FR-materials are aged.

Appendix 3: Effect of the type of nanoparticle on the hydrolysis of FR-PLAs

In order to determine if the hydrophilic character of clays plays a role during the hydrolytic degradation of flame retarded PLA, three kinds of Cloisite, i.e. 20A, 30B and Na⁺ (hydrophilic character of CNa⁺ > C30B > C20A) were incorporated into FR-PLA materials and then aged for 60 days under T/RH conditions.

The formation of voids, fractures and of a white layer is reported (**Figure 114**) after 28 days of ageing under T/RH exposure for the three materials (i.e. FR-PLA-C20A, FR-PLA-C30B and FR-PLA-CNa⁺).

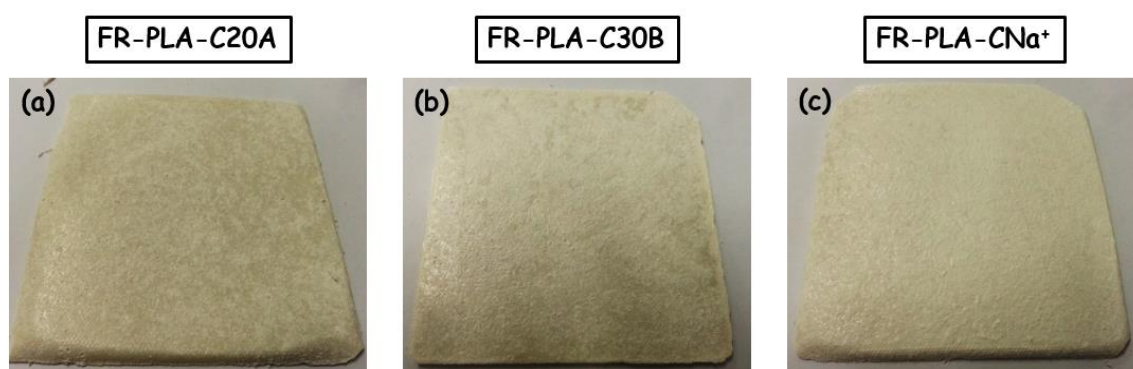


Figure 114: FR-PLA-C20A (a), FR-PLA-C30B (b) and FR-PLA-CNa⁺ (c) plates aged 28 days under T/RH conditions.

Physico-chemical properties of the materials were also studied all along the exposure to T/RH, i.e. the molecular mass (**Figure 115**), T_g (**Figure 116**), T_m (**Figure 117**) and crystallinity (**Figure 118**).

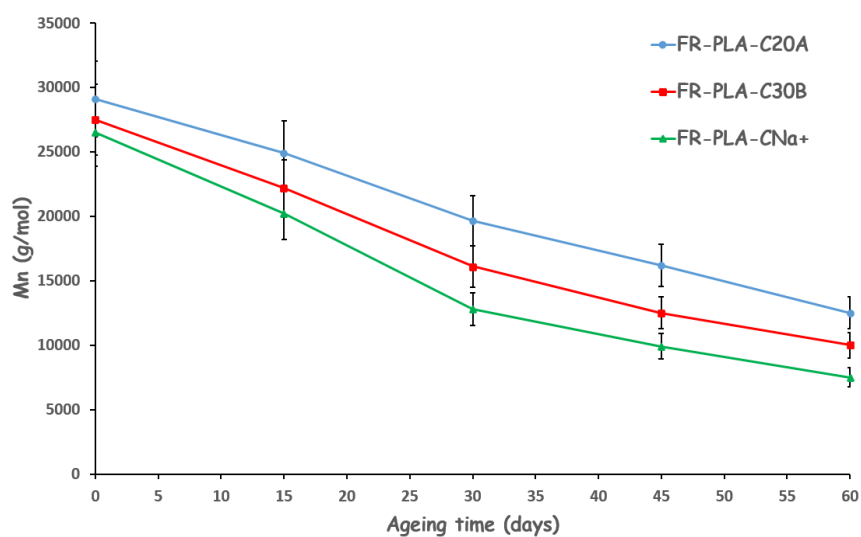


Figure 115: M_n versus ageing time of FR-PLA-C20A (\bullet), FR-PLA-C30B (\blacksquare) and FR-PLA-C30B (\triangle) samples aged under T/RH conditions.

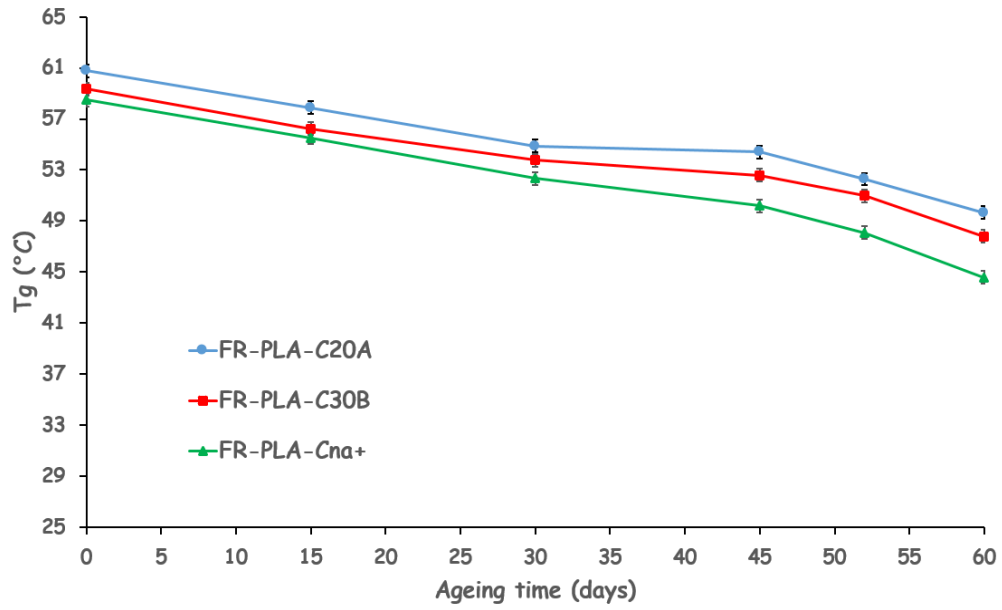


Figure 116: Evolution of glass transition temperature (T_g) of FR-PLA-C20A (\bullet), FR-PLA-C30B (\blacksquare) and FR-PLA-CNa⁺ (\blacktriangle) as a function of exposure time under T/RH conditions.

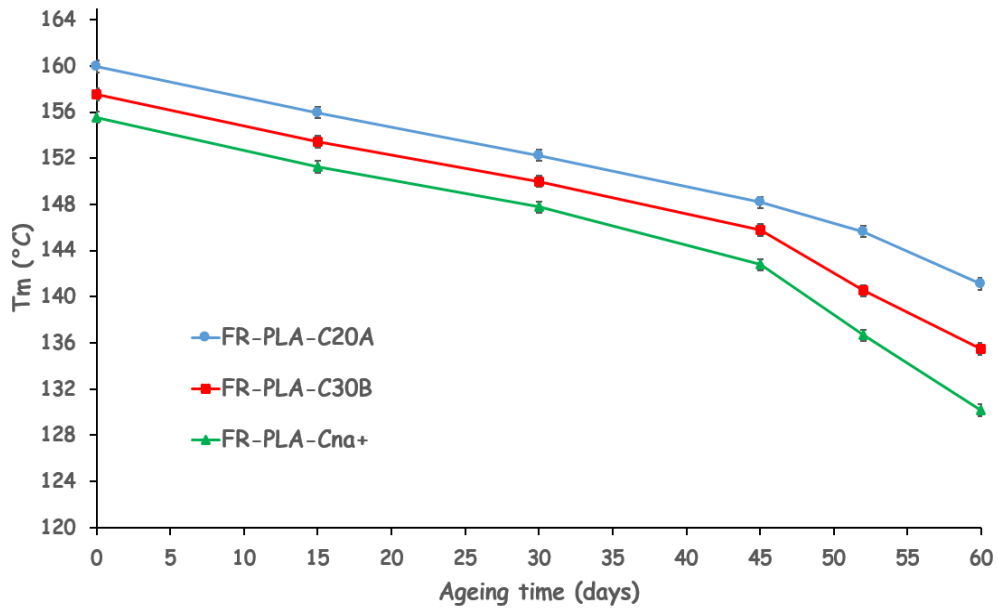


Figure 117: Evolution of melting temperature (T_m) of FR-PLA-C20A (\bullet), FR-PLA-C30B (\blacksquare) and FR-PLA-CNa⁺ (\blacktriangle) as a function of exposure time under T/RH conditions.

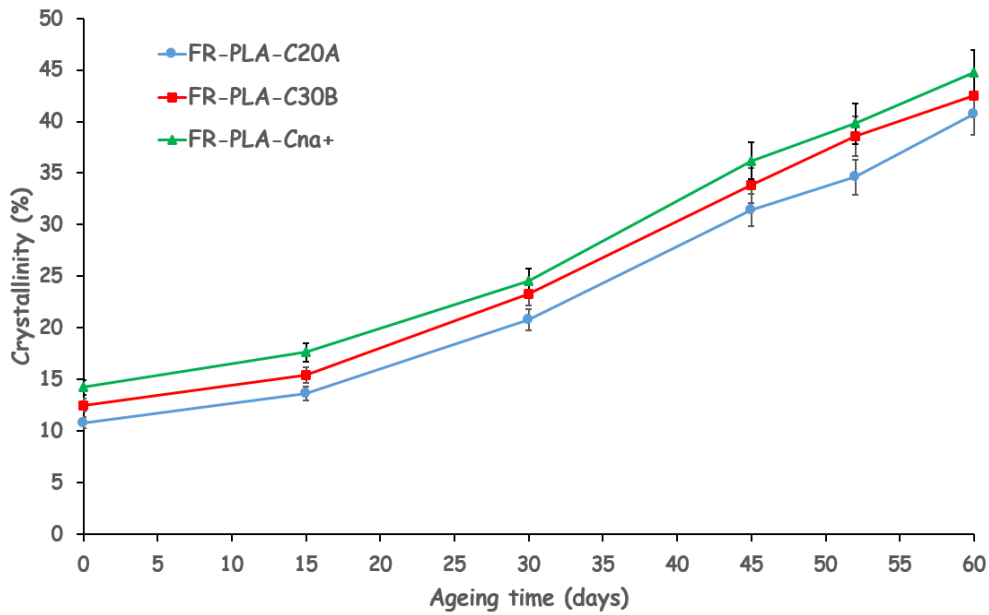


Figure 118: Evolution of crystallinity of FR-PLA-C20A (●), FR-PLA-C30B (■) and FR-PLA-CNa⁺ (△) as a function of ageing time under T/RH conditions.

Before ageing, M_n , T_g and T_m are higher with a lower crystallinity value for FR-PLA-C20A compared to FR-PLA-C30B then FR-PLA-CNa⁺. It appears that the molecular mass, T_g , T_m and crystallinity of the three materials exhibit the same behavior during ageing, whatever the formulation. Indeed, M_n , T_g and T_m of the three formulations decrease with increasing ageing exposure to T/RH. Crystallinity increases when ageing duration increase. Moreover, after ageing, M_n , T_g and T_m are still higher with a lower crystallinity value for FR-PLA-C20A compared to FR-PLA-C30B then FR-PLA-CNa⁺. This seem to indicate that the hydrophilic character of organoclays does not play a particular role during the degradation of the PLA matrix compared to the M_n . Indeed, the lower the M_n before ageing, the higher the impact of ageing on T_g , T_m and crystallinity.

Appendix 4: FTIR (ATR) spectra of FR-PLAs aged under T/RH and T/UV/RH exposure.

The behavior of FR fillers during ageing is confirmed by FTIR spectra recorded for both FR-PLAs during exposure to T/RH and T/UV/RH conditions (**Figure 119** and **Figure 120**). Indeed, characteristic bands of PLA (cf. **Table 1, p.29**), Melamine and APP (previously reported **p.144**) can be identified on the spectrum of unaged FR-PLA and FR-PLA-C30B. Furthermore, similar spectra are observed for both FR-PLAs after 35 days exposure to T/RH and 10 days exposure to T/UV/RH conditions (just before disintegration into powder) with no appearance of new peaks. As characteristic bands of Cloisite 30B are not observed in the FR-PLA-C30B spectra due to the relatively low loading of clays (i.e. 1 wt.-%), both FR-PLAs exhibit the same spectra.

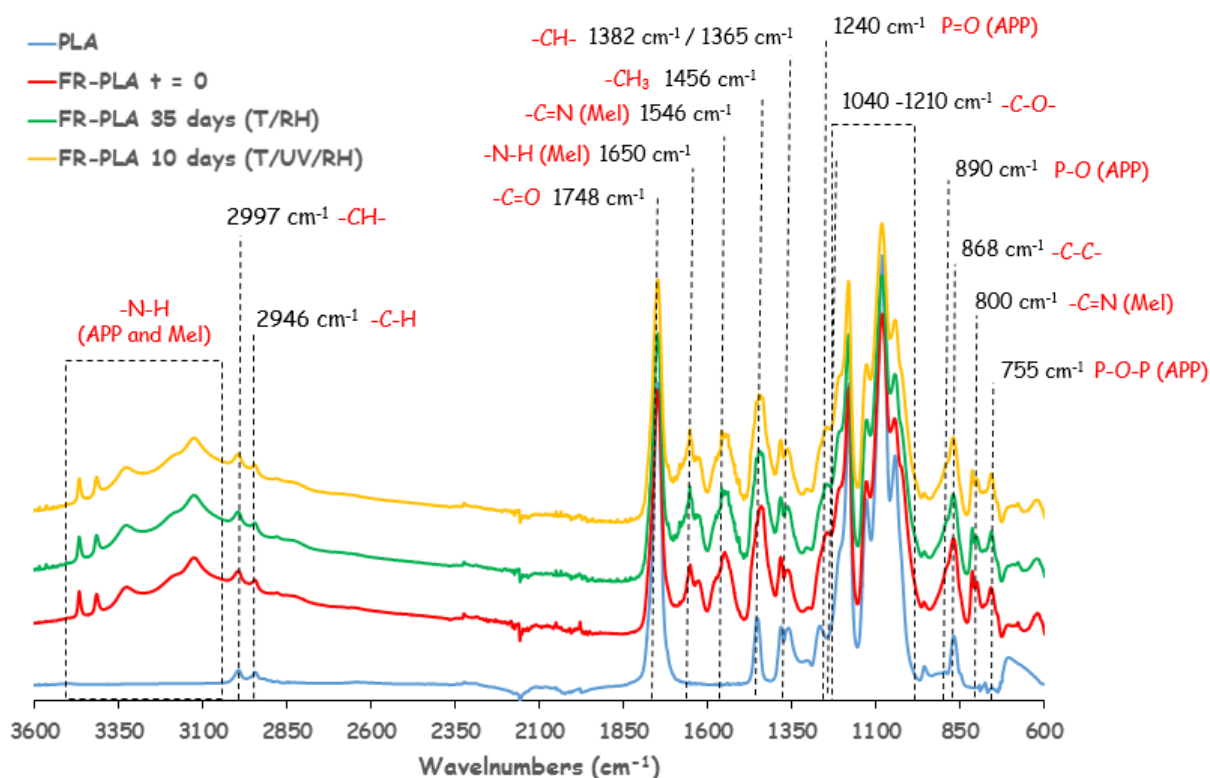


Figure 119: FTIR (ATR) spectra of PLA, FR-PLA, FR-PLA 105 days (T/RH) and FR-PLA 90 days (T/UV/RH) in the range of 600 to 3600 cm^{-1} .

Appendix

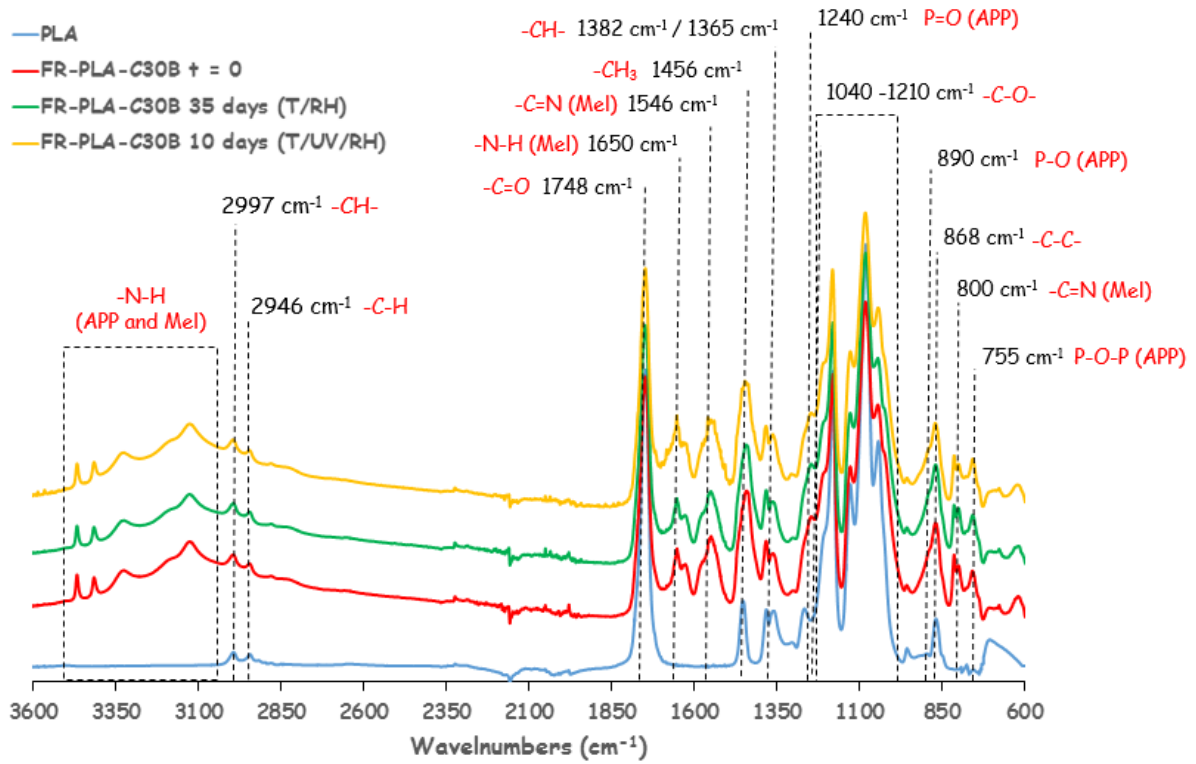


Figure 120: FTIR (ATR) spectra of PLA, FR-PLA-C30B, FR-PLA-C30B 105 days (T/RH) and FR-PLA-C30B 90 days (T/UV/RH) in the range of 600 to 3600 cm^{-1} .

Appendix 5: 2D HYSCORE principle

The 2D HYperfine Sub-level CORrelation (2D HYSCORE) is essentially a two dimensional electron spin-echo envelope modulation (ESEEM) experiment in which correlation is transferred from one electron spin manifold to another. A sequence of four microwave pulses is applied to the sample and the stimulated spin-echo produced is measured (**Figure 121**)

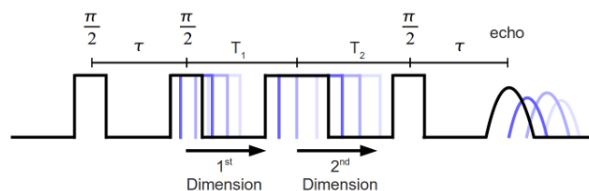


Figure 121: Example of 2D HYSCORE microwave pulses.

In a HYSCORE experiment, the time between the second $\pi/2$ and π pulse is varied in one dimension and the time between the π and third $\pi/2$ pulse is varied in a second dimension. A two dimensional Fourier transform gives the sample data below (**Figure 122**).

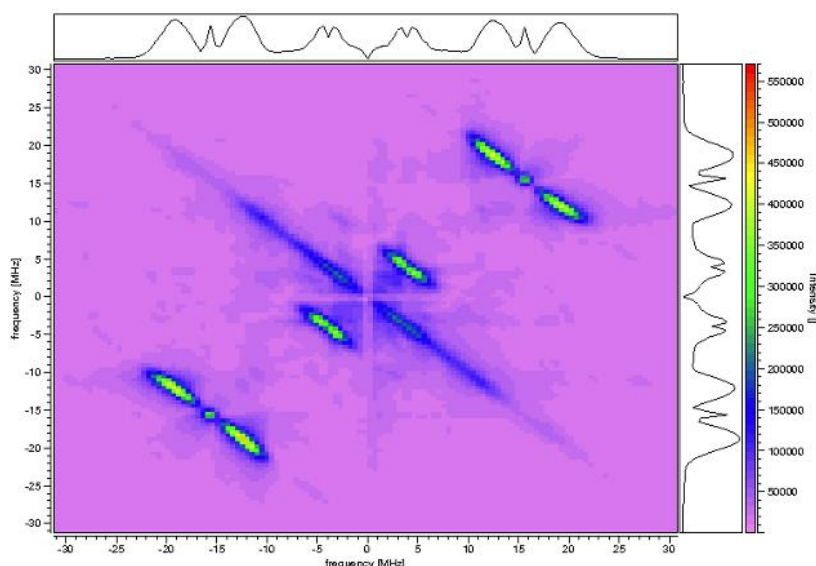


Figure 122: 2D HYSCORE spectrum of a coat standard sample.

As in an ESEEM experiment, the peaks observed are essentially an NMR spectrum of nuclei that are coupled to the electron. HYSCORE allows one to take a complicated ESEEM spectrum and extend the data into a second dimension. Peaks appearing in the upper right and lower left quadrants typically arise from nuclei in which the hyperfine coupling is less than the larmor frequency. They appear at the larmor frequency, separated by the hyperfine coupling. Peaks from nuclei in which the hyperfine interaction is greater than the larmor frequency appear in the upper left and lower right quadrants. The HYSCORE spectrum can get very complicated for nuclei with a spin of $I > 1/2$ with many peaks arising from the complication of additional nuclear zeeman and quadrupole levels. Even with the complexity of the spectra, HYSCORE on systems with multiple nuclei can make ESEEM spectra that would be difficult or impossible to interpret much more manageable.

Appendix 6: Thermal stability of pure compounds

The TGA curves of the pure polymer (PLA) and additives (Melamine, APP and Cloisite 30B) are depicted in **Figure 123**. PLA starts to decompose in one step around 280°C with no residue left at the end of the experiment, i.e. 800°C. APP decomposes in two steps, the first one between 250°C and 450°C corresponding to 14% weight loss due to water and ammonia release [282], leading to the formation of phosphoric acid. The second weight loss between 450°C and 700°C is linked to a 65% weight loss attributed to the sublimation of $P_4O_{10}\cdot H_2O$ [12, 282] with 13 wt.-% residue left at the end of the experiment. Melamine begins to decompose at 240°C, in one step with no residue at the end of the experiment, i.e. 800°C. It results in the formation of melam (stable up to 400°C), melem (stable up to 500°C) and melon (stable up to 600°C) [61]. The condensation of Melamine is accompanied by a release of ammonia [12, 61].

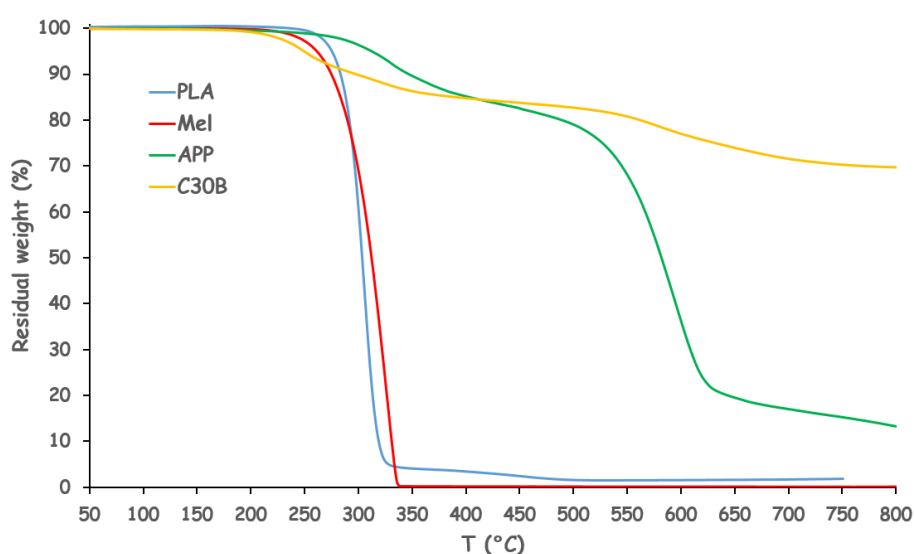


Figure 123: TGA curves of pure compounds, PLA (●), Mel (●), APP (●) and C30B (●) under air flow at 10°C/min.

Decomposition of C30B is well known and documented [283-285]. According to literature, this organoclay can decompose in 4 steps. These four steps of degradation can be retrieved in **Figure 123** and in particular in **Figure 124** which shows the rate of degradation (DTG) of pure compounds.

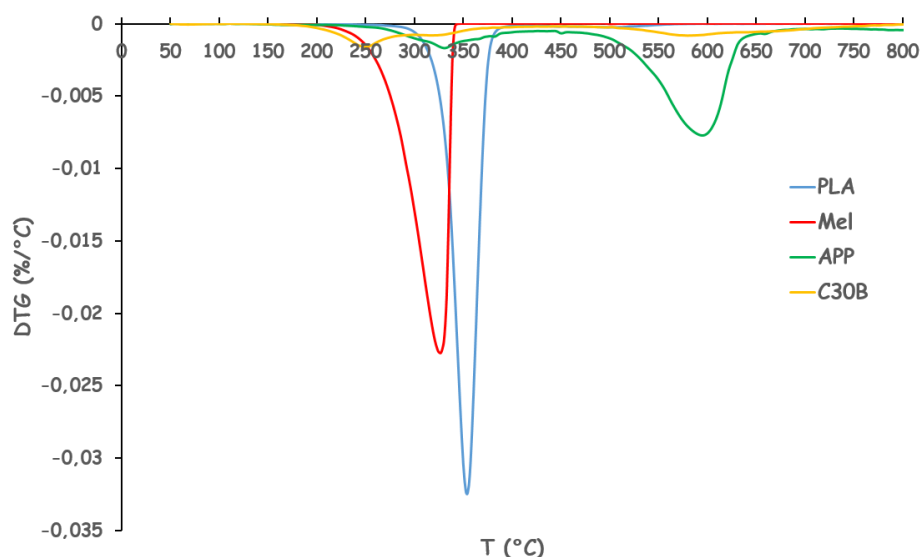


Figure 124: DTG of pure compounds, PLA (●), Mel (●), APP (●) and C30B (●) under air flow at 10°C/min.

The first step starts before 200°C and is linked to the desorption of water, oxygen and nitrogen absorbed in C30B. The second step (200°C to 450°C) results from the thermal degradation of the surfactant of Cloisite 30B. This second step is visible on the TGA curve in **Figure 123** (15% weight loss) and is normally constituted of two consecutive stages as observed in the DTG curve (**Figure 124**). From 200°C to 320°C, C30B releases water, carbon dioxide, alkane, alkene, aldehyde, carboxylic acid and amine. From 320°C to 450°C, water, alkane, alkene and alcohol are released [286]. From 450°C to 800°C, the 15% weight loss corresponds to the dehydroxylation of the aluminosilicate structure and to the release of degraded products of the surfactant. Researches in our lab have already confirmed this degradation process [287].

VIEILLISSEMENT D'ACIDE POLYLACTIQUE IGNIFUGÉ

RÉSUMÉ - Le but de ces recherches est d'étudier le vieillissement de l'acide polylactique (PLA) ignifugé. Trois vieillissements différents ont été étudiés i.e. température/ultra-violet (T/UV), température/humidité relative (T/RH) et température/ultra-violet/humidité relative (T/UV/RH). Afin de comprendre le rôle des retardateurs de flamme lors du vieillissement, l'étude de la dégradation du PLA vierge à tout d'abord été menée. Des méthodologies innovantes ont été développées et les propriétés physico-chimiques du polymère ont été caractérisées en fonction de la durée et du type d'exposition. Les mécanismes de dégradation dépendants du vieillissement (T/UV, T/RH et T/UV/RH) ont été élucidés et comparés à la littérature. L'influence des retardateurs de flamme (i.e. Mélamine, Polyphosphate d'ammonium et Cloisite 30B) lors du vieillissement des formulations ignifugées a ensuite été étudiée. Il a été prouvé que ces additifs ont une influence directe sur le vieillissement, au niveau des propriétés physico-chimiques et des mécanismes de dégradation. La masse molaire s'est révélée être cruciale dans la mesure où elle gouverne l'évolution des propriétés physico-chimiques du matériau durant le vieillissement, et donc sa durabilité. Sachant que le PLA est ignifugé par incorporation d'additifs retardateurs de flamme, il était primordial de comprendre l'effet du vieillissement sur ces additifs et donc leurs effets sur les propriétés feu du PLA. Il a ainsi été montré que les performances feu de ce matériau sont améliorées au cours du vieillissement, jusqu'à sa dégradation complète. Ces performances ont été corrélées avec l'évolution des propriétés physico-chimiques survenant au cours du vieillissement, présentant un rôle prépondérant sur la cinétique d'intumescence.

AGEING OF FLAME RETARDED POLYLACTIC ACID

ABSTRACT - This work deals with the ageing of flame retarded (FR) Polylactic acid (PLA). The impact of three accelerated ageing conditions i.e. temperature/ultra-violet (T/UV), temperature/relative humidity (T/RH) and temperature/ultra-violet/relative humidity (T/UV/RH) was studied. In order to understand the role of fire retardant additives on ageing of flame retarded PLAs, the first study was focused on neat PLA. Innovative methodologies were developed, the change in physico-chemical properties of the polymer was characterized as a function of ageing exposure and ageing duration. Moreover, the mechanisms of degradation occurring during T/UV, T/RH and T/UV/RH exposure were elucidated and compared to the literature. Then, the influence of flame retardants (i.e. Melamine, Ammonium polyphosphate and Cloisite 30B) on the ageing behavior of FR-PLAs was investigated. FR fillers were evidenced to have a direct influence on physico-chemical properties and mechanisms of degradation of the material during ageing. The molecular mass was reported to be a crucial parameter, as it is related to the physico-chemical properties and thus to the durability of the material. The main goal of flame retardants is to improve the flammability of PLA thus the effect of ageing on the fire properties of PLA was determined. It is noteworthy that the fire properties of flame retarded PLA are improved during ageing, until the complete degradation of the materials. These surprising performances were found to be correlated to the change in physico-chemical properties which play a key role on the kinetics of intumescence.